FINITE ELEMENT FORMULATION FOR THE ANALYSIS OF INTERFACES, NONLINEAR AND LARGE DISPLACEMENT PROBLEMS IN GEOTECHNICAL ENGINEERING

A THESIS

Presented to

The Faculty of the Division of Graduate Studies

By

Adolfo E. Zeevaert

In Parial Fulfillment

of the Requirements for the Degree

Doctor of Philosophy in Civil Engineering

Georgia Institute of Technology

September, 1980

FINITE ELEMENT FORMULATION FOR THE ANALYSIS OF INTERFACES, NONLINEAR AND LARGE DISPLACEMENT PROBLEMS IN GEOTECHNICAL ENGINEERING

Approved:

R. D. Barksdale, Chairman

G. F. Sowers

C. V. Smith

J. S. Lai

Date approved by Chairman September 18, 1980

ACKNOWLEDGMENTS

The author wishes to thank Dr. R. D. Barksdale, his principal advisor, for his continuous guidance, healthy discussions and encouragement during the preparation of this thesis. Sincere appreciation is extended to all the professors that have contributed to his professional formation, from his early student days. Special thanks to Regents Professor G. Sowers for his insight into real geotechnical problems and for being a member of the reading committee. Thanks are also extended to the members of the reading committee for their advice and patience: to Professors C. V. Smith and V. S. Lai, to Regents Professor S. Atluri for his advice and for being a member of the examining committee, and to Dr. Q. L. Robnett for his advice and laboratory data. Thanks are also extended to Professors B. Goodno, K. M. Will and L. F. Kahn for their early suggestions, to Dr. H. Murakawa and Dr. Kathiresan for their notes in Solid Mechanics and to the computer center staff of the Georgia Institute of Technology.

Finally, my deepest gratitude to my parents for all these years of understanding and support and to my brothers and sisters and my close friends that have in some way cared for me.

TABLE OF CONTENTS

Page

ACKNOWLEDGMENTS ii

LIST OF ILLUSTRATIONS v

LIST OF TABLES ix

NOMENCLATURE x

SUMMARY xv

Chapter

I. INTRODUCTION 1

Purpose of the Analytical Model
The Soil-Fabric System Problem
Objectives and Applications

II. REVIEW OF THE LITERATURE 6

General
Axisymmetric Elements
Interface Elements
Nonlinear Analysis
Plasticity and Visco-elasto-plasticity
Large Displacements, Finite Strain and Elasto-Plasticity
No Tension Analysis
Fabric Materials
Related Research
Summary

III. OVERVIEW OF THE FINITE ELEMENT APPROACH 33

Finite Element Model
Types of Finite Elements Used
Isoparametric Eight Node Quadrilateral Element
Formulation of the Strain-Displacement Transformation Matrices for Axisymmetric Solids

IV. SOIL-FABRIC MODEL 44

Interface Element
Fabric Element

Chapter Page

V. NONLINEAR ANALYSIS AND LARGE DISPLACEMENTS. . . . 64

Background
Total Lagrangean Formulation
Updated Lagrangean Formulation
Equations for the Nonlinear and Large Displacement Finite Element Formulation
Derivation of the Strain-Displacement Relation for Large Displacements
Initial Stress Stiffness Matrix
Procedure for Piecewise Solution of the Nonlinear Equations
Summary

VI. THE INTERFACE PROBLEM 95

Interface Behavior Including Large Displacements and Slip
Fabric Element Subjected to Large Displacements

VII. SOIL PLASTICITY 124

Introduction
Soil Plasticity
Summary

VIII. NO TENSION ANALYSIS 148

Introduction
Formulation of the No Tension Problem for Soils
Resilient Modulus of Elasticity
Summary

IX. COMPUTER CODE ORGANIZATION AND CAPABILITIES . . .171

General Description
Input-Output Capabilities
Summary

X. APPLICATIONS OF THE COMPUTER CODE 199

Examples

XI. CONCLUSIONS 237

XII. RECOMMENDATIONS FOR FURTHER STUDY 242

APPENDIX A 245

BIBLIOGRAPHY 253

LIST OF ILLUSTRATIONS

Figure		Page
3-1.	Representation of the Soil-Fabric System	34
3-2.	Finite Elements Used in the Model: Global Coordinate Axis.	36
4-1.	Interface Element.	45
4-2.	Uniform Load Applied at the Boundary of an Eight Node Isoparametric Element	47
4-3.	Total Nodal Displacement Axes of the Interface Element.	47
4-4.	Fabric Element Model-Axisymmetric Representation	56
4-5.	The Fabric Element in the Soil-Fabric System	57
4-6.	Soil-Fabric Finite Element Model	57
4-7.	Linear Approximation for the Fabric at the Soil-Fabric Interface.	59
4-8.	Fabric Element General Representation.	59
5-1.	Deformation and Stresses Due to Load Increments.	66
5-2.	Part of a Finite Element Mesh Showing Updated Nodal Coordinates.	93
5-3.	Graphical Representation of the Maximum Allowable Increment of Displacement for an Iteration	93
6-1.	General Case of Deformation for an Interface Element.	96
6-2.	Average Plane of Contact of an Interface Element	96
6-3.	General Case of Inclination of a Contact Plane with Corresponding Spring Elements	99
6-4.	Particular Case of Horizontal Interface	99
6-5.	Slip Forces Correction for Spring Elements	104

Figure		Page
6-6.	Maximum Shear Decomposition.	106
6-7.	Normal and Tangential Relative Displacements of Interface Element	106
6-8.	Fabric Element Sampling Points A and B for Two Point Numerical Integration.	120
6-9.	Change of Coordinates of Fabric Element.	120
7-1.	Elastic and Plastic Material Behavior.	129
7-2.	Mechanical Model of an Ideal Elasto-Plastic Material	129
7-3.	Yield Surface for Associated Plasticity.	132
7-4.	Elastic and Plastic Strains Defining H'.	132
8-1.	Cohesionless Material. Stress Modification for a No Tension Failure Condition	155
8-2.	Stress Modification in No Tension Analysis for $\sigma_3 > (\sigma_3)_{min}$	156
8-3.	Stress Modification Procedure [108].	157
8-4.	Tangential Stress Modification	158
8-5.	Sign Convection for Rotation of Axes	161
8-6.	Resilient Modulus Variation with Stress State. . .	161
8-7.	Local and Global Axes for Stratified Materials . .	170
9-1.	Flow Diagram of the Main Finite Element Program. .	173
9-2.	Flow Diagram for Subroutine BOPER: Strain Displacement Operator.	175
9-3.	Flow Diagram for Subroutine BLOPER: Strain Displacement Operator for Large Displacements. . .	176
9-4.	Flow Diagram for Subroutine ELASPD: Elastic-Plastic Constitutive Matrix.	178
9-5.	Sampling Points for the Eight Node Isoparametric Element.	178
9-6.	Flow Diagrams for Subroutine SPRSTIF: Interface Element Stiffness Matrix	181

Figure		Page
9-7.	Flow Diagram for Subroutine FABSTIF: Fabric Element Stiffness Matrix Subroutine.	182
9-8.	Norm for Maximum Displacement for a Given Iteration.	185
9-9.	Flow Diagram for Subroutine STRES1: Computation of Stresses and Strains.	186
9-10.	Flow Diagram for Subroutine TRANST: Transformation to True Cauchy Stress.	187
9-11.	Slip Algorithm in Subroutine STRES1 After Herrmann [59].	189
9-12.	Variation of the Computed σ-ε Relation with the Number of Load Increments.	195
9-13.	Interpolation of the Plasticity Parameter	197
10-1.	Mesh for the Stress Distribution Problem. Example No. 1.	202
10-2.	Boussinesq and Finite Element Results of the Vertical Stress Distribution. Example No. 1 . . .	203
10-3.	Meshes with 24 and 54 Elements Used in Example No. 2.	205
10-4.	Computed Vertical Stresses for a Two Layer System. Example No. 2	206
10-5.	Shear Stress at the Interface Elements for Homogeneous Material Horizontal Axis at 4.5 in Depth. Example No. 2	206
10-6.	Geometry and Finite Element Model of a Horizontally Loaded Fabric. Example No. 3	208
10-7.	Horizontally Loaded Fabric Results for Radial and Tangential Stress. Example No. 3.	210
10-8.	Gray Clay Parameters for Example No. 4	211
10-9.	Finite Element Model. Example No. 4	213
10-10.	Results of the Finite Element Formulation and the Experimental Results for the q_u-Test. Example No. 4.	213

Figure Page

10-11. Finite Element Model of a Footing over Soft Clay Uniform Load Conditions. Example No. 5. 214

10-12. Results for Uniform Load Condition. Example No. 5. 214

10-13. Plasticity Parameter $\bar{\sigma}$ vs. H'. Example No. 5 . . . 215

10-14. Two Layer Model. Rigid Concrete Footing over Compacted Sand. Example No. 6 217

10-15. Elasticity, Plasticity and Variable Modulus Constants for Two Layer. Example No. 6. 218

10-16. Finite Element Model of Footing over Two Layer. Example No. 6. 220

10-17. Vertical Stress and Strain Distributions. Example No. 6. 221

10-18. Soil-Fabric Laboratory Model. Example No. 7 . . . 223

10-19. Laboratory Material Parameters. Example No. 7 . . 224

10-20. Finite Element Models With and Without Fabric. Example No. 7. 226

10-21. Finite Element Program Computed Stress Distributions. Example No. 7. 227

10-22. Radial Stresses 0.75 inch Above the Interface. Example No. 7. 228

10-23. Fabric Stresses. Example No. 7. 228

10-24. Sampling Points at Failure for 7 psi and 56 psi of Applied Pressure. Example No. 7. 232

10-25. Total Load Displacement at the Surface. Example No. 7. 233

10-26. Surface vs. Interface Vertical Displacement. Example No. 7. 233

10-27. Deformed Mesh for the Soil-Fabric System. Example No. 7. 234

A-1. Stress Tensor Definitions. 248

A-2. Axisymmetric Axes (r,z,θ) and Cartesian Axes (x,y,z) 252

LIST OF TABLES

Table		Page
9-1.	Results with Variable Number of Load Increments.	196
10-1.	Computed Response of the Soil-Fabric Model. Deformations for the Center of the Loaded Area. Example No. 7.	231
10-2.	Permanent Deformations for 100 Cycles of Load Applications. Example No. 7	231

NOMENCLATURE

A	plasticity parameter function of strain hardening
AV	axisymmetric load factor
AVR,AVT	axial and tangential correction factors for fabric elements
$\underset{\sim}{B}$	strain-displacement transformation matrix, matrix relating relative displacements to nodal displacements for interface elements
$\underset{\sim}{\tilde{B}}$	total incremental strain displacement matrix
$\underset{\sim}{B}_L$	incremental strain-displacement matrix for large displacements
c	cohesion
$\underset{\sim}{C}_E$	center of axisymmetric model
$\underset{\sim}{D}$	stress strain constitutive matrix
$\underset{\sim}{D}_{ep}$	elastic-plastic constitutive matrix
det|J|	determinant of the Jacobian matrix
E	modulus of elasticity
E_1, E_2	modulus of elasticity in plane behavior and normal to the plane
E_r	resilient modulus of elasticity
E_A, E_B, E_C	resilient modulus for stress conditions A, B, and C
F_i, F_j, F_k	concentrated forces at nodes i,j,k
$\underset{\sim}{F}$	displacement gradient matrix or transformation matrix
{F}	nodal forces
$\underset{\sim}{F}_{int}$	internal forces at the interface
F	failure criterion

$\underset{\sim}{F}_o$	corrective nodal forces
G_2	shear modulus
H_i	interpolation or shape functions
H'	slope of the uniaxial stress-plastic strain curve
$[J]$	Jacobian matrix
J_2	second invariant
k	subgrade reaction modulus
K_s	shear spring coefficient
K_n	normal spring coefficient
K_{system}	system stiffness matrix
$\underset{\sim}{K}_T$	tangential stiffness matrix
$\underset{\sim}{K}_o$	small strains stiffness matrix
$\underset{\sim}{K}_L$	large displacements stiffness matrix
$\underset{\sim}{K}_\sigma$	initial stress stiffness matrix or geometry stiffness matrix
k'	failure criterion parameter
k_1	constant for computation of E_r
L	length of interface element
$\underset{\sim}{M}^o, \underset{\sim}{M}^I$	matrix constants for evaluation of failure criterion
n	constant for computation of E_r
P, P_{ex}	external forces
P_{UN}	unbalanced slip forces
P_{SPRING}	forces at the spring interface
P_{SLIP}	slip forces
P_{UB}	unbalanced force for the system
P_{int}	internal forces

P_{corr}	corrective forces
Q	plastic potential
q	uniform load
$\underset{\sim}{R}$	rotation matrix
R_i	body forces
R_s	stress ratio
RP,ZP	local coordinates axes of element
r	global coordinate axis
r_a	radial distance for sampling point
$\underset{\sim}{S}$	element stiffness matrix, second Piola-Kirchhoff stress
$\underset{\sim}{S}_{ie}$	interface element stiffness matrix
$\underset{\sim}{S}_f$	fabric element stiffness matrix
$\underset{\sim}{S}_{fL}$	fabric element stiffness matrix for large displacements
$\underset{\sim}{S}_{fI}$	fabric element stiffness matrix for small displacements
SRD,NRD	average shear and normal incremental relative displacement
S_r, S_θ, S_θ	deviator stresses
$\underset{\sim}{T}_\varepsilon, \underset{\sim}{T}_\theta$	transformation matrices
$\underset{\sim}{t}$	first Piola-Kirchhoff stress
$\underset{\sim}{t}_{si}$	surface tractions
$\underset{\sim}{u}$	nodal displacements
u,v	nodal displacements in r and z directions
u'	local axis displacement for fabric element
z	global coordinate axis
α	angle between horizontal r axis and ijk side of interface, angle to define direction of principal stresses

α'	failure criterion parameter
α_1	corrective angle
δ	increment of node displacement, or increment
$\Delta\delta$	average increment of relative displacement
$\delta\epsilon^I, \delta\epsilon^L$	linear and quadratic strain increments
$\{\frac{\partial F}{\partial \sigma}\}$	gradient vector
$\Delta\sigma$	incremental normal stress
$\Delta\tau$	incremental shear stress
$\Delta\sigma_a, \Delta\sigma_B, \Delta\sigma_C$	deviator stress for conditions A,B,C
$\Delta u, \Delta v$	relative displacements in the r and z directions
$\Delta \underset{\sim}{S}$	increment of second Piola-Kirchhoff stress
$\underset{\sim}{\varepsilon}$	strain
$\epsilon_e - \epsilon_p$	elastic and plastic strains
$\epsilon_r, \epsilon_r, \epsilon_\theta, \gamma_{rz}$	axisymmetric strain components
ϵ^I, ϵ^L	small and large displacements strains
θ	angle between principal stress direction and global axes
κ	hardening parameter
λ	proportionality constant
ν	Poisson's ratio
ν_1, ν_2	Poisson's ratio in plane and normal to the strata
$\underset{\sim}{\sigma}$	stress
σ_z	normal stress at the interface
$\sigma_1, \sigma_2, \sigma_3$	principal stresses
$\bar{\sigma}$	equivalent effective stress = $J_2^{1/2}$
$\bar{\bar{\sigma}}_o$	equivalent stress at yield
σ_m	average or mean normal stress

$\sigma_r, \sigma_\theta, \sigma_z$	axisymmetric normal stress components
$\overset{\nabla}{\sigma}{}^*$	corotational stress rate
$(\sigma_1)_{max}, (\sigma_3)_{min}$	maximum and minimum major principal stresses
σ_1'	major principal stress associated with σ_3 at failure
σ_n	normal stress
$\sigma_{\theta c}$	$= \sigma_1+\sigma_2+\sigma_3$
$\underset{\sim}{\tau}$	true Cauchy stress, shear stress
τ_{max}	maximum shear stress
τ_s	shear stress at the spring interface
$\tau_r{}^N, \tau_T{}^N$	true radial and tangential stresses for fabric at state N
τ_o	octahedral shear stress
ϕ	angle of internal friction
$\underset{\sim}{\psi}$	vector of unbalanced forces

SUMMARY

The use of fabric materials in soil construction projects has created an important need to theoretically predict their behavior using experimentally measured material properties. At sites where temporary roadways are constructed by placing stone over existing soft soil, the performance of the roadway is often unsatisfactory due to the development of large deformations and rutting with the application of repeated wheel loadings. The principal objective of the mathematical formulation is to model the behavior under load of a reinforced soil system, where a fabric is placed over a soft soil and covered with stone for use as a temporary haul road. This approach is now widely used to improve the behavior of temporary roadways, particularly where very soft soils are encountered. Available laboratory and full-scale tests of soil-fabric systems provide a sound basis for validating the theoretical model developed in this study.

The finite element method has gained wide acceptance for solving both static and dynamic geotechnical problems. The finite element solution presented in this study is applicable to the analysis of solid axisymmetric soil-fabric interaction problems.

The purpose of the theoretical and analytical

investigation is to define the stress distribution and the load-deformation characteristics of the soil-fabric system for varying geometries and material properties. Included in the mathematical formulation are such features as: nonlinear behavior of the soil and fabric materials, friction parameters of the interface, tension characteristics of the fabric materials, large displacements in finite deformation, "no tension" conditions of the cohesionless materials, and yielding of plastic materials. The mathematical model is a more complete approximation of the actual fabric-soil system than is presently available.

The principal features that were implemented in the finite element formulation to accurately model the problem are:

(a) Eight Node Isoparametric Element. Eight node isoparametric elements are used to model the soil and stone. This type of element permits using curved boundaries and gives accurate representation of the variation in stress and strain through the element.

(b) Nonlinear Material Behavior. The nonlinear behavior of the material is described by a uniaxial stress-strain curve. The program computes for the stress conditions, the corresponding elasticity matrix and/or the yield conditions of the elements.

(c) Anisotropy. For materials such as stone having different moduli of elasticity in two orthogonal directions,

the anisotropic elastic constants are used for an initial elastic analysis.

(d) Interface Modeling. With the use of six node spring elements, the interface stress conditions are computed; and the slip or separation condition between interfaces is established.

(e) Fabric or Membrane Flexible Elements. A special element is used to represent the fabric at the interface of stone and clay. In this thesis the term fabric element is used replacing a more general term flexible membrane element. The fabric element used can take only tension forces with compression or bending resistance not being permitted in this element. The fabric elements provide the "reinforcing" of the system and can have nonlinear material properties.

(f) Large Displacement. Nonlinear strain-displacement relations are included as an option. Hence, the solution is valid as the fabric-soil system undergoes large displacements.

(g) Incremental Loading. The load applied on the system is added in small increments to give a complete load-displacement history of the model. Equilibrium is checked after each load increment, and iterations performed to equilibrate unbalanced forces resulting from the nonlinear stress-strain and large deformation conditions.

(h) No-Tension Analysis. The fact that stone cannot take a significant level of tension is fully considered in

the no tension model. The model modifies the stresses for elements in failure and applies equilibrating forces for the introduced modification.

(i) Failure Conditions. The plasticity characteristics of each element for each material are taken into account by use of the Drucker-Prager yield criterion for each element. Associated plasticity is used together with a corresponding flow rule. The plasticity formulation is limited to small strains. The present finite element formulation does not include time effects due to viscosity or consolidation. Also not included are effects of rate of loading, inertia forces, strain softening and the local effects of the gravel punching into the soft soil.

CHAPTER I

INTRODUCTION

Purpose of the Analytical Model

The introduction of new synthetic fabric materials and their subsequent use in soil construction projects has created the need to predict their behavior under all types of loads and environmental conditions. Laboratory and full scale tests together with suitable analytical models provide valuable information for the design and utilization of the fabric materials. The use of woven and nonwoven fabrics, introduced in geotechnical projects in the late sixties, has increased at a very fast rate and it is certain that their use will be much more intensive in the future.

At sites where temporary roadways are constructed by placing gravel over the existing soft clay, the performance of the roadway is not always satisfactory. Large deformations and rutting due to multiple wheel load applications often develop. The gravel penetrates into the soft soil and large deformations are produced at the surface. To avoid this particular problem woven and nonwoven fabric materials are now often used. The fabric is placed over the soft clay to improve working conditions, prevent intrusions of the stone into the subgrade and "stiffen" the system.

The purpose of this study is to develop an analytical model that is able to predict the state of stresses and deformations of the soil-fabric system when the system is subjected to external loads. The finite element method is used to obtain the solution of this problem. The material design parameters used by the mathematical model are evaluated with appropriate laboratory tests that are in accordance with the constitutive laws of the analytical model.

An important matter to be investigated is: To what extent and what is the mechanism developed by flexible membrane elements embedded in the soil to improve the performance of roadways during construction and of conventional roadways subjected to multiple load applications? The answer requires the knowledge of all design parameters including the geometry of the problem, material properties of all elements of the system, pressure distribution, number of load applications, fabric properties and the interface friction parameters. Environmental loads, drainage, pore pressures and climate will also affect the system.

The present thesis presents the analytical solution of the soil-fabric system using the finite element method includes: nonlinear behavior of soil and fabric materials, the interface behavior of the soil-fabric system, shear transfer and potential slip at the interface, the membrane action of the fabric material, variation of stress distribution due to large displacements, "no tension" characteristics

of the gravel and yielding of the elasto-plastic materials. The mathematical model is formulated for an axisymmetric solid structure with the capability of representing interfaces and fabric materials. The present finite element formulation does not include time effects due to viscosity or consolidation. Strain softening, inertia forces, effect of pore pressures or local effects of the gravel punching into the soft soil are also not included. The normality condition used implies that too high rates of dilation for cohesionless soil under drained conditions [78] are obtained. The plasticity solution used is limited to small strain and small rotation of the elements.

The solution of this analytical study provides a more refined solution for the analysis to this complex problem, a close representation of the soil-fabric system's true behavior.

The Soil-Fabric System Problem

Gravel placed over soft clay and loaded at the surface penetrates into the soft soil and surface deformations are developed. Generally the fabric is placed over soft soil and compacted crushed stone or gravel is placed on top of the fabric. The fabric hence forms a boundary barrier between the gravel and the soft soil.

The fabric helps to prevent the intrusion of the gravel into the soft subsoil. Because of this action the fabric

material is stretched and acts as a membrane. An important question is: "To what extent the stress distribution of the system is changed?" The fabric changes the confining conditions of the material which can alter the stress distribution of the system. The effect of these changes on the interface shear stress distribution between soft subsoil and the fabric and between the fabric and the gravel has to be established. Also large displacements will influence the fabric membrane action due to geometry changes and need to be investigated. The confinement conditions of the gravel and the "no tension" characteristic of this material will affect the load distribution of the whole system. Finally the deformation pattern will provide information to evaluate the performance of the system under repeated loading conditions and the probable rutting of the roadway.

The model will predict the performance of the soil-fabric system including the stress distribution and the displacements due to single and approximate the multiple load application displacements.

Objectives and Applications

The main objective of the study is to analyze the soil-fabric system by using special mathematical formulations to represent the nonlinear mechanical properties, the large changes in geometry due to load application, the "no tension" properties of the gravel and the interface behavior. The

interface is modeled by a special finite element that permits determining the slip mode of the interface. In the course of this study it is shown that the finite element method is a powerful tool for the solution of geotechnical problems.

Incremental loading is used and a complete load-displacement history of the model is obtained after all the load has been applied. The results of the system include a complete stress-strain response together with the displacement behavior.

The system undergoes large displacements during loading. The mathematical model takes this condition into account and also the nonlinear mechanical characteristics of the materials. The formulation of the problem accounts for the use of practical material properties of the soil, fabric and interface that can be readily obtained from standard laboratory tests.

The mathematical formulation presented can also be applied in solving other important geotechnical problems such as: piles and piers, anchors in soil and rock, footings and retaining walls. All of these problems contain interfaces that can be modeled with the finite element formulation developed in this study.

CHAPTER II

REVIEW OF THE LITERATURE

General

The finite element method has gained wide acceptance among civil engineers. The method has been applied to a great variety of problems in geotechnical engineering [18,29, 32,39,49,50,59,75,111,116,137,140]. A computer search on finite elements, fabrics and nonlinear analysis provided a very extensive list of reports, theses and programs of related areas. The most relevant articles are given in the bibliography. The amount of research related to nonlinear analysis and modeling of the interface behavior of different materials has increased in the last ten years at a fast rate. Considerable work has also been done in the last five years on large displacement, finite elasticity and elasto-plasticity. Research involving layered systems, stress distribution and settlement is closely related with this study and will be reviewed briefly. The following subject areas are presented in this chapter with only the most relevant papers being cited

(a) Axisymmetric Elements

(b) Interface Elements

(c) Nonlinear Analysis

(d) Plasticity and Visco-elasto-plasticity

(e) Large Displacements, Finite Strain and Elasto-plasticity

(f) No Tension Analysis

(g) Fabric Materials

(h) Related Research

(a) Axisymmetric Elements

At the initial stages of development of the finite element method, reports by Wilson [131] and Argyris [1] used constant strain elements that were axisymmetric or three dimensional. The paper by Wilson [131] used triangular, constant strain, axisymmetric elements for the analysis of complex structures of the aerospace industry which are subjected to thermal and mechanical loads. Argyris [1] used tetrahedra elements for the analysis of 3-dimensional deformable bodies and extended the theory to problems of large displacements in the elastic and nonelastic range. Doherty, Wilson and Taylor [36] reported the use of higher order quadrilateral finite elements for the stress analysis of axisymmetric solids.

With the higher order elements, the bending characteristics are improved. The formulation presented is capable of performing thermal stress analysis of reentry space vehicle nose tips and plane structures. In a related paper by Wilson [132] the dynamic response of axisymmetric structures is analyzed for blast studies. Quadrilateral elements are used and the theory is extended to nonlinear materials. The derivation of the stiffness matrix is presented, and the bases

for the numerical integration are given.

With the introduction of higher order elements the accuracy of the resulting stress-strain distribution was improved since the elements had a linear or quadratic distribution of strain within the element. Fewer elements are needed for a certain structure representation to achieve the same accuracy. Improvements in numerical integration procedures were developed since it is not possible to compute in closed form the element stiffness matrix and the computer performs this task expediently. Presently many different kinds of higher order elements are used [147].

(b) Interface Elements

By definition the interface is the space or bonding agent between dissimilar materials, and many problems in civil engineering present interfaces. In the finite element representation the interface does not present a problem if the interface provides for full bond between the dissimilar materials. It is only necessary to assign the appropriate mechanical properties to the elements at both sides of the interface, and the problem is solved automatically. If the interface does not provide for full bond between adjacent dissimilar elements, a special kind of "bonding" is needed which is called an interface element.

Early studies of the behavior of interfaces were performed when the study of bond stress of steel bars in concrete was modeled using finite elements. Ngo and Scordelis

[95] used finite elements in the study of the behavior of reinforced concrete structures. The interface between the steel reinforcement and the concrete was represented by a set of two linear orthogonal springs without physical dimension. The effect of the assumed bond links was examined briefly, and the paper demonstrates the feasibility and potential of the finite element method for the analysis of reinforced concrete structures.

In rock mechanics the distribution of stresses in jointed rock can be modeled using finite element interface concepts. Goodman, Taylor and Brekke [50] introduced a model for the representation of the mechanics of jointed rock by means of a joint element that handles failure in tension or shear, rotation of blocks of rock and to a certain extent a collapse pattern. A modified plane strain computer program written by Wilson was used. The need for direct measurement of joint properties was recommended, especially of joint stiffness with large direct shear tests.

Zienkiewicz, Best, Dullage and Stagg [142] reported the analysis of nonlinear problems in jointed rock systems and soil mechanics. Stratified materials and joint elements were modeled using isoparametric finite elements. The joint element was a thin element described by two points with linear variation of strain in both directions. Examples of results for a tunnel and an arch dam were presented.

In the report by Heuze, Goodman and Bornstein [62],

joint elements having variable stiffness to account for fracture movements and "no tension" were analyzed for jointed rock, which is a medium that cannot resist tension upon load application. A finite element model accounted for joint perturbation with the use of joint elements of variable stiffness to account for movements along the fractures. The technique was applied for a bore hole jack deformability test, and the results were compared to measured values.

Ghaboussi, Wilson and Isenberg [49] developed a joint element for analyzing discontinuities such as joints, faults, and interfaces embedded within continuous systems. The relative motion along a joint surface defines slip when the shearing force exceeds the shear strength of the joint. Slip and debonding makes the joint nonlinear. The joint element defined the displacement degrees of freedom at the nodes of the element to be the relative displacements between opposing sides of the slip surface. The element stiffness matrix for the plane strain and axisymmetric cases were given.

Isenberg [70] presented the analysis and use of a computer code applicable to general three dimensional structures. The applications of this formulation include nonlinear properties, joint surfaces, anisotropy, time dependent material properties, gravity loading and the sequence of construction or excavation. The report compared the computations with the field measurements of a chamber excavated in argillaceous quarzite. Another problem considered which used interface

elements was the analysis of buried culverts where the interface is between the soil and the culvert.

Katona, Smith, Odello and Allgood [75] presented a computer program to perform a very complete analysis of buried culverts. The report includes a closed form elasticity solution and two levels of finite element method of analysis. Each solution characterizes the culvert-soil system by plane strain geometry and loading. The analytical model features incremental construction and nonlinear behavior for culvert and soil. The interface problem is treated in detail and defines several states for the interface condition.

The analytical treatment of interfaces needs to consider the mode behavior of the interface element with load. The mode behavior can be no slip, slip or separation. It is defined after each load increment and models the bonding characteristics of the system. A very extensive analysis of interface elements has been presented by Herrmann [58,59,60]. Herrmann presented an analysis of the interface problem and defined the importance of interfaces in structural engineering. The procedures developed by Herrmann use fictitious bond springs at the interface and the maximum bond stress is determined by Coulomb's Law. For shear stresses exceeding the maximum permitted by Coulomb's Law, the slip mode occurs in the element, the bond breaks and the stress distribution is changed. Relative movement occurs between the two mating surfaces and special analysis procedures are necessary to solve the problem.

The procedure is applied for only small displacements of the interface. The model presented accounts for both slippage and separation of the mating surfaces. Herrmann has applied his model to reinforced earth computations [61,111,119].

(c) Nonlinear Analysis

In soil mechanics practically all materials behave nonlinearly and accurate results of stress and displacement computations are obtained only if the nonlinearities are taken in account. To represent the stress-strain relation of soils Duncan and Chang [40] report a simple procedure for representing the nonlinear, stress-dependent, inelastic stress-strain behavior of soils. The relationship requires the cohesion and the angle of internal friction and four parameters derived from results of standard triaxial laboratory tests. From a theoretical standpoint it is desirable to include the effects of an intermediate principal stress, however from practical determinations it does not produce significant variations and the necessary tests are rarely performed. The stress-strain relation incorporates the nonlinear behavior in a simple way for the use of finite element analysis, but it may introduce errors in the value of the modulus of elasticity.

A finite element model that presents large displacements, even with the material in the elastic range, presents geometric nonlinearities. Stricklin, Haisler and von Riesemann [121] derived the geometric stiffness matrix for a pin-jointed

bar and for a triangular plane stress element using a direct energy formulation. A brief literature review on geometrically nonlinear problem solutions was given. The role of the initial stress stiffness matrix was discussed by Haisler, Stricklin and Stebbins [53], and a comparative study was presented of solution techniques for nonlinear algebraic or differential equations characterizing nonlinear structural behavior. The new solution procedures were compared for highly nonlinear problems with the Newton-Raphson method, incremental methods and iteration procedures.

Efforts have been made to improve the definition of the input parameters used by the mathematical models of soils in the paper by Domaschuk and Valliappan [37]. The stress system was separated into hydrostatic and deviatroic components for laboratory and field computations. They mentioned that the use of bulk and shear modulus instead of Young's modulus and Poisson's ratio is advantageous because both can be evaluated independently through laboratory tests and may be more readily related to the stress state in the field. The deformation parameters evaluated in this way were used in a finite element program to calculate the load settlement response of an oil storage tank with good success.

In a recent paper by Desai and Wu [31], the nonlinear behavior was incorporated in the numerical procedure by means of a general constitutive law that handles the most important parameters that control the behavior. The function used is

similar to the Ramberg-Osgood model and offers certain advantages over parabolas, hyperbolas and spline functions. It includes the hyperbola as a special case and incorporates the effects of confining pressure and stress paths in the model.

(d) Plasticity and Visco-Elasto-Plasticity

All soils behave as elasto-plastic-viscous materials. Depending on the type of material, each of these characteristics has differing levels of influence on the stress-strain-time relation. Several solutions have been proposed to modify the elastic finite element method for the solution of non-linear, plasticity and viscosity problems. Yamada, Yoshimura and Sakarai [135] presented a method for the solution of continuum elastic-plastic problems by means of a plastic stress-strain matrix, derived by inverting the Prandtl-Reuss plasticity equations, obeying the von Mises yield criterion. The approach uses small and varying increments of load sufficient to just cause yield in successive triangular elements.

Zienkiewicz has presented several papers involving plasticity solutions. In the paper by Zienkiewicz, Valliappan and King [141] the general formulation of the elasto-plastic matrix for any yield surface with an associated flow rule was presented. The "initial stress" computational method was proposed, and it was shown that the method yields a rapid convergence and permits large load increments without violating the yield criteria. Solutions for the von Mises, Coulomb and Drucker yield criteria were given. Assessment of the

equilibrium for lower bounds is provided by this methodology.

Nayak and Zienkiewicz [90] presented iterative processes for solving elasto-plastic problems together with associated and non-associated plasticity relations. Isoparametric elements were used that permit a smooth displacement distribution throughout the element. Numerical integration was recommended. Strain hardening as well as strain softening was studied and the advantages of the "initial stress" process emphasized.

Zienkiewicz and Cormeau [143] reported that the visco-plastic model of material behavior and the initial strain techniques for the solution of finite element models have been proved efficient. This model can reproduce creep phenomena and allows the treatment of non-associated plasticity and strain softening. The authors state that the elasto-visco-plastic algorithm presents a powerful, efficient and unifying process to approach a wide range of nonlinear problems. Two questions not resolved involve the most efficient way of dealing with large deformations and with dynamic effects.

Zienkiewicz, Humpheson and Lewis [144] presented elastic-ideally plastic formulations in which both associated and non-associated forms of behavior in soil mechanics are assumed. The formulation given allows layered configurations with variable properties to be handled in a general manner. In the paper by Yamada [136] the theoretical bases for the computer program COMPOSITE III are presented. A finite element

analysis scheme is presented that permits the material elastic-plastic creep as well as structural geometric nonlinearities. Creep is represented by a Voigt model. Specific features of the program include the visco-elastic behavior of unidirectional composites, incorporation of bond or joint elements and a routine for fracture analysis of matrix-reinforcement complex.

Runesson, Tagnfors and Wiberg [113] presented the computer implementation of a nonlinear finite element analysis that incorporates the problems associated with the two-phase media applicable to soil mechanics. Constitutive equations for the soil skeleton are assumed nonlinear while the pore water flow is assumed to obey Darcy's Law. Numerical examples show the versatility of the program.

Rich [110] presented the elastic-plastic stiffness matrix for axisymmetric finite elements. The triangular elements considered were characterized by linear displacement relationships and an average stress. The Prandtl-Reuss flow rule and the von Mises yield criterion were used. Comparison was given of stiffness terms obtained by numerical integration and those computed by closed form equations. Significant higher radial stiffness terms arising from numerical integration were reported for elements located near the line of axial symmetry, physically this means a higher resistance for displacement in the radial direction for points near the centerline of the axisymmetric model. Rich recommends to

verify that this stiffness variation does not affect the solution of the problem in question.

(e) Large Displacement, Finite Strain and Elasto-Plasticity

The finite element method is widely used for the solution of the small displacement, elastic structural and soil mechanics problems and for large displacement computations. Since the early versions of the finite element procedure, nonlinear solutions have been proposed and implemented. The following papers deal with this important phase of the solution of problems, that present material or geometrical nonlinearity and undergo large deformations.

Hibbit, Marcal and Rice [63] presented an incremental and piecewise linear finite element theory for large displacement, large strain for predicting the elasto-plastic behavior of metals. The resulting equations are similar to those for large displacement small strain problems, with the only additional term being an initial load stiffness matrix which depends on current loads and may be significant in some cases. The paper presents also a good literature review of previous work in this area.

Oden and Key [97] applied the finite element method to the problem of finite axisymmetric deformations of incompressible, elastic solids of revolution. Nonlinear stiffness relations were derived for a finite element procedure. These relations involve an additional unknown, the hydrostatic pressure, which needs the introduction of an

incompatibility condition for each element. Provisions are made to change the loading due to deformation. A good numerical example is presented of an infinitely long thick-walled cylinder subjected to internal pressure. This problem is of special interest because it is one of the few cases for large displacements for which the results can be compared with exact solutions [98].

Hofmeister, Greenbaum and Evensen [67] presented a method for large strain, elasto-plastic analysis of two dimensional structures. An incremental variational principle is used to develop the finite element equilibrium equations. The formulation includes an equilibrium check that reduces any cumulative error in nodal point equilibrium. Such errors are caused by linearizing the displacement equilibrium equations and can build up and lead to an incorrect answer. The equilibrium verification technique represents the major contribution of this paper.

Stricklin, Haisler and von Riesemann [122] presented a good literature review of the contributions in the analysis of structural problems exhibiting material nonlinearities and combined geometric-material nonlinearities. Attention was focused at evaluating the available computational and solution techniques.

Atluri [3] presented an extension of the hybrid stress finite element model for analysis of large deflection problems. This approach was originally developed for small strains.

The hybrid stress finite element model assumes an equilibrium stress field in the interior of the element and a displacement field at the boundary of the element, which inherently satisfies the interelement compatibility condition. An incremental approach is used together with the concept of initial stresses. Verification of the equilibrium of the initial stresses in the current reference geometry is included. The method leads to an incremental stiffness matrix and is easily adaptable to existing computer programs using the stiffness approach.

A finite element formulation for problems of large flow based on Hill [64] variational principle was reported by McMeeking and Rice [79]. The formulation is suited to isotropically hardening Prandtl-Reuss materials. Small strain finite element programs may be adapted using this procedure for problems involving arbitrary amounts of deformation and stress level. The paper explains the importance of a proper identification of the constitutive matrix.

Bathe, Ramm and Wilson [10] reviewed and derived the finite element incremental formulations for nonlinear static and dynamic analysis. The general formulations include large displacements, large strains and material nonlinearities. Elastic, hyperelastic (rubber-like) and hypoelastic elastic-plastic materials were considered. Isoparametric elements were used and the specific matrices needed in the computations were given. The solutions were presented of static and dynamic

problems involving large displacements and large strains.

Wifi [129] presented an incremental variational method to analyze axisymmetric elastic-plastic solids at large strains. The method was then applied to the problems of steel-forming and complete deep-drawing of a circular blank using a hemispherical punch. In this case the finite element method is applied to metal forming problems. A complete derivation of the finite strain computation was presented.

Yamada and Wifi [137] presented a general formulation of the finite element method including finite strains and elastic-plastic materials. An updated incremental finite element technique was applied to problems of shallow foundations of homogeneous as well as multilayer soils. The nonlinear material behavior and a modified Ramberg-Osgood formula was proposed for fitting the stress-strain curve. Isoparametric quadratic elements were used which are suitable for large strain situations.

Carter, Booker and Davis [15] presented the formulation and numerical solution for problems which involve finite deformations of an elasto-plastic material. The solution was applied to an elasto-plastic soil. The governing equations were given in rate form. Plastic failure is described by a general yield condition and plastic deformation by an arbitrary flow rule.

Chen and Davidson [22] presented an analytical study of static response of a homogeneous clay to loads. Emphasis

was placed in the incremental elastic-perfectly plastic material with the Drucker-Prager yield condition and its associated flow rule. The finite element method was applied and a step by step integration procedure used. Numerical solutions for four geomechanical problems were presented for plane strain conditions.

Murakawa and Atluri [83] presented the development and application of incremental finite element formulations for finite elasticity, using a promising complementary energy principle. The incremental analysis of finite deformations of nonlinear elastic solids in terms of Piola-Lagrange (First Piola-Kirchhoff) stresses was examined. An incremental hybrid stress finite element model is presented which permits the a priori relaxation of traction reciprocity condition at the interelement boundaries. The procedure is applied to the problem of stretching to twice its original length a sheet made of a nonlinear elastic compressible material.

Murakawa [85] has presented several finite element models based on a complementary energy principle for the analysis of finite deformation of nonlinear compressible and incompressible elastic solids. It was concluded that the general principle based on the Jaumann stress measure can lead to a rational and practical complementary energy principle involving the unsymmetric Piola-Lagrange stress and the rotation tensor as variables. The concept of hybrid finite element models was used for the derivation of incremental

hybrid type variational principles for total and updated Lagrangean formulations. Example problems of finite strain, plane stress deformations of compressible and incompressible, nonlinear elastic solids are solved, the results agree with literature solutions. In the report by Atluri [4] general variational theorems for the rate problem of classical elasto-plasticity, at finite strains were presented. The updated Lagrangean and the total Lagrangean rate forms in terms of alternate measures of stress and strain are critically studied from the point of view of their application. Attention is focused on the derivation of consistent complementary energy rate principles, which could form the basis of consistent and rational finite element methods. A literature review of formulations and applications of analysis of large strain elasto-plastic problems is presented.

(f) No Tension Analysis

Soil and rock materials cannot take tension forces or are limited in their tensile capabilities. A linear elastic solution will not give a correct distribution of stresses. It is therefore necessary to implement an analytical solution that represents the "no tension" characteristics such as the one presented by Zienkiewicz, Valliappan and King [140]. The authors show how solutions can be obtained by applying restraining forces in the tension direction and by evaluating the forces with an element by element integration. The structure is reanalyzed elastically with equal nodal forces

which are opposite in direction with their effect being added to the structure so as to eliminate tension forces.

The procedure is repeated until the tension forces are virtually negligible. The final solution complies with statics and presents a lower bound on the ultimate load of the structure. Examples of a dam, a tunnel and an underground power station are included using the no tension analysis.

Recently Raad and Figueroa [108] presented a method of analysis for granular materials based on the Mohr-Coulomb theory incorporated to the finite element method. The principal stresses of the base granular material were modifed at the end of each iteration, so they do not exceed the strength of the material as defined by the Mohr-Coulomb envelope. It was reported that a reasonable degree of convergence is attained after four iterations. The predicted vertical stresses are larger than those predicted by an elastic analysis or iterative techniques. For the bottom half of the granular base an elastic analysis predicts horizontal tensile stresses that do not correlate with measured values. With this method the horizontal stresses that are influenced by the variation of modulus with depth result in small compressive stresses. The method does not predict the magnitude of permanent deformations or accounts for variations in the strength properties of the granular material under repeated loads.

(g) Fabric Materials

The International Conference on the use of Fabrics in Geotechnics held in Paris in 1977 was a step forward to the increased use of fabric membranes as reinforcement or filters in soil construction programs. The trend of the conference was to present case histories on the use of fabrics in several projects. Instrumented field cases are available and tests on the mechanical properties of the fabric are reported. The analytical approaches of particular interest for this study [13,73] are reviewed here. A nonlinear finite element program [9] was used to predict the deformation pattern and stresses in the system. Bell, Greenway and Vischer [13] reported a field test of a road across muskeg that was "reinforced" with a fabric membrane. The analyses of the test section are given using the nonlinear program NONSAP. To simulate the "no tension" material of the embankment a Poisson's ratio equal to zero was used, and a very small elastic modulus for the horizontal direction assumed. No difference was found in computed deflections for systems with and without nonwoven fabrics, field measurements show a significant difference.

The conclusions of the report that appear justified for very low reinforced embankment roads, over very soft foundations are:

1. The main function of the fabric is to prevent local bearing failures.
2. Tension in the fabric depends on the modulus of the fabric.

3. Information about the mechanical properties of the fabrics must be available before rational designs are possible.

In the paper by Jessberger [73] an investigation is made concerning the inclusion of a non-woven synthetic fabric placed between a foundation soft soil and overlaying gravel. The results of plate bearing tests on a large scale investigation and a numerical analysis, contributes to the discussion of the improvement of the load bearing properties of a soil-gravel system with the inclusion of a fabric material. A numerical analysis with the finite element method was performed. It was assumed that the gravel cannot take tensile stresses, so a very small modulus of elasticity for the horizontal direction was assumed. A stress transfer analysis was executed until tensile stresses were not higher than a small limit value.

The results of the report show that in general the inclusion of the fabric increases the bearing capacity, but computed values show increases of 2% to 5% in contrast with field measurements which resulted in a 30% increase. Probably the finite element procedure did not model accurately the interface behavior. No comparison of deformations of both systems were reported and larger deformations will obviously improve the fabric behavior.

In the thesis by Kinney [76] a method was presented to quantify the structural changes a fabric makes in a high

deformation soil-fabric-aggregate system. The final result of the research is the development of a general design scheme for the use of the geotechnical fabric as structural reinforcement of the soil. A very complete review was presented of previous work that includes field experience, model tests, full-scale field tests, theoretical developments and design procedures. Description in detail of the experimental work performed and the fabric tension model are given. Effects are discussed of rutting, vehicle wander, regrading the rutted surface, fabric properties, subgrade strength, maximum frictional resistance, width and overlap, placement technique, position of the fabric in the profile and pretensioning, prestretching and anchorage.

By means of the laboratory model tests and the mathematical model that was used as the basis of the design scheme the following conclusions were given:

1. Fabrics improve stability of high deformation soil-fabric-aggregate system. The amount depends on geometry and fabric properties.
2. The fabric will increase the stability of the system as the amount of rutting increases.
3. The fabric changes the strain distribution of the profile.
4. For a soil-fabric-aggregate system with a thick deposit of uniform subgrade the displacements will be characterized by a fairly rigid block of

aggregate below the load moving down as a unit causing massive shear distortions in the subgrade.

5. The fabric causes a decrease in the normal stress on the subgrade under the load and an increase in the normal stress on the heaved portion.
6. The fabric tension model developed appears to represent the effects of the fabric laboratory tests reasonably well.
7. Vehicle wander must be controlled on a soil-fabric-aggregate system.
8. Fabric installation must be done carefully. Avoid wrinkles, sharp objects and unnecessarily slippery materials.
9. Fabric properties are significant to the response of the system.

Recommendations for further research included parametric studies to define situations, information on the frictional resistance between aggregate and fabric, evaluation of mechanical properties of the fabrics, field testing with adequate instrumentation.

(h) Related Research

Reinforced earth structures are currently used more frequently on soil and highway engineering construction projects. The behavior of the interface between soil and metal strips studied in the articles presented in Section (b) presents the basis for the solution of reinforced earth

problems. Descriptions of the behavior of these types of structures follow. Chang, Forsyth, and Beaton [17] have described the performance of a reinforced earth fill. The data resulting from an extensive instrumentation of an earth enbankment is compared with the predicted behavior. Field measurements include: strain of reinforcing strips, soil pressure, lateral movement, settlement, strip slippage and skin plate deformation.

The pull resistance and interaction of earthwork reinforcement and the soil was reported by Chang, Hannon and Forsyth [19]. Results indicate that the soil is not significantly strained until a proportional limit is reached on a load-deformation curve. The tests indicate that for the same surface area the bar mesh reinforcement has six times the pull resistance of a flat strip reinforcement and exhibited greater pull resistance in a dense cohesive soil than a less dense cohesionless soil. The increase of size mesh opening reduces the pull resistance of the bar mesh. The minimum length of a steel strip reinforcement required for a low-height reinforced earth wall was found to be at least 10 feet.

Romstad, Herrmann and Shen [110] and Shen, Romstad and Herrmann [119] analyzed and considered the theoretical behavior of reinforced earth structures. The reinforced earth is treated as a composite material with associated composite properties. The properties of the composite model are used in a finite element formulation. The composite model is

compared with a finite element model with separate elements for the soil and for the strips. The conclusions are that the composite representation is computer time economic and provides an accurate model of the system. The analysis indicates that the reinforced earth is a relatively rigid self-supporting unit. The geometry of the wall, the boundary conditions and the foundation affect the magnitude and distribution of the strip forces.

Determination of the skin plate thickness, corrosion and length (width of the wall) are not considered in the report. Needed are detailed studies of the pull out resistance to determine the strip length, the means of fixing or restraining the ends of the strip and the evaluation of the failure conditions during earthquakes.

A general finite element program for two dimensional models of soils and reinforced earth structures called REA was presented by Herrmann [58]. The program also includes incremental construction and excavation analysis capabilities and is a very general and complete program.

The analysis of layered systems has important practical applications in soil mechanics. The stress analysis of a layered system provides the means of predicting the probable settlement of the system for instant and long term loadings. Among many references on the subject Barksdale [6] presented an axisymmetric finite element model. This investigation developed a general nonlinear theory for the design of

flexible pavements. The proposed nonlinear theory was extended to include the calculation of both elastic and permanent deformations in multi-layered pavement systems, having material properties that vary with environmental changes, stress rate and number of load repetitions. The theory is verified using an idealized model pavement system with good agreement being observed between the measured and the calculated deflection profile of the slab.

Desai and Reese [29] analyzed and reported the results of foundations on single and double cohesive layers. The finite element method was used and an excellent correlation was obtained between laboratory results and the finite element model. A report on layered pavement systems was presented by Barksdale and Hicks [7], here the response of flexible pavement structural sections is predicted with reasonable good accuracy from dynamic laboratory determined material properties. A linear elastic finite element computer program or a nonlinear elastic program having iterative capability are used. The modulus of elasticity is stress dependent so the second solution was recommended. Predicting the actual response can be quite involved, due to nonlinear and inelastic behavior, anisotropy, changes with time of the material properties, uncertainties during construction and changes in environmental conditions. The report concludes with the recommendation that "The predicted behavior should always be compared with field observations, if it is

not satisfactory the theory should be revised."

Summary

The literature review provides valuable information for the development of the special finite element model of this study. The literature was closely reviewed and where appropriate applied. Only a few papers contain procedures and data for the solution of the soil-fabric problem. Procedures taken from finite element models applied to the space technology provided methods of analysis for the non-linear and large displacements formulations.

The information from such different sources needs to be applied with caution because a single paper may not contain the complete information or it was applied for a different use or computer environment. The accuracy of the solution of the equations of systems with large variations in stiffness and small relative displacements between nodes linked with rigid members is improved by using as degrees of freedom the relative displacements between the nodes [11,19,59]. In some cases this is not necessary if the appropriate computer environment is available [102].

The present study includes several load increments, together with all capabilities mentioned before, so it is of prime importance to apply efficient, accurate and as simple as possible mathematical procedures. Very sophisticated or computer inefficient methods should be identified

and not used.

The diversity of fields working on similar finite element models has produced a different nomenclature. An attempt to clarify this problem has been made [128], but still articles coming from such different fields as geotechnical, hydraulics, structural, heat transfer, mechanics, dynamics, and others make an overall nomenclature coordination of the mathematical model difficult to achieve.

The problem of fabric materials embedded in the soil does not have a special finite element that represents all the desired characteristics of the soil-fabric interface system. Multilayer analysis is the closest related research and provides guidelines on the type of model, range of deformations, and laboratory tests on similar models, that are valuable data for the comparison of the behavior of the system.

CHAPTER III

OVERVIEW OF THE FINITE ELEMENT APPROACH

Finite Element Model

The geotechnical engineer does not expect to obtain "mathematically exact" results for problems involving stratified clay, silt, sand or rocks. The nonlinear behavior of the soil, the environmental conditions of the site, the nondeterministic application of loads, the interaction between soil, foundation, and reinforcement and the changes in pore water pressure are some of the many variables encountered. The finite element method has proved for many applications to be a reliable way to solve with sufficient accuracy difficult engineering problems; applications are found in the theory of elasticity, plasticity, structures, water flow, heat transfer, dynamics, and many other areas [12,117].

The soil-fabric interaction problem is of a high order of difficulty. It involves nonlinear and plastic behavior of the materials, no tension characteristics of cohesionless soils, interfaces and reinforcement in the soil including large displacements. In Figure 3-1 the principal factors affecting the problem are shown. The finite element model developed in this study investigates the behavior of the soil-fabric interaction subjected to static monotonically increasing vertical loads. Inertia loads are neglected. With respect

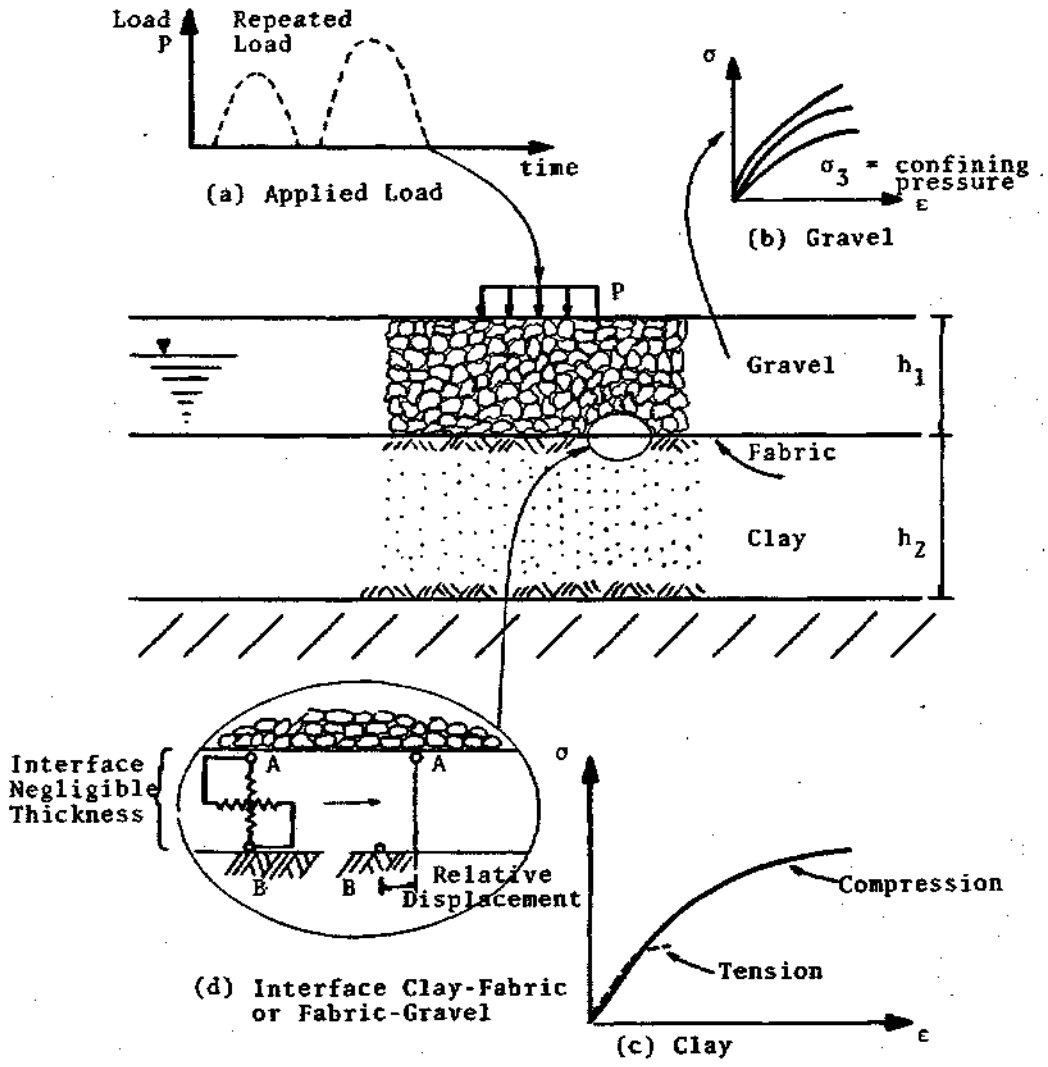

Figure 3-1. Representation of the Soil-Fabric System

to the soil-fabric interaction, special attention is given to the probable slip of the fabric with respect to the adjacent materials. Also, the no tension characteristics of the cohesionless crushed stone and gravels are modeled.

Types of Finite Elements Used

The soil-fabric system is represented in the finite element model developed by three types of elements: isoparametric eight-node elements, interface and fabric elements. For the clay and gravel the eight-node isoparametric element is used (Figure 3-2a). This element has quadratic interpolation functions that allow for a quadratic variation of displacements within the element and smoother variation of stresses and strains between adjacent elements. It can represent high stress gradient areas with a fewer number of elements than the linear quadrilateral or linear strain triangle.

The interface is modeled by six-node spring elements with three normal and three shear springs that allow for the computation of shear and normal stresses at the interface. The thickness of this interface element does not enter in the computations and the boundary nodes are coupled with the three side nodes of the adjacent eight node isoparametric element. This element is shown in Figure 3-2b. A complete derivation for this element is presented in Chapter IV.

To model the fabric, the reinforcing part of the system, a special fabric element was developed. This element

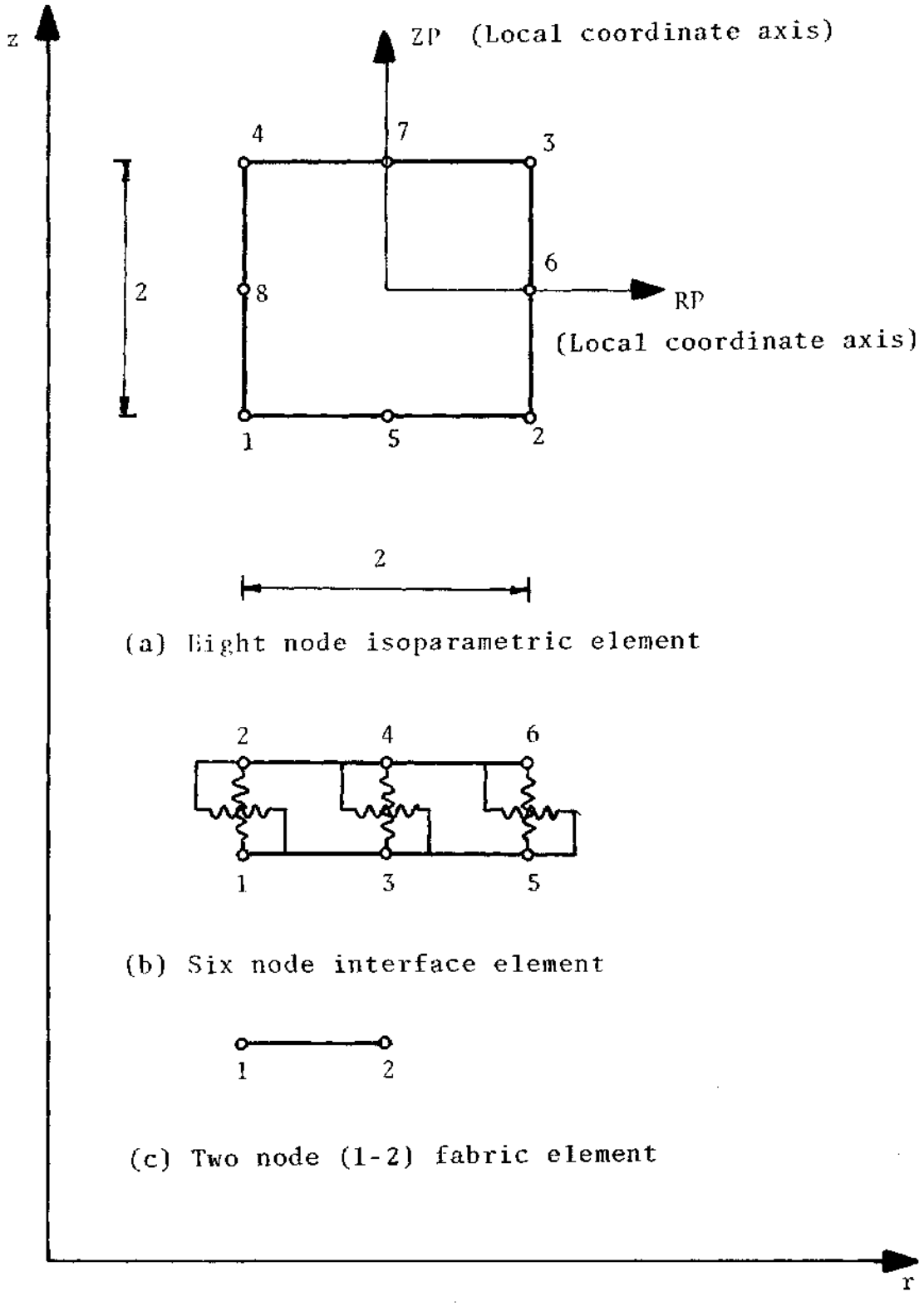

Figure 3-2. Finite Elements Used in the Model: Global Coordinate Axis

is a two dimensional element that approximates the membrane behavior of the fabric embedded in the soil. The element takes only tension forces. No bending or compression is taken by the fabric element.

The fabric element is placed between two layers of interface elements and acts as the reinforcing part of the system. It is shown in Figure 3-2c, and derivations are given in Chapter IV for the fabric element.

Isoparametric Eight-Node Quadrilateral Element

For representation of the clay and gravel layers, an eight-node isoparametric, axisymmetric element is used. It is shown in Figure 3-2a. This element with its quadratic shape functions has the capability to model curved boundaries and a quadratic variation of displacements within the element. It can follow the deformed geometry of the body and represent it accurately with a fewer number of elements than linear quadrilateral or triangular elements. The eight node isoparametric element is a powerful element, which has been proved accurate, useful and economic for many applications. It is reported in the literature on subjects dealing with nonlinearity [113], plasticity [15,145], large strains [137], and economy of the computer application of the element [41].

The general formulation for this element is extensive and available in the literature [11,47,147]. Just the most important aspects of the derivation are presented herein,

following the derivations given in [11].

Formulation of the Strain-Displacement Transformation Matrices $\underline{B}$ for Axisymmetric Solids

The use of isoparametric elements facilitates the formulation of the strain-displacement matrices for the elements of the system. The isoparametric finite element formulation by means of the shape or interpolation functions H_i, provides a direct relation between the values of the coordinates or displacements within the element and the nodal values of the coordinates and displacements [11].

The coordinates at any point within the element are given by:

$$r = \sum_{i=1}^{n} H_i r_i \qquad (1)$$

$$z = \sum_{i=1}^{n} H_i z_i \qquad (2)$$

where

r and z = global coordinates of the axisymmetric system

r_i and z_i = the coordinates of the nodes of the element

H_i = interpolation functions of RP and ZP

n = number of nodes of the element

With the shape functions (H_i) the displacements at any point of the element (u,v) can be computed if the displacements of the nodes (u_i,v_i) are known

$$u = \sum_{i=1}^{n} H_i u_i \tag{4}$$

$$v = \sum_{i=1}^{n} H_i v_i \tag{5}$$

For the eight-node isoparametric element the interpolation functions are given by the following expressions [11]:

$$\begin{aligned}
H_1 &= 0.25\ (1\text{-}RP)\ \ (1\text{-}ZP) - 0.5\ H_5 - 0.5\ H_8 \\
H_2 &= 0.25\ (1\text{+}RP)\ \ (1\text{-}ZP) - 0.5\ H_5 - 0.5\ H_6 \\
H_3 &= 0.25\ (1\text{+}RP)\ \ (1\text{+}ZP) - 0.5\ H_6 - 0.5\ H_7 \\
H_4 &= 0.25\ (1\text{-}RP)\ \ (1\text{+}ZP) - 0.5\ H_7 - 0.5\ H_8 \\
H_5 &= 0.50\ (1\text{-}RP^2)\ (1\text{-}ZP) \\
H_6 &= 0.50\ (1\text{-}ZP^2)\ (1\text{+}RP) \\
H_7 &= 0.50\ (1\text{-}RP^2)\ (1\text{+}ZP) \\
H_8 &= 0.50\ (1\text{-}ZP^2)\ (1\text{-}RP)
\end{aligned} \tag{6}$$

where ZP and RP are the coordinates of the point under consideration for the local coordinate axes of the element and vary from -1 to 1. Figure 3-2a shows an eight-node isoparametric element with the node numbering scheme and the local and global coordinate axes.

The strain displacement transformation matrix $\underset{\sim}{B}$ relates the strain at any point within the element, the nodal displacements $\underset{\sim}{u}$; as follows:

$$\underset{\sim}{\varepsilon} = \underset{\sim}{B} \cdot \underset{\sim}{u} \tag{7}$$

where $\underset{\sim}{\varepsilon}$ = strain vector.

$$\underset{\sim}{\varepsilon} = \left[\frac{\partial u}{\partial r} \quad \frac{\partial u}{\partial z} \quad \frac{u}{r} \quad \frac{\partial u}{\partial z} + \frac{\partial v}{\partial r}\right]^T \tag{8}$$

To derive the strain-displacement matrix $\underset{\sim}{B}$ the Jacobian operator $[J]^{-1}$ is required. It relates the natural or global coordinates (r,z) derivatives to the local coordinates (RP,ZP) and is computed by inverting the Jacobian matrix [J]:

$$[J] = \begin{bmatrix} \frac{\partial r}{\partial RP} & \frac{\partial z}{\partial RP} \\ \\ \frac{\partial r}{\partial ZP} & \frac{\partial z}{\partial ZP} \end{bmatrix} \tag{9}$$

then:

$$\frac{\partial}{\partial r} = [J]^{-1} \frac{\partial}{\partial RP} \tag{10}$$

$$\frac{\partial}{\partial z} = [J]^{-1} \frac{\partial}{\partial ZP} \tag{11}$$

where $[J]^{-1}$ is the inverse of the Jacobian matrix. Also the determinant of the Jacobian operator (det|J|) is utilized in the formulation of the element stiffness matrices, to transform

from the local coordinates to the global coordinates.

With equations (9), (10) and (11) the partial derivatives $\frac{\partial u}{\partial r}$, $\frac{\partial u}{\partial z}$, $\frac{\partial v}{\partial r}$ and $\frac{\partial v}{\partial z}$ are evaluated. Considering a specific point within an element having local coordinates RP and ZP we can write for the eight node isoparametric element:

$$\frac{\partial u}{\partial r} = \sum_{i=1}^{8} \frac{\partial H_i}{\partial r} u_i \tag{12}$$

$$\frac{\partial u}{\partial z} = \sum_{i=1}^{8} \frac{\partial H_i}{\partial z} u_i \tag{13}$$

$$\frac{\partial v}{\partial r} = \sum_{i=1}^{8} \frac{\partial H_i}{\partial r} v_i \tag{14}$$

$$\frac{\partial v}{\partial z} = \sum_{i=1}^{8} \frac{\partial H_i}{\partial z} v_i \tag{15}$$

Now the stress-displacement matrix $\underset{\sim}{B}$ can be formed. First by using equations (10) and (11) to compute the partial derivatives of the shape functions H_i, with respect to the global coordinates r,z. Second with the equations (12) to (15) and the definition of the $\underset{\sim}{B}$ matrix equation (7), we can form the matrix $\underset{\sim}{B}$ for a specific point in the element. The $\underset{\sim}{B}$ matrix is given by:

$$\underset{\sim}{B} = \begin{bmatrix} \frac{\partial H_1}{\partial r} & 0 & \frac{\partial H_2}{\partial r} & 0 & \cdots & \frac{\partial H_8}{\partial r} & 0 \\ 0 & \frac{\partial H_1}{\partial z} & 0 & \frac{\partial H_2}{\partial z} & \cdots & 0 & \frac{\partial H_8}{\partial z} \\ \frac{H_1}{r} & 0 & \frac{H_2}{r} & 0 & \cdots & \frac{H_8}{r} & 0 \\ \frac{\partial H_1}{\partial z} & \frac{\partial H_1}{\partial r} & \frac{\partial H_2}{\partial z} & \frac{\partial H_2}{\partial r} & \cdots & \frac{\partial H_8}{\partial z} & \frac{\partial H_8}{\partial r} \end{bmatrix} \quad (4 \times 16) \tag{16}$$

Using the strain-displacement matrix relation $\underset{\sim}{B}$, the stiffness and internal forces of the system can then be evaluated. The element stiffness matrix $\underset{\sim}{S}$ is given by

$$\underset{\sim}{S} = \int_V \underset{\sim}{B}^T \underset{\sim}{D} \underset{\sim}{B} \det|J| dv \tag{17}$$

where

$\underset{\sim}{B}$ = strain-displacement matrix

$\underset{\sim}{D}$ = elasticity matrix

$\det|J|$ is the determinant of the Jacobian matrix

v = volume of the element

The stiffness matrix $\underset{\sim}{S}$ can be evaluated by numerical integration using Gaussian quadrature. The axisymmetric analysis for an isotropic material results in the following form for $\underset{\sim}{D}$:

$$\underset{\sim}{D} = \frac{E(1-\nu)}{(1+\nu)(1-2\nu)} \begin{bmatrix} 1 & \frac{\nu}{1-\nu} & \frac{\nu}{1-\nu} & 0 \\ & 1 & \frac{\nu}{1-\nu} & 0 \\ & & 1 & 0 \\ \text{symmetric} & & & \frac{1-2\nu}{2(1-\nu)} \end{bmatrix} \tag{18}$$

where

E = modulus of elasticity

ν = Poisson's ratio

The general case for an anisotropic stratified material is presented in Chapter VIII.

The eight node isoparametric element presents several advantages over simpler elements. It includes the possibility of representing curved boundaries, a quadratic displacement variation between the nodes, and the use of fewer elements to model a certain problem and obtain good accuracy on stress and strain computations. The numerical work and the operation matrices are more elaborate than those needed for linear quadrilaterals or triangles, but the algorithms do not present extra difficulties for the programmer. The element has been compared with simpler and more complex elements [41] and is very convenient in overall efficiency and accuracy for the problems of this study where large displacements and deformed geometry are included.

CHAPTER IV

SOIL-FABRIC MODEL

Interface Element

A special interface element was developed to handle soil-fabric systems. The formulation of this element follows previous work on interface elements performed by Wilson [133], Goodman [50,51], Ghaboussi [49] and Herrmann [57,59,60].

The interface element selected complies with the compatibility requirements of the adjacent eight-node isoparametric element previously described. The interface or joint element is formed by six springs and six nodes (Figure 4-1a). The normal and shear spring coefficients computed as a foundation modulus or subgrade reaction (k), the ratio of stress divided by the displacement given in units $[F/L^3]$, are used for the computation of the equivalent axisymmetric springs of the interface element.

For the computation of the shear stress at the interface a very high subgrade reaction modulus (k) is assigned, so that the computed shear relative displacements are a very small number. Using the high modulus, the applied shear at the interface is computed and compared with the maximum shear resistance of the interface. In the problems analyzed in a CDC CYBER 74 values for the subgrade modulus of the order

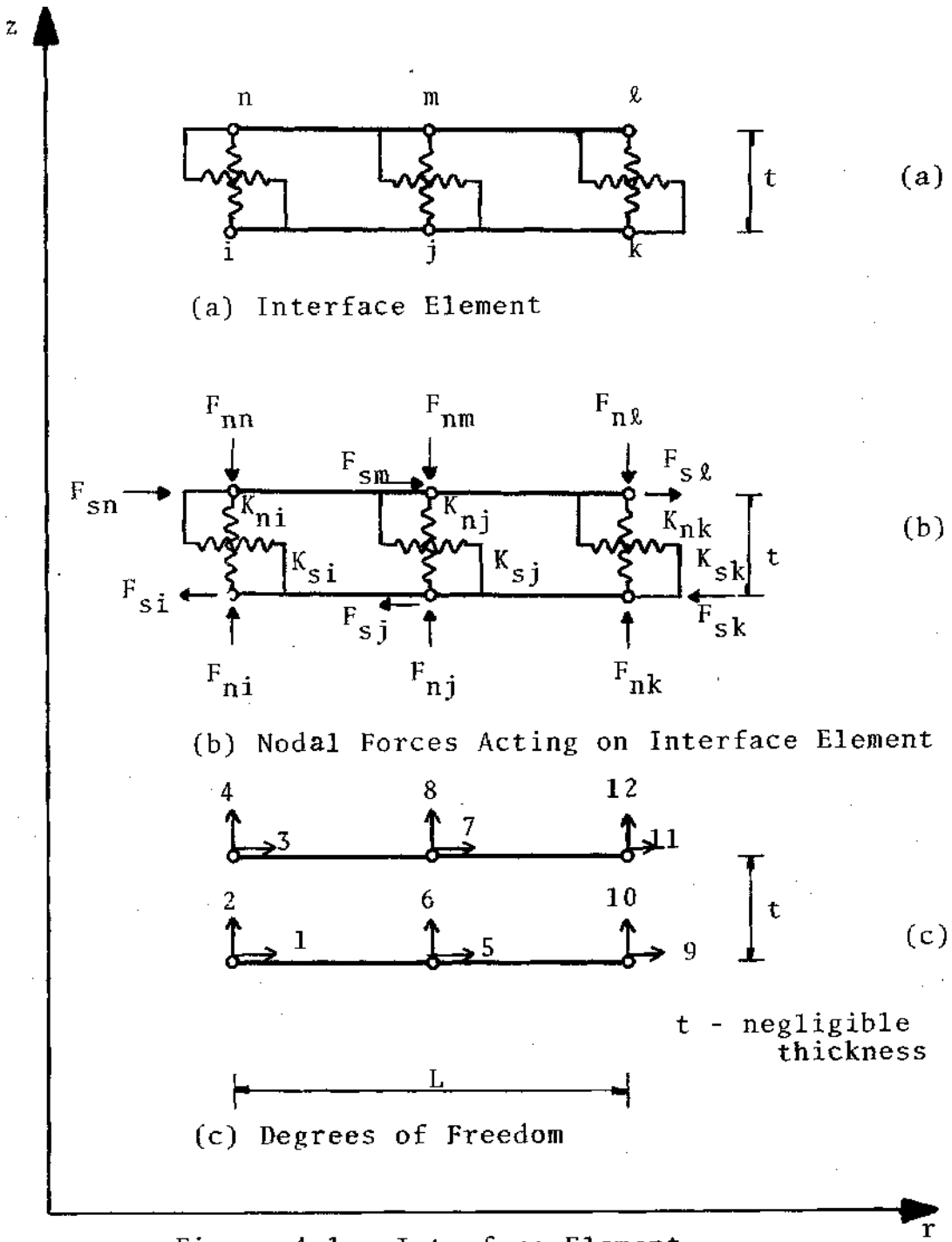

Figure 4-1. Interface Element

10^6 to 10^8 pci appear not to influence the results. When the spring shear is larger than the maximum allowable shear, a slip condition is achieved and only the maximum shear is applied at the interface.

Derivation of the External Load Vector

The external uniform loads are represented by concentrated equivalent forces in the finite element formulation. Equating the work done by the uniform load and the concentrated loads we can derive the axisymmetric load factors that are used to compute equivalent loads given a uniform stress distribution on a boundary of the eight node isoparametric element. The displacement distribution is quadratic between the nodes of the eight node axisymmetric elements, as shown in Figure 4-2. Assuming the nodes of the element boundary i, j and k, then we can obtain the energy equivalent concentrated loads by equating the work of both systems by:

$$F_n \times 1 = \int_{r_i}^{r_k} 2\pi r q \, H_n \cdot dr \qquad (1)$$

where

F_n = equivalent concentrated forces at the nodes i, j or k

q = uniform load acting perpendicular to the member

H_n = shape or interpolation function for the eight node isoparametric element function of RP

r = horizontal coordinate

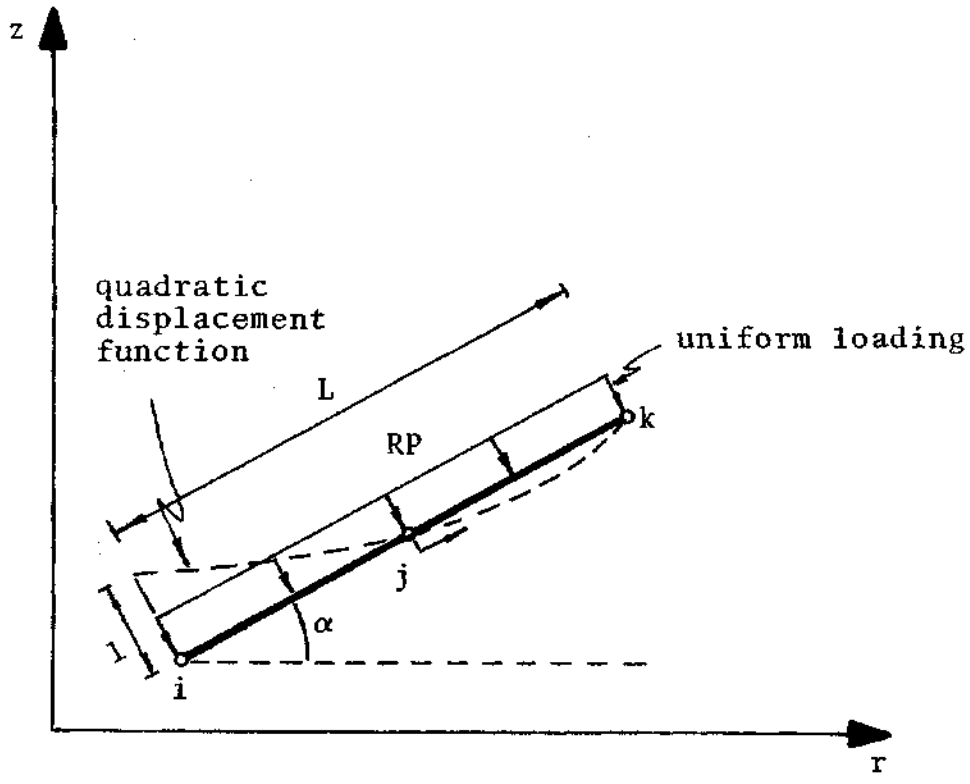

Figure 4-2. Uniform Load Applied at the Boundary of an Eight Node Isoparametric Element

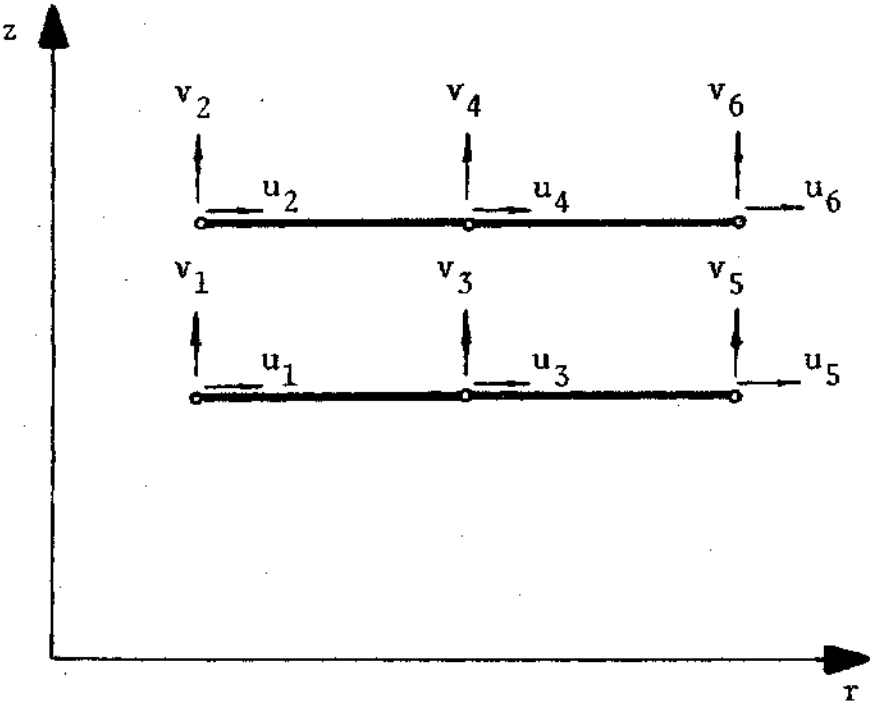

Figure 4-3. Total Nodal Displacements Axes of the Interface Element

Using local coordinates of the member (RP), we can write equation (1)

$$F_n = \int_{-1}^{1} 2\pi r q \, H_n \, dr \qquad (2)$$

where

$$n = i, j, k$$

$$r = r_{avg} + RP \times \frac{L}{2} \cos\alpha \qquad (3)$$

$$dr = \det |J| \, dRP = \frac{L}{2} \, dRP$$

α = initial angle between horizontal r axis and the ijk side at the start of load increment

Substituting r and dr in equation (2) for node i, the concentrated equivalent force taking $H_i = H_4$ for ZP = 1 is:

$$F_i = \int_{-1}^{1} 2\pi (r_{avg} + RP \times \frac{L}{2} \cos\alpha) q \cdot 0.5(RP^2 - RP) \frac{L}{2} \, dRP \qquad (4)$$

Performing the appropriate integrations then

$$F_i = \pi q \frac{L}{3} (r_{avg} - \frac{L}{2} \cos\alpha) \qquad (5)$$

where

$$r_{avg} = (r_i + r_j + r_k)/3 \tag{6}$$

L = length of side i-k

The same procedure is followed for nodes j and k which results in concentrated forces F_j and F_k given by:

$$F_j = \pi q L \frac{4}{3} r_{avg} = \frac{4}{3} \pi q L r_{avg} \tag{7}$$

and

$$F_k = \pi q \frac{L}{3} (r_{avg} + \frac{L}{2} \cos\alpha) \tag{8}$$

The axisymmetric load factors AV_i multipled by the uniform load q give the concentrated nodal forces.

$$F_i = AV_1 \times q$$
$$F_j = AV_2 \times q$$
$$F_k = AV_3 \times q$$

Then solving for the axisymmetric load factors with equations (5), (7) and (8):

$$AV_1 = \pi \frac{L}{3} \left(r_{avg} - \frac{L}{2} \cos\alpha\right)$$

$$AV_2 = \frac{4}{3} \pi L \, r_{avg} \qquad (9)$$

$$AV_3 = \pi \frac{L}{3} \left(r_{avg} + \frac{L}{2} \cos\alpha\right)$$

The axisymmetric load factors AV_i are employed in the derivation of the stiffness matrix of the interface element.

Derivation of the Interface Element

The interface element enables representing the shear and normal stresses at the interface in a simple way that can be coupled with the adjacent eight-node isoparametric elements. The interface is assumed to have a distributed foundation modulus or subgrade reaction k along its boundary. The units of k are (F/L^3) and is uniform within one element. An interface element is formed by six nodes and springs as shown in Figure 4.1a. In the model the concentrated springs replace the uniform distributed foundation modulus, k. The strain energy of a distributed uniform foundation modulus k is equated to the strain energy of a concentrated spring stiffness K at nodes i, j and k of Figure 4.1a. The strain energy equation applied to compute the concentrated force at mode i is:

$$\frac{1}{2} \int_{r_i}^{r_j} 2\pi r k \, \Delta u^2 \, dr = \frac{1}{2} K \, \Delta u_i^2 \qquad (10)$$

differentiating and equating to zero to obtain the stiffness in both systems

$$\int_{r_i}^{r_j} 2\pi r k \, \Delta u \, dr = K \cdot \Delta u_i = 0 \tag{11}$$

now $\Delta u = H_i \, \Delta u_i$ into (11)

$$k \int_{r_i}^{r_j} 2\pi r \, H_i \, \Delta u_i \, dr = K \cdot \Delta u_i \tag{12}$$

Thus the equivalent spring stiffness K is given by

$$K = \int_{r_i}^{r_j} 2\pi r \, H_i \, dr \cdot k \tag{13}$$

This integral is similar to equation (2) with k replacing q. This integral resulted in the axisymmetric load factors AV given in equation (9). The same operations are performed for nodes j and k, resulting in the concentrated spring stiffness that can be computed by

$$K_{sn} = AV_n \, k_s \tag{14}$$

$$K_{nn} = AV_n \, k_n \tag{15}$$

where n represents nodes i, j and k, as shown in Figure 4-1a. The total node displacements of the interface element for the 12 degrees of freedom of the element shown in Figure 4-1c are defined as:

$$\begin{Bmatrix} u \\ v \end{Bmatrix} = [u_i \; v_i \; u_j \; v_j \; u_k \; v_k \; u_\ell \; v_\ell \; u_m \; v_m \; u_n \; v_n]^T \tag{16}$$

The relative displacements are then given by:

$$\begin{aligned} \Delta u_i &= u_n - u_i & \Delta v_i &= v_n - v_i \\ \Delta u_j &= u_m - u_j & \Delta v_j &= v_m - v_j \\ \Delta u_k &= u_\ell - u_k & \Delta v_k &= v_\ell - v_k \end{aligned} \tag{17}$$

The interface element stiffness matrix $\underset{\sim}{S}_{ier}$ can now be assembled in terms of the relative displacements between the linked nodes, and is given by

$$\underset{\sim}{S}_{ier} = \begin{bmatrix} AV_i K_{si} & & & & & & & & & & & \\ & AV_i K_{ni} & & & & & & & & & & \\ & & AV_j K_{sj} & & & & 0 & & & & & \\ & & & AV_j K_{nj} & & & & & & & & \\ & & 0 & & & & & & & & & \\ & & & & & AV_k K_{sk} & & & & & & \\ & & & & & & & & & & & AV_k K_{nk} \end{bmatrix} \tag{18}$$

The relative displacements can be expressed in matrix form by

$$\Delta \underset{\sim}{u} = \underset{\sim}{B} \cdot \underset{\sim}{u} \tag{19}$$

where

$$\begin{Bmatrix} \Delta u_i \\ \Delta v_i \\ \Delta u_j \\ \Delta v_j \\ \Delta u_k \\ \Delta v_k \end{Bmatrix} = \begin{Bmatrix} u_n - u_i \\ v_n - v_i \\ u_m - u_j \\ v_m - v_j \\ u_\ell - u_k \\ v_\ell - v_k \end{Bmatrix} = \begin{bmatrix} -1 & 0 & 0 & 0 & 0 & 0 & 0 & 0 & 0 & 0 & 1 & 0 \\ 0 & -1 & 0 & 0 & 0 & 0 & 0 & 0 & 0 & 0 & 0 & 1 \\ 0 & 0 & -1 & 0 & 0 & 0 & 0 & 0 & 1 & 0 & 0 & 0 \\ 0 & 0 & 0 & -1 & 0 & 0 & 0 & 0 & 0 & 1 & 0 & 0 \\ 0 & 0 & 0 & 0 & -1 & 0 & 1 & 0 & 0 & 0 & 0 & 0 \\ 0 & 0 & 0 & 0 & 0 & -1 & 0 & 1 & 0 & 0 & 0 & 0 \end{bmatrix} \cdot \begin{Bmatrix} u_i \\ v_i \\ u_j \\ v_j \\ u_k \\ v_k \\ u_\ell \\ v_\ell \\ u_m \\ v_m \\ u_n \\ v_n \end{Bmatrix} \tag{20}$$

Now the interface element stiffness matrix $\underset{\sim}{S}_{ie}$ is given in terms of the total displacements by

$$\underset{\sim}{S}_{ie} = \underset{\sim}{B}^{T} \underset{\sim}{S}_{ier} \underset{\sim}{B} \tag{21}$$

The total displacements axes for the interface element are shown in Figure 4.3.

The interface element stiffness $\underset{\sim}{S}_{ie}$ can now be used for the formulation of the system stiffness. Since the whole derivation gives the stiffness matrix in closed form, numerical integration is not necessary.

Fabric Element

The fabric is the reinforcing element of the gravel-interface-clay system. To model the fabric a special axisymmetric, linear, two dimensional element is developed.

The fabric element only takes tension in the radial and tangential directions. Compression and bending are not taken by this element. Without bending resistance, the element will deform without restriction with applied transverse forces. This linear element is a two dimensional version of a one dimensional pin-end bar element.

A quadratic element with no bending capacity does not handle the equilibrium condition of the shear stresses developed along the curved element. Due to its curvature, membrane stresses alone cannot provide the equilibrium condition. For this reason a linear and not a quadratic element is used. The friction forces that are developed at the fabric are applied at the nodes of the element and depend

on many variables including:

(a) The friction and or adhesion between the clay and the fabric.

(b) The friction or "grip" between gravel and the fabric.

(c) The tension properties of the fabric.

(d) The gravel thickness that defines the stress field at the interface.

(e) The orientation and state of deformation of the fabric.

The two dimensional axisymmetric fabric element used in this investigation is shown in Figure 4-4 for undeformed and deformed conditions and in Figure 4-5 the soil-fabric finite element model is shown. The fabric-soil system is modeled by a fabric element and double layer of interface elements as shown in Figure 4-6, one interface element being placed above the fabric element and one below. Since the interface element was developed assuming a quadratic displacement distribution, incompatibility of displacements between the interface and the fabric element exists. To give a better approximation of the behavior of the interface and the fabric, two fabric elements are placed along the side of one interface element, as shown in Figure 4-6. Each fabric element extends from a node adjacent to a corner node to a node adjacent to a midside node of an eight node isoparametric element.

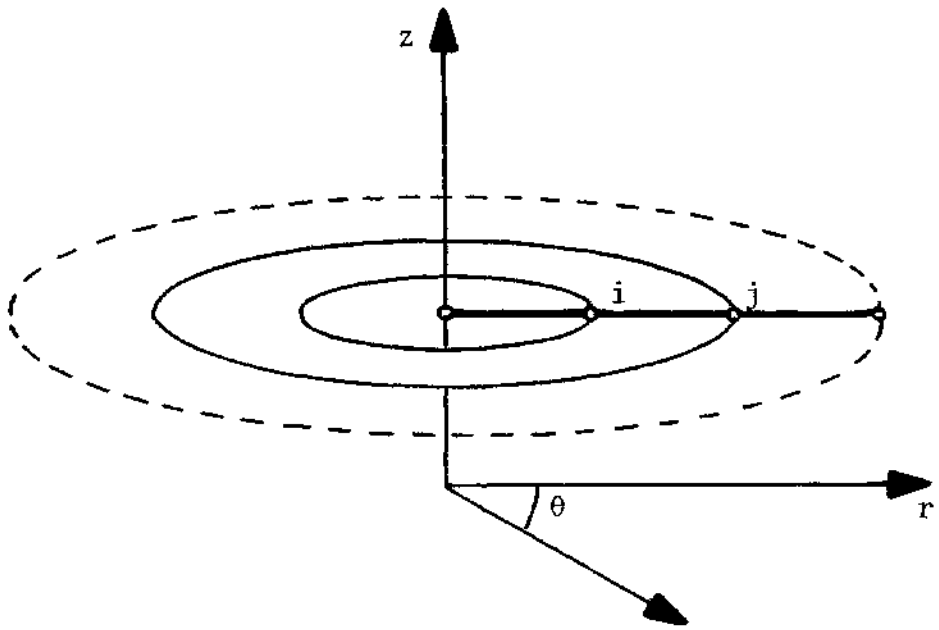

(a) Undeformed

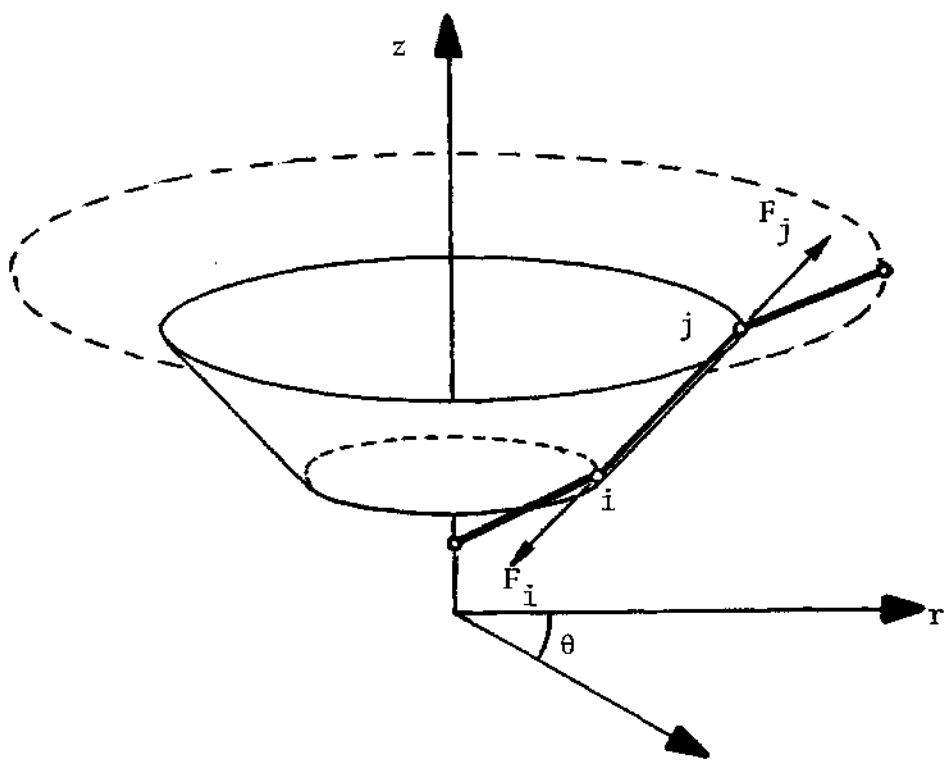

(b) Deformed

Figure 4-4. Fabric Element Model--Axisymmetric Representation

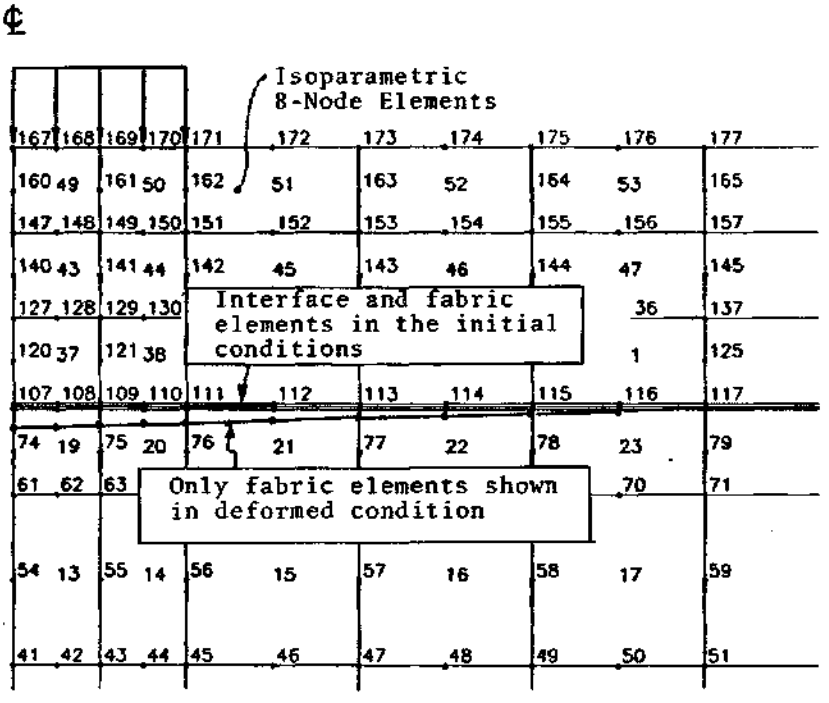

Figure 4-5. The Fabric Element in the Soil-Fabric System

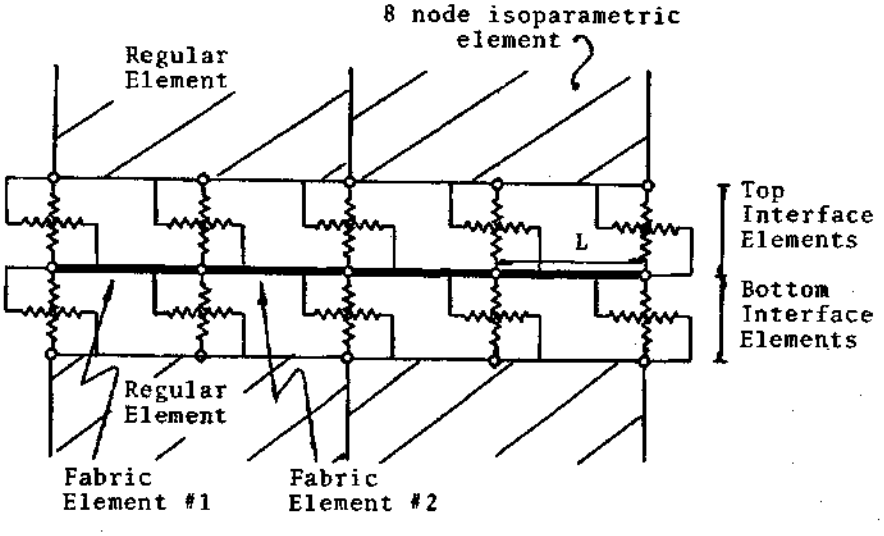

Figure 4-6. Soil-Fabric Finite Element Model

When the system undergoes displacement the interface will be represented by the model shown in Figures 4-5 and 4-7.

Fabric Element Derivation

The general representation of the linear, two dimensional axisymmetric fabric element is shown in Figure 4-8. The nodes of the element are i and j and the element forms an initial angle α with the horizontal r axis.

For the local coordinate system of the element labeled RP, the displacements are given by u'. Then the displacement interpolation values in terms of the global components u_1, v_1, u_2 and v_2 are given in matrix form by:

$$u' = \frac{1}{2} [\cos\alpha \ \sin\alpha] \begin{Bmatrix} (1-RP)u_1 + (1+RP)u_2 \\ (1-RP)v_1 + (1+RP)v_2 \end{Bmatrix} \tag{22}$$

The radial strain of the element is given by

$$\varepsilon_r = \frac{\partial u'}{\partial r} \tag{23}$$

and the tangential strain, assuming that only the displacement in the radial direction produces tangential strain, is given by:

$$\varepsilon_\theta = \frac{u'}{r} \cos\alpha \tag{24}$$

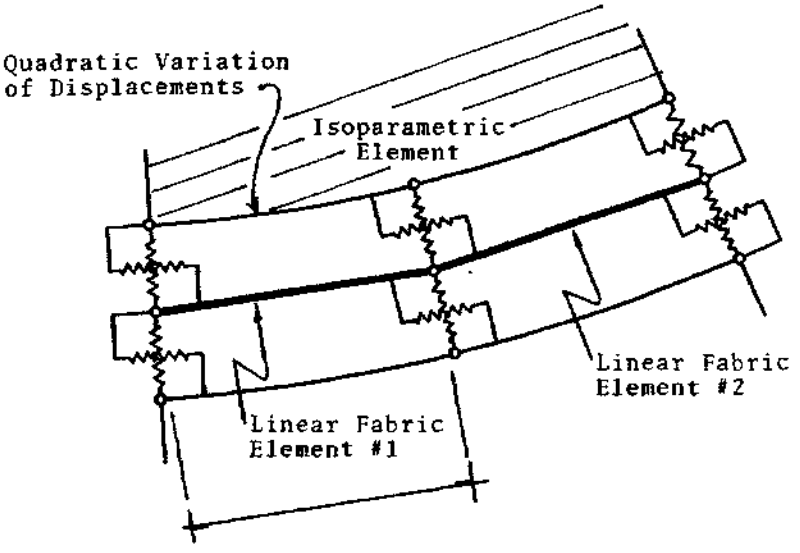

Figure 4-7. Linear Approximation for the Fabric at the Soil-Fabric Interface

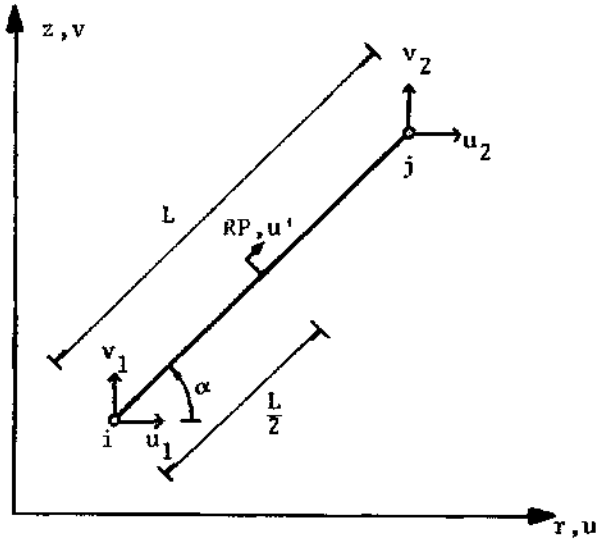

Figure 4-8. Fabric Element General Representation

The Jacobian matrix [J] relating the element length in the global coordinate system to the element length in the local coordinate system is given by:

$$[\underset{\sim}{J}] = \frac{L}{2} \tag{25}$$

where

$$L = [(r_j - r_i)^2 + (z_j - z_i)^2]^{1/2} \tag{26}$$

Converting equation (23) to the local coordinate axis RP:

$$\varepsilon_r = [\underset{\sim}{J}]^{-1} \frac{\partial u'}{\partial RP} = \frac{2}{L} \frac{\partial u'}{\partial RP} \tag{27}$$

Now the derivative of displacement u' with respect to RP from equation (22) is in matrix form:

$$\frac{\partial u'}{\partial RP} = [\cos \alpha \quad \sin \alpha] \begin{Bmatrix} -0.5\ u_1 + 0.5\ u_2 \\ \\ -0.5\ v_1 + 0.5\ v_2 \end{Bmatrix} \tag{28}$$

so the radial strain in terms of the global displacements, substituting (28) into (27) we have:

$$\varepsilon_r = \frac{2}{L}\frac{1}{2}\left[(u_2-u_1)\cos\alpha + (v_2-v_1)\sin\alpha\right]$$

$$\varepsilon_r = \frac{1}{L}\left[(u_2-u_1)\cos\alpha + (v_2-v_1)\sin\alpha\right] \tag{29}$$

where L is given by equations (26).

Substituting (22) into (24) for the tangential strain we have the expression:

$$\varepsilon_\theta = \frac{1}{2RI}\cos\alpha\ [\cos\alpha\ \sin\alpha] \begin{Bmatrix} (1-RP)u_1 + (1+RP)u_2 \\ (1-RP(v_1 + (1+RP)v_2 \end{Bmatrix} \tag{30}$$

where

$$RI = r = (r_j+r_i)/2 + RP \cdot \frac{L}{2}\cos\alpha \tag{31}$$

The strain nodal displacement equation is:

$$\underset{\sim}{\varepsilon} = \underset{\sim}{B}\cdot\underset{\sim}{u} \tag{32}$$

Then with expression (29) and (30) and with (32) we form the strain-displacement matrix $\underset{\sim}{B}$ for small strains

$$\begin{Bmatrix} \varepsilon_r \\ \varepsilon_\theta \end{Bmatrix} = \begin{bmatrix} -\frac{\cos\alpha}{L} & -\frac{\sin\alpha}{L} & \frac{\cos\alpha}{L} & \frac{\sin\alpha}{L} \\ (1-RP)\frac{\cos^2\alpha}{2RI} & \frac{(1-RP)\sin\alpha\cos\alpha}{2RI} & \frac{(1+RP)\cos^2\alpha}{2RI} & \frac{(1+RP)\sin\alpha\cos\alpha}{2RI} \end{bmatrix} \underset{\sim}{u} \tag{33}$$

Finally from (33) the strain-displacement matrix B is defined:

$$\underset{\sim}{B} = \begin{bmatrix} -\frac{\cos\alpha}{L} & -\frac{\sin\alpha}{L} & \frac{\cos\alpha}{L} & \frac{\sin\alpha}{L} \\ \frac{(1-RP)\cos^2\alpha}{2RI} & \frac{(1-RP)\sin\alpha\cos\alpha}{2RI} & \frac{(1+RP)\cos^2\alpha}{2RI} & \frac{(1+RP)\sin\alpha\cos\alpha}{2RI} \end{bmatrix} \tag{34}$$

Laboratory tests show the fabric material has different tension modulus E_f in orthogonal directions due to the method used in manufacturing. These mechanical characteristics of the fabric imply that the fabric is not axisymmetric. To treat the problem as an axisymmetric problem an average tension modulus of the fabric E_f is used. The average is computed from the tension modulus values in the main and transverse directions. The solution with the fabric with different tension modulus in both directions implies the use of a three dimensional model or an axisymmetric model using Fourier series to account for the fabric mechanical characteristics. Considering the complexities of the finite element

solution for the soil-fabric system, the use of a more sophisticated model would result in a prohibitive computer time for the nonlinear incremental analysis of the system. The matrix relating stress to strain or elasticity matrix $\underset{\sim}{D}$ is then given by:

$$D = \begin{bmatrix} E_f & 0 \\ 0 & E_f \end{bmatrix} \tag{35}$$

The stiffness of the fabric element $\underset{\sim}{S}_f$ is given by:

$$\underset{\sim}{S}_f = \int_A \underset{\sim}{B}^T \underset{\sim}{D} \underset{\sim}{B} \, dA \tag{36}$$

which is evaluated numerically as discussed in Chapter VI.

The interface and fabric elements presented provide an approximate model to represent the interface soil-fabric system in the finite element formulation. In the case of the fabric element by using straight portions of the fabric, the real curved surface in space is just approximated and the displacements developed are not complying with the continuity of the slope of the fabric membrane. For this reason the present fabric element is a simplification of the problem, but tests show that it represents adequately the fabric material in the soil-fabric system. Examples of the use of the fabric element are given in Chapter X.

CHAPTER V

NONLINEAR ANALYSIS AND LARGE DISPLACEMENTS

Background

The solution strategy for the finite element analysis of nonlinear systems and large displacements is based on the solution of incremental formulations of the problem. The load is applied to the model by increments, and computations of incremental and total stresses are performed for each load increment by solving a system of linear incremental equations of equilibrium of the system. The complete load-displacement behavior is obtained. In the nonlinear problem the nonlinearities arise from two different sources: geometric nonlinearities and material nonlinearity. The geometric nonlinearities are due to large displacements caused by the change in geometry of the body, and the material nonlinearities depend on the constitutive relation of the material. In many finite element applications the elastic-plastic or the elastic-strain hardening behavior is used to represent the material behavior.

The earliest solutions of the nonlinear finite element analysis treated the problem as multilinear making possible general analysis capabilities and solutions. Development of isoparametric elements enhanced the use of the nonlinear approach and provided an effective way to solve several

problems. In structural analysis these are solutions reported for beams and axisymmetric shells [53], large deflection of plates [86], large displacements of membranes [96], tensile strip problems, bending of bars [121] and deflections of shallow curved beams [2] among many others. In geotechnical engineering the material nonlinearity has been of prime interest for predicting settlement of footings on layered soils [29] together with procedures for the nonlinear analysis of soils [40] and analysis of layered systems [6].

The following two different procedures have been used in the solution of the incremental nonlinear finite element models:

(a) The total Lagrangean or Lagrangian formulation where all variables are referred to the initial configuration of the body, shown as state M in Figure 5-1a and uses a unique type of stresses. This procedure has been used by Oden [98], Hibbit, Marcal and Rice [63], Stricklin [121] and others. It was the first introduced and produced good results in static analysis.

(b) The updated Lagrangean formulation where all variables are referred to an updated configuration of the body in each load step. This procedure is called also Eulerian or moving coordinate. It was used by Bathe and Wilson [10], Yamada [136], Atluri [2,4], Stricklin [121], Murakawa [85], Zienkiewicz et al. [149], among other authors. It is recognized that this formulation presents more simplicity than the

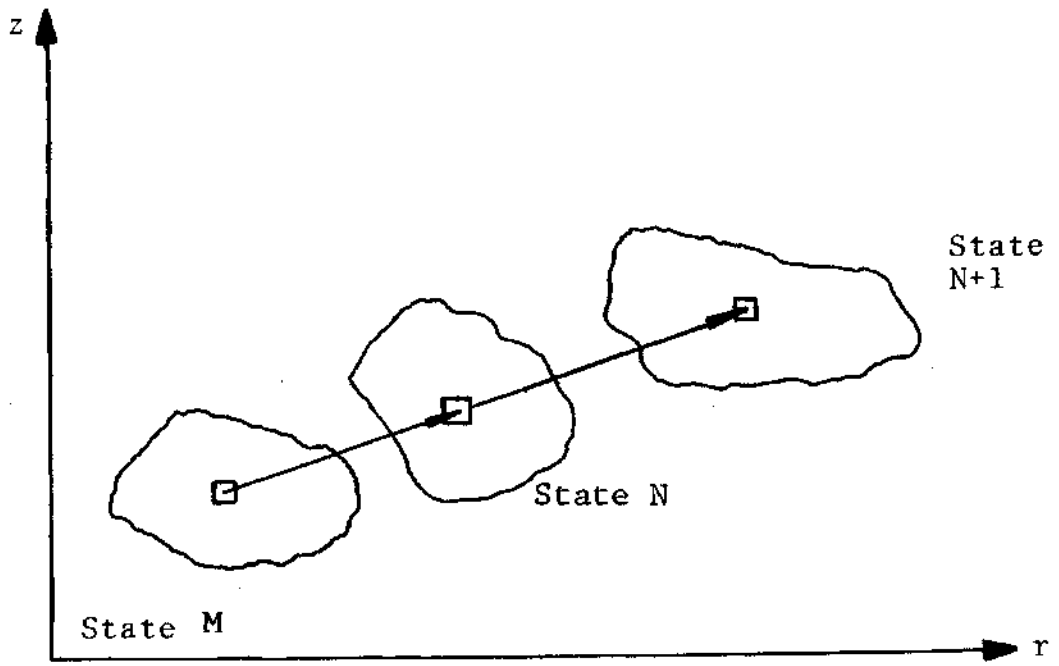

(a) Deformation of a body from initial state M to State N and N+1

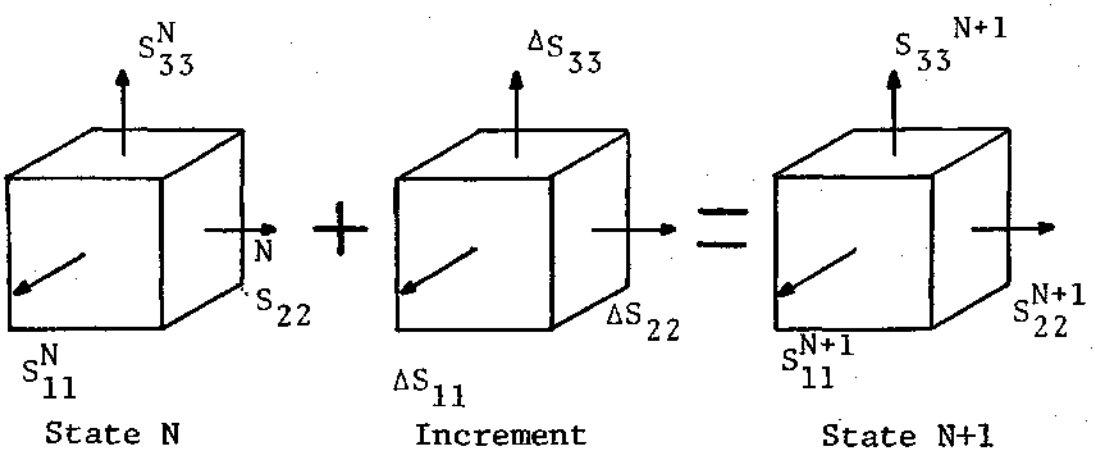

(b) Element stresses for the second Piola-Kirchhoff stress

Figure 5-1. Deformation and Stresses Due to Load Increments

total Lagrangean, especially for large displacements--small strain problems.

The two approaches have been studied and literature reviews are given in [2,4,10,98,136,149]. Both theoretical solutions should give identical results, although different authors report different results with variations up to 25% [10]. Probably the constitutive relations used, the number of increments and the equilibrium verification played an important role in these variations.

A brief presentation of the two approaches follows where matrix and tensorial notations are used following references [4,4A,83 and 85].

Total Lagrangean Formulation

The total Lagrangean approach for the solution of non-linear, incremental finite element problems refers all variables to the initial configuration of the body. Considering a load increment applied to a body which starts with an undeformed configuration at state M, then after the load increment is applied, the body will deform to a configuration N. With a second load increment the body will further deform to configuration N+1, as shown in Figure 5-1a. All variables are referred to the initial configuration of the body. The second Piola-Kirchhoff stresses at state N+1, according to the definitions for all the stresses used in this chapter given in Appendix A, are computed as follows:

$$\underset{\sim}{S}_{ij}^{N+1} = \underset{\sim}{S}_{ij}^{N} + \Delta\underset{\sim}{S}_{ij} \tag{1}$$

where

$\underset{\sim}{S}^{N+1}$ = second Piola-Kirchhoff stress at state N+1

$\underset{\sim}{S}^{N}$ = second Piola-Kirchhoff stress at state N

$\Delta\underset{\sim}{S}_{ij}$ = increment of the second Piola-Kirchhoff stress

The second Piola-Kirchhoff stress is a stress per unit area in the undeformed configuration of the body.

Now compute the true Cauchy stress at the end of the increment. For this case the increment of stress $\Delta\underset{\sim}{S}_{ij}$ is not additive to the true Cauchy stress at state N+1. To compute the true Cauchy stress $\underset{\sim}{\tau}^{N+1}$ at state N+1, the following transformation is needed:

$$\underset{\sim}{\tau}^{N+1} = \frac{1}{J^{N+1}} \underset{\sim}{F}^{N+1} \underset{\sim}{S}^{N+1} [\underset{\sim}{F}^{N+1}]^{T} \tag{2}$$

where

$\underset{\sim}{F}^{N+1}$ = displacement gradient matrix or transformation matrix

$$\underset{\sim}{F}^{N+1} = [\frac{\partial u^{N+1}}{\partial x}] \tag{3}$$

u = displacement vector

x = coordinates for the axisymmetric case: r, z, θ

$$J^{N+1} = \det[\frac{\partial u^{N+1}}{\partial x}] = \det |F^{N+1}| \tag{4}$$

The true Cauchy stress $\underset{\sim}{\tau}^{N+1}$ is the stress that results from

the application of the differential force acting on an oriented surface in the deformed configuration of the body.

In the total Lagrangean approach we solve for the increments of the second Piola-Kirchhoff stress $\Delta\underset{\sim}{S}$ and the increment in displacement $\Delta\underset{\sim}{u}$ and add these values to the state N values to obtain the conditions of state N+1. The transformation matrix is calculated using the gradient matrix $[\underset{\sim}{F}^N]$, whose transpose matrix $[\underset{\sim}{F}^N]^T$ found in Appendix A is given below:

$$[\underset{\sim}{F}^N]^T = \begin{bmatrix} 1 + \frac{\partial u}{\partial r} & \frac{\partial v}{\partial r} & 0 \\ \frac{\partial u}{\partial z} & 1 + \frac{\partial v}{\partial z} & 0 \\ 0 & 0 & 1 + \frac{u}{r} \end{bmatrix} \tag{5}$$

The main advantage of the total Lagrangean formulation is the use of a single reference configuration and a single type of stress, the second Piola-Kirchhoff stress. With it compute the true Cauchy stress with equation (2). A disadvantage is that the stiffness matrix for large displacements is quite complex to implement in the formulation and the equilibrium equations are rather complicated.

Updated Lagrangean Formulation

The updated Lagrangean approach is also called Eulerian, moving coordinate or updated [4,9,79,137]. This

formulation considers the changes in geometry with each load increment and all variables (stresses, strains and displacements) are referred to the immediately previous configuration of the body. The equations of equilibrium are simpler than the total Lagrangean formulation. For each load increment a reference configuration N is used for the solution of the incremental variables. A disadvantage of the updated Lagrangean formulation is that the computation of stresses needs a step by step procedure. The initial stress in state N is the true Cauchy stress $\underset{\sim}{\tau}^N$, this stress is given per unit area in N, in the orthogonal axes r, z and θ for the axisymmetric problem. The definition of the true Cauchy stress and a graphical representation is given in Appendix A.

The incremental stress decomposition for the updated Lagrangean formulation is represented by:

$$\underset{\sim}{S}^{N+1} = \underset{\sim}{\tau}^N + \Delta\underset{\sim}{S}^N \qquad (6)$$

where

$\underset{\sim}{S}^{N+1}$ = components of the second Piola-Kirchhoff stress at N+1 referred to N at the end of the increment

$\underset{\sim}{\tau}^N$ = components of the true Cauchy stress tensor

$\Delta\underset{\sim}{S}^N$ = components of the second Piola-Kirchhoff stress increment referred to configuration N (Truesdell stress increment).

With the values of $\underset{\sim}{S}^{N+1}$ computed, we use the transformation

$$\underset{\sim}{\tau}^{N+1} = \frac{1}{J^{N+1}} \underset{\sim}{F}^{N+1} \underset{\sim}{S}^{N+1} [\underset{\sim}{F}^{N+1}]^T \tag{7}$$

to compute the true Cauchy stress at the state N+1, which is the initial stress for state N+2.

The first Piola-Kirchhoff stress in state N+1 as referred to N is:

$$\underset{\sim}{t}^{N+1} = \underset{\sim}{\tau}^{N} + \Delta \underset{\sim}{t}_{N}^{N+1} \tag{8}$$

where in general

$$\underset{\sim}{\tau}^{N} = \frac{1}{J^{N}} \underset{\sim}{F}^{N} \underset{\sim}{S}^{N} [\underset{\sim}{F}^{N}]^T \tag{9}$$

Now the strategy is to calculate $\Delta \underset{\sim}{S}$ or $\Delta \underset{\sim}{t}$ and then calculate $\underset{\sim}{S}^{N+1}$ or $\underset{\sim}{t}^{N+1}$ and with the help of the transformation matrix $\underset{\sim}{F}$ given in equation (5), calculate by means of equation (7) the true Cauchy stress at state N+1 represented by $\underset{\sim}{\tau}^{N+1}$ and given for the end of the increment.

Equations for the Nonlinear and Large Displacement Finite Element Formulation

Using the updated Lagrangean approach and taking as reference the configuration of the body at state N, the true total stress $\underset{\sim}{\tau}^{N+1}$ at state N+1 referred to N is given by equation (7). The total strain in state N+1 referred to N is $\underset{\sim}{\varepsilon}$ and the total displacements in N+1 referred to the orthogonal base vectors in N are $\underset{\sim}{u}$. Using standard tensor

notation the strains are given by:

$$\varepsilon_{ij} = \frac{1}{2}\,[u_{i,j} + u_{j,i} + u_{k,i}\,u_{k,j}] \tag{10}$$

The commas in the above expression indicate differentiation.

The virtual strains are computed with:

$$\delta\varepsilon_{ij} = \frac{1}{2}\,\delta[u_{i,j} + u_{j,i} + u_{k,i}\,u_{k,j}] \tag{11}$$

Employing the principle of virtual work [147] we can formulate the equations of equilibrium of the system by computing the virtual work of the external forces and equating it to the negative change of the internal energy, which gives:

$$\int_{V_N} [(\tau^N_{ij} + \Delta S_{ij})\delta\varepsilon_{ij} - (R^N_i + \Delta R^N_i)\delta u_i]dv - \int_{S_N} [(t^N_{s_i} + \Delta t_{s_i})\delta u_i]ds = 0 \tag{12}$$

where

$\underset{\sim}{R}_i$ = body forces

t_{s_i} = surface tractions

V_N = volume of the body at state N

S_N = surface of body at state N

Substituting equation (11) into (12) gives

$$\int_{V_N} \{\tau_{ij}^N \frac{1}{2} [\delta u_{i,j} + \delta u_{j,i}] - R_i^N \delta u_i\} dv - \int_S t_{s_i}^N \delta u_i$$

$$+ \int_{V_N} [\Delta S_{ij} \frac{1}{2} \delta [u_{i,j} + u_{j,i} + u_{k,i} u_{k,j}]$$

$$+ \tau_{ij}^N \cdot \frac{1}{2} \delta [u_{k,i} u_{k,j}] - \Delta R_i \delta u_i] dv - \int_S [\Delta t_{s_i} \delta u_i] ds = 0 \tag{13}$$

For state N to be in equilibrium the first row of equation (13) must be equal to zero. Thus the first row gives a check of the accuracy of the solution for each load increment since it represents the unbalance of the system. Now use a piecewise linearization solution of the problem and assume that equilibrium is satisfied at the state N. For the incremental body forces and external pressures for the interval we can define the incremental equations of equilibrium. The nonlinear term $\{\Delta S_{ij} u_{k,i} u_{k,j}\}$ of equation (13) is dropped here to obtain a linear solution for the increment which gives

$$\int_{V_N} [\Delta S_{ij} \cdot \frac{1}{2} \delta [u_{i,j} + u_{j,i}] + \tau_{ij}^N \cdot \frac{1}{2} \delta [u_{k,i} u_{k,j}]$$

$$- \Delta R \delta u_i] dv - \int_s [\Delta t_{s_i} \delta u_i] ds = 0 \tag{14}$$

The linear and quadratic strain increments are respectively:

$$\delta\varepsilon_{ij}^{I} = \frac{1}{2}\delta[u_{i,j} + u_{j,i}] \tag{15}$$

$$\delta\varepsilon_{ij}^{L} = \frac{1}{2}\delta[u_{k,i}u_{k,j}] \tag{16}$$

The total strain is given by

$$\varepsilon_{ij} = \varepsilon_{ij}^{I} + \varepsilon_{ij}^{L} \tag{17}$$

Since stresses, body forces and surface tractions do not change during virtual displacements

$$\tau_{ij}^{N}\ \delta\varepsilon_{ij}^{L} = \delta(\tau_{ij}^{N}\ \varepsilon_{ij}^{L}) \tag{18}$$

$$\Delta R_i\ \delta u_i = \delta(\Delta R_i u_i) \tag{19}$$

$$\Delta t_{si} \cdot \delta u_i = \delta(\Delta t_{si} u_i) \tag{20}$$

Substituting expressions (15) through (20) into (14) gives

$$\int_{V_N} [\Delta S_{ij}\delta\varepsilon_{ij}^{I} + \tau_{ij}^{N}\delta\varepsilon_{ij}^{L} - \Delta R_i\delta u_i]dv - \int_{S_N} [\Delta t_{si}\delta u_i]ds = 0 \tag{21}$$

where

ΔS_{ij} = second Piola-Kirchhoff stress increment

τ_{ij}^{N} = true Cauchy stress in state N

ΔR_i = body forces load increment contribution

Δt_s = external tractions load increment contribution

The integration and stiffness matrices derivation from equation (14) show that in the above expressions the term $\{\Delta S_{ij}\ \delta\varepsilon_{ij}^{I}\}$ provides the conventional small displacement stiffness matrix, and the term $\{\tau_{ij}^{N}\ \delta\varepsilon_{ij}^{L}\}$ provides the initial stress stiffness matrix. When the second order term $\{\Delta S_{ij}\ u_{k,i}\ u_{k,j}\}$ is retained in the derivations, then the equation of equilibrium includes large displacement strain terms; and the large displacement stiffness matrix of the elements is included in the computations. This is shown in the next section. The equation of equilibrium is then

$$\int_V [\Delta S_{ij}\delta\varepsilon_{ij}^{I} + \Delta S_{ij}\delta\varepsilon_{ij}^{L} + \tau_{ij}^{N}\delta\varepsilon_{ij}^{L} - \Delta R_i\delta u_i]dv - \int_{S_N} [\Delta t_{si}\delta u_i]ds = 0 \qquad (22)$$

The first three terms provide the small displacements, large displacements and initial stress stiffness matrices, respectively.

Equation (22) is used to generate the system of piecewise equations of equilibrium for the finite element model. The general unbalanced case of the system was represented by equation (13) and by grouping terms gives

$$\int_V \tilde{\underset{\sim}{B}}^T \underset{\sim}{\sigma} dv - \underset{\sim}{P} = \underset{\sim}{\psi}(u) \tag{23}$$

where

$\int_V \tilde{\underset{\sim}{B}}^T \underset{\sim}{\sigma} dv$ = internal forces of the element

$\tilde{\underset{\sim}{B}}$ = total strain displacement matrix

$\underset{\sim}{\psi}(u)$ = vector of unbalanced forces equal to the sum of external and internal generalized forces corresponding to the first row of equation (13)

$\underset{\sim}{P}$ = vector of external forces

$\underset{\sim}{\sigma}$ = stress of the element

The increase in strain for large displacements can be computed with

$$\underset{\sim}{d\varepsilon} = \tilde{\underset{\sim}{B}}\ \underset{\sim}{du} \tag{24}$$

where

$$\tilde{\underset{\sim}{B}} = \underset{\sim}{B} + \underset{\sim}{B}_L(u) \tag{25}$$

$$d\tilde{\underset{\sim}{B}} = d\underset{\sim}{B}_L \tag{26}$$

$\underset{\sim}{B}$ = incremental strain-incremental displacement matrix for small displacements

$\underset{\sim}{B}_L$ = incremental strain-incremental displacement matrix for large displacements

$\bar{\underset{\sim}{B}}$ = complete strain-displacement matrix

The $\underset{\sim}{B}$ matrices are also called strain-displacement matrices.

$d\varepsilon$ = strain increment

du = displacement increment

The derivation of $\underset{\sim}{B}_L$ is presented in the next section.

The stresses in each element can be computed using the constitutive equation for linear analysis

$$\underset{\sim}{\sigma} = \underset{\sim}{D}\ (\underset{\sim}{\varepsilon} - \underset{\sim}{\varepsilon}_o) + \underset{\sim}{\sigma}_o \tag{27}$$

where

$\underset{\sim}{D}$ = stress-strain constitutive matrix (formula (18) Chapter III)

ε_o, σ_o = initial strain and stress terms

For an elasto-plastic analysis the elasticity matrix $\underset{\sim}{D}$ is replaced by $\underset{\sim}{D}_{ep}$. The derivation and nomenclature of the elasto-plastic matrix $\underset{\sim}{D}_{ep}$ is given in Chapter VII. Equations (22) and (23) are equivalent; differentiating (23) we have a system of incremental equations of equilibrium,

$$d\underset{\sim}{\psi} = \int_V d\bar{\underset{\sim}{B}}^T \underset{\sim}{\sigma} dv + \int_V \bar{\underset{\sim}{B}}^T d\underset{\sim}{\sigma} dv = \underset{\sim}{K}_T du \tag{28}$$

defining $\underset{\sim}{K}_T$ as the tangential stiffness matrix for the load increment. Differentiating equation (27) and substituting it and equations (24) and (25) into (28) after performing the matrix operations according to [147] gives:

$$d\psi = \{\int_V d\underset{\sim}{B}_L^T \sigma dv + \int_V \underset{\sim}{B}^T \underset{\sim\sim}{D}\underset{\sim}{B} dv + \int_V (\underset{\sim}{B}^T \underset{\sim\sim}{D}\underset{\sim}{B}_L + \underset{\sim}{B}_L^T \underset{\sim\sim}{D}\underset{\sim}{B}_L + \underset{\sim}{B}_L^T \underset{\sim\sim}{D}\underset{\sim}{B}) dv\} du \tag{29}$$

The stiffness matrices $\underset{\sim}{K}_o$ and $\underset{\sim}{K}_L$ are defined by:

$$\underset{\sim}{K}_o = \int_V \underset{\sim}{B}^T \underset{\sim\sim}{D}\underset{\sim}{B} dv \tag{30}$$

$$\underset{\sim}{K}_L = \int_V (\underset{\sim}{B}^T \underset{\sim\sim}{D}\underset{\sim}{B}_L + \underset{\sim}{B}_L^T \underset{\sim\sim}{D}\underset{\sim}{B}_L + \underset{\sim}{B}_L^T \underset{\sim\sim}{D}\underset{\sim}{B}) dv \tag{31}$$

In the above expressions $\underset{\sim}{K}_o$ is the usual small strain stiffness matrix and $\underset{\sim}{K}_L$ is the stiffness matrix due to large displacements that includes second order strain terms. Now we have also from the first term of the right side of equation (29) the initial stress stiffness matrix, $\underset{\sim}{K}_\sigma$, which is also called the geometric matrix and given by:

$$\underset{\sim}{K}_\sigma = \int_V d\underset{\sim}{B}_L^T \underset{\sim}{\sigma} dv \tag{32}$$

The general equation of incremental equilibrium as a function of the defined stiffness matrices is obtained by substituting equations (30) through (32) into (29) giving:

$$d\underset{\sim}{\psi} = (\underset{\sim}{K}_o + \underset{\sim}{K}_L + \underset{\sim}{K}_\sigma) du = \underset{\sim}{K}_T du \tag{33}$$

Derivation of the Strain-Displacement Relation for Large Displacements

The strain terms for finite deformation of the axisymmetric solid are given by the following expressions, with the complete derivations given in Appendix A.

$$\varepsilon_r = \frac{\partial u}{\partial r} + \frac{1}{2}\left[\left(\frac{\partial u}{\partial r}\right)^2 + \left(\frac{\partial v}{\partial r}\right)^2\right] \tag{34}$$

$$\varepsilon_z = \frac{\partial v}{\partial z} + \frac{1}{2}\left[\left(\frac{\partial u}{\partial z}\right)^2 + \left(\frac{\partial v}{\partial z}\right)^2\right] \tag{35}$$

$$\varepsilon_\theta = \frac{u}{r} + \frac{1}{2}\left(\frac{u}{r}\right)^2 \tag{36}$$

$$\gamma_{rz} = \frac{\partial u}{\partial z} + \frac{\partial v}{\partial r} + \left[\frac{\partial u}{\partial r}\frac{\partial u}{\partial z} + \frac{\partial v}{\partial r}\frac{\partial v}{\partial z}\right] \tag{37}$$

where

ε_r = radial strain

ε_z = vertical strain

ε_θ = tangential strain

γ_{rz} = shear strain (engineering definition)

The total strain formulas given in equations (34) to (37) can be decomposed into infinitesimal strain terms and finite strain terms which gives

$$\varepsilon = \varepsilon^I + \varepsilon^L = \begin{Bmatrix} \varepsilon_r^I \\ \varepsilon_z^I \\ \varepsilon_\theta^I \\ \gamma_{rz}^I \end{Bmatrix} + \begin{Bmatrix} \varepsilon_r^L \\ \varepsilon_z^L \\ \varepsilon_\theta^L \\ \gamma_{rz}^L \end{Bmatrix} \tag{38}$$

where

ε^I = small or infinitesimal strain components

ε^L = large or finite strain components

Then the contribution of the large displacements terms are:

$$\varepsilon_r^L = \frac{1}{2}\left[\left(\frac{\partial u}{\partial r}\right)^2 + \left(\frac{\partial v}{\partial r}\right)^2\right] \tag{39}$$

$$\varepsilon_z^L = \frac{1}{2}\left[\left(\frac{\partial u}{\partial z}\right)^2 + \left(\frac{\partial v}{\partial z}\right)^2\right] \tag{40}$$

$$\varepsilon_\theta^L = \frac{1}{2}\left(\frac{u}{r}\right)^2 \tag{41}$$

$$\gamma_{rz}^L = \left[\frac{\partial u}{\partial r} \cdot \frac{\partial u}{\partial z} + \frac{\partial v}{\partial r} \cdot \frac{\partial v}{\partial z}\right] \tag{42}$$

Now define $\underset{\sim}{\theta}_r$ and $\underset{\sim}{\theta}_z$ as:

$$\underset{\sim}{\theta}_r = \begin{Bmatrix} \frac{\partial u}{\partial r} \\ \\ \frac{\partial v}{\partial r} \end{Bmatrix} \qquad \theta_z = \begin{Bmatrix} \frac{\partial u}{\partial z} \\ \\ \frac{\partial v}{\partial z} \end{Bmatrix} \tag{43}$$

The large displacements strain term $\underset{\sim}{\epsilon}^{L}$ can be defined in matrix form using equations (39) to (43) as:

$$\underset{\sim}{\epsilon}^{L} = \frac{1}{2} \underset{\sim}{A}\ \underset{\sim}{\theta} \tag{44}$$

where

$$\underset{\sim}{A} = \begin{bmatrix} \underset{\sim}{\theta}_r^T & 0 & 0 \\ 0 & \underset{\sim}{\theta}_z^T & 0 \\ 0 & 0 & \frac{u}{r} \\ \underset{\sim}{\theta}_z^T & \underset{\sim}{\theta}_r^T & 0 \end{bmatrix} \tag{45}$$

and

$$\underset{\sim}{\theta} = \begin{Bmatrix} \underset{\sim}{\theta}_r \\ \underset{\sim}{\theta}_z \\ \frac{u}{r} \end{Bmatrix} \tag{46}$$

Using the large strain term definitions given by equations (39) to (42) and equations (43) to form the appropriate $\underset{\sim}{A}$ and $\underset{\sim}{\theta}$ matrices, the terms forming equation (44) can then be expanded to give

$$\underset{\sim}{\varepsilon}^{L} = \frac{1}{2}\begin{bmatrix} \frac{\partial u}{\partial r} & \frac{\partial v}{\partial r} & 0 & 0 & 0 \\ 0 & 0 & \frac{\partial u}{\partial z} & \frac{\partial v}{\partial z} & 0 \\ 0 & 0 & 0 & 0 & \frac{u}{r} \\ \frac{\partial u}{\partial z} & \frac{\partial v}{\partial z} & \frac{\partial u}{\partial r} & \frac{\partial v}{\partial r} & 0 \end{bmatrix} \begin{Bmatrix} \frac{\partial u}{\partial r} \\ \frac{\partial v}{\partial r} \\ \frac{\partial u}{\partial z} \\ \frac{\partial v}{\partial z} \\ \frac{u}{r} \end{Bmatrix} \tag{47}$$

Applying the chain rule of differentiation to equation (44) gives for $d\underset{\sim}{\varepsilon}^{L}$ [147]:

$$d\underset{\sim}{\varepsilon}^{L} = \frac{1}{2}\, d\underset{\sim}{A}\cdot\underset{\sim}{\theta} + \frac{1}{2}\,\underset{\sim}{A}d\underset{\sim}{\theta} = \underset{\sim}{A}d\underset{\sim}{\theta} \tag{48}$$

Also defining $\underset{\sim}{\theta}$ as:

$$\underset{\sim}{\theta} = \underset{\sim}{G}\cdot\underset{\sim}{u} \tag{49}$$

and differentiating we have:

$$d\underset{\sim}{\theta} = \underset{\sim}{G}\cdot d\underset{\sim}{u} \tag{50}$$

where

$\underset{\sim}{u}$ = nodal displacements vector

Substituting (50) into (48)

$$d\underset{\sim}{\varepsilon}^{L} = \underset{\sim}{A}\cdot\underset{\sim}{G}\cdot d\underset{\sim}{u} \tag{51}$$

Then $\underset{\sim}{B}_L$ is immediately obtained from equation (51)

$$\underset{\sim}{B}_L = \underset{\sim}{A}\cdot\underset{\sim}{G} \tag{52}$$

and

$$d\underset{\sim}{\varepsilon}^{L} = \underset{\sim}{B}_L\cdot d\underset{\sim}{u} \tag{53}$$

Since $\underset{\sim}{\theta}$ is a vector formed partially by the partial derivatives of the displacements with respect to the global coordinate axes r and z, the matrix $\underset{\sim}{G}$ is given by the multiplication of the inverse of the Jacobian matrix by the partial derivatives of the interpolation functions. These functions given by equation (6) of Chapter III and the operators equations (10) and (11) also from Chapter III, are applied to obtain the partial derivatives in the following matrix operations:

$$\begin{Bmatrix} \frac{\partial u}{\partial r} \\ \\ \frac{\partial u}{\partial z} \end{Bmatrix} = [J]^{-1} \begin{bmatrix} \frac{\partial H_1}{\partial RP} & 0 & \frac{\partial H_2}{\partial RP} & 0 & \cdots & \frac{\partial H_8}{\partial RP} & 0 \\ \\ \frac{\partial H_1}{\partial ZP} & 0 & \frac{\partial H_2}{\partial ZP} & 0 & \cdots & \frac{\partial H_8}{\partial ZP} & 0 \end{bmatrix} \underset{\sim}{u} \tag{54}$$

$$\begin{Bmatrix} \frac{\partial v}{\partial r} \\ \\ \frac{\partial v}{\partial z} \end{Bmatrix} = [J]^{-1} \begin{bmatrix} 0 & \frac{\partial H_1}{\partial RP} & 0 & \frac{\partial H_2}{\partial RP} & \cdots & 0 & \frac{\partial H_8}{\partial RP} \\ 0 & \frac{\partial H_1}{\partial ZP} & 0 & \frac{\partial H_2}{\partial ZP} & \cdots & 0 & \frac{\partial H_8}{\partial ZP} \end{bmatrix} \underset{\sim}{u} \quad (55)$$

where $[J]^{-1}$, H_i, RP and ZP were defined in Chapter III with formulas (6) and (9). The tangential strain term factor $\frac{u}{r}$ in terms of the shape functions is given by:

$$\frac{u}{r} = \frac{1}{r_a} [H_1 \quad 0 \quad H_2 \quad 0 \quad H_3 \quad \cdots \quad H_8 \quad 0] \quad \underset{\sim}{u} \qquad (56)$$

where r_a is the radial distance for the sampling point under consideration. Substituting equation (43) into equation (46) we have:

$$\underset{\sim}{\theta} = \begin{Bmatrix} \frac{\partial u}{\partial r} \\ \\ \frac{\partial v}{\partial r} \\ \\ \frac{\partial u}{\partial z} \\ \\ \frac{\partial v}{\partial z} \\ \\ \frac{u}{r} \end{Bmatrix} \qquad (57)$$

Letting $\underset{\sim}{G}_1$ and $\underset{\sim}{G}_2$ represent the first two right side terms of equations (54) and (55) we have:

$$\begin{Bmatrix} \frac{\partial u}{\partial r} \\ \\ \frac{\partial u}{\partial z} \end{Bmatrix} = \underset{\sim}{G}_1 \cdot \underset{\sim}{u} \tag{58}$$

$$\begin{Bmatrix} \frac{\partial v}{\partial r} \\ \\ \frac{\partial v}{\partial z} \end{Bmatrix} = \underset{\sim}{G}_2 \cdot \underset{\sim}{u} \tag{59}$$

The rows of $\underset{\sim}{G}_1$ and $\underset{\sim}{G}_2$ are computed evaluating the first two terms of the right side of equations (54) and (55) and assembled to comply with (49) and (57). This allows to form matrix $\underset{\sim}{G}$ for the computation of $\underset{\sim}{B}_L$ given by (53).

Having also defined $\underset{\sim}{B}$ and $\underset{\sim}{D}$ by equations (16) and (18) of Chapter III respectively, the stiffness matrix due to large displacements $\underset{\sim}{K}_L$ can be computed using equation (31) and a numerical integration procedure. For the eight node isoparametric element a nine point numerical integration may be applied [147].

Initial Stress Stiffness Matrix

The initial stress stiffness matrix is obtained from the third term of the integral equation (22).

$$\int_V \tau_{ij}^N \, \delta\varepsilon_{ij}^L \, dv \tag{60}$$

where

τ_{ij}^{N} = true Cauchy stress at the start of the increment N to N+1

$\delta\varepsilon_{ij}^{L}$ = increment of quadratic strain terms

For the axisymmetric case

$$\tau_{ij}^{N} = \begin{bmatrix} \sigma_r & \tau_{rz} & 0 \\ \tau_{rz} & \sigma_z & 0 \\ 0 & 0 & \sigma_\theta \end{bmatrix} \tag{61}$$

and $\underset{\sim}{\varepsilon}^{L}$ is given by expressions (39) to (42) for large displacement computations.

For the Cartesian three dimensional coordinate space we have

$$\tau_{ij}^{N}\delta\varepsilon_{ij}^{L} = \tau_{11}\delta\varepsilon_{11}^{L} + 2\tau_{12}\delta\varepsilon_{12}^{L} + 2\tau_{13}\delta\varepsilon_{13}^{L} + \tau_{22}\delta\varepsilon_{22}^{L} + 2\tau_{23}\delta\varepsilon_{23}^{L} + \tau_{33}\delta\varepsilon_{33}^{L} \tag{62}$$

Further, for the particular axisymmetric case under consideration equation (62) can be reduced to

$$\tau_{ij}^{N}\delta\varepsilon_{ij}^{L} = \tau_{11}\delta\varepsilon_{11}^{L} + 2\tau_{12}\delta\varepsilon_{12}^{L} + \tau_{22}\delta\varepsilon_{22}^{L} + \tau_{33}\delta\varepsilon_{33}^{L}$$

$$= \tau_r\delta\varepsilon_r^{L} + 2\tau_{rz}\delta\varepsilon_{rz}^{L} + \tau_z\delta\varepsilon_z^{L} + \tau_\theta\delta\varepsilon_\theta^{L} \tag{63}$$

The derivatives used for the computation of the large displacement terms were given by equation (49)

$$\underset{\sim}{\theta} = \underset{\sim}{G} \cdot \underset{\sim}{u} \tag{49}$$

With the use of $\underset{\sim}{G}$, the large displacement strains $\underset{\sim}{\varepsilon}^{L}$ are evaluated in terms of $\underset{\sim}{u}$, using equation (49) considering the order of the derivatives in $\underset{\sim}{\theta}$ and the appropriate matrix multiplication of the rows of $\underset{\sim}{G}$, to obtain the large displacement strain terms

$$\delta\varepsilon_{ij}^{L} = \frac{1}{2}\delta[u_{k,i}\ u_{k,j}] \tag{16}$$

The resulting derivatives are substituted into equation (60). A similar procedure for the computation of the initial stiffness matrix was presented in [63] for the general three dimensional case. The initial stress stiffness term of the equation of equilibrium (22) is now derived for the axisymmetric case. By the principle of virtual work the initial stress stiffness matrix $\underset{\sim}{K}_{\sigma}$ is obtained:

$$\int_V \tau_{ij}^{N}\delta\varepsilon_{ij}^{L}dv = \delta u^{T}\Big[\int_V \{\tau_{11}^{N} \cdot (\underset{\sim}{G}_1^{T} \cdot \underset{\sim}{G}_1 + \underset{\sim}{G}_2^{T} \cdot \underset{\sim}{G}_2)$$

$$+ 2\tau_{12}^{N}\ (\underset{\sim}{G}_1^{T} \cdot \underset{\sim}{G}_3 + \underset{\sim}{G}_2^{T} \cdot \underset{\sim}{G}_4) + \tau_{22}^{N} \cdot (\underset{\sim}{G}_3^{T} \cdot \underset{\sim}{G}_3$$

$$+ \underset{\sim}{G}_4^{T} \cdot \underset{\sim}{G}_4) + \tau_{33}^{N} \cdot (\underset{\sim}{G}_5^{T} \cdot \underset{\sim}{G}_5)\}dv\Big]u \tag{64}$$

where in G_i, i is the row number of matrix $\underset{\sim}{G}$ defined in (49). The m and n element of the initial stress stiffness matrix $\underset{\sim}{K}_\sigma$ is given by

$$K_\sigma[m,n] = \tau_r^N (G_{1,m} \cdot G_{1,n} + G_{2,m} \cdot G_{2,n})$$

$$+ 2\tau_{rz}^N (G_{1,m} \cdot G_{3,n} + G_{2,m} \cdot G_{4,n})$$

$$+ \tau_z^N (G_{3,m} \cdot G_{3,n} + G_{4,m} \cdot G_{4,n})$$

$$+ \tau_\theta^N (G_{5,m} \cdot G_{5,n}) \qquad (65)$$

The first and second subscripts denote the row and column of $\underset{\sim}{G}$, and m and n vary from 1 to 16 in the eight node isoparametric element.

The general stiffness matrix of the element for the load increment is given by $\underset{\sim}{K}_T$, the tangential stiffness matrix:

$$\underset{\sim}{K}_T = \underset{\sim}{K}_o + \underset{\sim}{K}_L + \underset{\sim}{K}_\sigma \qquad (66)$$

which is used for the solution of the incremental equations of equilibrium (28).

Procedure for the Piecewise Solution of the Nonlinear Equations

The nonlinear analysis of the system is performed using an incremental and iterative procedure. The incremental solutions are verified for equilibrium after each load increment. Iterations are performed to insure the equilibrium

condition. The convergence criterion for each load increment tests the maximum displacement increment of any node. The maximum allowable displacement increment or norm is set after the computation of the maximum total elastic displacement. The maximum allowable displacement is given as a small fraction of the total elastic displacement and can be changed depending on the accuracy desired for the computation. The nonlinearity and the large displacement analysis are included in the present piecewise solution by the implementation of the large displacements and initial stress stiffness matrices and the elastoplastic constitutive relation of the materials, excluding rotation within the element.

The system stiffness matrix is assembled in the usual manner including contributions of the isoparametric and fabric elements. The stiffness of the interface elements is computed in a closed form and included in the global stiffness. The piecewise incremental solution for the nonlinear analysis of the finite element model is as follows:

(a) For the first load increment no initial stresses act on the system and the $\underset{\sim}{K}_L$ and $\underset{\sim}{K}_\sigma$ stiffness matrices are zero.

(b) The system of equations is solved as a linear system with an initial stiffness matrix $\underset{\sim}{K}_o$ and an applied load equal to the first load increment.

$$\underset{\sim}{K}_o \; \underset{\sim}{\Delta u} = \underset{\sim}{\Delta P} \tag{67}$$

$$\Delta \underset{\sim}{u} = \underset{\sim}{K}_o^{-1} \Delta \underset{\sim}{P} \tag{68}$$

where

$\Delta \underset{\sim}{P}$ = load increment

$\underset{\sim}{K}_o$ = system initial stiffness matrix

$\Delta \underset{\sim}{u}$ = displacement increment due to $\Delta \underset{\sim}{P}$

The load increment $\Delta \underset{\sim}{P}$ is computed as the total load divided by the number of load increments

$$\Delta P = \frac{P}{NI} \tag{69}$$

NI = number of load increments.

(c) For the first load increment the stresses are computed for the initial coordinates (geometry) of the system.

(d) Within each load increment, the nodal coordinates are updated at the end of each iteration, and the new r and z coordinates are used for the next load increment as shown in Figure 5-2.

(e) The large displacement stiffness matrix, initial stress stiffness matrix and the elasto-plastic stress-strain matrix are included in the stiffness computations. The stiffness matrices are updated for each iteration.

(f) For subsequent load increments or iterations the

increase and total stresses are computed by following the next procedure.

The incremental second Piola-Kirchhoff stress $\Delta\underset{\sim}{S}$ is added to the initial true Cauchy stress $\underset{\sim}{\tau}^{N}$ of state N to obtain the total second Piola-Kirchhoff stress $\underset{\sim}{S}^{N+1}$ at state N+1, from equation (6).

$$\underset{\sim}{S}^{N+1} = \underset{\sim}{\tau}^{N} + \Delta\underset{\sim}{S} \tag{6}$$

(g) The computation of the true Cauchy stress for state N+1 can be obtained using the transformation of equation (7)

$$\underset{\sim}{\tau}^{N+1} = \frac{1}{J^{N+1}} \underset{\sim}{F}^{N+1} \underset{\sim}{S}^{N+1} [\underset{\sim}{F}^{N+1}]^{T} \tag{7}$$

This will be the initial stress for the next load increment (or iteration).

In equation (7) J^{N+1} and $[F^{N+1}]^{T}$ are given by equations (4) and (5) respectively. The gradient matrix $[F^{N+1}]^{T}$ is found in Appendix A. Further

$$[\underset{\sim}{F}^{N+1}]^{T} = \begin{bmatrix} 1 + \frac{\partial u}{\partial r} & \frac{\partial v}{\partial r} & 0 \\ \frac{\partial u}{\partial z} & 1 + \frac{\partial v}{\partial z} & 0 \\ 0 & 0 & 1 + \frac{u}{r} \end{bmatrix} \tag{5}$$

$$J^{N+1} = \det|F^{N+1}| = (1 + \frac{\partial u}{\partial r})(1 + \frac{\partial v}{\partial z})(1 + \frac{u}{r}) - \frac{\partial v}{\partial r} \cdot \frac{\partial u}{\partial z} (1 + \frac{u}{r}) \tag{4}$$

Where both computed for the load increment in turn.

(h) After each load increment or iteration, equilibrium is verified applying equation (23). The resulting unbalanced forces are reversed and applied to the finite element model, and the computed maximum displacement of the iteration is compared with an established norm for the maximum allowable displacement of the system. The maximum allowable displacement is a percentage of the maximum total elastic displacement of the system, taken from 3% to 5% depending on the accuracy needed.

In Figure 5-3 a graphical description of the iteration procedure is shown for one load increment and three iterations. Convergence during iterations is assumed to have been achieved when $\Delta\delta_i$ is

$$\Delta\delta_i < (0.03 \text{ to } 0.05)\ \delta_{max} \tag{70}$$

where

δ_{max} = maximum elastic total displacement of any node under the influence of the total load assuming linear elastic response of the model.

The values of 0.03 to 0.05 were used for the problems presented in this study and they seem to provide the necessary equilibrium condition. If other geometry or materials are used the norm should be revised.

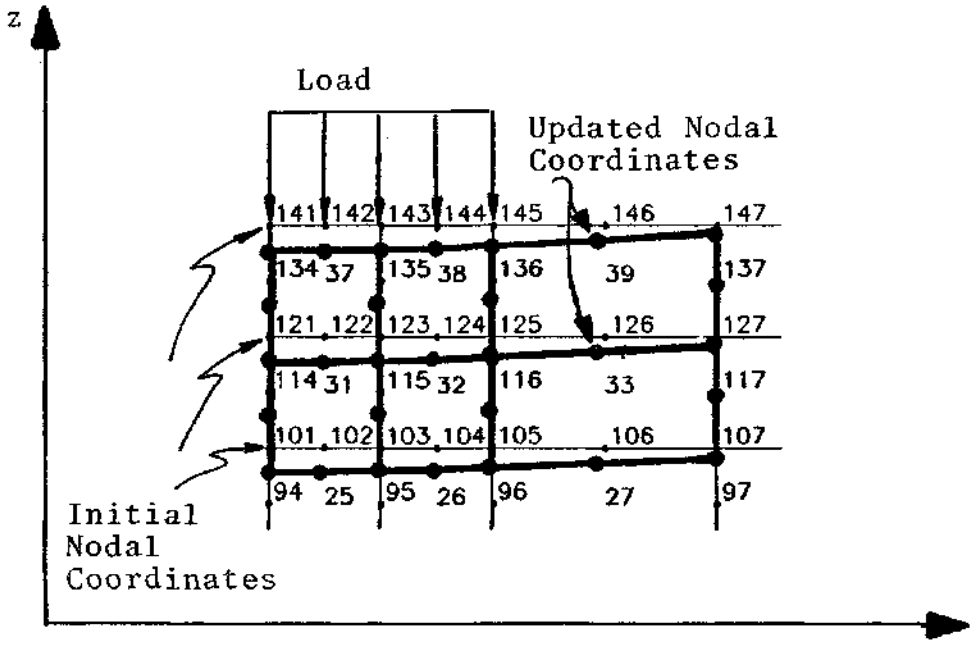

Figure 5-2. Part of a Finite Element Mesh Showing Updated Nodal Coordinates

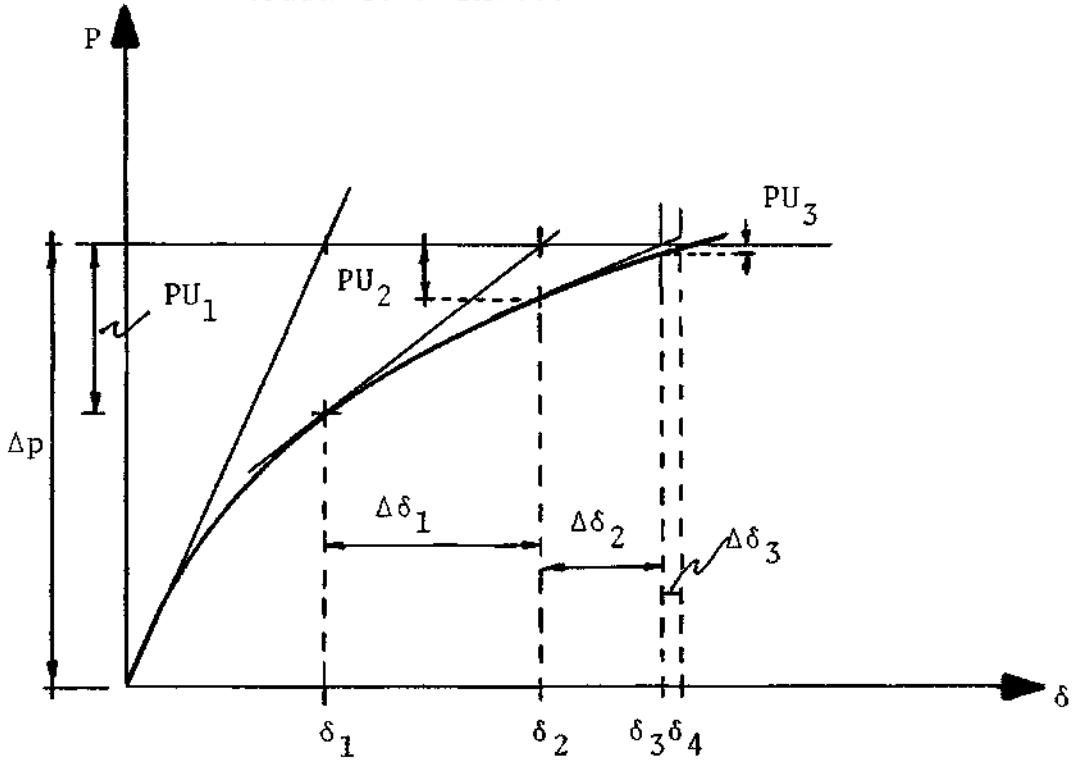

Figure 5-3. Graphical Representation of Maximum Allowable Increment of Displacement for an Iteration

Figure 5-3 shows a first unbalanced force that increases the total displacement δ by $\Delta\delta_1$ to give a total displacement δ_2 and a new unbalanced force PU_2. The procedure is repeated until $\Delta\delta_1$ is smaller than the given maximum allowable displacement for the iteration.

Summary

The updated Lagrangean formulation was presented which modifies the geometry of the model after each load increment and iteration. The element geometry is changed so the stiffness matrix of the system must be recalculated. The use of eight node isoparametric elements allows the direct computation of the element stiffness for curved deformed elements.

Updating the stiffness matrix of the system increases the computation time compared with a Newton-Raphson procedure but the number of iterations in each load increment are reduced. The stresses for the updated Lagrangean formulation are slightly more difficult to compute than the total Lagrange formulation, due to the step by step procedure applied. The stress increments are Piola-Kirchhoff stresses and need to be transformed to true Cauchy stresses. The large displacement option increases the computation time required for the numerical solution of the problem by a large percentage. For example for a typical finite element idealization of layered systems having 24 to 54 elements the computation time is approximately doubled.

CHAPTER VI

THE INTERFACE PROBLEM

Interface Behavior Including Large Displacements and Slip

The interface elements presented in Chapter IV will translate, rotate and deform due to load application. For large displacements and slip at the interface several special computations are necessary. The interface element having six springs as shown in Figure 6-1 deforms and hence has a different geometry at the end of each load increment. Since the program updates coordinates and stiffness for each load increment and iteration, this condition must be included in the derivation of the stiffness for the interface element. The following derivation takes this change into account using engineering approximations. Stresses are computed after each iteration, and the mode of behavior (no slip, slip or separation) of the element is established.

For a general case the initial configuration of the interface element is shown in Figure 6-1a. The interface element is deformed due to load application as shown in Figure 6-1b.

The normal and shear stresses are applied normal and tangential to the interface. In general a curved surface

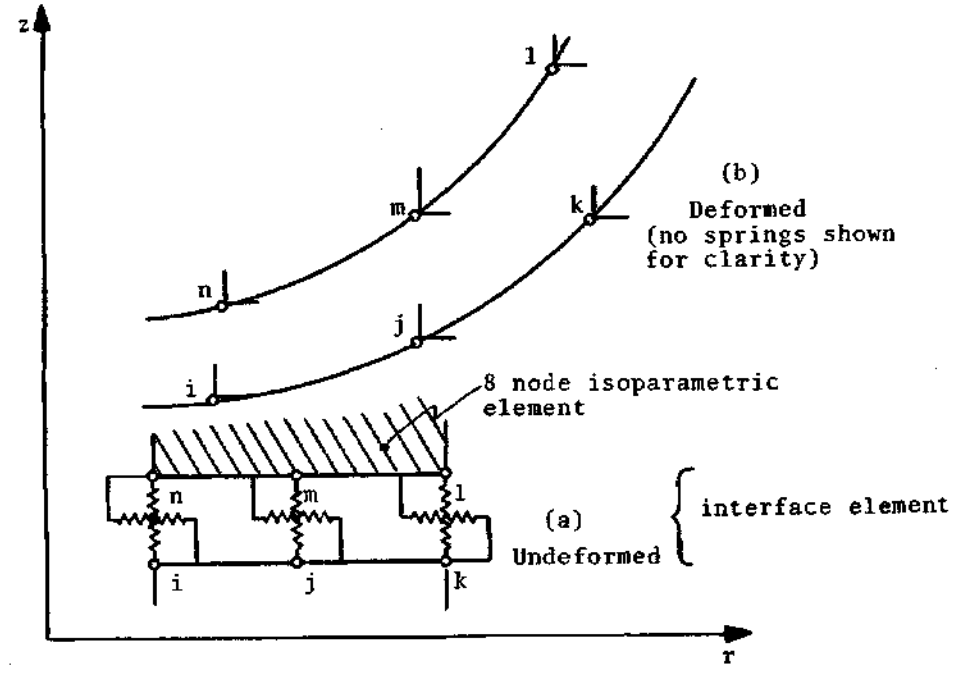

Figure 6-1. General Case of Deformation for an Interface Element

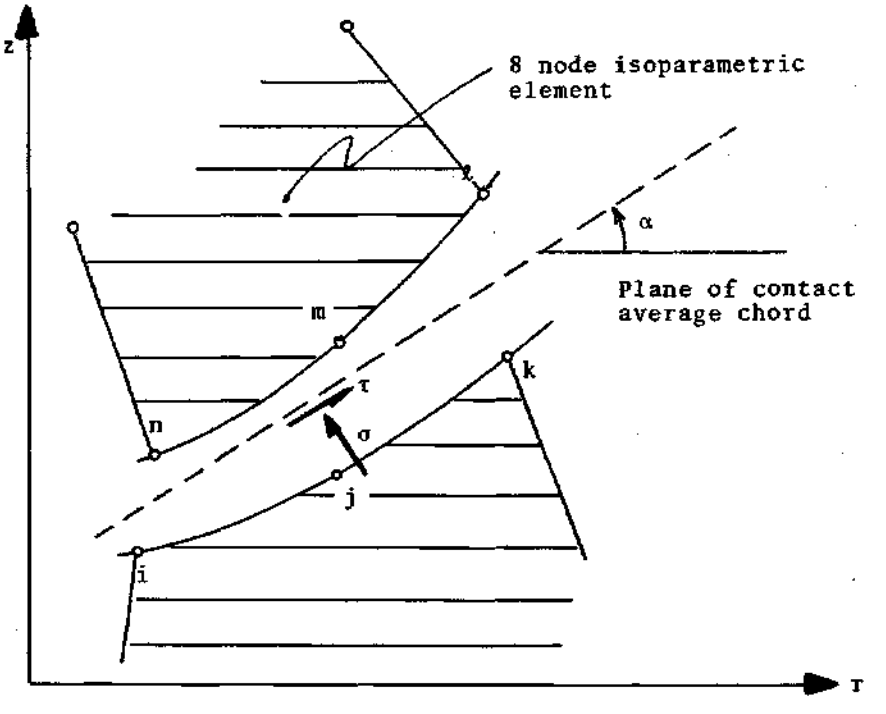

Figure 6-2. Average Plane of Contact of an Interface Element

will result after application of load and after the nodal coordinates have been updated. The curved surface is replaced in the model by conical plane segments of contact planes that are represented by the interface elements. The advantage of using planes is that the shear and normal forces are computed directly. There is no need to establish moment equilibrium equations for the curved surface, and the interface mode behavior is established with the mechanical elements acting at the interface. The geometrical approximation is close to the deformed surface of the interface as shown in Chapter X in the verification examples.

To define the behavioral mode of the element with respect to the adjacent element, all points over a segment of interface spanned by a single element (i-j-k and n-m-l, Figure 6-1a) are assumed in the same behavioral mode [60]. An engineering formulation is to compute for the interface element a representative average plane of contact, using the average chord that spans between the extreme nodes of an interface element, as shown in Figure 6-2.

This average chord will set the direction of the contact plane and the interface springs between the interface element and the regular element representing clay or gravel. The angle of inclination of the interface, α, with the horizontal r axis is computed by

$$\alpha = \tan^{-1} \frac{z_\ell + z_k - z_n - z_i}{r_\ell + r_k - r_n - r_i} \qquad (1)$$

The general case for the contact plane is shown in Figure 6-3. In case of a small number less 0.01 inch, in the denominator of equation (1), the angle α is set to 90°. The particular case of $\alpha = 90°$ is of interest for the solution of vertical interfaces. Several geotechnical problems can be analyzed by using this type of interface element such as piles, piers, and anchors.

The angle of inclination will allow computing the interface stiffness with their appropriate values. Then the transformation of the element stiffness to the global system is defined by

$$\underset{\sim}{S}_{ie} = \underset{\sim}{R}^{T}\underset{\sim}{S}\underset{\sim}{R} \tag{2}$$

where

$\underset{\sim}{S}_{ie}$ = interface element stiffness matrix for the global system

$\underset{\sim}{S}$ = interface element stiffness matrix for the local element axis

$\underset{\sim}{R}$ = rotation transformation matrix given by placing $\underset{\sim}{R}_L$ in the diagonal where

$$\underset{\sim}{R}_L = \begin{bmatrix} \cos\alpha & \sin\alpha \\ -\sin\alpha & \cos\alpha \end{bmatrix} \tag{3}$$

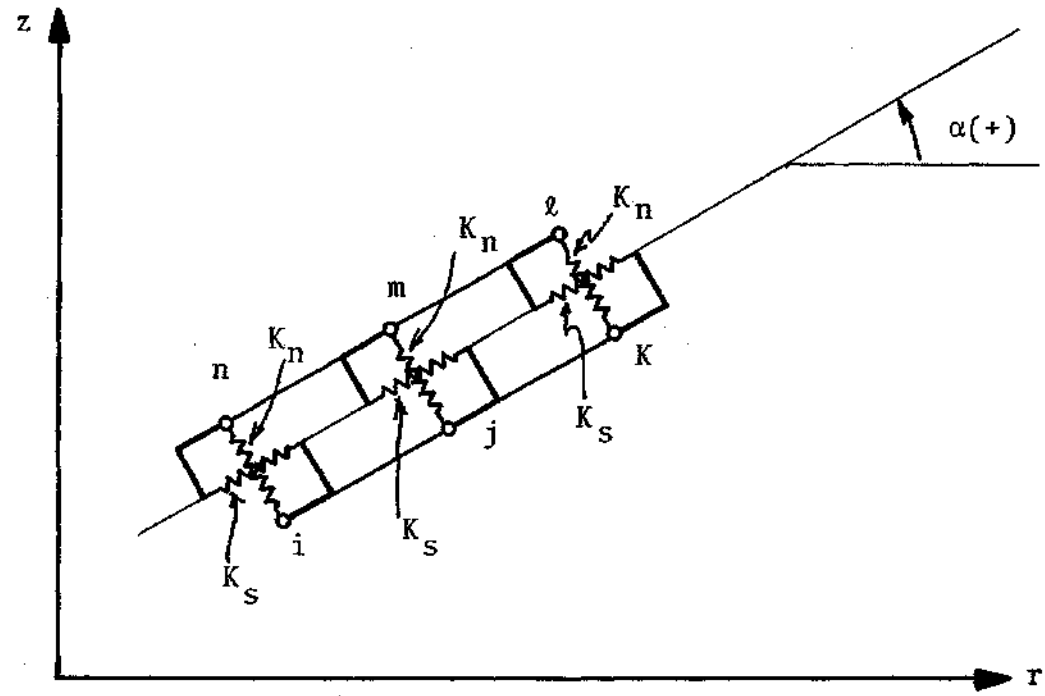

Figure 6-3. General Case of Inclination of a Contact Plane with Corresponding Spring Elements

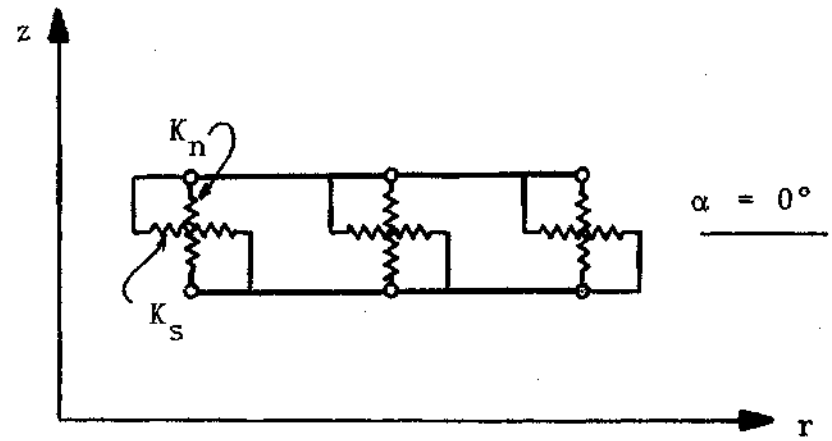

Figure 6-4. Particular Case of Horizontal Interface

and $\underset{\sim}{R}$ is a 12 x 12 matrix with diagonal elements for each spring equal to $\underset{\sim}{R}_L$, where α is the angle of inclination of the contact plane of the interface element. The angle α is measured between the r axis and the contact plane; counterclockwise is positive. Note that the direction defined by α coincides with the direction of a shear spring element (see Figure 6-3). The transformation needs to be applied to the three links of each interface element. The spring coefficients K_s and K_n (defined in Chapter IV, equations (14 and 15)) are taken as large numbers made as small as possible to give a negligible fictitious deformation which is negligible and still allow enough approximation in the computation of the interface shear stresses.

In the examples values of 4×10^6 and 9×10^6 psi for subgrade modulus k_s and k_n respectively give enough accuracy for the computer system used (CDC-Cyber 74) with 16 decimal places in single precision. Extremely large numbers for k_s or k_n present accuracy problems for the interface stress computation.

For the computation of the equivalent springs for each node of the interface element the axisymmetric load distribution factors presented in Chapter IV, equation (9), are applied. The results give a zero equivalent force and consequently zero spring force at the i node of an element that is placed with node i at the axis of symmetry. When computing the equivalent concentrated springs using axisymmetric load factors, a spring of zero stiffness is found to be located at the axis of symmetry due to the assumption of uniform vertical stress distribution

and quadratic displacement distribution along the interface element.

A computation of the actual stress distribution for the geometry of this problem was analyzed for depths of gravel of 4 to 12 inches and loaded radius areas of 3 inches. The stress distribution shows a maximum variation of about 3% from the axis of symmetry, node i to node j at 1.5 inch from the center, which justifies the assumption of uniform distribution. For the elements of the interface that share a node with the axis of symmetry, in order to have a spring at the centerline a linear displacement distribution is assumed, instead of the original quadratic distribution, between adjacent nodes parallel to the fabric represented by i and j. This particular case results in the axisymmetric load factor (AV) for i node of 1/3 of the value of the factor for node j, then:

$$AV_i = 1/3\ AV_j \tag{4}$$

This approximation is used only for the nodes of the elements of the interface that share a node with axis of symmetry, and it does not affect the shear spring coefficients, since the node is fixed in the horizontal direction.

Computation of Forces Due to Slip

The shear and normal stresses define the mode of behavior of an interface element. The interface element has three possible modes of behavior: (1) no slip, (2) slip and

(3) separation. In the no slip mode the shear forces are computed by means of the shear springs at the interface. The slip of an interface element means that the maximum allowable shear force has been "exceeded" by the computed shear of the spring forces of the interface.

For the slip case special computations are necessary. The element's contact plane direction is computed and the shear forces and normal stresses are applied at the nodes taking in account the direction of the contact plane. For the case of slip, the maximum shear stress, applying Mohr-Coulomb failure law [120] is computed by:

$$\tau_{max} = c + \sigma_z \tan\phi \qquad (5)$$

where

τ_{max} = maximum shear force

c = cohesion between the dissimilar materials

σ_z = normal stress at the interface

ϕ = angle of internal friction between the materials

When the spring shear stress is larger than τ_{max}, the difference in forces is applied to the system as an unbalanced force.

Calling P_{SLIP} the slip force which is the force computed with the maximum shear stress τ_{max} average for the element, the correction applied to the system (in other words the forces not taken by the elements in the slip mode) are:

$$P_{UN} = P_{SPRING} - P_{SLIP} \tag{6}$$

where for each spring

P_{UN} = unbalanced slip force

P_{SPRING} = forces at the spring interface

P_{SLIP} = slip force

Now the force of the spring can be computed by:

$$P_{SPRING} = \frac{\tau_s}{\tau_{max}} \cdot P_{SLIP} \tag{7}$$

τ_s = shear stress in the spring interface

τ_{max} = maximum shear stress

Then the unbalanced force P_{UN}, substituting equation (7) into (6) is given by:

$$P_{UN} = P_{SLIP} \left(\frac{\tau_s}{\tau_{max}} - 1 \right) \tag{8}$$

Now P_{UN} is applied to the system in the opposite direction to equilibrate the excess of force computed by the springs only for one iteration. Iterations are performed until the system is in equilibrium or an unstable system is encountered when the remaining spring elements are not able to take the total unbalanced shear force. The interface shear spring elements already in the slip mode are replaced by the corresponding P_{SLIP} forces, that are applied to the system. The slip forces are permanent if the element remains in the slip mode. In Figure 6-5 a graphical representation of the slip condition

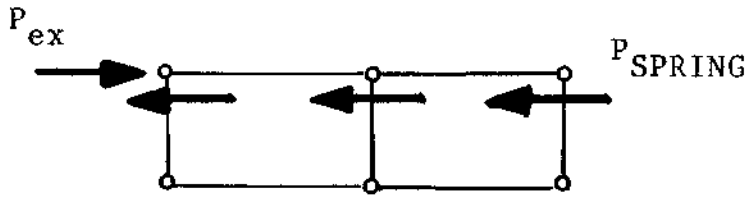

(a) Initial P_{SPRING} forces at the interface

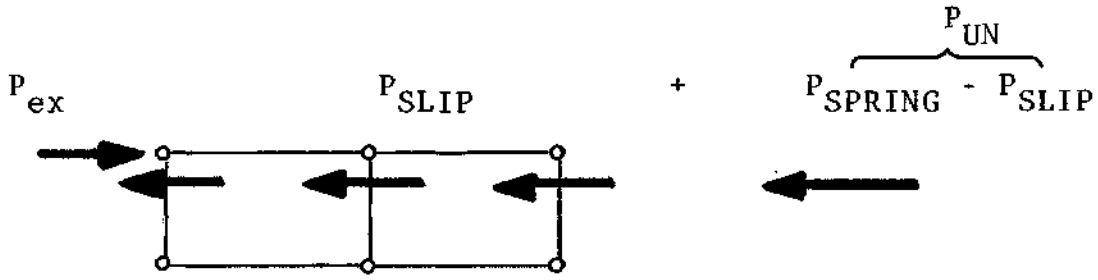

(b) Maximum shear forces

P_{UN} = unbalanced slip force applied to system in next iteration in opposite direction

P_{ex} = external load

P_{SPRING} = force taken by the springs

P_{SLIP} = maximum shear forces taken by the element

Figure 6-5. Slip Forces Correction for Spring Elements

correction is shown.

To compute the slip force P_{SLIP} for a general case of an interface element having a contact plane making an angle α with the horizontal, the nodal force components for the interface element due to the maximum shear stress are shown in Figure 6-6 and given by the next equations for the r,z coordinate axes:

$$P_{SLIP} = \left\{ \begin{array}{l} F_1 = \Delta\tau_{max} \cos\alpha \; AV_i \\ F_3 = -F_1 \\ F_5 = \Delta\tau_{max} \cos\alpha \; AV_j \\ F_7 = -F_5 \\ F_9 = \Delta\tau_{max} \cos\alpha \; AV_k \\ F_{11} = -F_9 \\ F_2 = \Delta\tau_{max} \sin\alpha \; AV_i \\ F_4 = -F_2 \\ F_6 = \Delta\tau_{max} \sin\alpha \; AV_j \\ F_8 = -F_6 \\ F_{10} = \Delta\tau_{max} \sin\alpha \; AV_k \\ F_{12} = -F_{10} \end{array} \right\} \qquad (9)$$

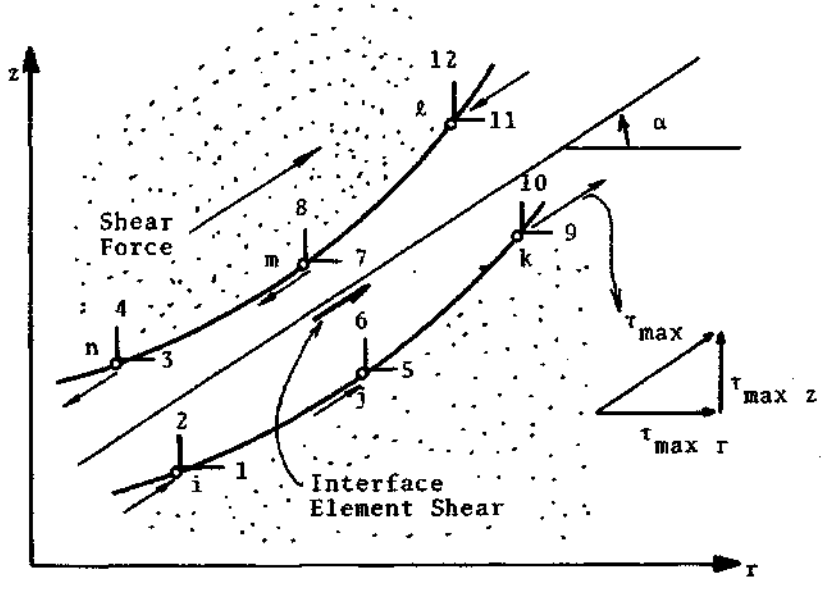

Figure 6-6. Maximum Shear Decomposition

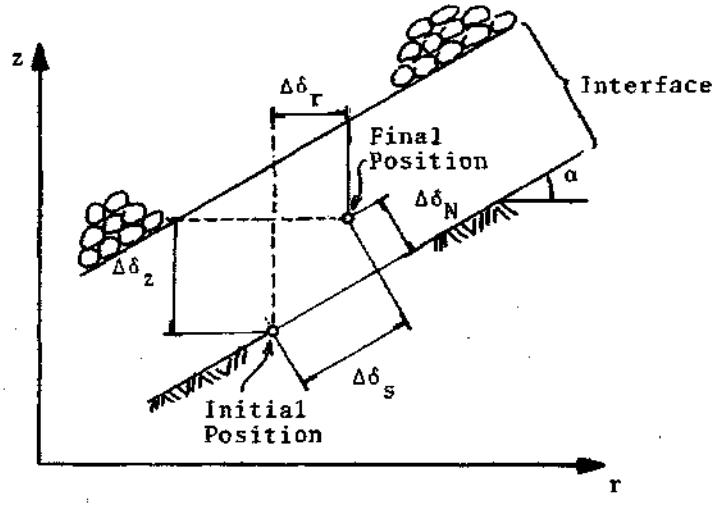

Figure 6-7. Normal and Tangential Relative Displacements of Interface Element

where

$\Delta\tau_{max}$ = maximum shear stress

α = angle of inclination from equation (1)

AV_i, AV_j and AV_k are the axisymmetric distribution factors derived in Chapter IV, equation (9).

To compute the internal forces at the interface the interface element stiffness matrix $\underset{\sim}{S}_{ie}$ and the computed displacements $\underset{\sim}{u}$ are used; the forces are given by the matrix equation:

$$\underset{\sim}{F}_{int} = \underset{\sim}{S}_{ie} \cdot \underset{\sim}{u} \tag{10}$$

where

$\underset{\sim}{F}_{int}$ = internal forces at the interface

The internal forces, the maximum shear stress, the applied external loads and the computed slip forces in the case of elements in the slip mode will permit using them in a computation routine and set the system in equilibrium complying with the maximum shear stress requirements.

Procedure for the Computation Process

A. First increment. Iterate the following steps.

1. For the first load increment no slippage is assumed and the slip flag is set to zero.
2. Compute the average relative displacements, in the r and z coordinate directions using the global coordinate system.

$$\Delta\delta_z = (\delta_4+\delta_8+\delta_{12}-\delta_2-\delta_6-\delta_{10})/3$$

$$\Delta\delta_r = (\delta_3+\delta_7+\delta_{11}-\delta_1-\delta_5-\delta_9)/3 \qquad (11)$$

where

$\Delta\delta_z, \Delta\delta_r$ = average increment of relative displacements in z and r directions, respectively

δ_n = increment of node displacement for the load increment.

At the center of the element axis the vertical relative displacement is approximated by the centroid value.

$$\Delta\delta_z = \delta_8-\delta_6 \qquad (12)$$

3. Compute the direction of the contact surface, which is given by the α angle measured from the horizontal axis r, as shown in Figure 6-2.

4. Compute the normal and tangential relative incremental displacements for the direction of the interface. As shown in Figure 6-7, $\Delta\delta_S$ is the relative shear displacement and $\Delta\delta_N$ is the relative normal displacement. The average normal incremental relative displacement, NRD, is:

$$NRD = \Delta\delta_z\cos\alpha-\Delta\delta_r\sin\alpha \qquad (13)$$

and the average incremental shear relative displacement, SRD, is:

$$SRD = \Delta\delta_z \sin\alpha + \Delta\delta_r \cos\alpha \tag{14}$$

5. The increment in normal stress

$$\Delta\sigma = K_n \cdot NRD \tag{15}$$

and the increment in shear stress

$$\Delta\tau = K_s \quad SRD \tag{16}$$

6. Accumulate the stresses of the spring elements for complete bond, for iteration j the shear stress is:

$$\tau^j = \tau^i + \Delta\tau^j \tag{17}$$

where

τ^i = shear stress previous iteration i

$\Delta\tau^j$ = increment of shear stress for the iteration

Then compute the normal stress of the element, $\sigma_n{}^j$

$$\sigma_n{}^j = \sigma_n{}^i + \Delta\sigma^j \tag{18}$$

where

σ_n^i = normal stress from previous iteration i

$\Delta\sigma^j$ = increment in normal stress for the iteration

7. Compute the maximum shear τ_{max} with the use of Mohr-Coulomb failure law:

$$\tau_{max} = c + \sigma_n \tan\phi \tag{19}$$

where

c = cohesion or adhesion between the interface materials

ϕ = interface angle of internal friction between the interface materials

8. Determine mode behavior of the element. First test for slip:

$$\text{If } |\tau_{max}| < \tau^j, \text{ slip is occurring;} \tag{20}$$

$$\text{if } |\tau_{max}| > \tau^j, \text{ no slip takes place.}$$

The algorithm to set the mode behavior is given in [60] and is presented in Chapter IX.

The test for slip involves the case above and the case below the interface. If slip occurs, the slip flag is set to one which sets the behavioral mode of the particular interface element for the next load increment. For the no slip condition the flag is set to zero, and for separation it is set to two.

If the system has elements in the slip mode then iterations are necessary to comply with the general equilibrium of the system. For the elements in slip, the spring shear stiffness is neglected and iterations performed with the unbalanced force applied to the system. This force is given by the equilibrium equation of the system:

$$P_{UB} = P_{ex} - (P_{int} + P_{corr} - P_{slip}) \tag{21}$$

where

P_{UB} = unbalanced force

P_{ex} = external forces

P_{int} = internal forces

$P_{corr} = P_{SLIP} \cdot \frac{\tau_s}{\tau_{max}}$

P_{SLIP} = slip force given by equation (9)

τ_s = spring shear stress

τ_{max} = maximum shear stress given by Mohr-Coulomb's law

10. At the end of the iteration process the actual bond stress for the case of no slip is the stress computed due to the shear springs. For the case of slip in the maximum shear stress computed by Mohr-Coulomb Law, resulting in the P_{SLIP} forces.

11. For the case of separation, forces equal in magnitude but in opposite direction to the internal forces of the interface are applied to the system, and both shear and normal stiffness spring coefficients are set to zero. The

forces are applied as an internal force of the system, and equilibrium iterations are performed.

B. Subsequent Load Increments

1. The system is in equilibrium and now the load increment with the additional P_{SLIP} forces are applied to the system. The P_{SLIP} forces substitute for the neglected shear springs. The applied load to the system is then P which is given by:

$$P = P_{INC} + P_{SLIP} \tag{22}$$

P_{INC} = increment of load

P_{SLIP} = forces due to SLIP for elements in the slip mode

2. Steps 2 to 11 from Part A are executed for the new load increment.

Fabric Element Subjected to Large Displacements

After introducing the higher order terms into the computation of displacements, a modified strain displacement matrix $\underset{\sim}{B}$ is needed. Following the general formulation for large displacements of the isoparametric eight node elements given in Chapter V, a similar derivation is presented for the fabric element.

The radial strain with the higher order terms included is given by:

$$\varepsilon_r = \frac{\partial u'}{\partial r} + \frac{1}{2}\left(\frac{\partial u'}{\partial r}\right)^2 \tag{23}$$

where

u' = local "axial" displacement of the member

r = horizontal axis

Using the local coordinate axis RP to define the axial displacement u', the equations (22) to (24) of Chapter IV and equation (36) of Chapter V, then for the tangential strain we have:

$$\varepsilon_\theta = \frac{u'}{r}\cos\alpha + \frac{1}{2}\left(\frac{u'}{r}\cos\alpha\right)^2 \tag{24}$$

Dividing the strains into small or infinitesimal displacement terms and finite displacement terms that correspond to the higher order terms, the total strain is given by:

$$\underset{\sim}{\varepsilon} = \underset{\sim}{\varepsilon}^I + \underset{\sim}{\varepsilon}^L \tag{25}$$

where

$\underset{\sim}{\varepsilon}^I$ = small displacements strain

$\underset{\sim}{\varepsilon}^L$ = large displacements strain

The superscript L is used for finite displacement terms so the higher order strain terms are:

$$\varepsilon_r^L = \frac{1}{2}\left(\frac{\partial u'}{\partial r}\right)^2 \tag{26}$$

$$\varepsilon_{\theta}^{L} = \frac{1}{2}\left(\frac{u'}{r}\cos\alpha\right)^2 \tag{27}$$

Equations (26) and (27) in matrix form are given by:

$$\underset{\sim}{\varepsilon}^{L} = \begin{Bmatrix} \varepsilon_r^L \\ \varepsilon_\theta^L \end{Bmatrix} = \frac{1}{2}\begin{bmatrix} \frac{\partial u'}{\partial r} & \frac{\partial u'}{\partial r} \\ \frac{u'}{r}\cos\alpha & \frac{u'}{r}\cos\alpha \end{bmatrix}\begin{Bmatrix} \frac{\partial u'}{\partial r} \\ \frac{u'}{r}\cos\alpha \end{Bmatrix} \tag{28}$$

then we can define $\underset{\sim}{\varepsilon}^{L}$ in terms of $\underset{\sim}{A}$ and $\underset{\sim}{\theta}$ the two matrices of the right side of equation (28).

$$\underset{\sim}{\varepsilon}^{L} = \frac{1}{2}\underset{\sim}{A}\underset{\sim}{\theta} \tag{29}$$

Differentiating ε^{L} and using the chain rule

$$d\underset{\sim}{\varepsilon}^{L} = \frac{1}{2}\, d\underset{\sim}{A}\cdot\underset{\sim}{\theta} + \frac{1}{2}\underset{\sim}{A}d\underset{\sim}{\theta} = \underset{\sim}{A}d\underset{\sim}{\theta} \tag{30}$$

Refer to [147] for a complete derivation of matrix equation (30).

Using formulas (29) and (30) from Chapter IV, the derivative of the displacement u' with respect to r according to the definitions given in equations (23) and (24) of the same Chapter is:

$$\frac{\partial u'}{\partial r} = \frac{1}{L} \left[-\cos\alpha \ -\sin\alpha \ \cos\alpha \ \sin\alpha\right] \begin{Bmatrix} u_1 \\ v_1 \\ u_2 \\ v_2 \end{Bmatrix} \tag{31}$$

and

$$\frac{u'}{r}\cos\alpha = \frac{1}{2RI}\left[(1-RP)\cos^2\alpha \ (1-RP)\sin\alpha\cos\alpha \ (1+RP)\cos^2\alpha \ \ldots \right.$$
$$\left. \ldots \ (1+RP)\sin\alpha\cos\alpha\right] \begin{Bmatrix} u_1 \\ v_1 \\ u_2 \\ v_2 \end{Bmatrix} \tag{31a}$$

where

$$RI = (r_i+r_j)/2 + (RP\cdot L/2)\cos\alpha$$

Defining a matrix $\underset{\sim}{G}$ that multipled by the displacement vector $\underset{\sim}{u}$ gives the strain terms defined in equations (31) and (31a):

$$\underset{\sim}{\theta} = \underset{\sim}{G}\cdot\underset{\sim}{u} \tag{32}$$

where

$$\underset{\sim}{\theta} = \begin{Bmatrix} \dfrac{\partial u'}{\partial r} \\ \\ \dfrac{u'}{r}\cos\alpha \end{Bmatrix}$$

Then by substituting equations (31) and (31a) in (32) we have the expression:

$$\begin{Bmatrix} \frac{\partial u'}{\partial r} \\ \\ \frac{u'}{r}\cos\alpha \end{Bmatrix} = \begin{bmatrix} -\frac{\cos\alpha}{L} & -\frac{\sin\alpha}{L} & \frac{\cos\alpha}{L} & \frac{\sin\alpha}{L} \\ \\ \frac{(1-RP)\cos^2\alpha}{2\cdot RI} & \frac{(1-RP)\sin\alpha\cos\alpha}{2\cdot RI} & \frac{(1+RP)\cos^2\alpha}{2\cdot RI} & \frac{(1+RP)\sin\alpha\cos\alpha}{2\cdot RI} \end{bmatrix} \tag{33}$$

Equations (29) and (30) of Chapter IV are equivalent to the matrix equation (33) just derived. The definition of the strain-displacement matrix given by equation (32) of Chapter IV is equated to equation (33) and for this case

$$\underset{\sim}{G} = \underset{\sim}{B} \tag{34}$$

Differentiating equation (32) and substituting $d\theta$ into equation (30) we have

$$d\underset{\sim}{\varepsilon}^L = \underset{\sim}{A}\cdot\underset{\sim}{G}\cdot du \tag{35}$$

The strain-displacement matrix for large displacements is now obtained directly from (35) and is given by:

$$\underset{\sim}{B}_L = \underset{\sim}{A}\cdot\underset{\sim}{G} \tag{36}$$

Now the element stiffness matrix including higher order terms can be evaluated. In the following sections the derivation of the stiffness matrix of a fabric element is presented.

Computations and Numerical Integration of the Stiffness Matrix for the Fabric Element

The stiffness matrix of a fabric element is given by:

$$\underset{\sim}{S}_f = \int_V \underset{\sim}{B}^T \underset{\sim}{D} \underset{\sim}{\bar{B}} dv \tag{37}$$

Since there is no thickness associated with this element

$$\underset{\sim}{S}_f = \int_A \underset{\sim}{B}^T \underset{\sim}{D} \underset{\sim}{\bar{B}} dA \tag{38}$$

where

$$\underset{\sim}{\bar{B}} = \underset{\sim}{B} + \underset{\sim}{B}_L \tag{39}$$

and the stress-strain relation is:

$$\underset{\sim}{D} = \begin{bmatrix} E_f & 0 \\ 0 & E_f \end{bmatrix} \tag{40}$$

as defined in Chapter IV. The matrix multiplication of $\underset{\sim}{B}^T \underset{\sim}{D} \underset{\sim}{B}$ results in four terms and the element stiffness matrix for the fabric is

$$S_f = \int_A (\underset{\sim}{B}^T \underset{\sim}{D} \underset{\sim}{B} + \underset{\sim}{B}^T \underset{\sim}{D} \underset{\sim}{B}_L + \underset{\sim}{B}_L^T \underset{\sim}{D} \underset{\sim}{B} + \underset{\sim}{B}_L^T \underset{\sim}{D} \underset{\sim}{B}_L) dA \tag{41}$$

where $\underset{\sim}{B}$ and $\underset{\sim}{B}_L$ were defined in equation (34) of Chapter IV and (36) respectively.

The first term $\int_A \underset{\sim}{B}^T \underset{\sim}{D}\underset{\sim}{B}\, dA$ corresponds to the regular small displacement stiffness matrix of the element $\underset{\sim}{S}_{fI}$ and the remaining three terms form

$$\underset{\sim}{S}_{fL} = \int_A (\underset{\sim}{B}^T \underset{\sim\sim}{D}\underset{\sim}{B}_L + \underset{\sim}{B}_L^T \underset{\sim\sim}{D}\underset{\sim}{B} + \underset{\sim}{B}_L^T \underset{\sim\sim}{D}\underset{\sim}{B}_L)\, dA \tag{42}$$

which is the finite displacement stiffness contribution matrix.

The matrix multiplication and numerical integration for the four terms of (41) can be performed for each element and incorporated into the general stiffness matrix of the system. The numerical integration used for this element is a two point numerical integration, and the derivation is as follows:

$$\int_A (\beta) r\, d\theta\, dr = \int_{-1}^{1} (\beta) r\, d\theta \det J\, dRP \tag{43}$$

where β is the factorized terms in parentheses of equation (41). Since the coordinate transformation is given by:

$$dr = \det|J|\, dRP \tag{44}$$

and r is given by

$$r = ((r_i + r_j)/2) + RP \cdot \frac{L}{2} \cos\alpha \tag{45}$$

Now define RI as:

$$RI = r = ((r_i+r_j)/2) + RP(r_j-r_i)/2 \tag{46}$$

For example, for the $\underset{\sim}{B}^T\underset{\sim\sim}{D}\underset{\sim}{B}$ term of equation (42) we have the element stiffness matrix of the fabric element for small strains given by:

$$\underset{\sim}{S}_{fI} = \int_{-1}^{1} RI \cdot 2\pi \; \underset{\sim}{B}^T\underset{\sim\sim}{D}\underset{\sim}{B} \det|J| dRP \tag{47}$$

where the determinant of the Jacobian for a linear element is

$$\det|J| = \frac{L}{2}$$

Finally the stiffness matrix of the fabric element can be numerically integrated by:

$$\underset{\sim}{S}_{fI} = \pi L \sum_{i=1}^{n} RI \cdot \underset{\sim}{B}^T\underset{\sim\sim}{D}\underset{\sim}{B} \cdot WT \tag{48}$$

where

n = number of sampling points

WT = weight factor for a two point numerical integration [147]

For the two point numerical integration used, WT = 1 (see Figure 6-8), the element stiffness matrix is:

$$\underset{\sim}{S}_{fI} = \pi L \sum_{k=1}^{2} r_k \underset{\sim}{B}^T\underset{\sim\sim}{D}\underset{\sim}{B} \tag{49}$$

The numerical integration computations for equation (42) are performed in the same way as explained above with the

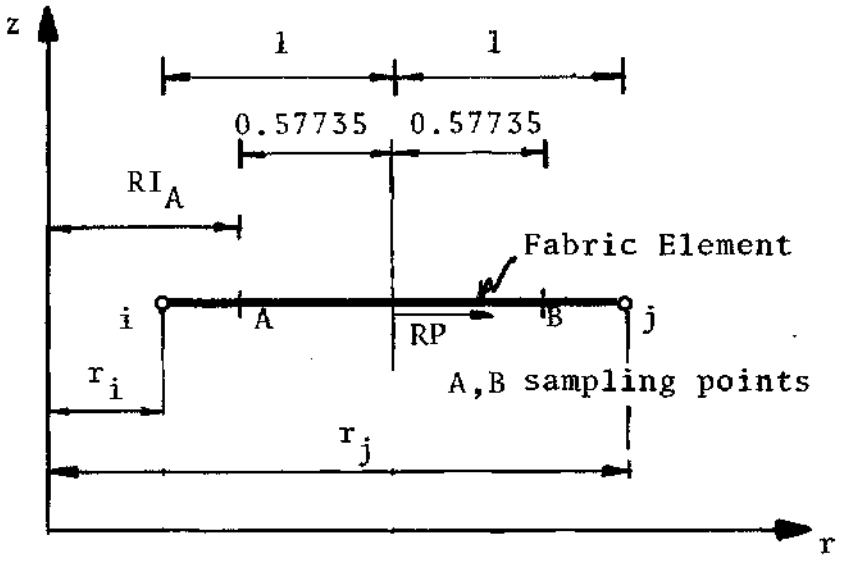

Figure 6-8. Fabric Element Sampling Points A and B for Two Point Numerical Integration

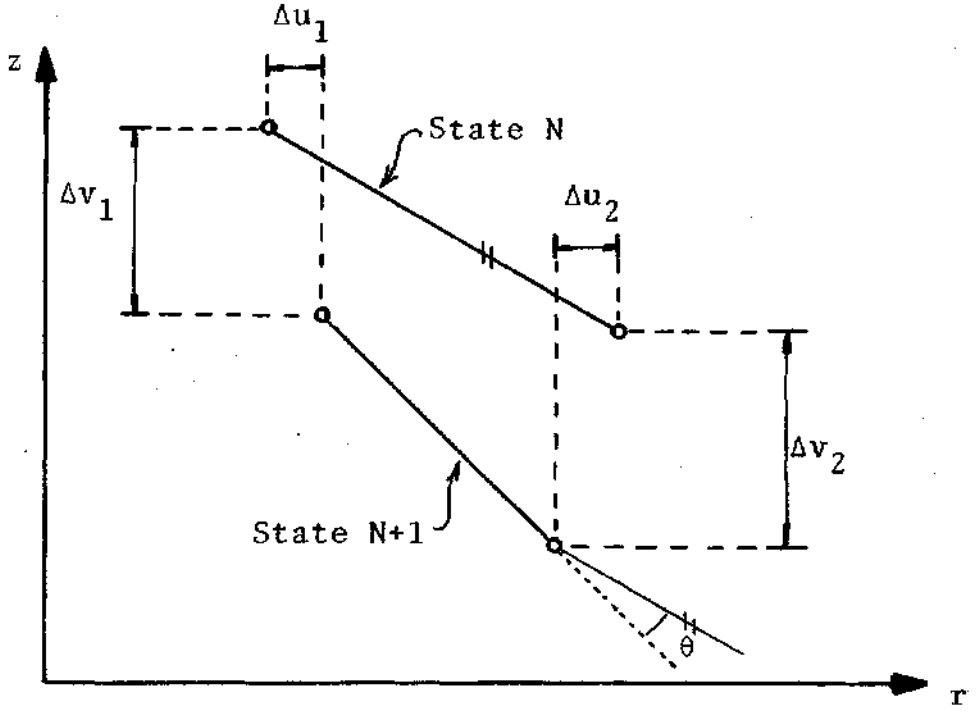

Figure 6-9. Change of Coordinates of Fabric Element

appropriate use of $\underset{\sim}{B}$ and $\underset{\sim}{B}_L$.

The large displacement stiffness can only be computed after applying the first load increment since the terms are a function of the derivatives of the displacements with respect to the system coordinates. All stiffness terms are then placed in the general stiffness matrix of the system. A small increment of displacement is needed for accurate computation of stresses.

Fabric Element--Stress Transformation

Assume a fabric element at state N. Due to the current load increment it deforms to state N+1 with the change in coordinates of the nodes i and j given by Δu_1, Δu_2, Δv_1 and Δv_2 as shown in Figure 6-9.

The computations for stress and strain for the element are performed for two-sampling points and the average value is taken as representative of the response of the element. Due to large displacements the length and area of the element will change and a correction for the new geometry is needed. The corrected axial stress is obtained by multiplying the axial stress obtained by the correction factor AVR due to change in area given by:

$$AVR = \frac{[(r_i+r_j)/2]_N}{[(r_i+r_j)/2]_{N+1}} \tag{50}$$

which is the ratio of the radial distance of the centroid of the element for state N and N+1 (Figure 6-9).

For the tangential stress correction the change of area will be given approximately by the change in length of the element. The tangential stress factor is then:

$$AVT = \frac{[(r_j-r_i)^2 + (z_j-z_i)^2]_N^{1/2}}{[(r_j-r_i)^2 + (z_j-z_i)^2]_{N+1}^{1/2}} \tag{51}$$

The true radial and tangential stresses for large displacements are computed using for the radial stress the following transformation:

$$\tau_r^{N+1} = (\tau_r^N + \Delta S_r) \cdot AVR \tag{52}$$

and for the tangential stress:

$$\tau_T^{N+1} = (\tau_T^N + \Delta S_T) AVT \tag{53}$$

where

ΔS_r = computed radial stress increase for the current load increment

ΔS_T = computed tangential stress increase for the current load increment

τ_r^N and τ_T^N = true radial and tangential stress for state N

τ_r^{N+1} and τ_T^{N+1} = true radial and tangential stress for state N+1

The complex problem of a flexible membrane embedded in the soil is solved by a linear fabric element which approximates the true behavior of the membrane. The fabric element presented is not stressed by initial vertical differential displacements. The differential vertical displacements are accounted for in the following iterations and load increments. The large displacement strain terms are also computed after the first load increment since they are a function of the displacements.

As a result large load increments can not be initially applied since the fabric stresses would be poorly approximated. In Chapter X an example is presented of a two dimensional model of a fabric element subjected to tension and compared with the theoretical elastic solution. The behavior of the fabric element in the soil-fabric system is also presented in the examples given in Chapter X where a system is compared with and without fabric.

CHAPTER VII

SOIL PLASTICITY

Introduction

The theory of elasticity in soil mechanics has been a valuable tool to obtain approximate solutions to many geotechnical problems. Inaccuracies occur when linear elastic behavior is assumed since geotechnical materials experience nonlinear behavior from early stages of load application. The soil does not follow Hooke's law, and frequently in localized zones enters a plastic flow state at low stress levels. A second valuable tool in soil mechanics is the theory of stability or limit load analysis. Collapse loads are computed satisfying statics and using a compatible stress distribution. The method has produced many solutions in geotechnical problems such as the analysis and design of footings, retaining walls and slope stability [123,124]. The theory of consolidation and viscosity effects are also very important considerations in geotechnical engineering.

Several of the classic texts in soil mechanics, elasticity and plasticity [123,124,127] present the basis of the soil plasticity theory. A brief review of the most important theories used in soil mechanics follows. In 1773 Coulomb developed the shear resistance in form of the present Coulomb law. In 1857 Rankine considered limit plastic equilibrium,

which is defined by slip surfaces together with the computational procedures for the pressures produced by the soil in active and passive states. Mohr in 1882 presented the theory to compute the principal stresses and the state of stresses in any plane. Mohr's formulas together with Coulomb's law form the Mohr-Coulomb failure criteria for soils. Recent laboratory tests have shown that the failure criteria of soils is closely represented by Mohr-Coulomb law [31,33].

By 1900 Kotter developed a method for the computation of limit loads on slip surfaces combining equilibrium and failure conditions. K. Terzagi in his 1943 text [123] presented the methods and solutions for many of the limit load soil mechanics problems that required computation of limit loads.

These theories, however, neglect the stress-strain behavior of the soil materials that can be important for the prediction of the actual behavior of the soil structure.

The analysis of the plastic behavior of metals developed the basis for the theory of plasticity [64,127]. Von Mises in 1913 established the assumptions for the yield criteria for metals which has also been applied to concrete. Failure analysis for metals and the development of the plasticity theory are the basis of the soil plasticity theory. For soils the original von Mises yield criterion needs extensions and modifications to improve the representation soil behavior.

Analytical and experimental models have been used to verify the complex mechanical behavior of soil materials using the von Mises yield criteria and several extensions and modifications proposed for different soil materials [33,90,92, 137,144]. It is important to state that viscosity and consolidation are not directly considered in the development of the finite element formulation. These effects can be considered indirectly in an approximate way by proper correlation with the laboratory test procedures.

To include the changes in soil behavior due to changes in the confining conditions an extended von Mises yield criterion was proposed by Drucker-Prager [38]. This yield criterion in the context of the finite element method can be readily used for the analysis of elastic-plastic soil materials [33], as shown in the next derivations.

Soil Plasticity

Geotechnical materials experience at all load levels a certain amount of plastic behavior; and upon load removal sand, clay or silt experience a recoverable elastic deformation and a permanent plastic deformation. The total strain of the body can be expressed as the sum of the elastic and plastic strains

$$\varepsilon = \varepsilon_e + \varepsilon_p \tag{1}$$

where

ε = total strain

ε_e = elastic strain

ε_p = plastic strain

Unloading a material will immediately determine if the material is elastic, with no permanent deformations, or plastic, with permanent deformations in which the stress-strain curve is stress history dependent. In the finite element formulation the soil materials can be successfully represented by an elasto-plastic model [33,90,137,141].

Repeated loadings applied to an elasto-plastic material cause the accumulation of permanent and displacements which may be important for the actual design and operation of the soil structure or foundation. For this reason it is important to be able to predict the nonlinear and plastic behavior of the subsoil. The present mathematical formulation includes the nonlinear and plastic characteristics of the soil materials and takes these important parameters into account in the general formulation of this study. The applied load is taken by the effective stresses, and the only provision to include pore pressures is as concentrated node loads in the system; no special formulations are included for pore pressures.

By means of the uniaxial stress-strain relationship and the unloading of the material it is possible to determine if the material is elastic or plastic. The plastic material will show permanent strains, ε_p, as shown in Figure 7-1. The

plastic or permanent deformation begins when the yield stress σ_y is reached, the mechanical models of the elastic and plastic behaviors are a spring and a friction bar as shown in Figure 7-2.

The material can be represented by a perfectly elastic-plastic model shown in Figure 7-1a or a strain hardening non-linear model shown in Figure 7-1b.

In a general state of stresses the concept of yield stresses must be generalized. For most of the engineering materials R. von Mises in 1913 proposed the following yielding hypothesis, using octahedral shear stress or octahedral stress as it is commonly called and the aid of a principal stress plot. von Mises criterion states that yielding occurs at a constant value of $9\tau_0^2$ where τ_0 is the octahedral shear stress. From the magnitude of the shearing stress on a plane it can be shown [120] that

$$9\tau_0^2 = (\sigma_1-\sigma_2)^2 + (\sigma_2-\sigma_3)^2 + (\sigma_3-\sigma_1)^2$$

or

$$\tau_0 = 1/3\ [(\sigma_1-\sigma_2]^2 + (\sigma_2-\sigma_3)^2 + (\sigma_3-\sigma_1)^2]^{1/2} \qquad (2)$$

where

$\sigma_1,\sigma_2,\sigma_3$ = principal stresses.

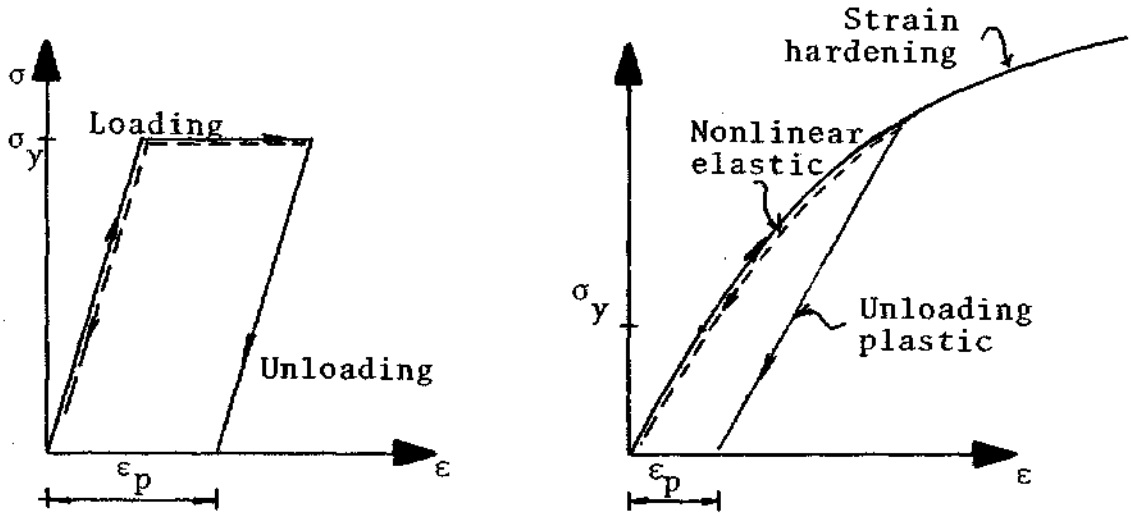

(a) Ideally plastic material

(b) Nonlinear material strain hardening or softening

Figure 7-1. Elastic and Plastic Material Behavior

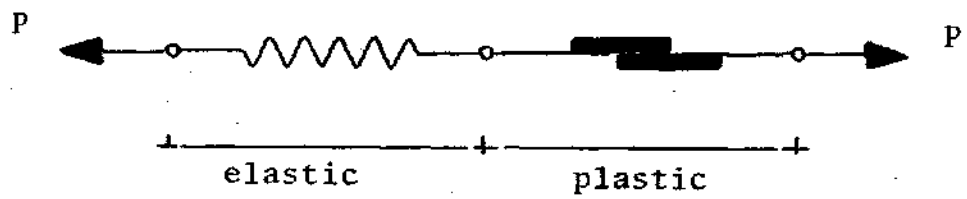

Figure 7-2. Mechanical Model of an Ideal Elasto-Plastic Material

This relationship is then used in the basic equations of plasticity. It is useful to introduce also the following formulas used in the derivation of the plasticity parameters of the material. The average or mean normal stress σ_m is given by:

$$\sigma_m = \frac{1}{3} (\sigma_1+\sigma_2+\sigma_3) = \frac{1}{3} (\sigma_r+\sigma_z+\sigma_\theta) \tag{3}$$

where

$\sigma_r, \sigma_\theta, \sigma_z$ = axisymmetric normal stress components.

And the second invariant J_2 is given by several analytical expressions, with two of them being as follows

$$J_2 = \frac{1}{6} (\sigma_1-\sigma_2)^2 + (\sigma_2-\sigma_3)^2 + (\sigma_3-\sigma_1)^2 \tag{4}$$

or in terms of the cylindrical coordinates r, z and θ.

$$J_2 = \frac{1}{2} (S_r^2 + S_\theta^2 + S_z^2) + \tau_{rz}^2 \tag{5}$$

where

$$\begin{aligned} S_r &= \sigma_r-\sigma_m \\ S_\theta &= \sigma_\theta-\sigma_m \\ S_z &= \sigma_z-\sigma_m \end{aligned} \tag{6}$$

and τ_{rz} is the shear stress acting on plane rz.

Comparing equations (2) and (4) we can show that

$$J_2 = \frac{3}{2} \tau_0^2 \tag{7}$$

Following the concept of yielding proposed by von Mises, several yield criteria can be established for the general state of multiaxial stress. It is postulated that yielding occurs if the stresses satisfy the yield criterion.

$$F(\sigma,\kappa) = 0 \tag{8}$$

where

F = failure criterion

σ = stress state

κ = hardening parameter

The yield condition can be visualized as a surface in the n-dimensional space of stress, with the position of the surface dependent on the instantaneous value of the strain hardening parameter κ. The yield surface is shown in Figure 7-3. Yielding first begins when $\bar{\sigma}$ exceeds $\bar{\sigma}_0$. This condition can be determined by experiment, as shown in Figure 7-4a.

The basic constitutive relation that defines the plastic strain increments in relation to the yield surface is the flow rate or normality principle, first suggested by von Mises. The following hypothesis appears to be acceptable [147]. The increment of plastic strain is given by

$$d\epsilon_p = \lambda \frac{\partial F}{\partial \sigma} \tag{9}$$

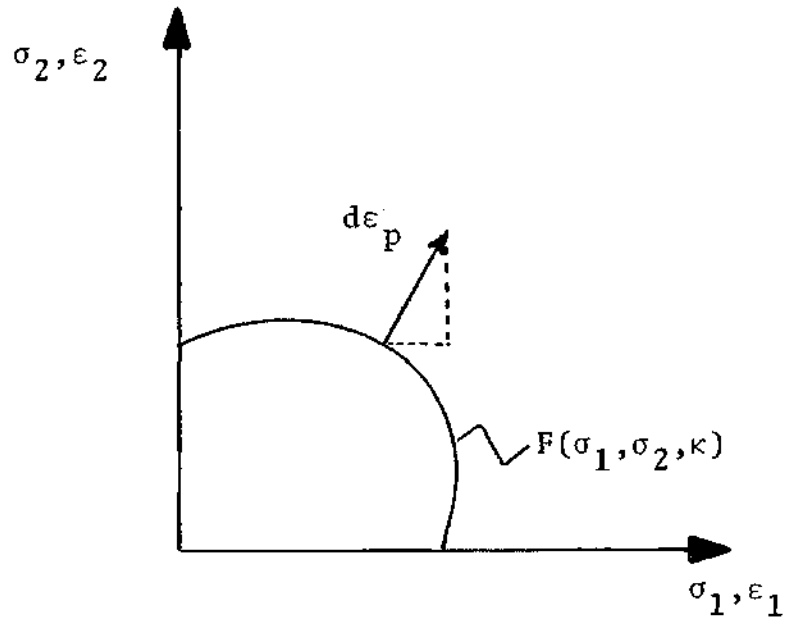

Figure 7-3. Yield Surface for Associated Plasticity

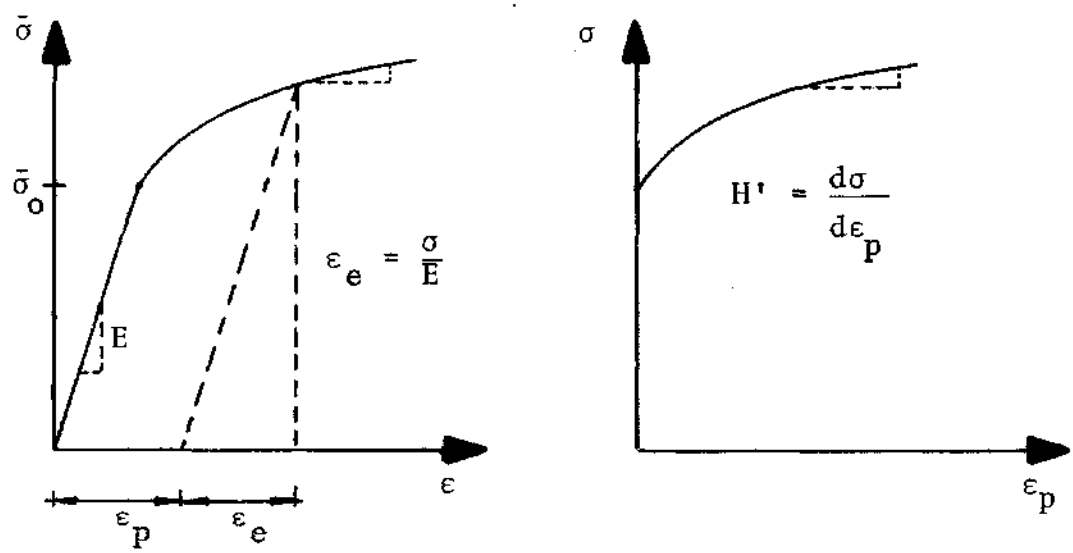

(a) Initial yield and subsequent plastic behavior

(b) Stress-plastic strain curve

Figure 7-4. Elastic and Plastic Strains Defining H'

where

λ = a proportionality constant yet undetermined

This rule is known as the normality principle because it requires that the plastic strain increment vector be normal to the yield surface in the space of n-dimensions as shown in Figure 7-3. An elimination of the restriction that plastic stress be normal to the yield surface and the above rule can be obtained by specifying a plastic potential Q as a function of the stress and the hardening factor κ:

$$Q = Q(\sigma,\kappa) \tag{10}$$

The plastic potential Q defines the plastic strain increment similar to equation (9) as:

$$d\varepsilon_p = \lambda \frac{\partial Q}{\partial \sigma} \tag{11}$$

If the plastic potential Q = F, the case is known as associated plasticity. When this relation is not satisfied, the plasticity is nonassociated.

Using equations (1) and (11) and the elasticity matrix $\underset{\sim}{D}$ we can write

$$d\varepsilon = \underset{\sim}{D}^{-1} d\sigma + \lambda \frac{\partial Q}{\partial \sigma} \tag{12}$$

When plastic yield is occurring the stresses are on the yield surface given by equation (8); differentiating it we can write:

$$dF = \frac{\partial F}{\partial \sigma_1} d\sigma_1 + \frac{\partial F}{\partial \sigma_2} d\sigma_2 + \ldots + \frac{\partial F}{\partial \kappa} d\kappa = 0 \tag{13}$$

Defining

$$\frac{\partial F}{\partial \kappa} d\kappa = -A \cdot \lambda \tag{14}$$

we can write equation (13) as:

$$\{\frac{\partial F}{\partial \sigma}\}^T \, d\underset{\sim}{\sigma} - A\lambda = 0 \tag{15}$$

where A is a parameter function of the strain hardening characteristics of the material.

Equations (12) and (15) in matrix form are

$$\begin{Bmatrix} d\varepsilon \\ 0 \end{Bmatrix} = \begin{bmatrix} \underset{\sim}{D}^{-1} & \frac{\partial Q}{\partial \sigma} \\ \{\frac{\partial F}{\partial \sigma}\}^T & -A \end{bmatrix} \begin{Bmatrix} d\sigma \\ \lambda \end{Bmatrix} \tag{16}$$

Multipling the first row by $\{\frac{\partial F}{\partial \sigma}\}^T \underset{\sim}{D}$ we have:

$$\{\frac{\partial F}{\partial \sigma}\}^T \, d\sigma = \{\frac{\partial F}{\partial \sigma}\}^T \, \underset{\sim}{D} \, d\varepsilon - [\{\frac{\partial F}{\partial \sigma}\}^T \, \underset{\sim}{D} \{\frac{\partial Q}{\partial \sigma}\}]\lambda \tag{17}$$

Substituting the first row of the matrix in equation (16) into the second row gives:

$$\{\frac{\partial F}{\partial \sigma}\}^T \, \underset{\sim}{D} \, d\varepsilon - [\{\frac{\partial F}{\partial \sigma}\}^T \, \underset{\sim}{D} \, \frac{\partial Q}{\partial \sigma} + A]\lambda = 0 \tag{18}$$

Now λ is obtained from (18) and substituted into (17). In this way λ is eliminated obtaining:

$$d\sigma = \underset{\sim}{D} \, d\varepsilon - \underset{\sim}{D} \, \frac{\partial Q}{\partial \sigma} \, \frac{\{\frac{\partial F}{\partial \sigma}\}^T \, \underset{\sim}{D}}{\{\frac{\partial F}{\partial \sigma}\}^T \, \underset{\sim}{D} \, \frac{\partial Q}{\partial \sigma} + A} \, d\varepsilon \tag{19}$$

Rearranging terms the stress-strain relation becomes:

$$d\sigma = \underset{\sim}{D} \, d\varepsilon - \frac{\underset{\sim}{D}\{\frac{\partial Q}{\partial \sigma}\}\{\frac{\partial F}{\partial \sigma}\}^T \, \underset{\sim}{D}}{\{\frac{\partial F}{\partial \sigma}\}^T \, \underset{\sim}{D} \, \{\frac{\partial Q}{\partial \sigma}\} + A} \, d\varepsilon \tag{20}$$

Defining the elasto plastic matrix, $\underset{\sim}{D}_{ep}$ we have:

$$\underset{\sim}{D}_{ep} = \underset{\sim}{D} - \frac{\underset{\sim}{D}\{\frac{\partial Q}{\partial \sigma}\}\{\frac{\partial F}{\partial \sigma}\}^T \, \underset{\sim}{D}}{\{\frac{\partial F}{\partial \sigma}\}^T \, \underset{\sim}{D}\{\frac{\partial Q}{\partial \sigma}\} + A} \tag{21}$$

The matrix $\underset{\sim}{D}_{ep}$ is symmetric only for associated plasticity, and takes the place of the elasticity $\underset{\sim}{D}$ matrix in the non-linear incremental analysis. Here associated plasticity is used in the formulation.

The parameter A is a function of the strain hardening properties of the materials and here only strain hardening materials are represented. The parameter A can be obtained from a uniaxial stress-strain test, making use of the failure-criterion and the flow rule used as will be shown in the next paragraphs.

The yield surface or failure criterion for soil materials has been represented by the Mohr-Coulomb law and a mathematically expedient approximation given by Drucker-Prager [38] represented by the failure surface equation, F, given by the following formula:

$$F = 3\alpha'\sigma_m + \bar{\sigma} - K = 0 \tag{22}$$

if $F > 0$ the material is not elastic and corresponds to the yielding part of the strain-stress curve. The parameters used in equation (22) are as follows [147]:

$$\alpha' = \frac{2\sin\phi}{\sqrt{3}\ (3-\sin\phi)} \tag{23}$$

$$K = \frac{6c\ \cos\phi}{\sqrt{3}\ (3-\sin\phi)} \tag{24}$$

$$\sigma_m = \frac{J_1}{3} = \frac{1}{3}(\sigma_r + \sigma_\theta + \sigma_z) \tag{25}$$

or

$$\sigma_m = \frac{1}{3}(\sigma_1+\sigma_2+\sigma_3)$$

The equivalent effective stress $\bar{\sigma}$ is given by

$$\bar{\sigma} = J_2^{1/2} = [\frac{1}{2}(S_r^2 + S_\theta^2 + S_z^2) + \tau_{rz}^2]^{1/2} \tag{26}$$

or

$$\bar{\sigma} = [\frac{1}{6}[(\sigma_1-\sigma_2)^2 + (\sigma_2-\sigma_3)^2 + (\sigma_3-\sigma_1)^2]]^{1/2}$$

where

$$S_r = \sigma_r - \sigma_m$$

$$S_\theta = \sigma_\theta - \sigma_m \tag{27}$$

$$S_z = \sigma_z - \sigma_m$$

With the failure criterion established we can now compute the gradient vector $\{\frac{\partial F}{\partial \sigma}\}$ used in equation (21) and use it for the computation of the elastic-plastic matrix $\underset{\sim}{D}_{ep}$ and in the determination of parameter A.

Differentiating equation (22) we have

$$\frac{\partial F}{\partial \sigma} = \frac{\partial}{\partial \sigma} (3\alpha' \sigma_m + \bar{\sigma} - K) \tag{28}$$

in terms of the partial derivatives using the chain rule then:

$$\frac{\partial F}{\partial \sigma} = \frac{\partial F}{\partial \sigma_m} \frac{\partial \sigma_m}{\partial \sigma} + \frac{\partial F}{\partial J_2} \frac{\partial J_2}{\partial \sigma} \tag{29}$$

The terms of equation (29) are found by differentiating equation (22):

$$\frac{\partial F}{\partial \sigma_m} = 3\alpha' \tag{30}$$

$$\frac{\partial \sigma_m}{\partial \sigma_r} = \frac{1}{3}; \quad \frac{\partial \sigma_m}{\partial \sigma_z} = \frac{1}{3}; \quad \frac{\partial \sigma_m}{\partial \sigma_\theta} = \frac{1}{3} \tag{31}$$

$$\left.\begin{aligned} \frac{\partial J_2}{\partial \sigma_r} &= \frac{1}{3} (2\sigma_r - \sigma_z - \sigma_\theta) \\ \frac{\partial J_2}{\partial \sigma_z} &= \frac{1}{3} (-\sigma_r + 2\sigma_z - \sigma_\theta) \\ \frac{\partial J_2}{\partial \sigma_\theta} &= \frac{1}{3} (-\sigma_r - \sigma_z + 2\sigma_\theta) \end{aligned}\right\} \tag{32}$$

$$\frac{\partial J_2}{\partial \tau_{rz}} = 2\tau_{rz}$$

$$\frac{\partial F}{\partial J_2} = \frac{1}{2}\frac{1}{J^{1/2}} = \frac{1}{2\bar{\sigma}} \tag{33}$$

Arranging terms of these derivatives in matrix form we have:

$$\left[\frac{\partial \sigma_m}{\partial \sigma}\right]^T = \frac{1}{3}\begin{bmatrix} 1 & 1 & 1 & 0 \end{bmatrix} \tag{34}$$

Further the first term of the right side of equation (29) is

$$\frac{\partial F}{\partial \sigma_m} \cdot \frac{\partial \sigma_m}{\partial \sigma} = \frac{\partial F}{\partial \sigma_m} \underset{\sim}{M^\circ}\ \underset{\sim}{\sigma} = 3\alpha' \cdot \underset{\sim}{M^\circ}\ \underset{\sim}{\sigma} \tag{35}$$

where

$$M^\circ = \frac{1}{9\sigma_m}\begin{bmatrix} 1 & 1 & 1 & 0 \\ 1 & 1 & 1 & 0 \\ 1 & 1 & 1 & 0 \\ 0 & 0 & 0 & 0 \end{bmatrix} \tag{36}$$

and the second term for equation (29) is

$$\frac{\partial F}{\partial J_2}\ \frac{\partial J_2}{\partial \sigma} = \frac{1}{2\bar{\sigma}} \cdot \underset{\sim}{M^I} \cdot \underset{\sim}{\sigma} \tag{37}$$

where

$$M^I = \begin{bmatrix} 2/3 & -1/3 & -1/3 & 0 \\ -1/3 & 2/3 & -1/3 & 0 \\ -1/3 & -1/3 & 2/3 & 0 \\ 0 & 0 & 0 & 2 \end{bmatrix} \tag{38}$$

Finally the gradient vector is given by the following expression

$$\{\frac{\partial F}{\partial \sigma}\} = (\frac{\partial F}{\partial \sigma_m} \cdot \underset{\sim}{M}^\circ + \frac{\partial F}{\partial J_2} \underset{\sim}{M}^I)\, \underset{\sim}{\sigma} \tag{39}$$

If associated plasticity is used

$$\{\frac{\partial Q}{\partial \sigma}\} = \{\frac{\partial F}{\partial \sigma}\} \tag{40}$$

and the elasto-plastic matrix $\underset{\sim}{D}_{ep}$ from equation (21) is:

$$\underset{\sim}{D}_{ep} = \underset{\sim}{D} - \frac{\underset{\sim}{D}\{\frac{\partial F}{\partial \sigma}\}\{\frac{\partial F}{\partial \sigma}\}^T \underset{\sim}{D}}{A + \{\frac{\partial F}{\partial \sigma}\}^T \underset{\sim}{D} \{\frac{\partial F}{\partial \sigma}\}} \tag{41}$$

$\underset{\sim}{D}$ = elasticity matrix.

$\{\frac{\partial F}{\partial \sigma}\}$ = given in equation (39)

A = plasticity parameter

Parameter A is a function of the plasticity characteristics of the material. For this study it was computed using the results of a uniaxial stress-strain test. The definition of the variables involved in the computation of parameter A follow. From equation (15) the value of A is given by:

$$A = \frac{1}{\lambda} \{\frac{\partial F}{\partial \sigma}\}^T \{d\sigma\} \tag{42}$$

The flow rule defines the value of λ as:

$$\lambda = \frac{d\epsilon_p}{\frac{\partial F}{\partial \sigma_z}} \tag{43}$$

where

$d\epsilon_p$ = increment in uniaxial plastic strain

Introducing equation (43) into equation (42) we have

$$A = \frac{\frac{\partial F}{\partial \sigma_z}}{d\epsilon_p} \{\frac{\partial F}{\partial \sigma}\}^T \{d\sigma\} \tag{44}$$

Using the results from a uniaxial stress-strain test the stresses are:

$$\sigma_2 = \sigma_3 = \tau_{13} = 0; \quad \sigma_1 = \sigma_z \tag{45}$$

and the parameters:

$$\sigma_m = \sigma_z/3 \quad S_r = -\sigma_z/3 \quad S_\theta = -\sigma_z/3 \quad S_z = 2\sigma_z/3; \quad \bar{\sigma} = \sigma_z/\sqrt{3}$$

The gradient vector for the uniaxial test is computed applying equation (39)

$$\{\frac{\partial F}{\partial \sigma}\} = \frac{\alpha'}{3\sigma_m}\begin{bmatrix} 1 & 1 & 1 & 0 \\ 1 & 1 & 1 & 0 \\ 1 & 1 & 1 & 0 \\ 0 & 0 & 0 & 0 \end{bmatrix}\begin{Bmatrix} 0 \\ \sigma_z \\ 0 \\ 0 \end{Bmatrix} + \frac{1}{2\bar{\sigma}}\cdot\frac{1}{3}\begin{bmatrix} 2 & -1 & -1 & 0 \\ -1 & 2 & -1 & 0 \\ -1 & -1 & 2 & 0 \\ 0 & 0 & 0 & 2 \end{bmatrix}\begin{Bmatrix} 0 \\ \sigma_z \\ 0 \\ 0 \end{Bmatrix}$$

$$\{\frac{\partial F}{\partial \sigma}\} = \alpha' \begin{Bmatrix} 1 \\ 1 \\ 1 \\ 0 \end{Bmatrix} + \frac{1}{2\sqrt{3}} \begin{Bmatrix} -1 \\ 2 \\ -1 \\ 0 \end{Bmatrix} \qquad (46)$$

The term $\frac{\partial F}{\partial \sigma_z}$ is now obtained directly from (46)

$$\frac{\partial F}{\partial \sigma_z} = \alpha' + \frac{1}{\sqrt{3}} \qquad (47)$$

Substituting equations (46) and (47) into (44) gives the definition of parameter A:

$$A = (\alpha' + \frac{1}{\sqrt{3}})\ \frac{1}{d\varepsilon_p} \begin{Bmatrix} \alpha' - \frac{1}{2\sqrt{3}} \\ \alpha' + \frac{1}{\sqrt{3}} \\ \alpha' - \frac{1}{2\sqrt{3}} \\ 0 \qquad 0 \end{Bmatrix}^T \begin{Bmatrix} 0 \\ d\sigma_z \\ 0 \\ 0 \end{Bmatrix} \qquad (48)$$

After performing the matrix operations, the expression for the computation of A for a uniaxial stress-strain test is obtained.

$$A = \frac{d\sigma_z}{d\varepsilon_p} (\alpha' + \frac{1}{\sqrt{3}})^2 \tag{49}$$

where

$$\frac{d\sigma_z}{d\varepsilon_p} = H' = \text{slope of the uniaxial stress plastic strain curve} \tag{50}$$

The graphical representation of H' is shown in Figure 7-4b. Equation (48) shows that other conditions of testing will induce changes in the value of $\{\frac{\partial F}{\partial \sigma}\}$ that need to be accounted for in the computation of the value of A.

Stress Rate Definitions

According to Prager [107A] the simplest constitutive equation considered in the theory of plasticity involves the tensors of stress and rate of deformation and describes a rigid perfectly plastic behavior. The elastic effects must be added to obtain the total elasto-plastic rate of deformation. The stress rate must satisfy the following condition: If a stressed continuum undergoes a rigid body motion and the stress field is independent of time, when referred to a coordinate system that participates in this motion, the stress rate must vanish. This restriction is not severe enough to lead to a unique definition of stress rate, and many definitions of stress rate are hence found in the literature.

If the small strain elastic-plastic coefficients are to be used, then the additional factor to be considered is that the measure of stress and strain increments must be of a form independent of the current rate of rigid body motion [63]. A linear relation between the Jaumann stress increment and the increments of deformation tensor should be used since these are appropriate true stress and strain increments, which are invariant with respect to rigid body motions.

Jaumann's stress rate [4], $\overset{\nabla}{\sigma}{}^{*}$, also called corotational rate of Kirchhoff stress, measures the rate of change of the stress components in a coordinate system that participates in the rotation of the material. Atluri [4] uses the Jaumann stress rate and defines the computations needed to apply the correct stress rate for the finite strain plasticity problems. Here the conventional whole element local coordinate system may not be sufficient for higher order elements, because finite rotations within the element may take place. In the present study, the Jaumann stress rate was not used. The second Piola-Kirchhoff stresses are computed for the increment of stress, and the true Cauchy stress is computed at the end of the load increment.

The elasto-plastic constitutive matrix $\underset{\sim}{D}_{ep}$ is an explicit expression relating stress changes to strain changes

$$d\underset{\sim}{\sigma} = \underset{\sim}{D}_{ep}\, d\underset{\sim}{\varepsilon}$$

For the incremental procedure presented, the increment of stress $d\underset{\sim}{\sigma}$ is given by the second Piola-Kirchhoff stress, and the increment of strain according to the Green-Lagrange strain definition. The resulting $\underset{\sim}{D}_{ep}$ is symmetric for associated plasticity. The rotation effects might be important for large displacement plasticity problems. New research should involve methods to include the Jaumann type of stress rates in the large displacement plasticity problems.

Summary

A general formulation for the analysis of soil plasticity is presented that includes cohesive and cohesionless materials. The Drucker-Prager failure criterion is proposed and complemented with the appropriate plastic parameters obtained from standard soil mechanics laboratory tests. Unconfined and regular triaxial tests are employed for the plastic parameter determination. The parameter computation, however, is considerably simpler if the uniaxial stress-strain test results are used. The real soil behavior is quite complex since in general it is not plastic or totally frictional. Clays for example might present a residual stress after reaching a peak stress and sands and gravel present no tension characteristics. The present model takes into account the hydrostatic conditions for the computation of the failure criterion. The cohesion and angle of internal friction of the material are parameters that influence the

failure condition as can be seen in equation (22). No provisions are included for variation of the angle of internal friction with confinement.

The soil is modeled by a strain-hardening material with provision for the particular case of elastic-perfectly plastic material for which parameter H' from equation (50) is zero. The gradient computation $\{\frac{\partial F}{\partial \sigma}\}$ is basic to establish an elastic plastic stress-strain relation and can be readily obtained using equation (39). The computation of the gradient vector $\{\frac{\partial F}{\partial \sigma}\}$ by means of formula (39) involves the use of the total true Cauchy stress. For the computation of the plasticity parameters the effective stress $\bar{\sigma}$ is used computed in terms of the true Cauchy stresses. The increase in volume or dilatation predicted by the failure criteria used in the finite element plasticity theory is larger than found in cohesionless material tests [33,78]. To improve this situation more sophisticated theories for clay and cohesionless materials have been recently presented [78,113,145] and discussions of the validity of the theories have produced lively debates [33]. No theory is at the present time totally accepted. The approach presented in this thesis implements the most important plasticity relations for the soil-fabric problem.

The Drucker-Prager failure criterion is a useful computation tool. Since there are uncertainties in laboratory tests and variations in the plasticity parameters, until more correlations are performed a better model is not justified.

The examples presented in Chapter X show that the model provides good estimates of stress-strain fields and the soil-fabric behavior under repeated cyclic loads. Experimental data from another investigation [29] are used also to verify the proposed plasticity theory.

CHAPTER VIII

NO TENSION ANALYSIS

Introduction

The elementary theory of elasticity is applied to analyze and solve many geotechnical problems. The material behavior is usually assumed linear and isotropic, with the material having the same properties in tension and in compression. In soil mechanics problems, these assumptions are not satisfied for most geotechnical materials encountered. However, experience demonstrates that elasticity solutions generally provide the geotechnical engineer with useful approximations for many problems and are used for analysis and design. Most of the materials in geotechnical engineering have a limited tension capacity or no tension capacity at all. These materials need special considerations, and their analysis is the subject of this chapter.

In the elastic analysis of layered systems linear elastic solutions provide reasonably accurate estimates for vertical stress and vertical displacements, but relatively poor estimates of horizontal stresses, displacements and strains [7,39,108]. According to a linear elastic analysis, an applied vertical load at the surface of an unstabilized layer resting on soil produces tensile stresses in the lower half of the base layer. If the base is a cohesionless

material, such as gravel, sand or any low capacity tension material, the tensile stresses cannot be taken by these materials. The results are that an elastic analysis will give tension stresses that do not correspond to the actual stresses [108]. Cohesionless materials such as gravel, crushed stone or sand subjected to repeated loads behave in a nonlinear and anisotropic manner [8,78,103], this behavior makes the analytical problem very complex. The disposition of the load with respect to the geometry of the model produces in some cases stress concentrations and tensile zones that cannot be taken by the soil materials. For these conditions a special analyses is required. The no tension problem is also encountered in rock mechanics, where rock joints are present or cracks appear due to load application. Solutions for rock mechanics problems have been given using special finite element formulations [49,50,51,139,140,142]. Recently several failure criteria in accordance with plasticity theory have provided methods of analysis of cohesionless materials [33,78,103,108]. Shear dilatancy effects are not included in the present study. Extensive laboratory testing and correlation with the proposed analytical formulations are required in order to verify the proposed methods.

Formulation of the No Tension Problem for Soils

Cohesionless materials and clays with low tensile strength present a nonlinear anisotropic behavior. An

accurate formulation of these materials is complex. The nonlinearity, no tension and anisotropy are some of the problems encountered. The no tension problem has been solved for rock mechanics [140,141], and the application of this method was implemented for the soil-fabric system, with limited success. The finite element model of the soil fabric system with variable resilient modulus of elasticity for the cohesionless materials resulted in a very slow convergence rate; seven iterations per load increment were not sufficient to equilibrate the system at low stress levels. After several tests the no tension procedure similar to the reference by Zienkiewicz et al. [140] was abandoned.

A recent plane strain finite element formulation for layered systems was presented by Raad and Figueroa [108]. The formulation included a granular layer with no cohesion resting on top of soil. The no tension or low tension capacity of the granular layer is considered. This method of analysis was implemented into the present soil-fabric finite element method. The extended von Mises or Drucker-Prager failure criteria was used as a three dimensional extension to the Mohr-Coulomb law for axisymmetric conditions. For the failure criteria represented by F, the analytical formulation is given by

$$F = \alpha' \sigma_m + \bar{\sigma} - K \qquad (1)$$

where α', σ_m, $\bar{\sigma}$ and K were given in equations (23) to (27) in Chapter VII. In $F > 0$ the material is in a failure state.

Now assume that the cohesionless material complies with Mohr-Coulomb law and computations by the finite element method show that the state of stress at a sampling point in an element is at failure. The following method is presented for handling the no tension characteristics of the granular material. The method includes equilibrium verification after each load increment or iteration, and modifies the state of stress to comply with Mohr-Coulomb law given by:

$$\tau = c + \sigma_n \tan\phi \tag{2}$$

where

τ = shear stress

c = cohesion

σ_n = normal stress

ϕ = angle of internal friction

For the procedure presented here, the soil mechanics sign convention is followed with tension being taken as negative and compression as positive. The Mohr-Coulomb law in terms of the principal stresses [123] applied for the r-z plane is:

$$\sigma_1 = \sigma_3 \frac{1+\sin\phi}{1-\sin\phi} + 2c \frac{\cos\phi}{1-\sin\phi} \tag{3}$$

With some algebraic transformations we obtain:

$$\sigma_1 = \sigma_3 \tan^2 (45 + \phi/2) + 2c \tan (45 + \phi/2) \qquad (4)$$

where

σ_1 = major principal stress

σ_3 = minor principal stress

c = cohesion

ϕ = angle of internal friction

In the finite element procedure, the principal stresses and strains are computed for each of the sampling or integration points of the eight node isoparametric element (see Chapter IX) using Gaussian Quadrature. The principal stresses in the r-z plane are given for the axisymmetric condition in terms of the vertical, radial and shear stresses by the following equations:

$$\sigma_1 = \frac{\sigma_r+\sigma_z}{2} + \sqrt{\left(\frac{\sigma_r-\sigma_z}{2}\right)^2 + \tau_{rz}^2} \qquad (5)$$

$$\sigma_2 = \frac{\sigma_r+\sigma_z}{2} - \sqrt{\frac{\sigma_r-\sigma_z}{2} + \tau_{rz}^2} \qquad (6)$$

The direction of the principal stresses is given by α, where

$$\alpha = \frac{1}{2} \tan^{-1} \frac{2\tau_{rz}}{\sigma_r-\sigma_z} \qquad (7)$$

The angle α is measured counter-clockwise from the r axis to

the direction of the major principal stress σ_1. Then defining α_1 as:

$$\alpha_1 = \alpha \pm 90° \tag{8}$$

For α negative use a minus sign in equation (8). For the case of $\sigma_r < \sigma_z$ the appropriate direction is given by α_1, using equation (8) and the value of α obtained from equation (7). This will give the appropriate quadrant of the direction for the major principal stress. The failure criterion is tested for each sampling point using equation (1) at the end of each iteration. For the case of $F > 0$ the sampling point is at failure and the principal stresses are corrected so their Mohr circles just touch the Mohr-Coulomb failure envelope. The correction is applied following the procedure given in [108] with modifications for an axisymmetric model.

With the computed vertical stress σ_z and equation (4) the maximum $(\sigma_1)_{max}$ and minimum $(\sigma_3)_{min}$ limiting principal stress states are defined, these comply with Mohr-Coulomb law and can be represented by the following expressions:

$$(\sigma_1)_{max} = \sigma_z \tan^2 (45 + \phi/2) + 2c \tan (45 + \phi/2) \tag{9}$$

$$(\sigma_3)_{min} = \sigma_z \tan^2 (45 - \phi/2) - 2c \tan (45 - \phi/2) \tag{10}$$

The computed principal stresses at the end of each iteration, σ_1 and σ_3, should not exceed or be smaller than $(\sigma_1)_{max}$ and $(\sigma_3)_{min}$, respectively (see Figure 8-1). Also σ_1 should not exceed the value given by σ_1' which is the major principal stress associated with σ_3 at failure, as shown in Figure 8-2b and given by:

$$\sigma_1' = \sigma_3 \tan^2 (45 + \phi/2) + 2c \tan (45 + \phi/2) \qquad (11)$$

If the principal stresses σ_1 and σ_3 exceeded the failure conditions, after the modification the principal stresses will comply with Mohr-Coulomb failure criteria, and the material will be in a perfectly plastic failure state. The algorithm for the stress modification procedure [108] is given in Figure 8-3 and the detailed flow diagram used in the computer code is given in Chapter IX. In the axisymmetric problem after computing the maximum and minimum principal stresses σ_1 and σ_3, the value of the computed tangential stress σ_θ is compared with σ_1 and σ_3 and substituted for σ_1 when $\sigma_\theta > \sigma_1$ or for σ_3 when $\sigma_\theta < \sigma_3$. Both cases are shown in Figure 8-4.

For modifying the tangential stress σ_θ from the original principal stress state, a stress ratio is defined, R_s, and applied to obtain the modified stress. The stress ratio is:

$$R_s = \frac{\sigma_3 - \sigma_2}{\sigma_3 - \sigma_1} \qquad (12)$$

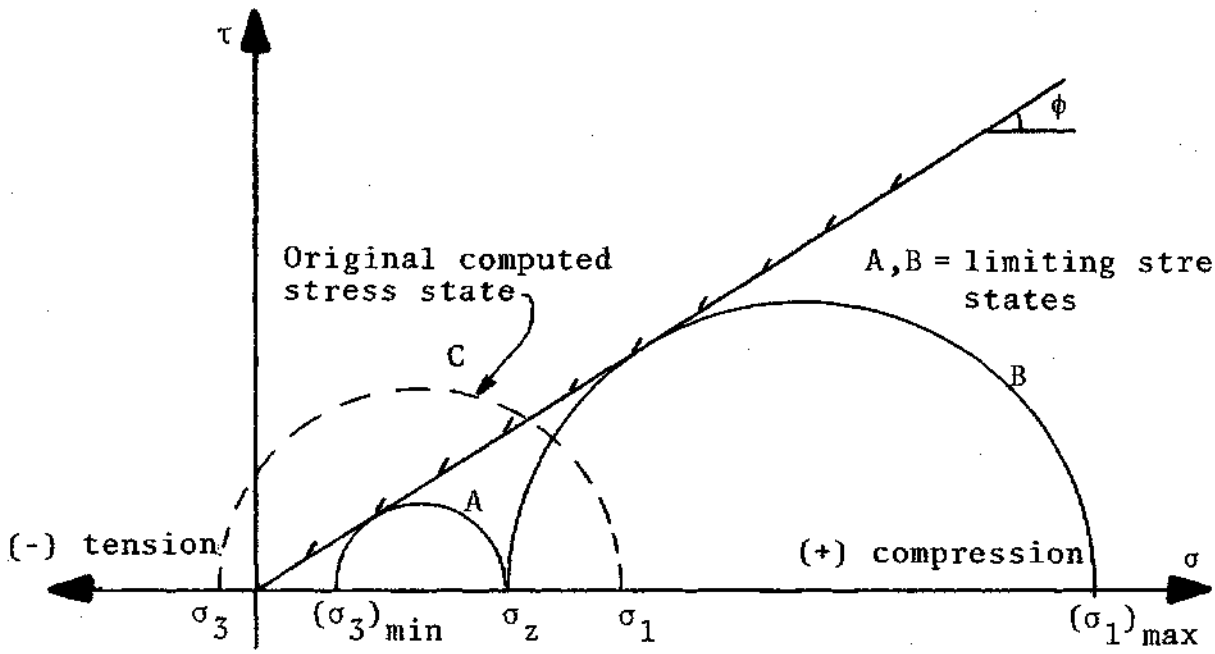

(a) Original computed stress state

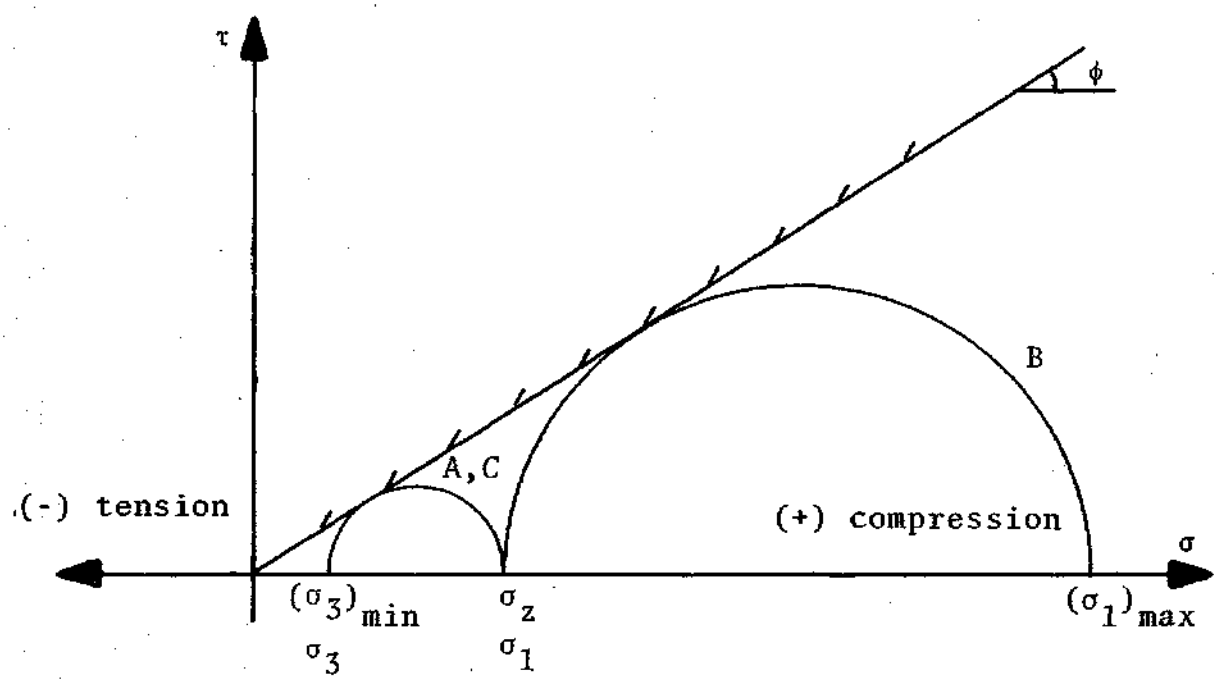

(b) Modified stress state

Note: Soil mechanics sign convention used here.

Figure 8-1. Cohesionless Material. Stress Modification for a No Tension Failure Condition ($\sigma_3 < (\sigma_3)_{min}$)

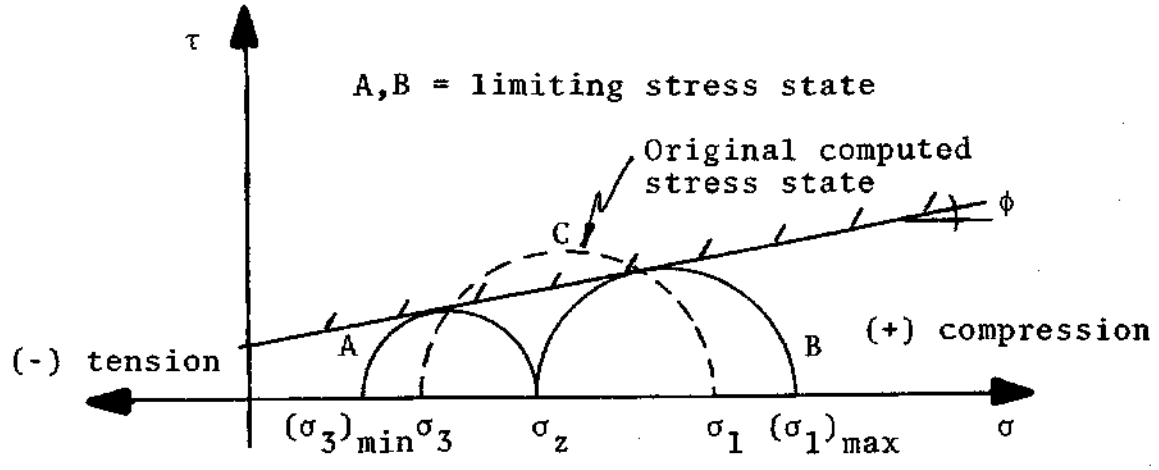

(a) Original computed stress state

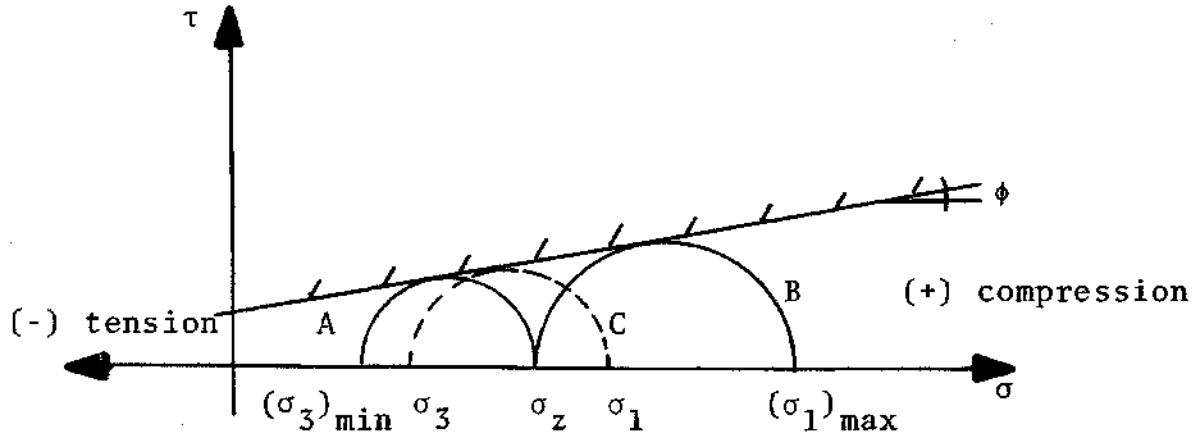

(b) Modified stress state
Note Soil Mechanics Sign Convention Used Here.

Figure 8-2. Stress Modification in No Tension Analysis for $\sigma_3 > (\sigma_3)_{min}$

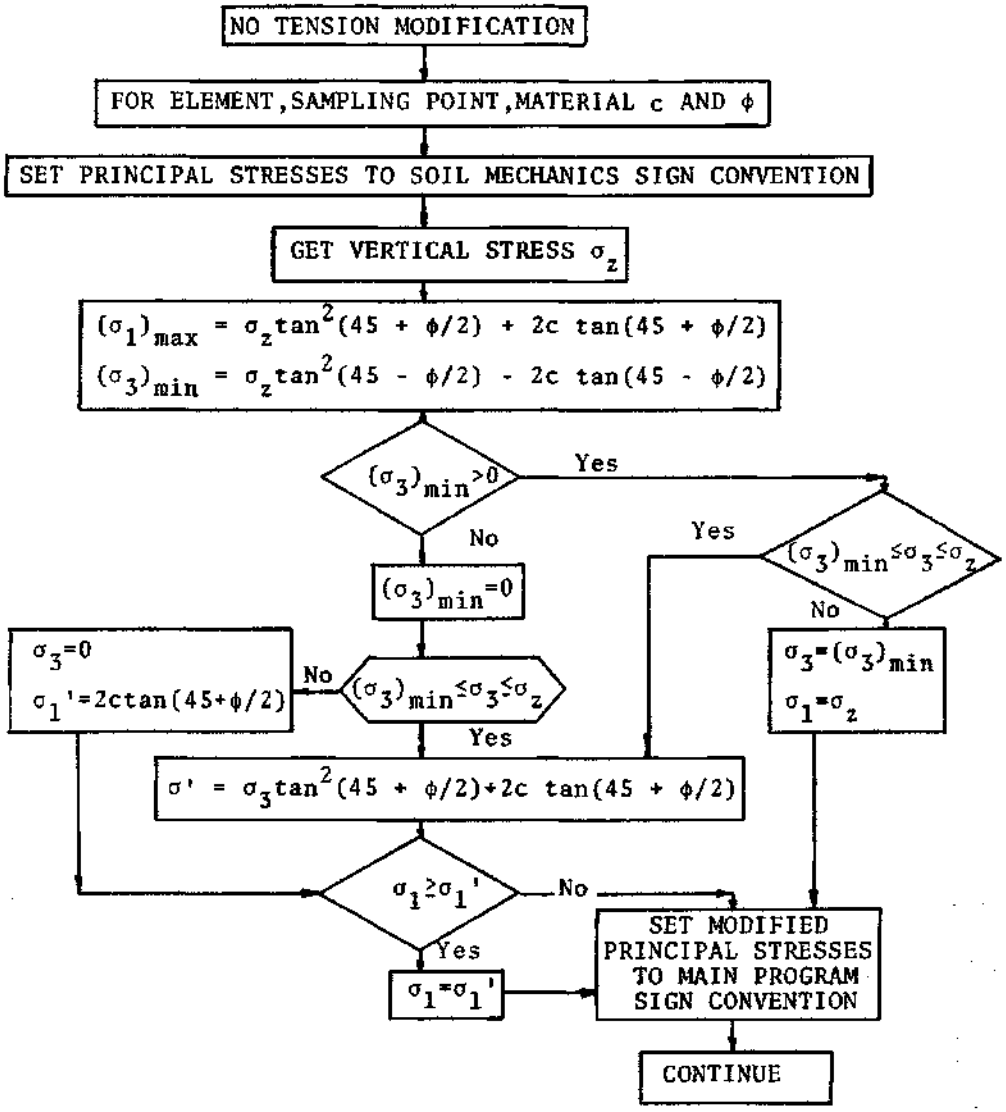

Figure 8-3. Stress Modification Procedure [108]

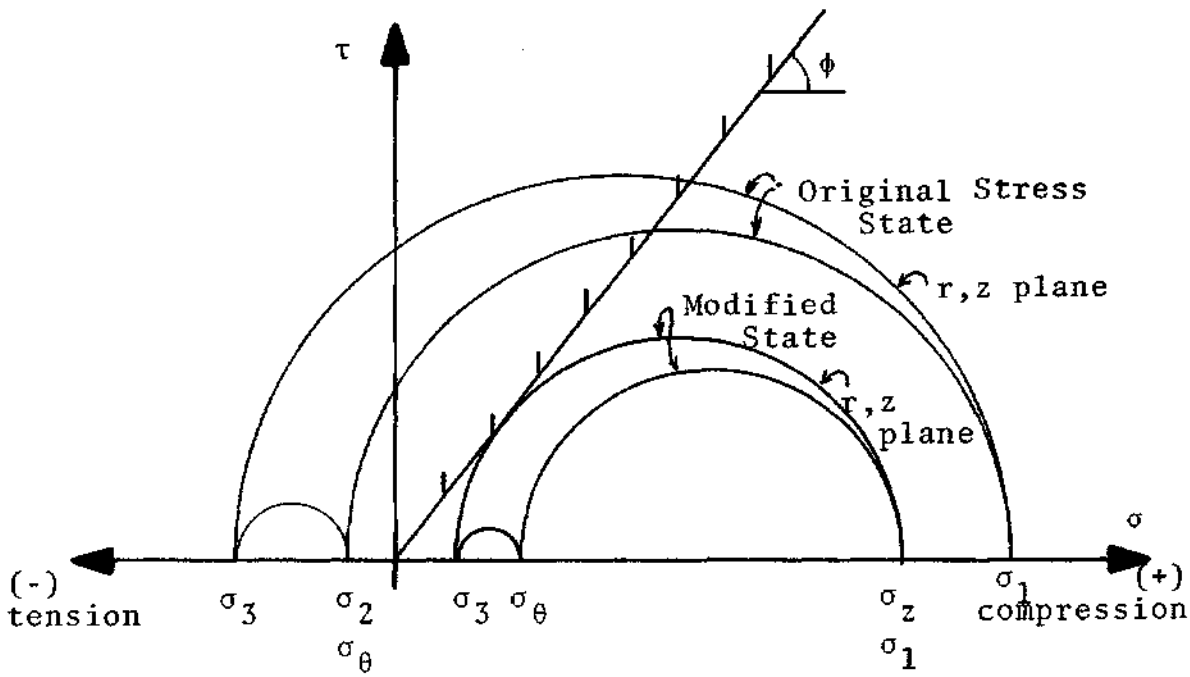

(a) Modified state of stresses for $\sigma_\theta < \sigma_3$ (r,z plane)

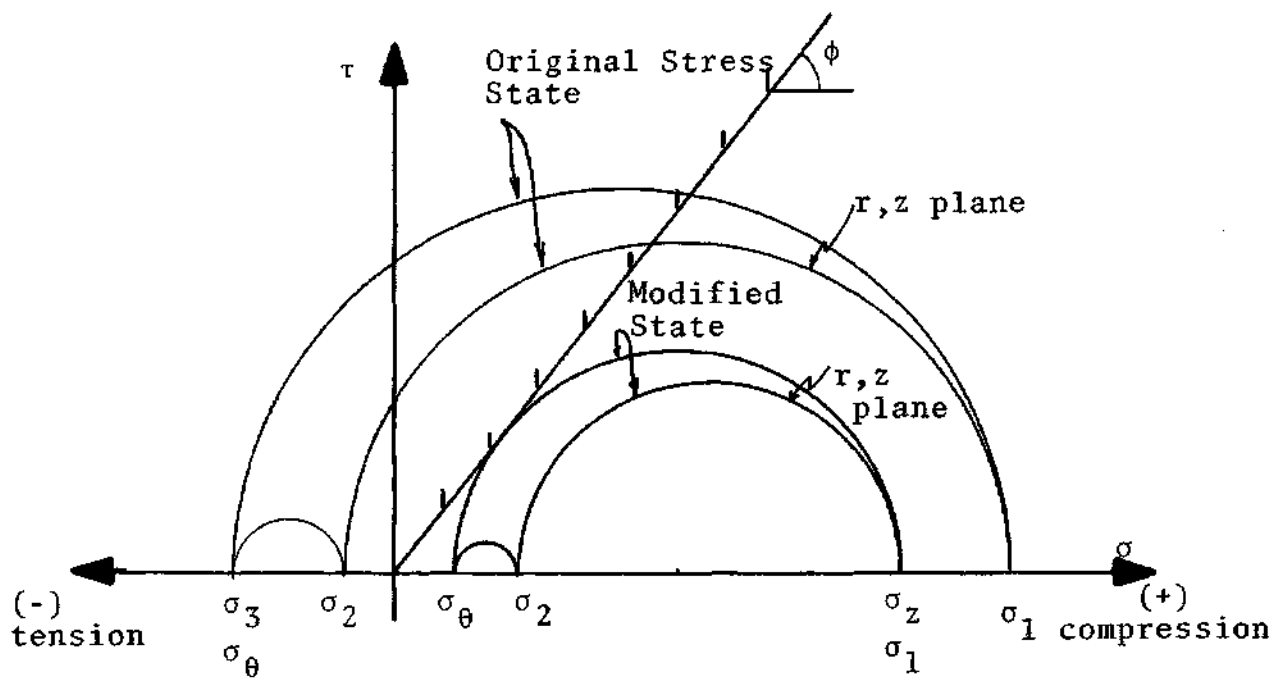

(b) Modified state of stresses for $\sigma_\theta > \sigma_3$ (r,z plane)

Note: Soil mechanics sign convention used here.

Figure 8-4. Tangential Stress Modification

This stress ratio is applied to the intermediate stress to obtain the modified intermediate stress σ_2. For the case of $\sigma_\theta < \sigma_3$ the modified tangential stress $\sigma_\theta = \sigma_2$ is given by

$$\sigma_2 = \sigma_3 + R_s (\sigma_1 - \sigma_3) \tag{13}$$

Now the principal stresses associated with the r' - z' plane are transformed to the r,z,θ coordinate axes to obtain the modified stresses σ_r, σ_z, σ_θ and τ_{rz}.

The computation of the stress transformation that relates the local coordinate (principal stress) system (r',z') and the global coordinate system (r,z) is derived in [25,139] and given by

$$\underset{\sim}{\sigma}' = \underset{\sim}{T}_\sigma \underset{\sim}{\sigma} \tag{14}$$

or

$$\underset{\sim}{\sigma} = \underset{\sim}{T}_\varepsilon \underset{\sim}{\sigma}' \tag{15}$$

where

σ' = stress in the local coordinate system, r' - z'

σ = stress in the global coordinate system, r - z

and the transformation matrix $\underset{\sim}{T}_\varepsilon$ is

$$\underset{\sim}{T}_{\varepsilon} = \begin{bmatrix} \cos^2\theta & \sin^2\theta & 0 & -2\sin\theta\cos\theta \\ \sin^2\theta & \cos^2\theta & 0 & 2\sin\theta\cos\theta \\ 0 & 0 & 1 & 0 \\ \sin\theta\cos\theta & -\sin\theta\cos\theta & 0 & \cos^2\theta - \sin^2\theta \end{bmatrix} \tag{16}$$

The angle θ is the angle clockwise from r' to r, as shown in Figure 8-5.

It can be demonstrated [25] that

$$\underset{\sim}{T}_{\varepsilon} = \underset{\sim}{T}_{\sigma}^{T} \tag{17}$$

To apply equation (15) the angle θ is needed between the direction of principal stresses and the r,z global axes. The angle θ is defined by computing the angle α that the major principal stress makes with the horizontal r axis. From Mohr's circle for the corrected stresses, 2α is given by:

$$2\alpha = \cos^{-1} \frac{2\sigma_z - \sigma_1 - \sigma_3}{\sigma_1 - \sigma_3} \tag{18}$$

For a negative shear (that produces clockwise moments if applied at the face perpendicular to the (+) direction of axis r), then α' gives the angle between the major principal stress and the horizontal r axis, computed by

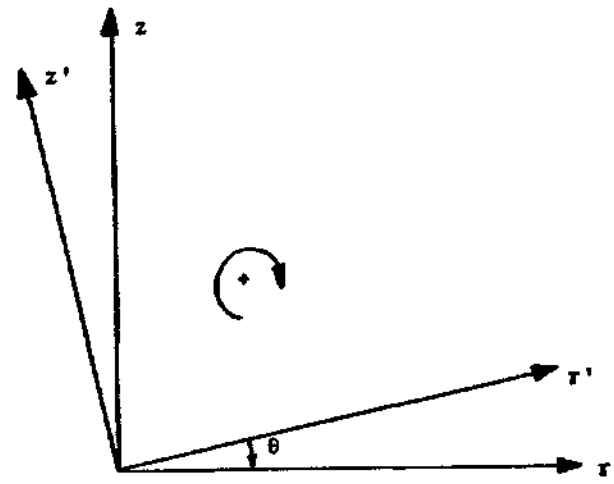

Figure 8-5. Sign Convention for Rotation of Axes.

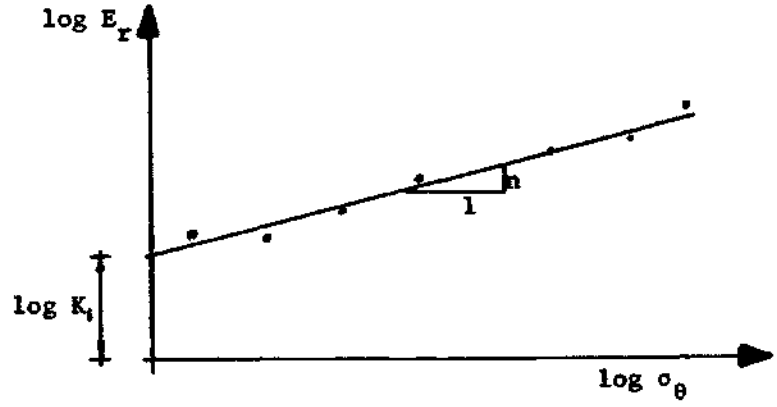

(a) Cohesionless Materials. Resilient Modulus Variation with Confinement.

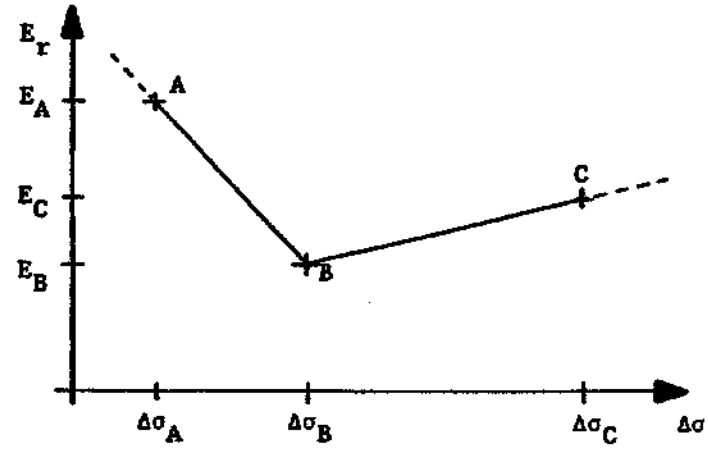

(b) Cohesive Materials. Resilient Modulus Variation with Deviator Stress.

Figure 8-6. Resilient Modulus Variation with Stress State.

$$2\alpha' = 360° - 2\alpha \tag{19}$$

If $\sigma_z = \sigma_1$ no transformation is required since the direction of principal stresses corresponds to the r,z axes and:

$$\sigma_r = \sigma_3 \tag{20}$$

$$\tau_{rz} = 0$$

To use the matrix transformation $\underset{\sim}{T}_\varepsilon$ from equation (16) the angle $\theta = \alpha$ and the σ_r, σ_z, σ_θ and τ_{rz} stresses can be evaluated with equation (15).

Using the computed stresses, the failure conditions at each sampling point are evaluated. If a sampling point falls outside the failure criterion the stress modification procedure is applied to that point.

For the system to remain in equilibrium, the difference between the originally computed state of stress and the modified state of stress is used to determine the nodal forces by numerical integration. These corrective nodal forces are applied to the system in the next iteration or load increment in order to maintain equilibrium. The corrective nodal forces are given integrating numerically the following expression:

$$\underset{\sim}{F}_o^n = \int_v B^T \Delta\sigma_o^{rz} dv \tag{21}$$

where

B^T = strain-displacement matrix

$\Delta\sigma_o^{rz} = \sigma_i - \sigma_m$ = applied stress modification

σ_i = initial state of stresses

σ_m = modified state of stresses.

In the application of the no tension and plasticity procedures, the load increment should be as small as practical limits on computer time allows. Use of a small load increment will produce stress states in the system that are close to the failure envelope and hence only requires a small amount of correction. Also using small load increments the development can be observed of the no tension or plasticity condition at the sampling points (slip in the case of interface elements present). A complete load-deformation history of the system is obtained.

Resilient Modulus of Elasticity

Considerable attention has been given to the variation of the modulus of elasticity with confinement [8,115,138]. Particular attention is devoted to the resilient modulus of elasticity and the application of dynamic repeated loads [8,116] used in predictions of base course rutting as a function of load repetitions.

For cohesionless soils the resilient modulus of elasticity can be computed with the following formula [8]

$$E_r = k_1 \sigma_{\theta c}^{n} \tag{22}$$

where

k_1 = ordinate at log $\sigma_{\theta c}$ = 0 in the log E-log σ_θ plot, constant

n = slope of the E_r vs σ_θ line on a log E-log-σ_θ plot

and

$$\sigma_{\theta c} = \sigma_1 + \sigma_2 + \sigma_3 \tag{23}$$

This type of formula is given by several authors. Recently more elaborate formulas have been presented [34,78,103]. The simple nature of equation (22) allows a straight forward application in the context of the finite element formulation presented here.

The value of the resilient modulus E_r is computed using equation (22) at the start of the iteration using the last previously obtained values for the principal stresses. The values of k_1 and n are obtained from triaxial repeated load tests for various confining conditions as shown in Figure 8-6a.

For cohesive materials the resilient modulus can also be represented in a different form [108]. A bilinear law can represent the variation of the resilient modulus with the deviator stress as shown in Figure 8-6b. The resilient modulus formula for cohesive materials is for $(\sigma_1 - \sigma_3) < \Delta\sigma_B$:

$$E_r = E_B + \frac{(\Delta\sigma_B - \Delta\sigma) \cdot (E_A - E_B)}{\Delta\sigma_B - \Delta\sigma_A} \quad (24)$$

and for $(\sigma_1 - \sigma_3) > \Delta\sigma_B$

$$E_r = E_B + \frac{(\Delta\sigma - \Delta\sigma_B)(E_C - E_B)}{\Delta\sigma_C - \Delta\sigma_B} \quad (25)$$

where

E_A, E_B, E_C = resilient modulus for conditions A,B,C

$\Delta\sigma_A, \Delta\sigma_B, \Delta\sigma_C$ = deviator stresses for conditions A,B,C

$\Delta\sigma$ = deviator stress for which E_r is computed

Summary

The computed modulus of elasticity is used in the stiffness determination for the next iteration. The corrected stresses in each iteration are used to compute the internal forces, the equilibrium of the system and the unbalanced forces, that are applied to the system in the next iteration. Iterations are performed until convergence is achieved as described in Chapters V and IX.

The variation of the resilient modulus of elasticity with confinement is quite important as illustrated in the following example. Consider a granular layer 4.5 inches thick placed on top of clay. Dynamic triaxial tests on a crushed stone gave the following constants: $k_1 = 1242$; $n = 0.762$ for E_r in psi. Using a linear elastic two layer

analysis we can compute the resilient modulus due to only body weight. The resilient modulus is about 200 psi at a depth of 0.75 inches and 750 psi at a depth of 3 inches. If a uniform circular load of 10 psi and 3 inches in radius is applied at the surface, the modulus increases to 13000 psi at a depth of 0.75 inches and reduces to 300 psi at the 3 inch depth, due to tensile stresses developed in the radial and tangential directions.

Repeated load triaxial tests are used to evaluate the resilient modulus parameters k_1 and n for the computation of E_r. From repeated load tests using constant confining pressure, the stress-plastic strain curves are obtained and the plasticity parameter H' determined, as explained in Chapter VII.

To evaluate the response of a soil-fabric system to load repetitions, the load and unload cycles need to be computed one at a time. As an engineering approximation for estimating the permanent deformation in such a system, the total number of load repetitions can be divided into several intervals. The values of the parameters n, k_1 and H' are then computed for the average conditions within the interval. The total permanent deformation response will be the sum of the average permanent deformatiom multiplied by the number of load repetitions applied within the interval.

The stress modification procedure used basically follows the one given in [108] modified for the axisymmetric

conditions and incorporating Drucker-Prager failure criteria. An approximate procedure to compute the intermediate principal stress is proposed and Mohr-Coulomb law is used to modify the stresses and comply with the failure criteria. For elements with sampling points in failure, a perfect plasticity is assumed and their contribution to the element stiffness is accumulated with the usual numerical integration described in Chapter IX. Results for a two layer system and a soil-fabric system are presented in Chapter X.

Anisotropy

The soil-plasticity theory and the no tension procedure previously presented assume isotropic conditions. In some cases the anisotropic characteristics of the materials are too important to be disregarded in the analysis. In the present formulation the anisotropic conditions can be introduced for the initial elastic computation. In this way a better initial estimate is obtained of the stress state in the system where no tension and plasticity are developed. For example, a system consisting of a cohesionless material placed over a soil and the subgrade elements elasticity modulus in the horizontal direction is set equal to zero or a very small value. The computed stresses using the anisotropic idealization are then used as initial values in the analysis. The no tension procedure described in this Chapter is used in subsequent iterations and load increments. In the next paragraphs the derivations for the use

of the anisotropic elasticity matrix are presented.

The anisotropic characteristics of the cohesionless materials play a very important role in the behavior of a layered soil system and the computations of the stress-strain relationships are affected by them. The general three dimensional elasticity strain-stress relations [139] for an anisotropic stratified layered system in terms of the inplane and normal to the strata elastic modulus and Poisson's ratios are given as follows:

$$
\begin{aligned}
\varepsilon_z &= \frac{\sigma_z}{E_2} - \nu_2 \frac{\sigma_r}{E_2} - \nu_2 \frac{\sigma_\theta}{E_2} \\
\varepsilon_r &= -\nu_2 \frac{\sigma_z}{E_2} + \frac{\sigma_r}{E_1} - \nu_1 \frac{\sigma_\theta}{E_1} \\
\varepsilon_\theta &= -\nu_2 \frac{\sigma_z}{E_2} - \nu_1 \frac{\sigma_r}{E_1} + \frac{\sigma_\theta}{E_1} \\
\gamma_{zr} &= \frac{\tau_{rz}}{G_2}
\end{aligned}
\qquad (26)
$$

where

E_1, ν_1 = modulus of elasticity and Poisson's ratio that correspond to the in-plane behavior

E_2, ν_2, G_2 = the modulus of elasticity, Poisson's ratio, and shear modulus respectively, that correspond to the behavior normal to the strata.

The geometry and axes are shown in Figure 8-7. The stress-strain matrix $\underset{\sim}{D}'$ is given by

$$\underset{\sim}{D}' = \frac{E_2}{(1+\nu_1)\ell}\begin{bmatrix} n(1-n\nu_2^2) & n\nu_2(1+\nu_1) & (\nu_1+n\nu_2^2)n & 0 \\ n\nu_2(1+\nu_1) & (1-\nu_1^2) & n\nu_2(1+\nu_1) & 0 \\ (\nu_1+n\nu_2^2)n & n\nu_2(1+\nu_1) & n(1-n\nu_2^2) & 0 \\ 0 & 0 & 0 & m(1+\nu_1)\ell \end{bmatrix} \quad (28)$$

where

$$n = \frac{E_1}{E_2}$$

$$m = \frac{G_2}{E_2} \quad (27)$$

and $$\ell = 1-\nu_1-2n\nu_2^2$$

Now the stress-strain relationship for the coordinate system with the axis z' normal to the strata is:

$$\sigma' = \underset{\sim}{D}'\varepsilon' \quad (29)$$

The stress transformation that relates the local coordinate system (r',z') and the global coordinate system (r,z) is given in equation (16), the matrix operations are defined in

equations (15)-(17).

In summary, considering anisotropic soil conditions, a better estimate of the initial elastic stress distribution in the system is obtained which results in a faster convergence when the next load increments are applied.

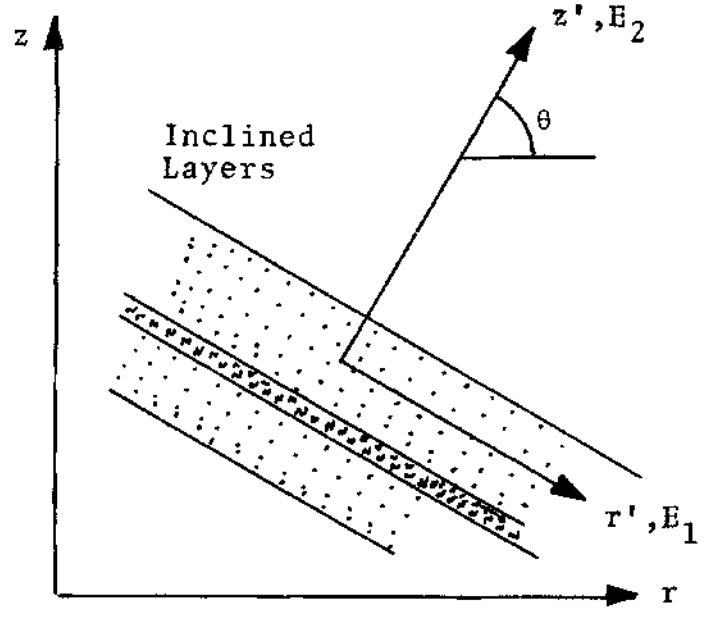

Figure 8-7. Local and Global Axes for Stratified Materials

CHAPTER IX

COMPUTER CODE ORGANIZATION AND CAPABILITIES

General Description

The theoretical development of the soil-fabric finite element formulation given in Chapters III to VIII is implemented into a computer code for the solution of the finite element model of the soil-fabric system. The finite element program analyzes linear or nonlinear axisymmetric solids, models interfaces between dissimilar materials and analyzes the behavior of the interface. Higher order strain terms can also be included in the analyses by using an option. No tension analysis for materials with small or nonexistent tension capacity is also a feature of the program. Fabric elements can be introduced into the system by the special elements described in Chapter VI. Plasticity analysis is limited to small displacements of the system. The program enables a geotechnical engineer to model layered systems with interfaces and can be applied to other axisymmetric problems like piles, piers and anchors.

The program was written in FORTRAN IV and implemented for a CDC-CYBER 74 computer, and has the capability of easily increasing or decreasing the total storage requirements depending on the size of mesh to be analyzed. As presently dimensioned the program needs a total storage capacity of

165000 bits and solves problems up to 200 nodal points and 60 elements where 25 elements may be of the interface type. Maximum values accepted by the computer code are 15 different type of materials, 25 pressure loads and a total stiffness matrix vector of 18000 storage locations. The maximum bandwidth (MBAND) is then MBAND = 18000/NUMNP*2 where NUMNP = number of nodal points. For 200 nodal points the maximum MBAND is hence 45. For a particular problem MBAND is computed by MBAND = (maximum difference between nodal points of an element - 1)2.

The organization of the program consists basically of a main program that handles input, initializations, calls the appropriate subroutines and outputs part of the results. Twelve subroutines are used to perform the required computations. The flow diagram of the main program is shown in Figure 9-1. The original elastic version of the program was written by R. D. Barksdale [6].

The input of the program consists basically of geometry, type of elements, type of materials and mechanical characteristics of the materials. The boundary conditions and pressure loads need also to be specified together with the number of load increments and whether a small or large displacement problem is to be solved. Examples of several problems are shown in Chapter X.

The finite element method requires the solution of a system of equations (refer to Chapter V, equation (33)), given by

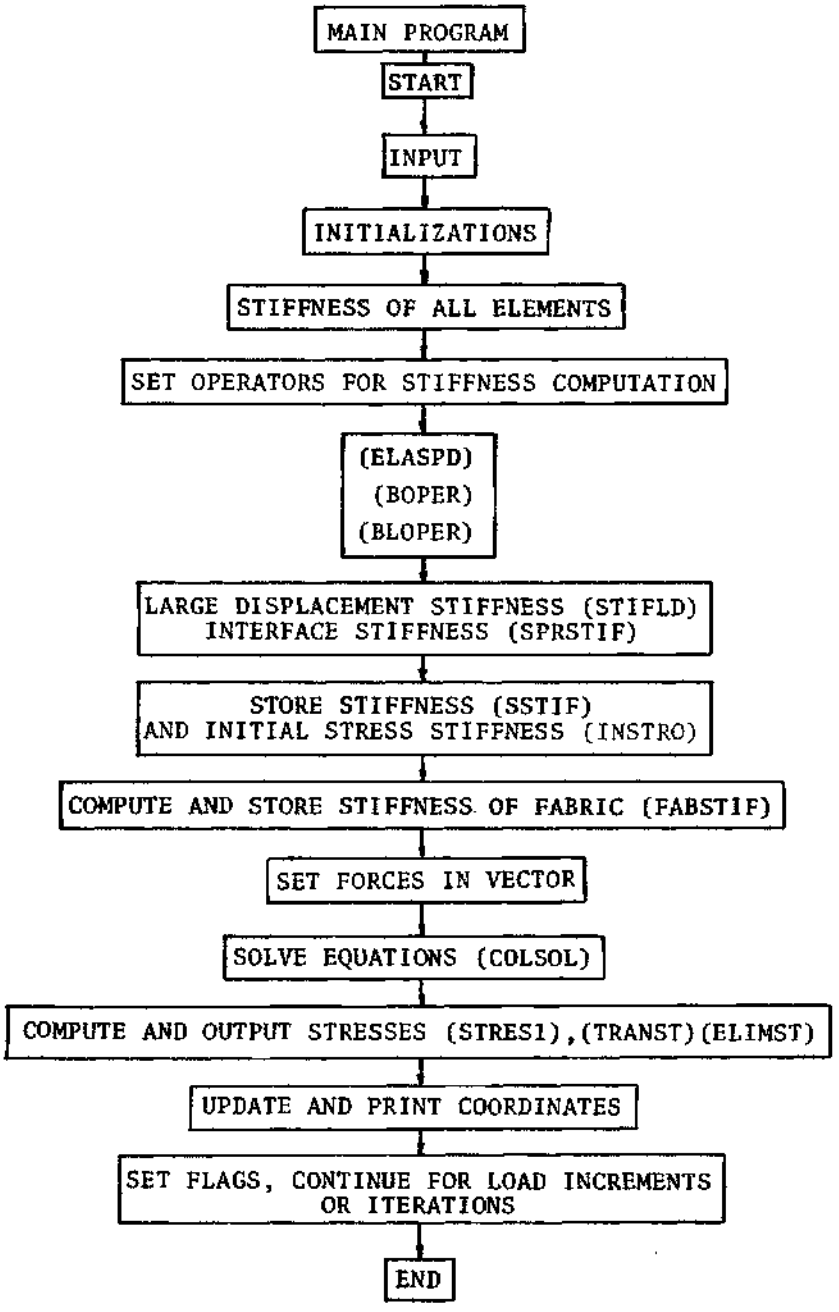

Figure 9-1. Flow Diagram of the Main Finite Element Program

$$d\psi = K_T du \tag{1}$$

The computation of the stiffness of the elements is basic to the solution of the problem. For the eight node isoparametric elements the following routines perform the numerical computations: BOPER, BLOPER, ELASPD, STIFLD and SSTIF. Subroutine BOPER computes the strain-displacement operator or $\underset{\sim}{B}$ matrix for the small displacement theory of the eight node isoparametric axisymmetric elements. The derivation of this matrix is presented in Chapter III and the generalized flow diagram of BOPER is shown in Figure 9-2. In order to include higher order strain terms the large displacement option LDFLAG is set to 1 and then subroutine BLOPER is called. This subroutine performs the necessary operations to obtain the large displacement $\underset{\sim}{B}_L$ matrix defined in Chapter V. In Figure 9-3 the flow diagram of BLOPER is shown. Since BLOPER depends on the displacements it is called after the first load increment is applied. For the initial elastic load increment the anisotropic conditions of the material can be introduced in the model. After the initial load increment, the program computes the variable modulus corresponding to the evaluated confining pressure and uses this value in the current load increment computations. When the material behaves nonlinear after the yielding point is reached, the elasto plastic matrix $\underset{\sim}{D}_{ep}$ is computed by routine ELASPD. The theoretical derivation of $\underset{\sim}{D}_{ep}$ limited to small strains was

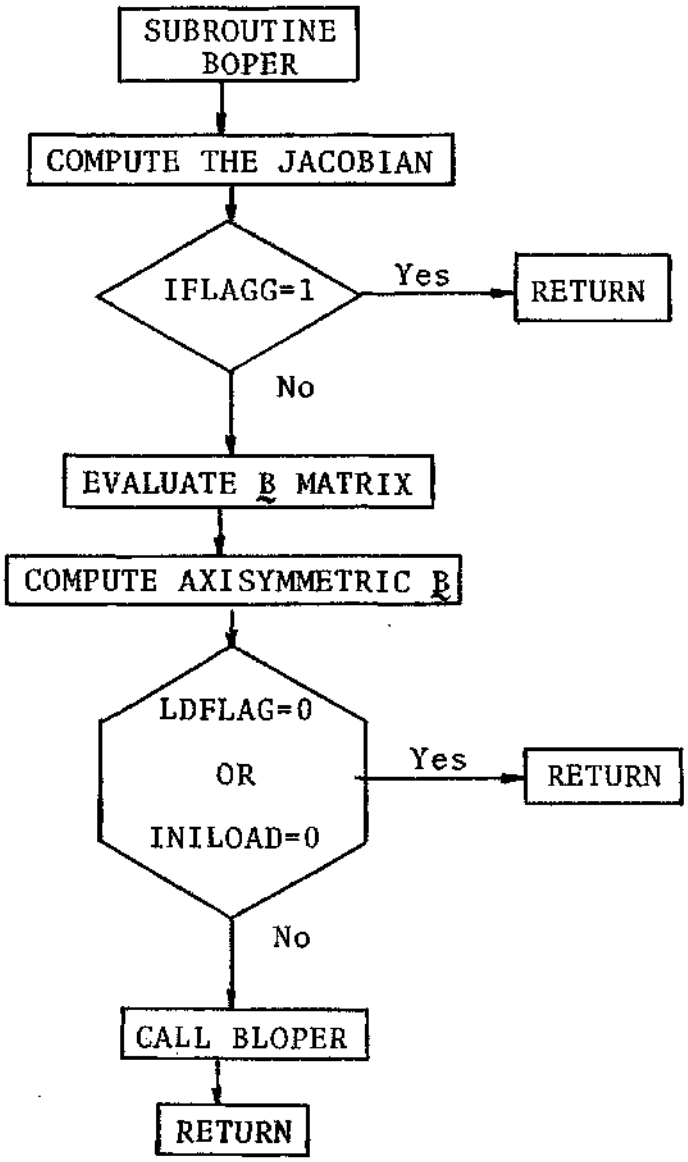

Figure 9-2. Flow Diagram for Subroutine BOPER: Strain-Displacement Operator

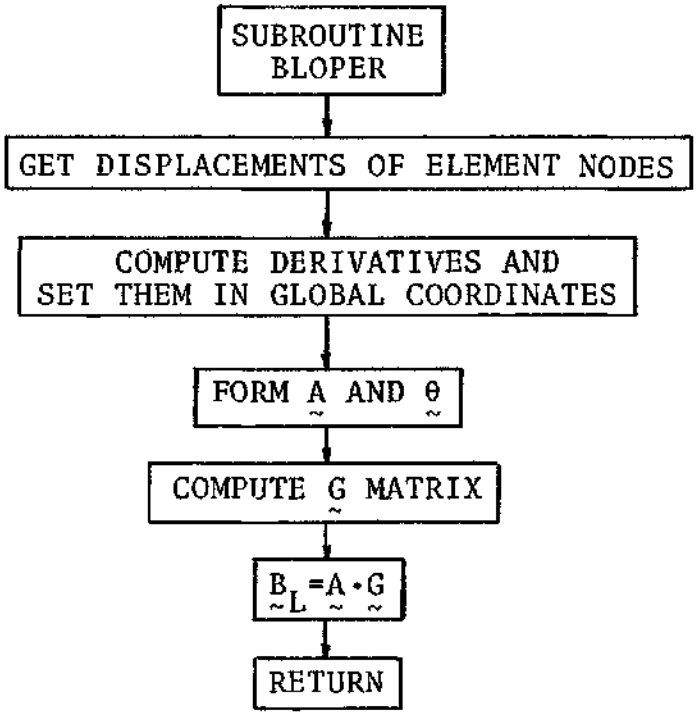

Figure 9-3. Flow Diagram for Subroutine BLOPER; Strain-Displacement Operator for Large Displacements

presented in Chapter VII and the general flow diagram is shown in Figure 9-4.

To compute the element stiffness matrix $\underset{\sim}{S}$ all matrices are now ready and $\underset{\sim}{B}^T\underset{\sim}{\underset{\sim}{D}}\underset{\sim}{B}$ is evaluated for each sampling point of each element. The program utilizes a nine point numerical integration scheme shown in Figure 9-5. For the large displacement computations the total stiffness matrix of the element is given by formulas (31,32) and (33) of Chapter V. Each of the $\underset{\sim}{B}^T\underset{\sim}{\underset{\sim}{D}}\underset{\sim}{B}$ terms are numerically integrated so that

$$\int_V \underset{\sim}{B}^T\underset{\sim}{\underset{\sim}{D}}\underset{\sim}{B}\, dv = \sum_{i=1}^{9} \underset{\sim i}{B}^T\underset{\sim i}{\underset{\sim}{D}}\underset{\sim i}{B} \cdot WT_i \qquad (2)$$

where WT_i is a weight factor for the sampling point i, where the numerical integration is performed. For the eight node axisymmetric, isoparametric element with nine sampling points we have [11,25,147]

$WT = CA(N) \cdot CA(n) \cdot 2\pi \cdot RI \cdot \det|J|$

$RI = RP(N) \times DELRH + RAVG$

$CA(1) = CA(3) = 0.555556$

$CA(2) = 0.888889$

$PR(N)$ = local r coordinate for sampling point N

$DELRH$ = average half of the element radial length

$\det|J|$ = determinant of the Jacobian matrix (see Chapter III).

After each sampling point is integrated the element stiffness is stored into the general stiffness matrix of the system by calling subroutine SSTIF.

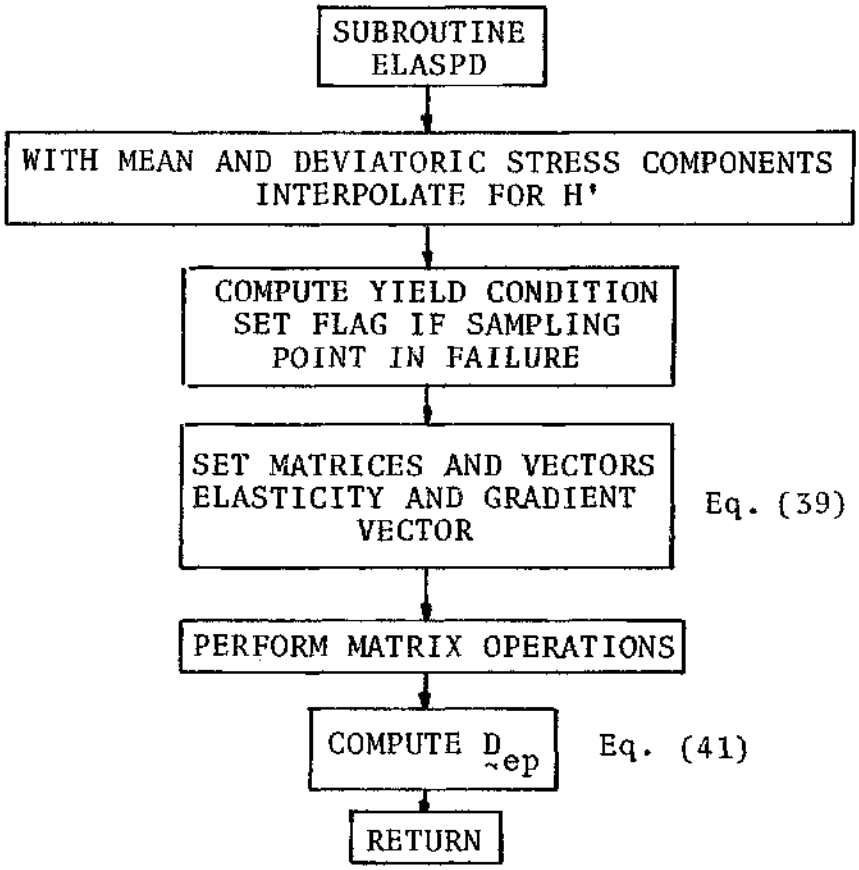

Equation numbers refer to Chapter VIII

Figure 9-4. Flow Diagram for Subroutine ELASPD: Elastic-Plastic Constitutive Matrix

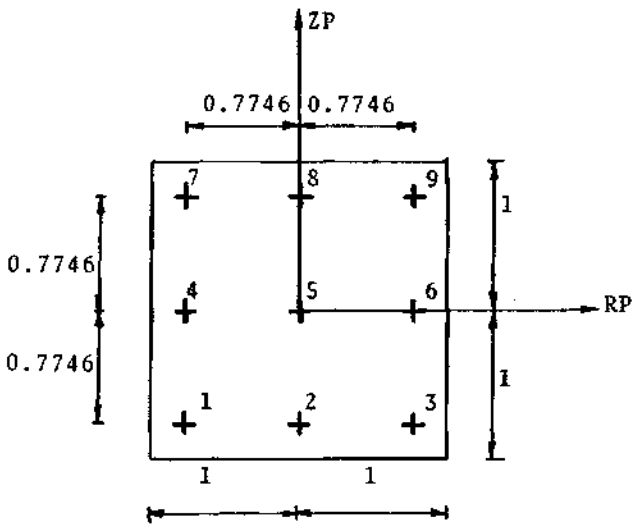

Figure 9-5. Sampling Points for the Eight Node Isoparametric Element

To solve the system of equations a symmetric, narrow banded equation solver [11] is used (subroutine COLSOL). The stiffness matrix of the system is stored in the following way in vector A:

$$\underset{\sim}{K}_{system} = \begin{bmatrix} \overbrace{a_{11} & a_{12} & a_{13}}^{MBAND} & 0 & 0 & 0 \\ & a_{22} & a_{23} & a_{24} & 0 & 0 \\ & & a_{33} & a_{34} & 0 & 0 \\ & & & a_{44} & a_{45} & 0 \\ \text{symmetric} & & & & a_{55} & 0 \\ & & & & & a_{66} \end{bmatrix} \tag{3}$$

The elements of $\underset{\sim}{K}$ are stored by columns from the diagonal term up to the bandwidth, MBAND, in a vector $\underset{\sim}{A}$ as follows:

$$A = [a_{11} \quad a_{22} \quad a_{12} \quad a_{33} \quad a_{23} \quad a_{13} \quad a_{44} \quad a_{34} \cdots$$
$$a_{24} \quad a_{55} \quad a_{45} \quad 0 \quad a_{66} \quad 0 \quad 0] \tag{4}$$

MBAND is the bandwidth of the matrix and is computed by

$$MBAND = (MD+1) \cdot 2 \tag{5}$$

where

MD = maximum difference between node numbers of an element

For the interface elements the stiffness matrix is computed in a closed form by subroutine SPRSTIF. The flow diagram is shown in Figure 9-6 and the mathematical procedure is presented in Chapter VI. The interface element stiffness matrix is then stored in the general stiffness of the system with subroutine SSTIF.

The stiffness of the two dimensional fabric axisymmetric element is computed and stored by subroutine FABSTIF following the computation procedure delineated in Chapter VI. A general flow diagram is shown in Figure 9-7. At this point the general stiffness matrix of the system, consisting of stiffness matrices from isoparametric eight node elements, interface elements and fabric elements is assembled in the vector $\underset{\sim}{A}$.

In the input preparation the program asks for the weight flag LWFLAG. If LWFLAG=0 the total body weight and external pressures are applied by increments. If LWFLAG=1 the full body weight is applied first in one increment and then the external pressures and node loads are applied in NUMLI, a specified number of load increments. The total specified node displacements and loads are applied in the first load increment. The load vector $\underset{\sim}{P}$ is assembled in the main program. The body forces are integrated numerically and applied as concentrated forces to the corresponding nodes. The external pressures

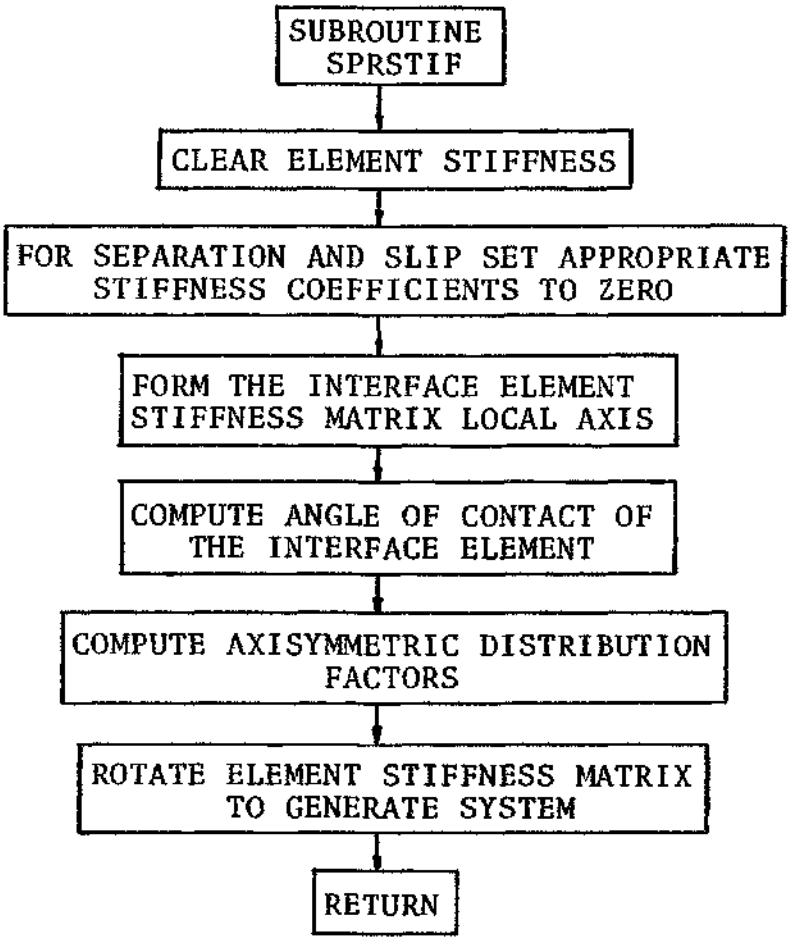

Figure 9-6. Flow Diagram for Subroutine SPRSTIF: Interface-Element Stiffness Matrix

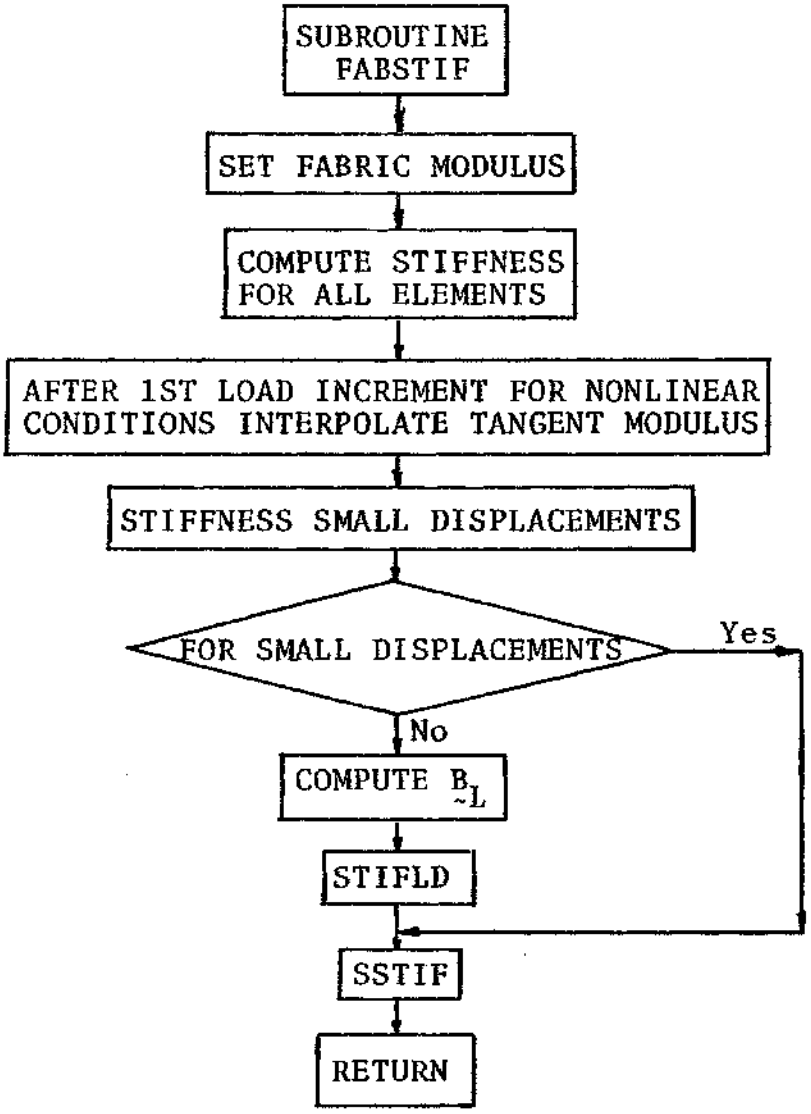

Figure 9-7. Flow Diagram for Subroutine FABSTIF: Fabric Element Stiffness Matrix Subroutine

are distributed to as concentrated forces the nodes in a consistent form with the axisymmetric distribution functions, AV presented in Chapter IV.

Boundary conditions and nodal displacements are also specified for a given nodal restraint. A large term (1×10^{11}) is multiplied by the diagonal term and stored in the appropriate location of the direction of the restraint in order that negligible displacements are computed in the restraint direction. In the program the vector MAXA[N] specifies the location of the diagonal term of the general stiffness matrix for the N-degree of freedom [11]. This is a convenient way to locate the diagonal terms stored in vector $\underset{\sim}{A}$. The solution of the system of equations gives the values of the displacements for all degrees of freedom of the system.

The total external load is applied in NUMLI increments. The first load increment is solved assuming linear elastic response. The maximum elastic displacement of the system when subjected to full load is then calculated using the displacements obtained from the first load increment. A norm is set as a percentage of the maximum elastic displacement of any node in the system, with appropriate values being between 3% and 5%. The maximum displacement of any of the nodes for the iteration is compared with the norm and the program will stop iterating for the load increment when the maximum displacement of the iteration is less than the norm. A value of 5% is taken when no norm is input to the program.

In Figure 9-8 a load-displacement curve of the system is shown and graphically presents the maximum allowable displacement per iteration (norm). The program sets ITFLAG=1 if the maximum displacement of the iteration is larger than the norm and iterates until this value is smaller than the given norm. Then the program prints the message: ITERATION DISPLACEMENTS LESS THAN:,

After applying a load increment the program tests for equilibrium computing internal and external loads. The unbalanced forces given by equation (23) of Chapter V are applied to the system to restore equilibrium, for the case of nonlinear analysis.

Using the computed displacements the stresses and strains are computed by means of subroutine STRES1, the corresponding flow diagram is shown in Figure 9-9. The routine initializes constants and computes the elasticity matrix of the elements for each sampling point. Computes the stresses and strains and calling the subroutine TRANST, see Figure 9-10, the true Cauchy stress and the accumulation of stresses is performed by increments as explained in Chapter V. Subroutine STRES1 also computes the principal stresses and strains.

The failure condition is then computed for each sampling point. For points in failure outside the failure envelope, the stress modification of Chapter VIII is applied by calling subroutine ELIMST (refer to the flow diagram in

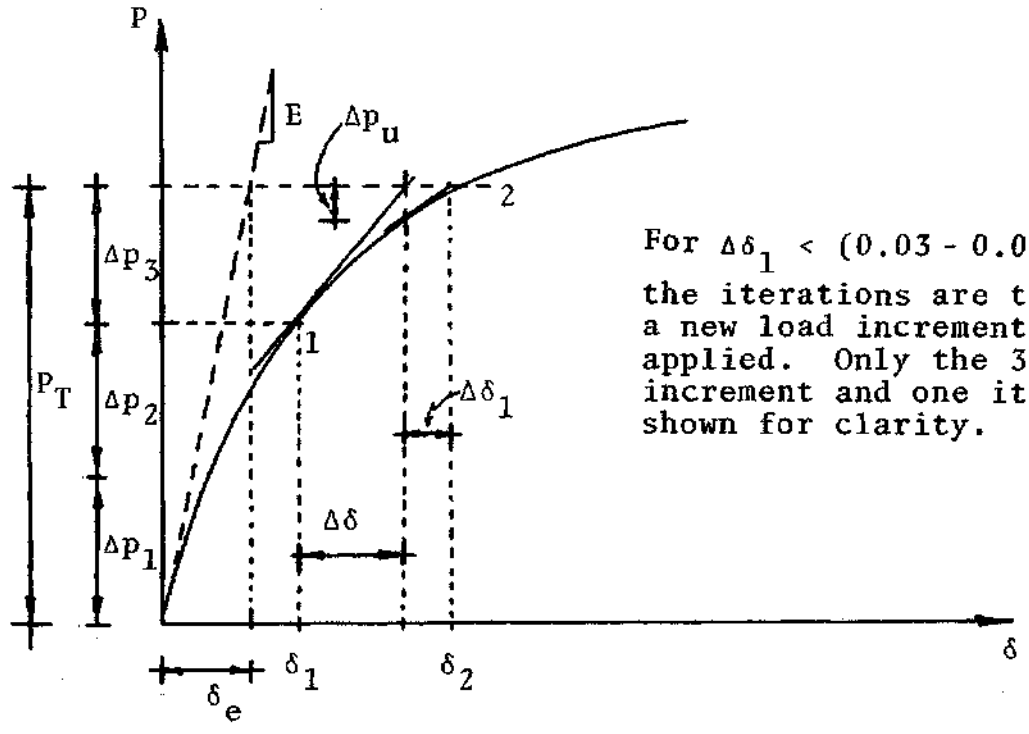

P_T = total applied load

Δp = applied load increment from 1 to 2

δ_e = total elastic displacement

δ_1 = displacement of start of load increment

$\Delta \delta$ = computed increment of displacement

Δp_u = unbalanced force for the load increment

$\Delta \delta_1$ = increment of displacement due to unbalanced force for iteration 1

δ_2 = displacement at end of iteration 1

Figure 9-8. Norm for Maximum Displacement for a Given Iteration

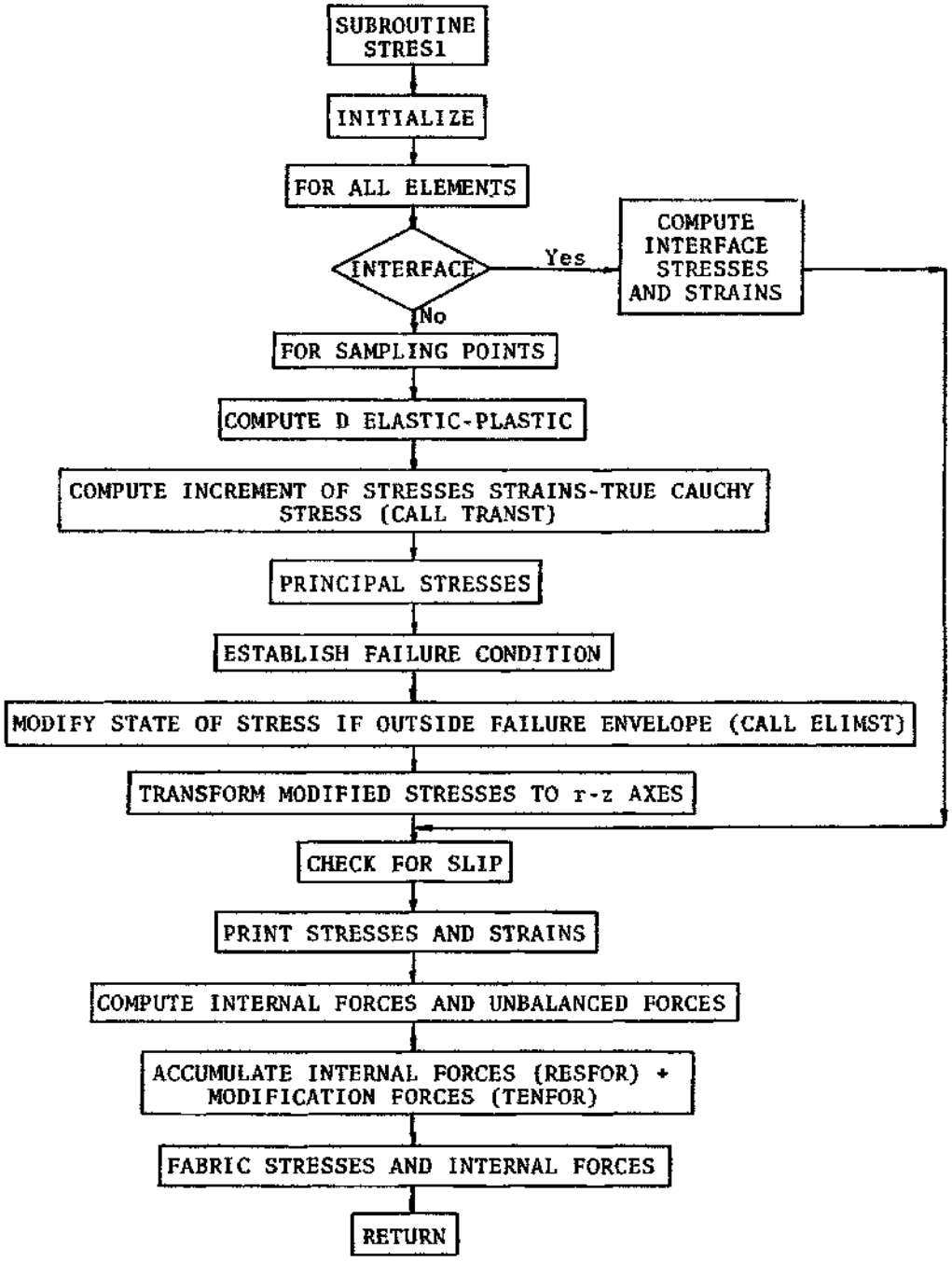

Figure 9.9. Flow Diagram for Subroutine STRES1: Computation of Stresses and Strains

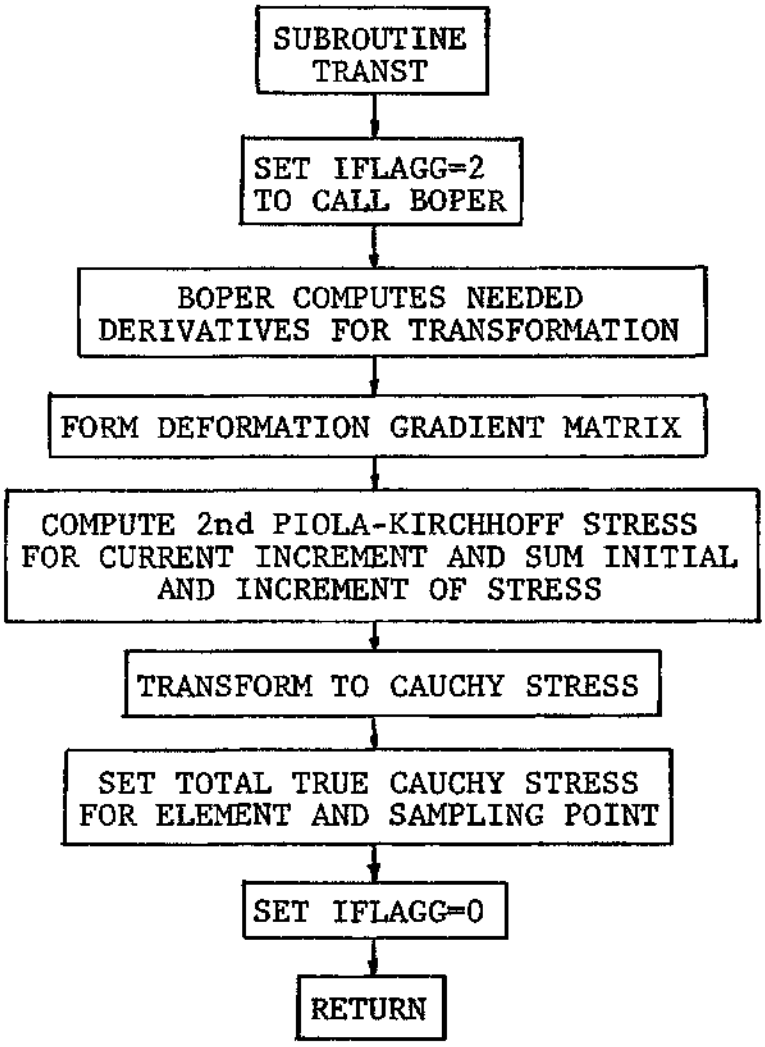

Figure 9-10. Flow Diagram for Subroutine TRANST: Transformation to True Cauchy Stress

Figure 8-3 of Chapter VIII). The modified stresses replace the original computed stresses which fall outside the failure envelope. To maintain equilibrium the forces that produced the stress modification are applied to the system in the next iteration.

Subroutine STRES1 outputs the stresses and strains for all the elements. The stress is given for the centroid of each element although the computation is performed for the nine sampling points of each element and can be printed if desired.

The final part of STRES1 computes the internal forces for the isoparametric eight node elements, interface elements, and fabric elements and stores the internal forces in the array PRES. The modification forces due to sampling points outside the failure envelope are also stored in PRES.

In STRES1 using the stresses previously computed the slip conditions of the interface elements are defined and the appropriate slip forces are calculated. The flow diagram showing the slip algorithm proposed by Herrmann [59] is shown in Figure 9-11. The complete slip computation process is presented in Chapter VI. In formula (21), Chapter VI, the unbalanced forces due to slip are given.

Finally after control leaves STRES1 the main program writes the total displacements, updates nodal coordinates and writes internal and unbalanced forces. Depending on the value of the flag ITFLAG, the program either iterates or increases

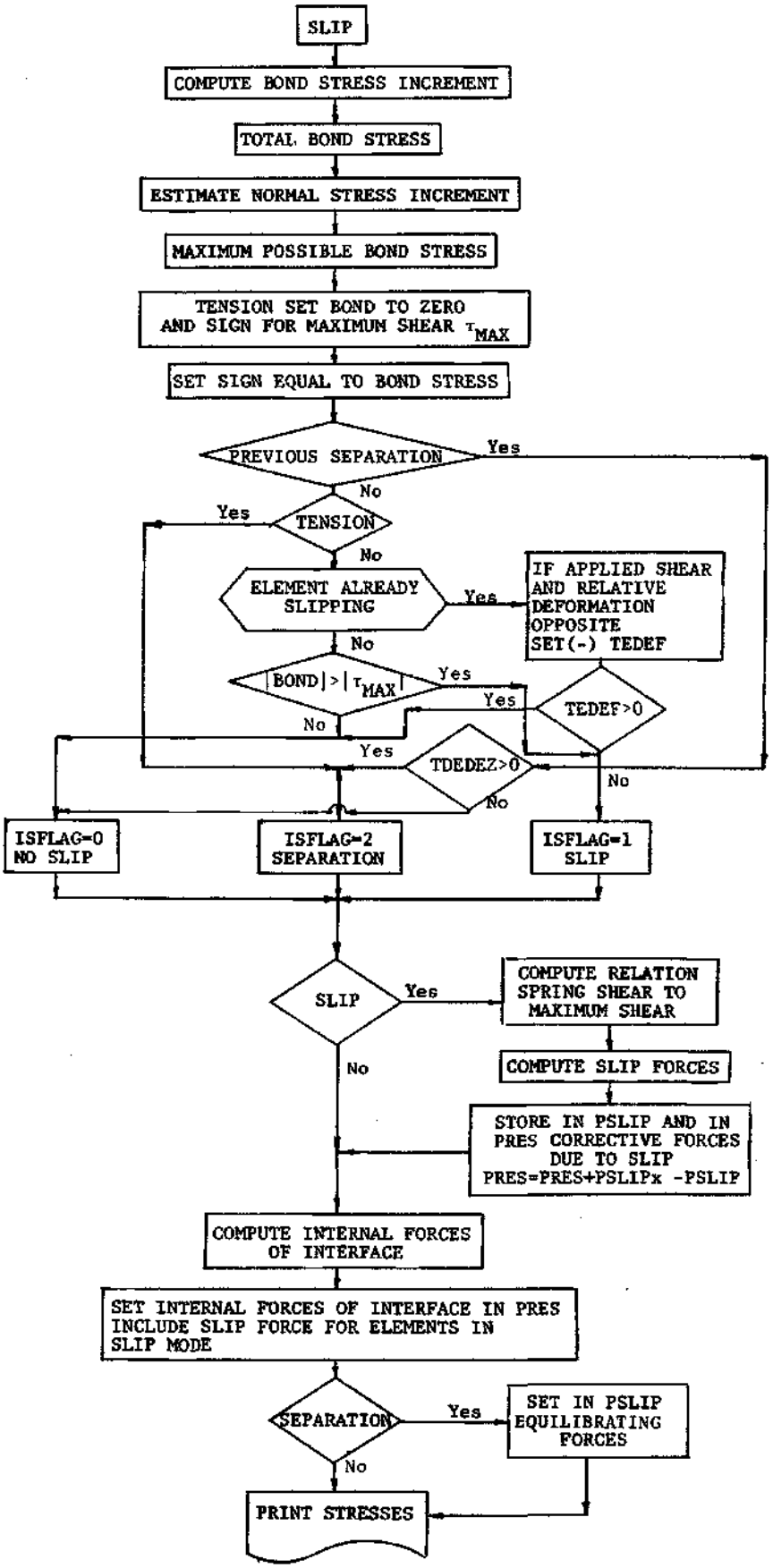

Figure 9-11. Slip Algorithm in Subroutine STRES1 after Herrmann [59].

the load by a load increment. If the program does not converge in eight iterations for one load increment it automatically stops giving a message: NUMBER OF ALLOWABLE ITERATIONS EXCEEDED. A list of some of the causes of no convergence follows:

(i) The load increment is too large

(ii) Unbalanced conditions exist due to geometry

(iii) Material near failure produces unbalanced conditions

(iv) Fabric elements are too large

(v) Mesh is too coarse to compute the stresses accurately

Input-Output Capabilities

The processing of the computer code for the soil-fabric system requires the following information. Any units may be used, but they must be consistent throughout the example. The dimensional units are given in parentheses with F = force, L = length and (°) = degrees.

(a) Geometry

Number of nodes, elements, interface elements and fabric elements, nodal coordinates, element topology, scale factors

(b) Material Properties

For each material the following data is necessary:

Unit weight (F/L^3)

Modulus of elasticity (r and z directions) (F/L^2)

Poisson's Ratio (r and z directions)

Shear modulus (F/L^2); $G = E/2(1 + \nu)$

Tension modulus (F/L^2)

Equivalent stress at yield ($\bar{\sigma}_o$)(F/L^2)

Cohesion (F/L^2)

Angle of internal friction (°)

Tensile strength (F/L^2)

The plasticity parameters are defined by a collection of pairs of values with $\bar{\sigma}(F/L^2)$ and H'. For the computation of the variable modulus with confinement (following Chapter VIII), the following data is required:

Cohesionless and cohesive materials: The constants k_1 and n are needed.

Cohesive materials: Three values of $E_r(F/L^2)$ vs $\Delta\sigma(F/L^2)$ (resilient modulus vs derivator stress).

(c) Fabric Properties

Elastic limit in tension (F/L)

Tension modulus (F/L)

Cohesion (F/L^2) and angle of friction (°) between the fabric and the adjacent materials,

Fabric incidences

(d) Interface properties

Shear subgrade modulus, k_s (F/L^3), normal subgrade modulus, k_n (F/L^3), cohesion and internal friction of interface

(e) External pressures and concentrated loads

Number of load increments, nodes of application,

magnitude of the loads (F/L^2)

(f) Boundary Conditions

Fixed, free r and z directions, free r or z directions

(g) Options

Application of the body weight first, before external pressures are applied or combined with external pressures, large displacement strain terms or usual small strain definitions, constant or variable resilient modulus for clay or silt, output of stresses and strains or stresses and principal stresses.

A control card after the execution of the program will output incremental displacements, stresses of all sampling points, internal and unbalanced forces.

(h) Norm

Maximum allowable displacement for the iteration from 3% to 5%. The last value taken as a default if no value is given.

The output capabilities of the computer program give a complete state of stress, strain and deformation of the finite element model. For each load increment and iteration the following information is printed out. A list of the output follows:

(a) Printing of all input data for verification. Then for each element or nodal point in each load increment or iteration the following values are printed:

(b) Stresses and strains: radial, vertical, tangential and shear for the centroid of each element. Optional to print principal stresses and strains.

(c) For interface elements prints the mode behavior: no slip, slip or separation and the shear and normal stress at the interface.

(d) Radial and tangential stresses and strains for the fabric elements.

(e) If the stresses exceed the failure condition of the material a message with the element number and the sampling point where the failure conditions were exceeded is printed.

(f) The total nodal displacements.

By including a special control card at the end of the execution of the program, the following additional results are also printed:

(g) The computed increment of displacements corresponding to all load increments,

(h) Stresses and strains for all sampling points,

(i) The updated nodal coordinates.

(j) The internal and unbalanced forces after each load increment (optional).

Summary

The computer program developed predicts the response of axisymmetric solids to loads. The material can behave in a linear elastic or nonlinear plastic form. The no tension

characteristics of the cohesionless materials are taken in account and interfaces with or without fabric materials are modeled. The load is applied in increments and a complete stress-displacement history of the soil-fabric system is obtained.

The accuracy of the solution obtained with the finite element formulation of the soil-fabric system, due to the several features of the program depends on the input parameters and their correct representation of the nonlinearity of the materials modeled. The number of load increments used will affect the results and the total computer time required by the program. A very small number of load increments will not provide enough accuracy and the stress state computed might be considered outside the failure envelope. On the other hand too many load increments will make the program very costly to run. The plasticity example of Chapter X provides interesting data on the accuracy obtained as a function of the number of load increments used.

The example No. 4 is used here to compare the results for 4, 8 and 12 load increments, using the experimental results as basis of comparison. A maximum allowable displacement ratio of 0.05 was used. The stress-strain relationship is given in Figure 9-12 and the variations are shown in Table 9-1 for an applied unit load of 6 psi.

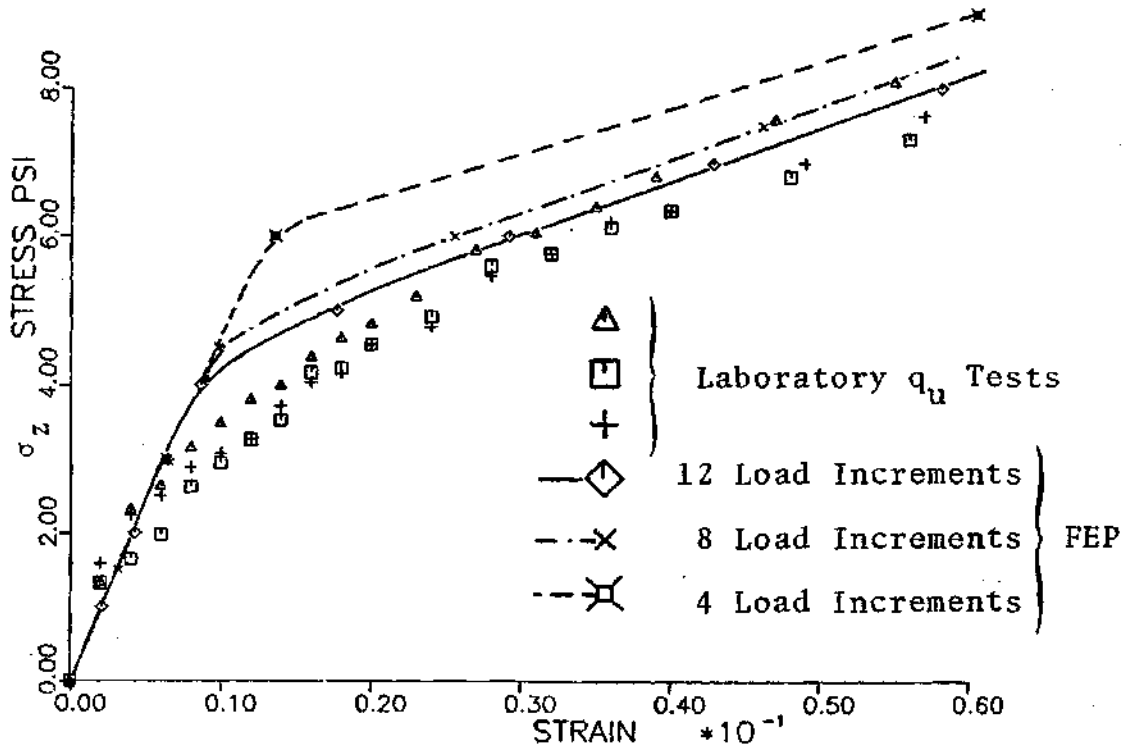

Figure 9-12. Variation of the Computed σ-ε Relation with the Number of Load Increments

Table 9-1. Results with Variable Number of Load Increments

Number of Load Increments	Strain for 6 psi	% of Experimental Result
4	0.0136	42.5
8	0.0256	80.0
12	0.0300	93.8

Figure 9-12 and Table 9-1 show that four load increments did not give acceptable results, eight increments yield an estimate within 20% of the measured value and twelve load increments resulted in a difference of 6%. The load level corresponded to 50% of the failure load of the specimen.

Using 4 load increments, the maximum displacement ratio of 0.05 was reduced to 0.02. No significant improvement on the computed strains and displacements was obtained. If the number of load increments is large the increase in stresses for all elements will provide with a detailed sequence of the elements (sampling points) that go into failure. Also, a better estimate of the stresses in the system can be obtained. For this reason it is important to keep the load increment small.

Computation of stresses at sampling points near the axis of symmetry presents problems due to the tangential terms in the $\underset{\sim}{B}$ matrix that are functions of $\frac{1}{r}$ [110]. A centroidal

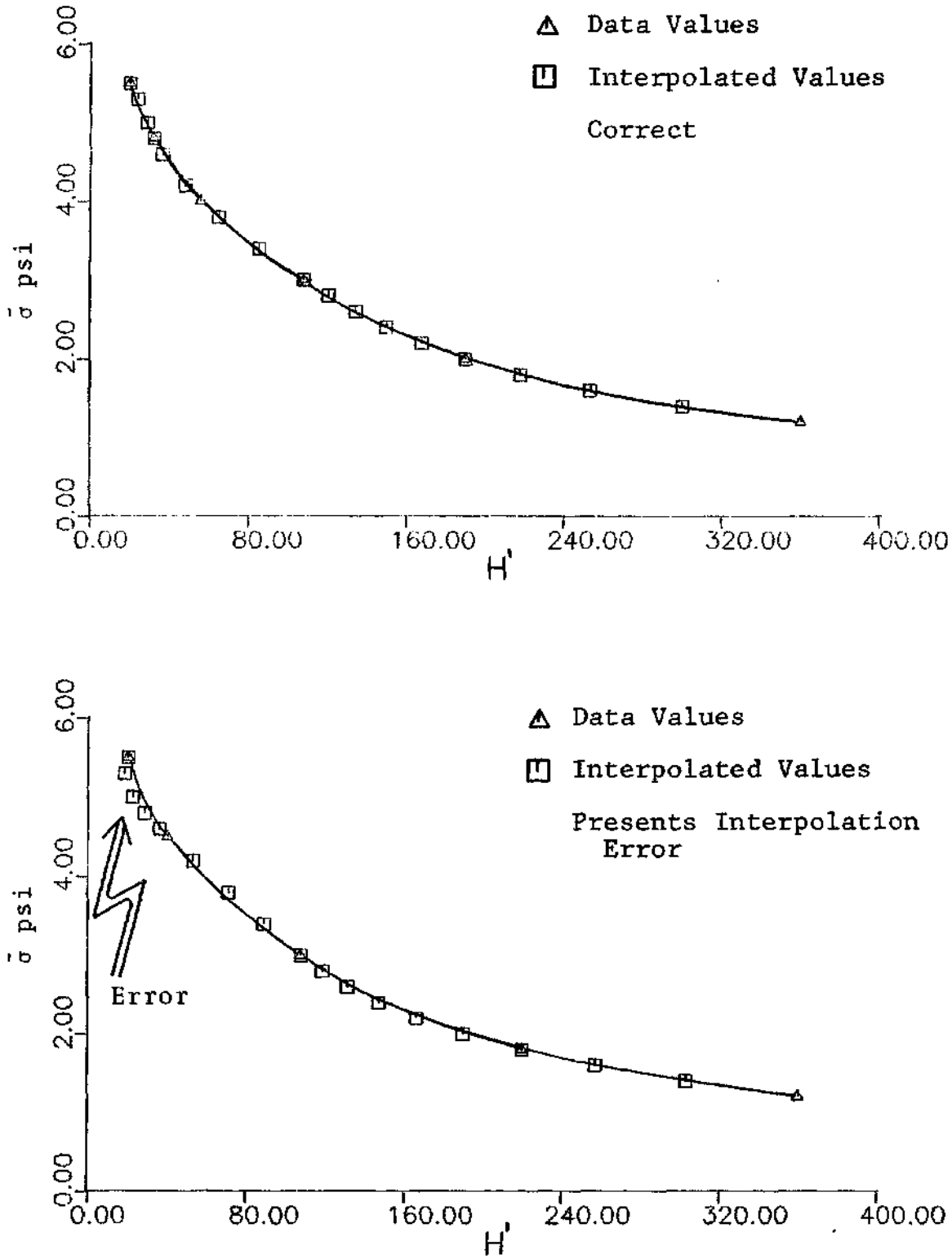

Figure 9-13. Interpolation of the Plasticity Parameter

value should be taken for those elements [25] especially if $r << a$, where a is the length of the element in the radial direction. Use of the centroidal values were failure to provide good estimates as shown in the examples of Chapter X.

The nonlinear material properties input to the program should be plotted and verified before using them in the finite element model. The interpolation routine of the program is based on a Lagrangian interpolation formula [45]. This formula might present problems, particularily at small values of H', for the representation of unevenly spaced data in higher order polynomials. It is advisable to compare the experimental curve with values obtained by interpolation. Figure 9-13 shows a problem that can occur. Some authors [137] suggest giving a mathematical formula for the variation of H'. In these cases extra parameters to define the behavior of H' with $\bar{\sigma}$ are needed.

CHAPTER X

APPLICATIONS OF THE COMPUTER CODE

The computer code developed calculates the load application deformation characteristics of a multilayer system. At the present even with our advanced computer technology it is still not feasible to model the complete repeated load test, due to the large number of load applications. We can analyze the soil-fabric model for material parameters obtained at selected numbers of load applications and assign a range of load repetitions over which these parameters are taken as constants. To follow any other approach would result in excessive computer time.

For the verification of the program several individual tests were performed, this provided means to check the various elements that constitute the program.

The verification of the program consisted of

(a) Individual tests on the response of the elements that form the soil-fabric model: eight node isoparametric elements, fabric elements, plastic behavior, no tension, interface elements and slip. Laboratory results and theoretical solutions were used to evaluate the results of these tests. The numerical operations performed by each subroutine were hand calculated for numerous test cases and compared with the program results.

(b) Elastic analysis on the behavior of the complete finite element formulation.

(c) Small and large displacement comparisons of obtained results with solutions given in the literature.

(d) Computations of stresses and deformations for the soil-fabric system for parameters selected for a certain number of load applications and comparison with laboratory measurements. All dimensions in the examples are given in inches and FEP stands for the finite element program developed in this thesis. Several selected examples used in verifying the program are as follows:

Example No. 1: Stress Distribution Boussinesq Type Problem

The application of a circular load over an homogeneous half space was solved in 1885 by Boussinesq and is given in several textbooks [123,125,127]. This example presents the results obtained by the finite element program (FEP) for a linear elastic, isotropic finite depth model and compares them with the Boussinesq solution. The theoretical Boussinesq solution for the problem of a circular, uniform load applied at the boundary of an infinite layer needs corrections, due to the depth of the rigid layer [107].

The soil-fabric finite element model is solved for several load increments and iterations, therefore it needs an optimum size mesh which gives enough accuracy with the

minimum number of nodes. A mesh of only 16 elements is used to evaluate the accuracy of a small number of elements mesh and the problems associated with the elements close to the axis of symmetry of the model.

The geometry is similar to the geometry of the laboratory tests for the soil-fabric system. The material properties of the 16 element mesh are shown in Figure 10-1. An applied circular vertical load of 3 inches in radius is applied to the system. The stress distribution along a vertical axis below the circular load is shown for the axis of symmetry, the theoretical Boussinesq half space solution and the corrected stress distribution due to the rigid layer position.

Boussinesq solution for the vertical stress along a vertical axis offset 0.5 radius of the loaded area is compared with the finite element program solution for the same axis shown in Figure 10-2. Good results are obtained with the 16 element mesh. It can be observed that the rigid layer correction is about 10% of the total stress at a depth of 18 inches. The program computed values include all sampling points, at the 0.5 r_o offset axis and gives acceptable approximation with this small number of elements mesh.

Example No. 2: Stress Distribution--

Two Layer Elastic Solid

Two layer elastic solutions provide the analysis of infinite half space where layers of different elastic

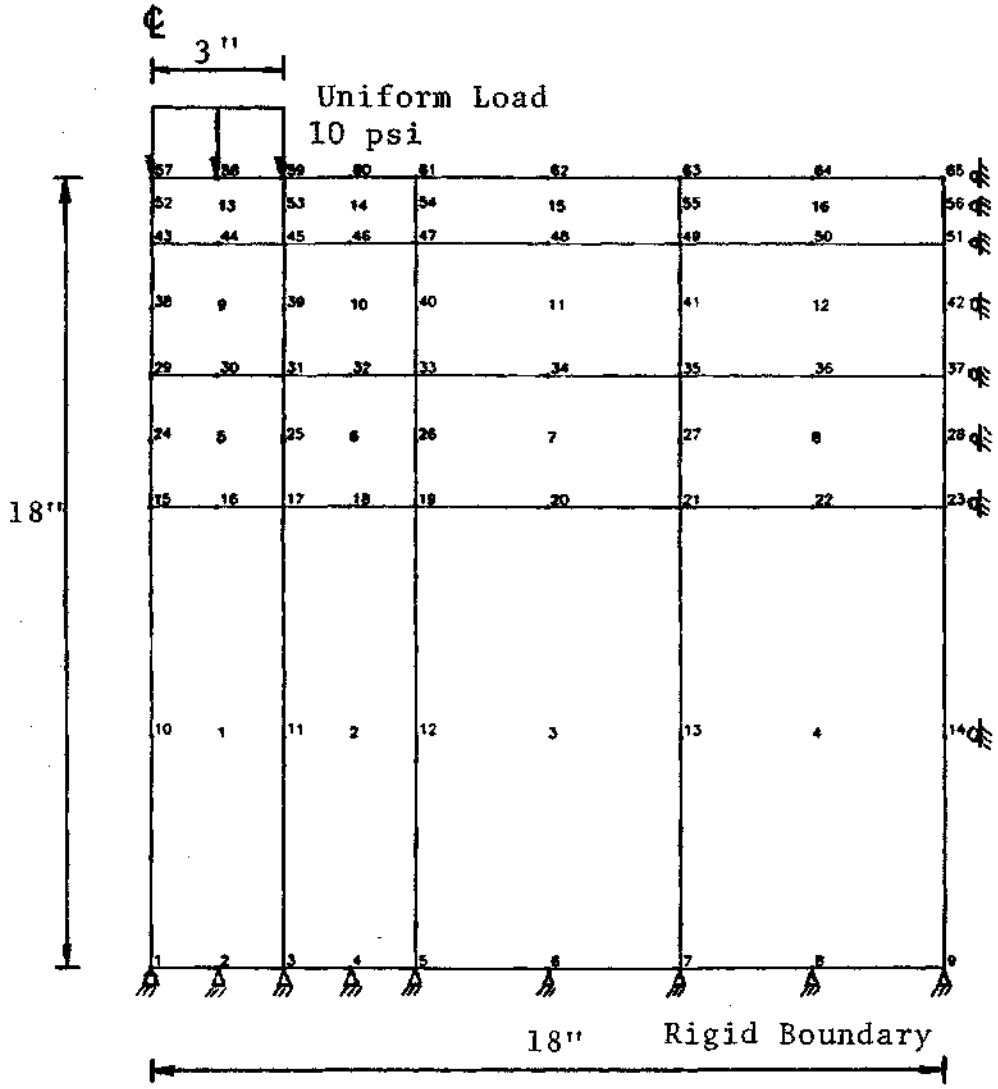

Data: Homogeneous Material
E = 2000 psi
ν = 0.4

Note: Nodes of vertical boundary restrained horizontally and base nodes fixed.

Figure 10-1. Mesh for the Stress Distribution Problem. Example No. 1

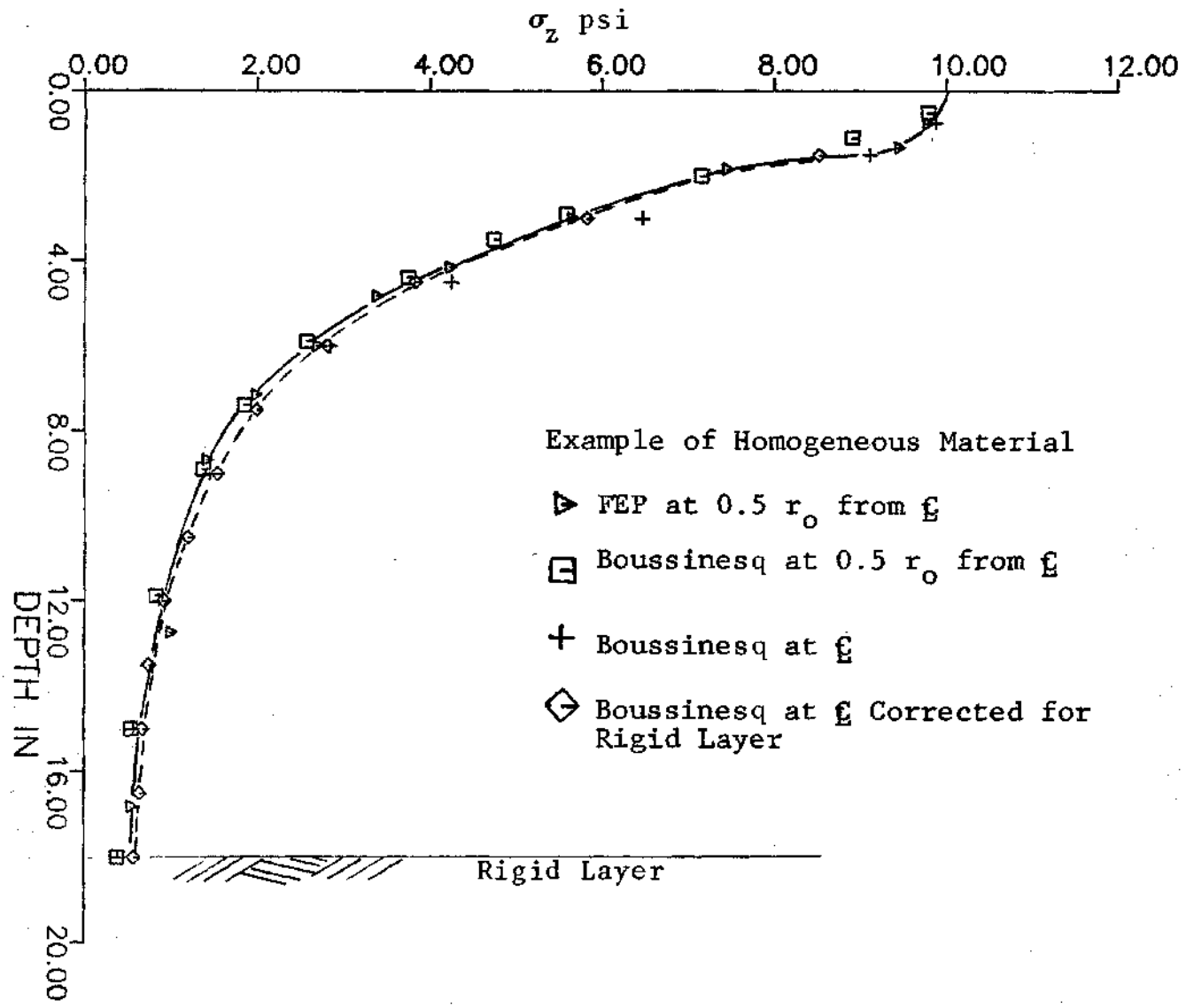

Figure 10-2. Boussinesq and Finite Element Results of the Vertical Stress Distribution. Example No. 1

constants form a two layer system, loaded at the surface with a uniform circular load of radius r_o. The elastic solution to this problem [48] provides with approximate results that can be compared with the finite element models shown in Figure 10-3.

For the solution of multiple increment/iteration problem, the total number of nodes in the model plays a definite role in the total computer time needed. Therefore, comparisons of two proposed meshes and their accuracy on stress-strain computations are presented.

The accuracy of both meshes (Figure 10-3), one with 24 and the other with 54 elements, is compared with the two layer linear elastic solution given in [48] where interpolated values were used to obtain the corresponding elastic constants for the finite element model.

The computed stresses given in Figure 10-4 show maximum differences of vertical stress for the 54 and 24 element mesh of 5% and of 15% with the interpolated two layer infinite depth solution: the unit weight of the material was included in the stress computations and the two layer elastic solution values are interpolated for the centerline of the load. The FEP results are for an axis offset 0.5 r_o from the centerline.

To verify the accuracy of the interface elements the following example was performed:

Taking both meshes with homogeneous material the shear at the interface was computed and compared with the Boussinesq

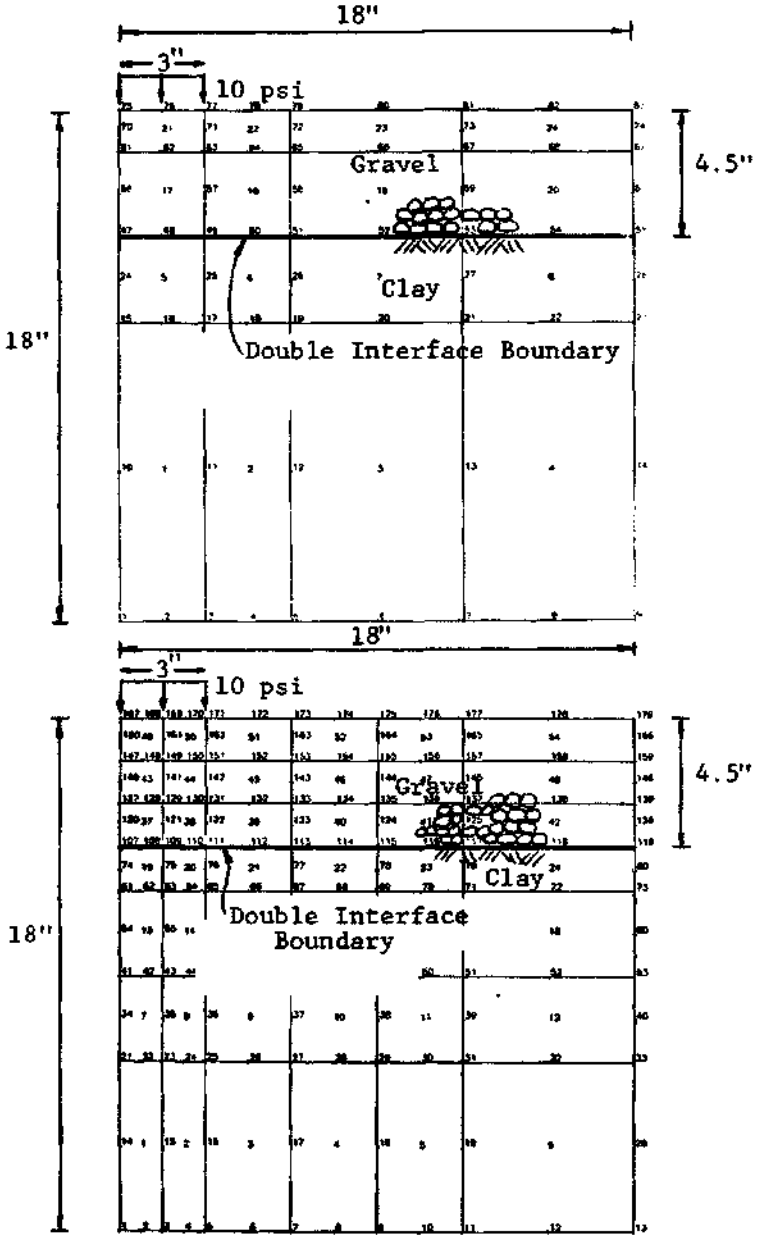

Note: Nodes on vertical boundary retained horizontally and base nodes fixed.

Figure 10-3. Meshes with 24 and 54 Elements Used in Example No. 2

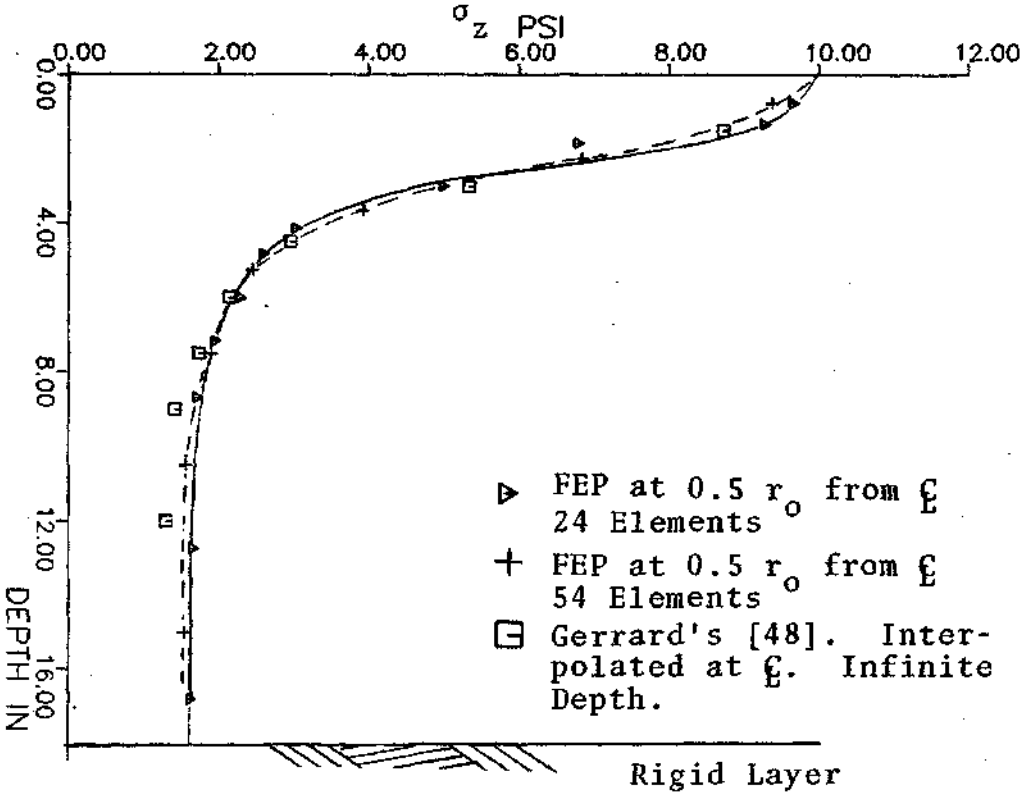

Figure 10-4. Computed Vertical Stress for a Two Layer System. Example No. 2.

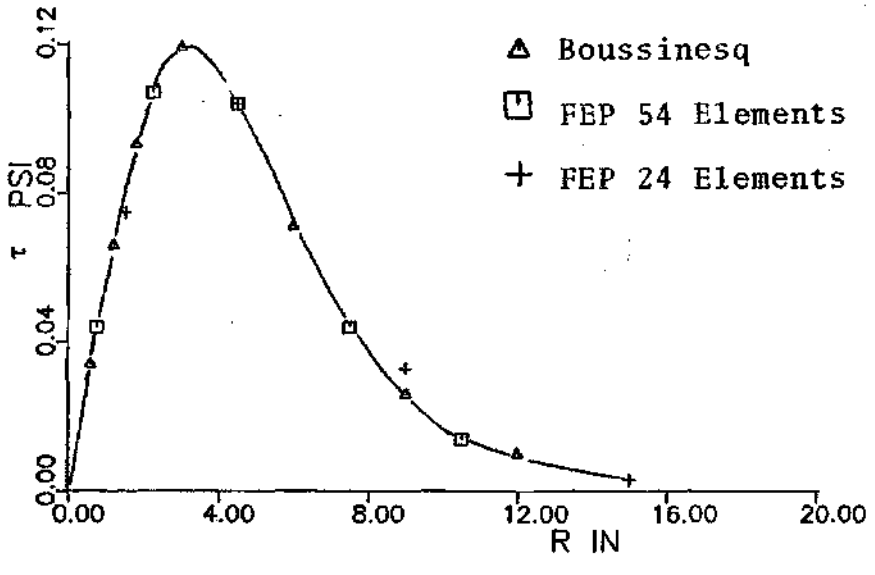

Figure 10-5. Shear Stress at the Interface Elements for Homogeneous Material Horizontal Axis at 4.5 in Depth. Example No. 2

theoretical solution, both meshes and the theoretical results are shown in Figure 10-5. The 54 element mesh gives a maximum difference of 6% and the 24 element mesh 19% of the theoretical Boussinesq result for the shear stress at a depth of 4.5 inch. As would be expected more accuracy is obtained with the 54 element mesh.

Example No. 3: Horizontally Loaded Fabric Element

The theoretical exact elastic analysis of a two dimensional fabric model loaded in tension in the horizontal direction is compared with the results obtained with the FEP computer code. The variation of the radial and tangential stresses along the radius are presented. All data is shown in Figure 10-6.

To aid the stability of the model four eight node isoparametric elements were included below the fabric with a very low modulus of elasticity, in order to run this special case with the general purpose computer code developed. The fabric model consists of eight fabric elements as shown in Figure 10-6.

The theoretical linear elastic, small displacement solution can be found in the literature [72]. The radial and tangential stresses for an external uniform load are given by:

$$\sigma_r = \frac{P_2 R_2^2}{R_2^2 - R_1^2} \left(1 - \frac{R_1^2}{r^2}\right) \qquad (1)$$

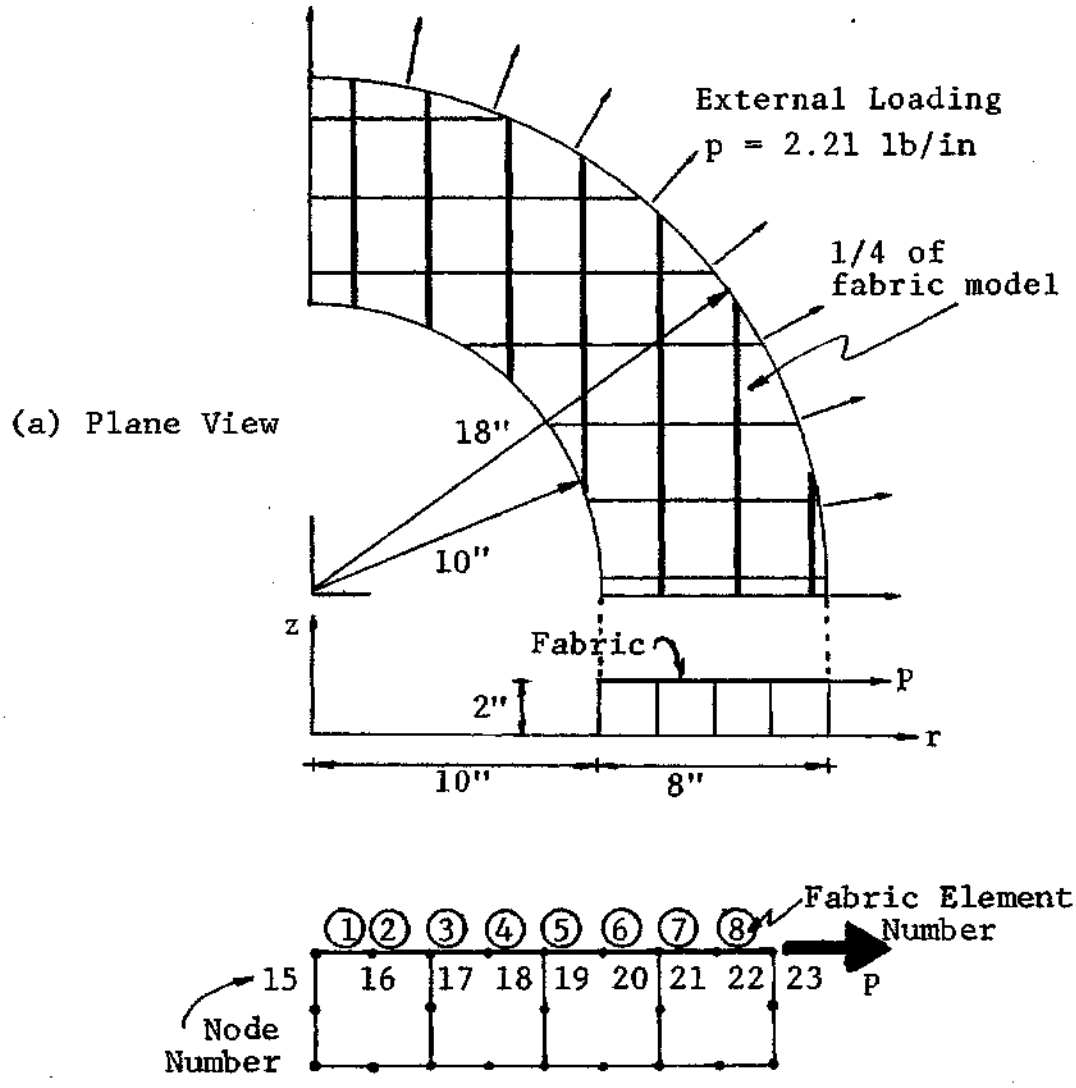

(a) Plane View

(b) Section View of Axisymmetric Model

Data: Two dimensional fabric axisymmetric model
Interior radius = 10 inch
Exterior radius = 18 inch
Tension Modulus = 1000 lb/in
Elastic Limit = 20 lb/in
Tension Load (2π) = 250 lb

Figure 10-6. Geometry and Finite Element Model of a Horizontally Loaded Fabric. Example No. 3

$$\sigma_\theta = \frac{P_2 R_2^2}{R_2^2 - R_1^2}\left(1 + \frac{R_1^2}{r^2}\right) \qquad (2)$$

where

R_1 and R_2 = interior and exterior radius

P_2 = external unit load

The comparison of the theoretical computations and the program results is given in Figure 10-7. As can be observed the eight fabric element model gave excellent results with maximum differences of 1.4%.

Plasticity Examples

In the next two examples applications of the soil-plasticity theory developed in Chapter VII are presented. An unconfined compressive strength test, q_u-test and a load test of a circular footing over soft clay, reported in the literature [29], are analyzed with the finite element program.

Example 4: Unconfined Compression Test

The axisymmetric conditions of an unconfined compressive strength test (q_u test) permit using the finite element formulation for the analysis. The soil is a soft gray clay used in soil-fabric laboratory tests. The soil index properties, stress-strain curves and the elasticity and plasticity parameters are all given in Figure 10-8. The finite element model having 16 elements used to represent the soil specimen is shown in Figure 10-9.

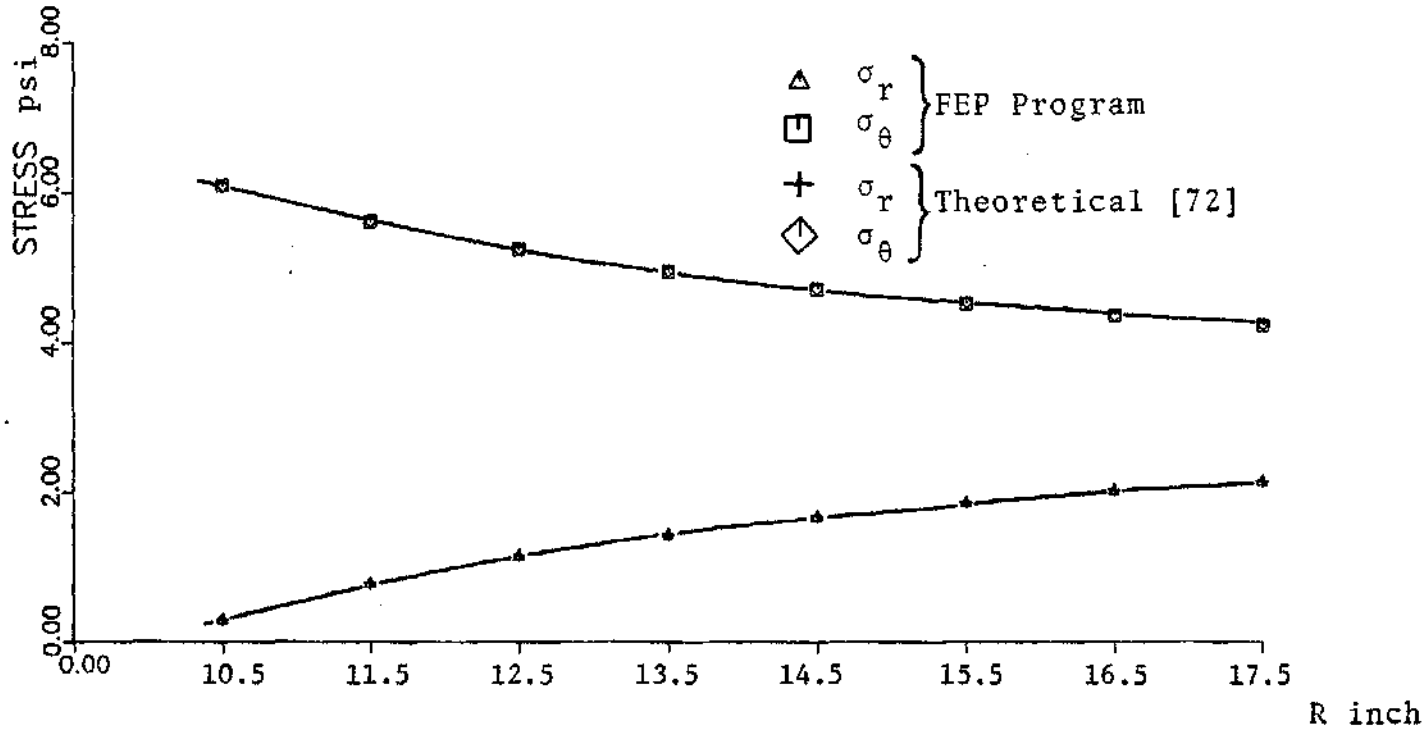

Figure 10-7. Horizontally Loaded Fabric Results for Radial and Tangential Stress. Example No. 3

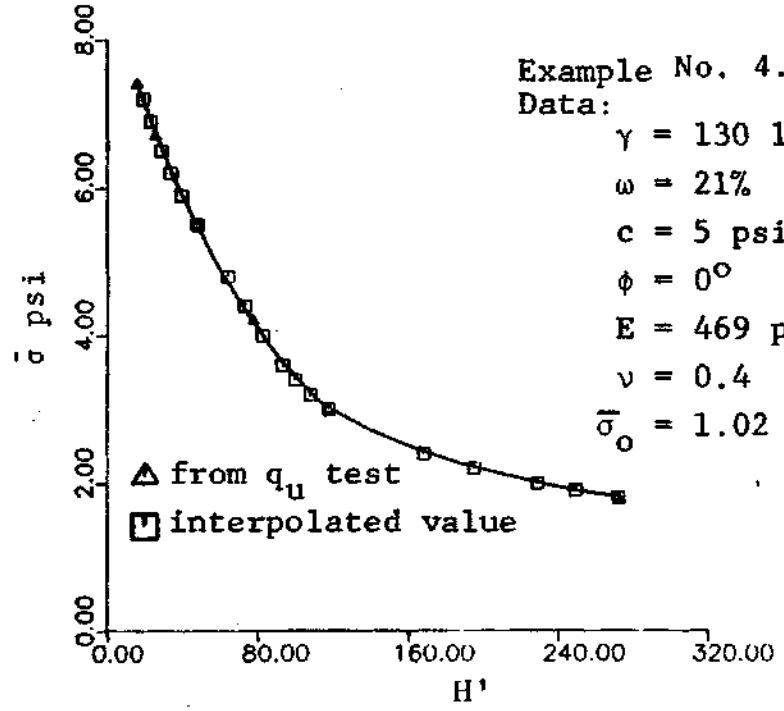

(a) Index Properties and Elasto-Plastic Parameters

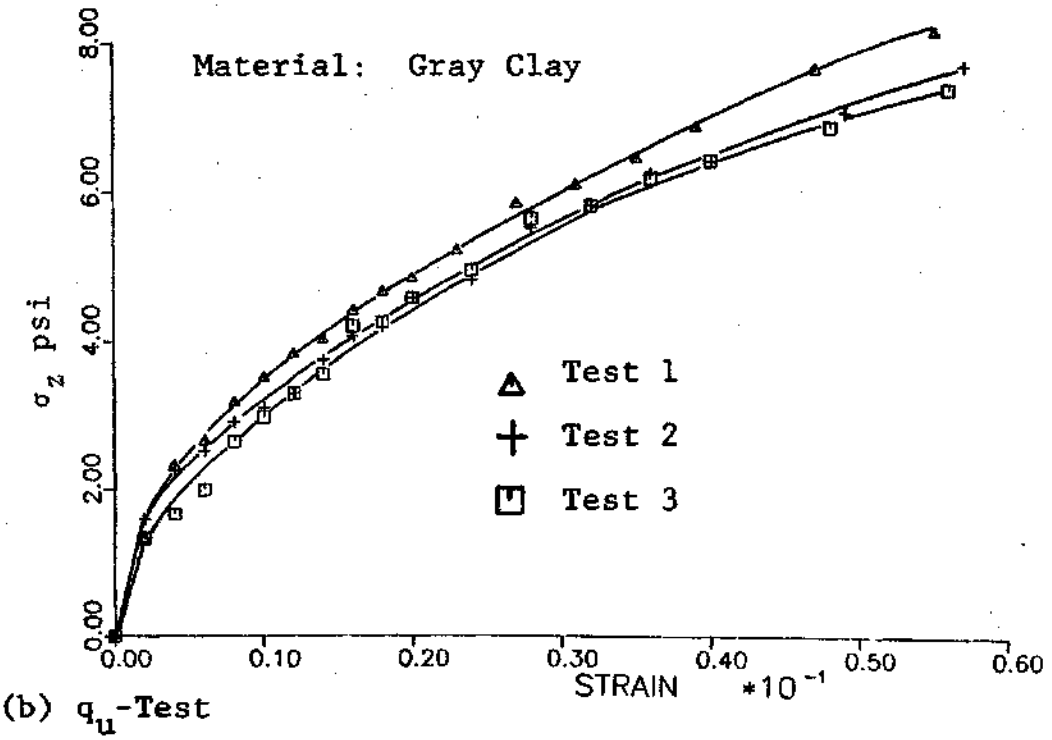

(b) q_u-Test

Figure 10-8. Gray Clay. Parameters for Example No. 4

In Figure 10-10 a comparison is presented of the q_u-test stress-strain results and the elastic-plastic finite element results for the small strain and the large displacement options. The results of the small and large displacement option show good agreement until strains of 5%. For strains larger than 6% the small displacement option still resulted in a good approximation of the elasto-plastic behavior of the sample, while the large displacement option started to drift from the experimental results. There are several possible reasons that result in the apparent better approximation of the small displacement option: (1) Time and viscosity effects are not included, and (2) The experimental results do not include measured lateral deformations. Therefore a comparison could not be made of lateral strains to further verify that correct parameters were used. The maximum allowable deformation per iteration used in the example was 0.05.

Example 5: Circular Footing Over Soft Clay

Many tests of footings over soft clay are reported in the literature. Reference [29] was chosen due to the detail shown in the laboratory tests performed on the material. The paper also gives the results for rigid and uniform loading conditions. The laboratory test of a footing on soft clay was modeled by the mesh shown in Figure 10-11 where the geometry and the applied load are shown.

An average modulus of elasticity was used for the clay.

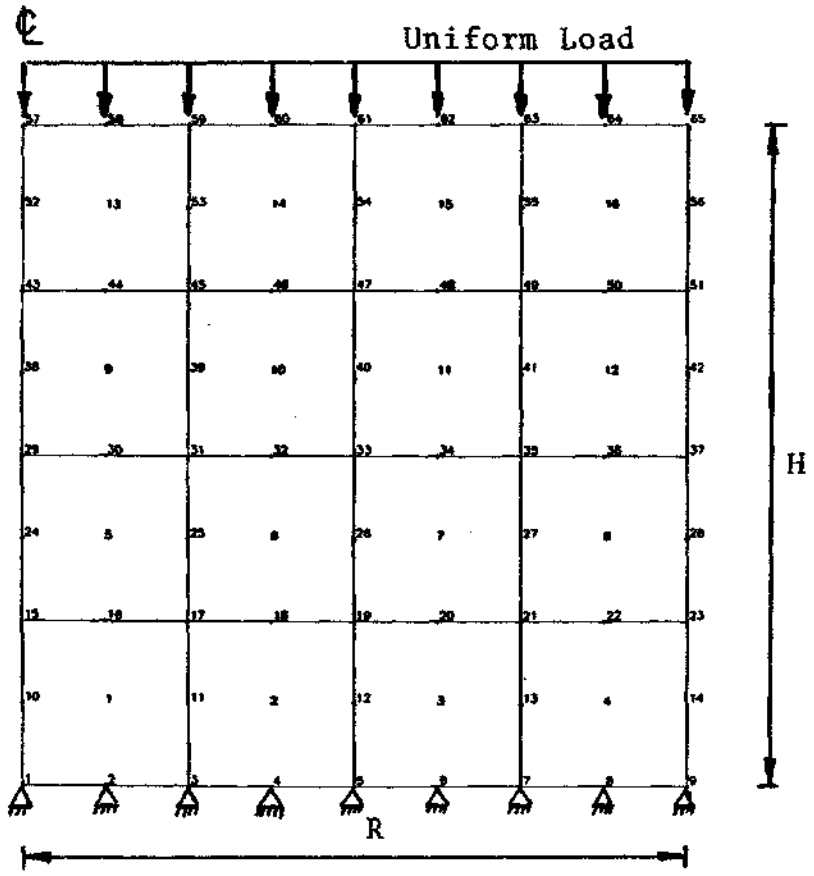

Figure 10-9. Finite Element Model. Example No. 4.

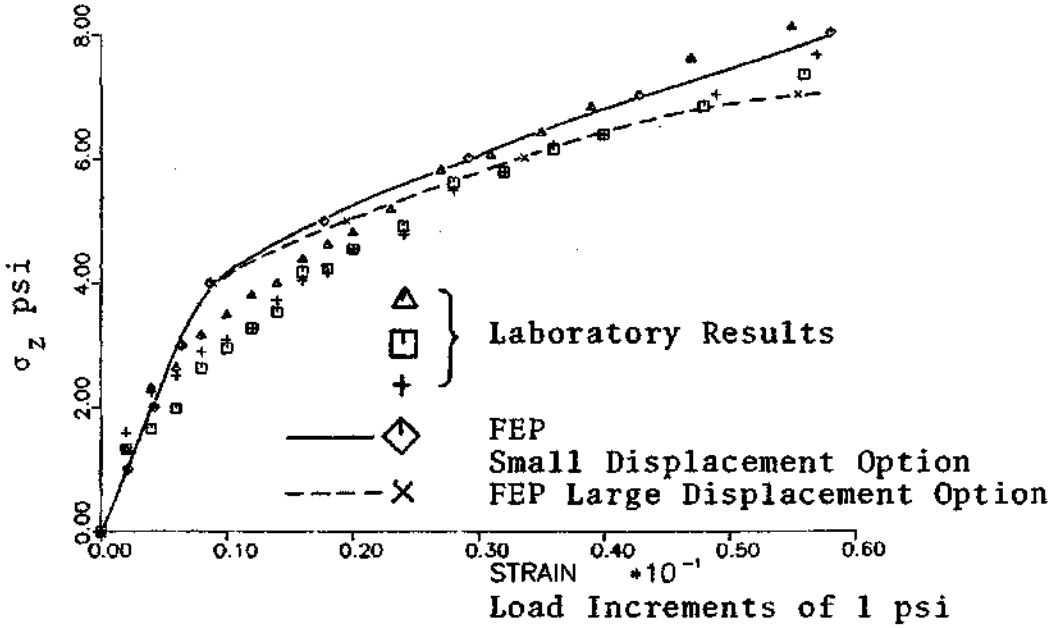

Figure 10-10. Results of the Finite Element Formulation and the Experimental Results for the q_u-Test of Example No. 4

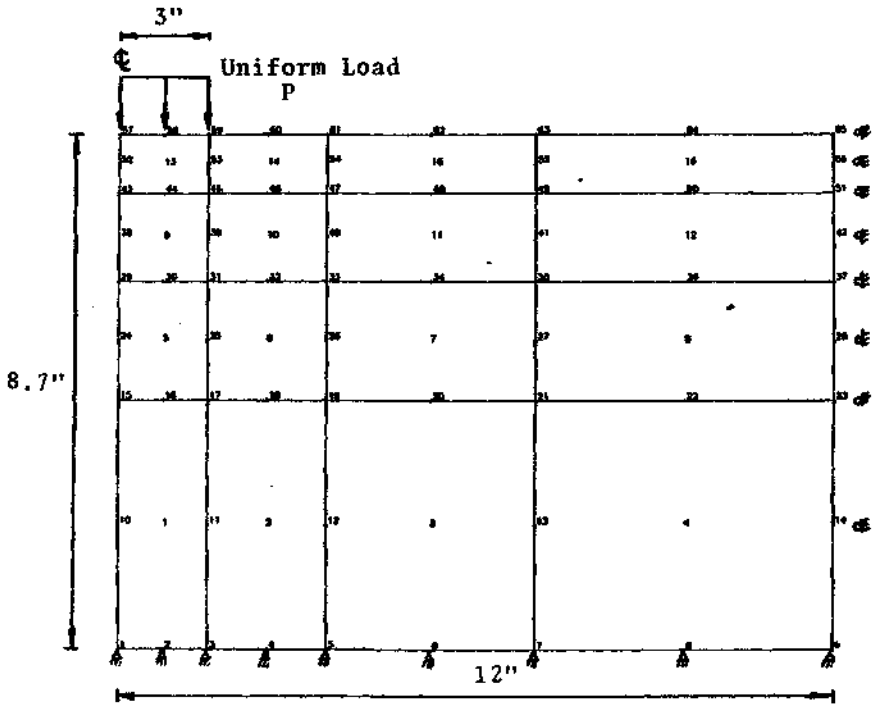

Figure 10-11. Finite Element Model of a Footing Over Soft Clay--Uniform Load Conditions. Example No. 5

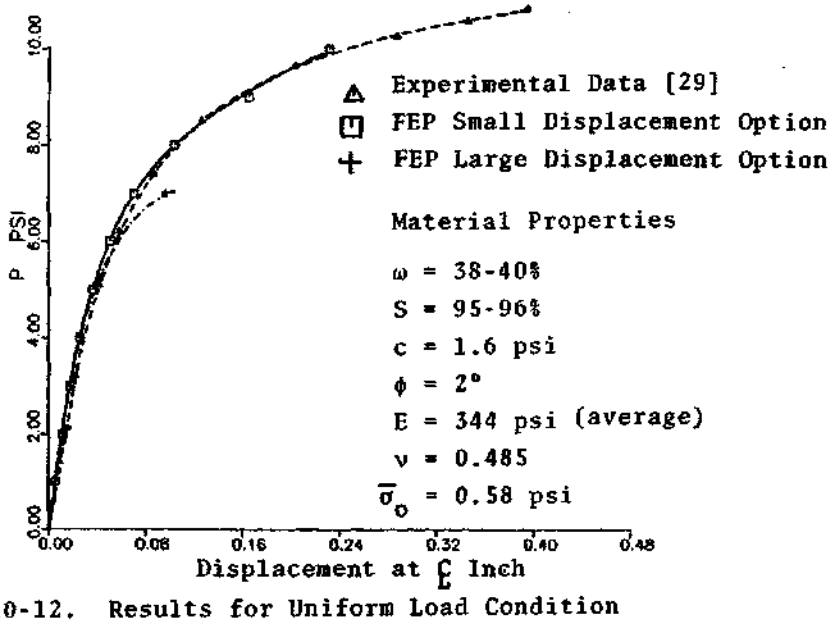

Figure 10-12. Results for Uniform Load Condition Example No. 5

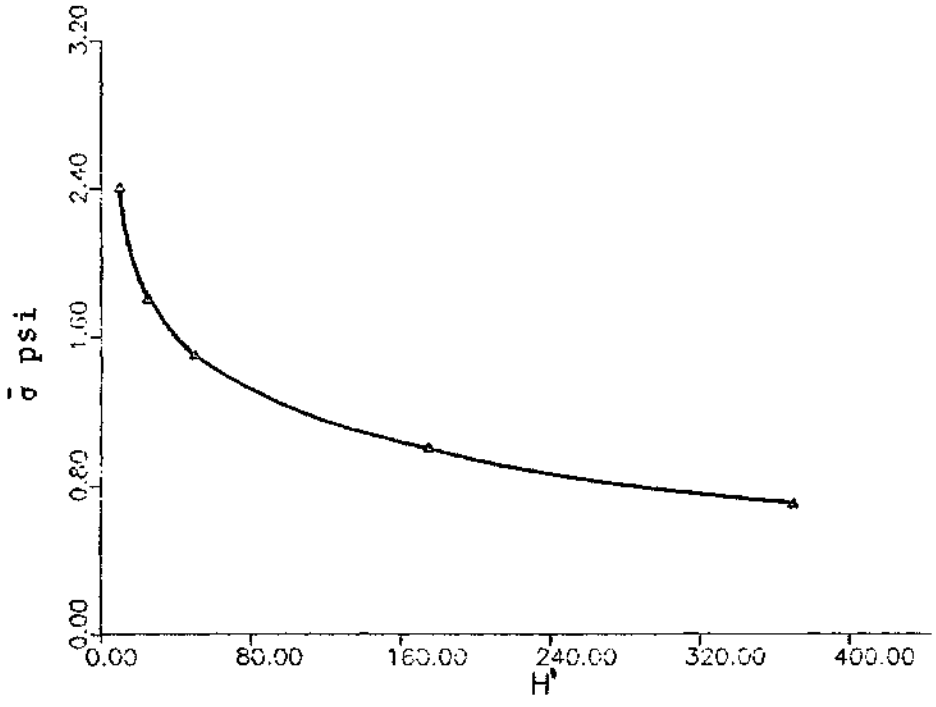

Figure 10-13. Plasticity Parameter $\bar{\sigma}$ vs. H' Example No. 5.

The plasticity parameter H' was computed from the average value of three triaxial tests at confining pressures of 0, 10 and 20 psi. The variation of the plasticity parameter H' is given in Figure 10-13. The load was applied in increments of 1 psi until failure occurred at 11 psi. Figure 10-12 shows that until 10 psi very good correlation of the computed applied stress-displacement relation for the small displacements theory was obtained. Results show maximum differences of 7%. With the large displacement option the maximum applied load of 7 psi was not in equilibrium in 8 iterations. At 6 psi the computed displacements show a difference of 9% with the experimental result uncertainties previously mentioned in example No. 4 contributed to an apparent better approximation of the small strain theory.

Example No. 6: No Tension Analysis in a Two Layer System

Detailed measurements of the stress and strain distribution of 18 inch diameter footings over compacted sand, compacted crushed stone, sandy clay placed over micaceous clayey silt were presented by Intraprasart [68]. The cases of compacted sand and compacted crushed stone are of interest for the application of the no tension analysis of Chapter VIII. In these tests a rigid circular concrete footing on compacted sand overlying a soft micaceous silty clay is studied. The computed stress distribution is compared with the laboratory measurements of reference [68]. In Figure 10-14, the geometry

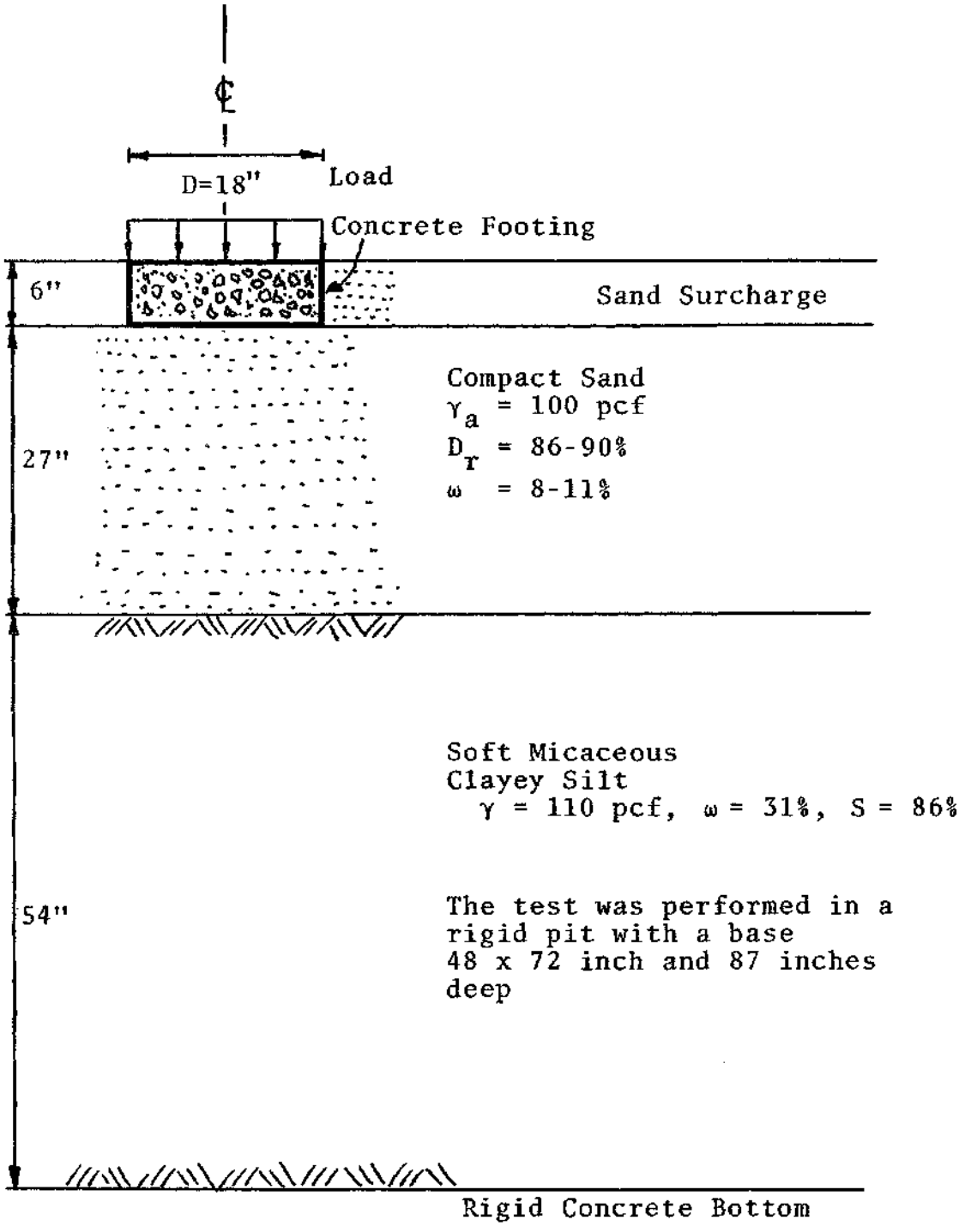

Figure 10-14. Two Layer Model. Rigid Concrete Footing over Compacted Sand. Example No. 6.

	E psi	ν	k_1	n	ϕ	c psi	$\bar{\sigma}_o$ psi
Sand	5000	0.485	2250	0.276	45°	0	11.5
Clay	500	0.4	715	0.43	10	3	1.7
Concrete	3.4×10^6	0.4					

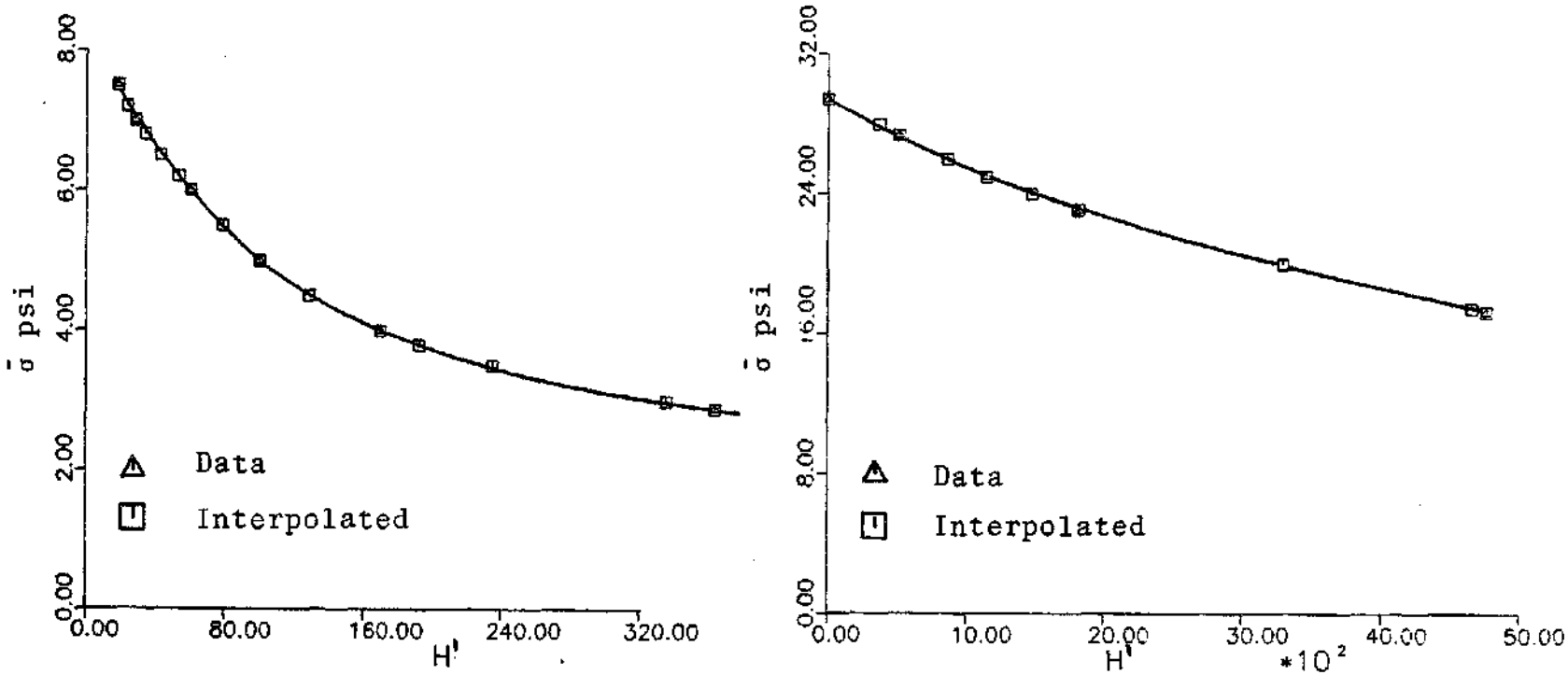

(a) Clay plasticity parameter H'

(b) Sand plasticity parameter H'

Figure 10-15. Elasticity, Plasticity and Variable Modulus Constants for Two Layer. Example No. 6

of the model is shown. A variable elastic modulus with confinement is used in the finite element computations. The parameters k_1 and n for the clayey silt and the compacted sand were computed in the form given by equation (22) of Chapter VIII. A Poisson's ratio of 0.485 was used for the sand to account for the high lateral stress due to the compact condition of the sand. The mechanical properties of the materials are given in Figure 10-15 and the finite element model is shown in Figure 10-16. The computed and measured vertical stresses and strains are shown in Figure 10-17. The stresses computed by the finite element program are for offsets from the axis of 2.25 in and 6.75 inch. The laboratory measurements of reference [68] were performed at 4.0 inch offset from the center of the load. The computed vertical stresses and strains show for depths with $z/D > 1$ small differences between computed and measured values. The largest difference is 20%. Large differences with the measured values for depths corresponding to z/D less than 0.5 were obtained with the computer program.

The computed vertical strain distribution is similar in shape with strain measurements in sand loaded with rigid footing [54,114]. In the computer solution the entire body weight was applied first and the corresponding stress dependent elasticity modulus computed. One reason for the relatively large differences in vertical stress and strains near the loaded area could be due to the initial stress state

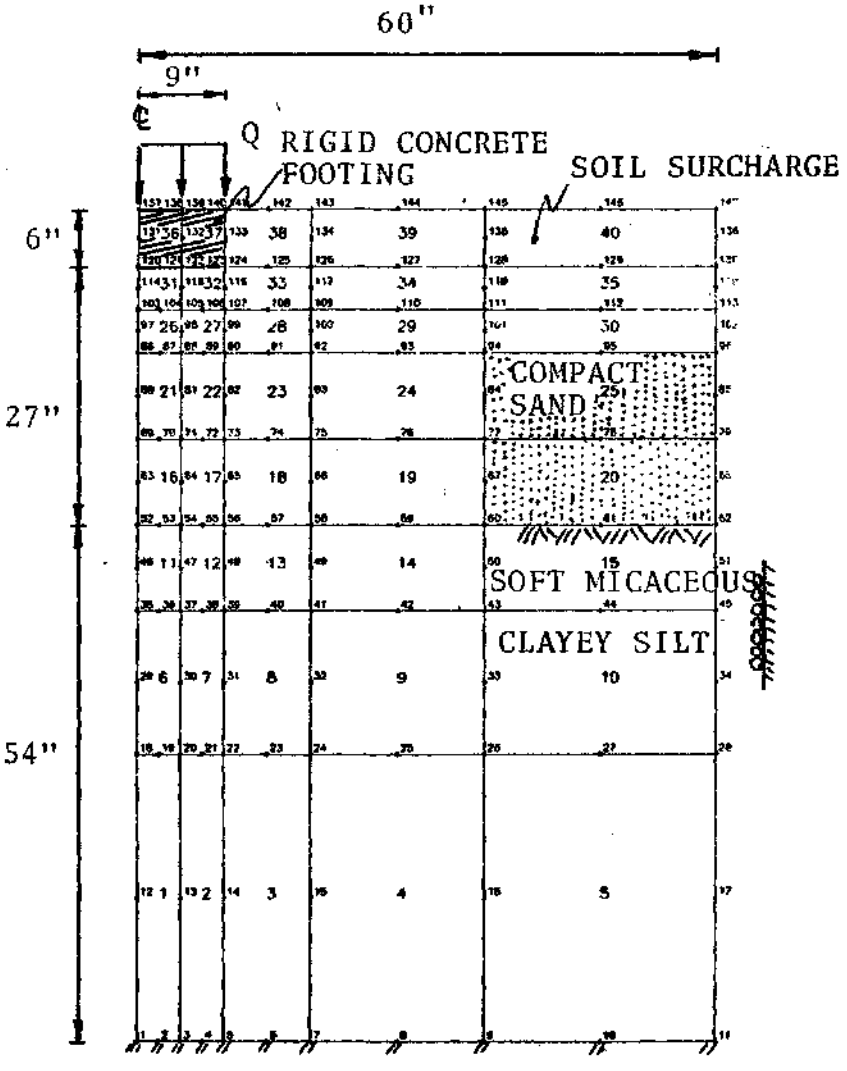

Vertical boundaries nodes fixed horizontally. Base nodes fixed in r and z directions

Figure 10-16. Finite Element Model of Footing over Two Layer. Example No. 6

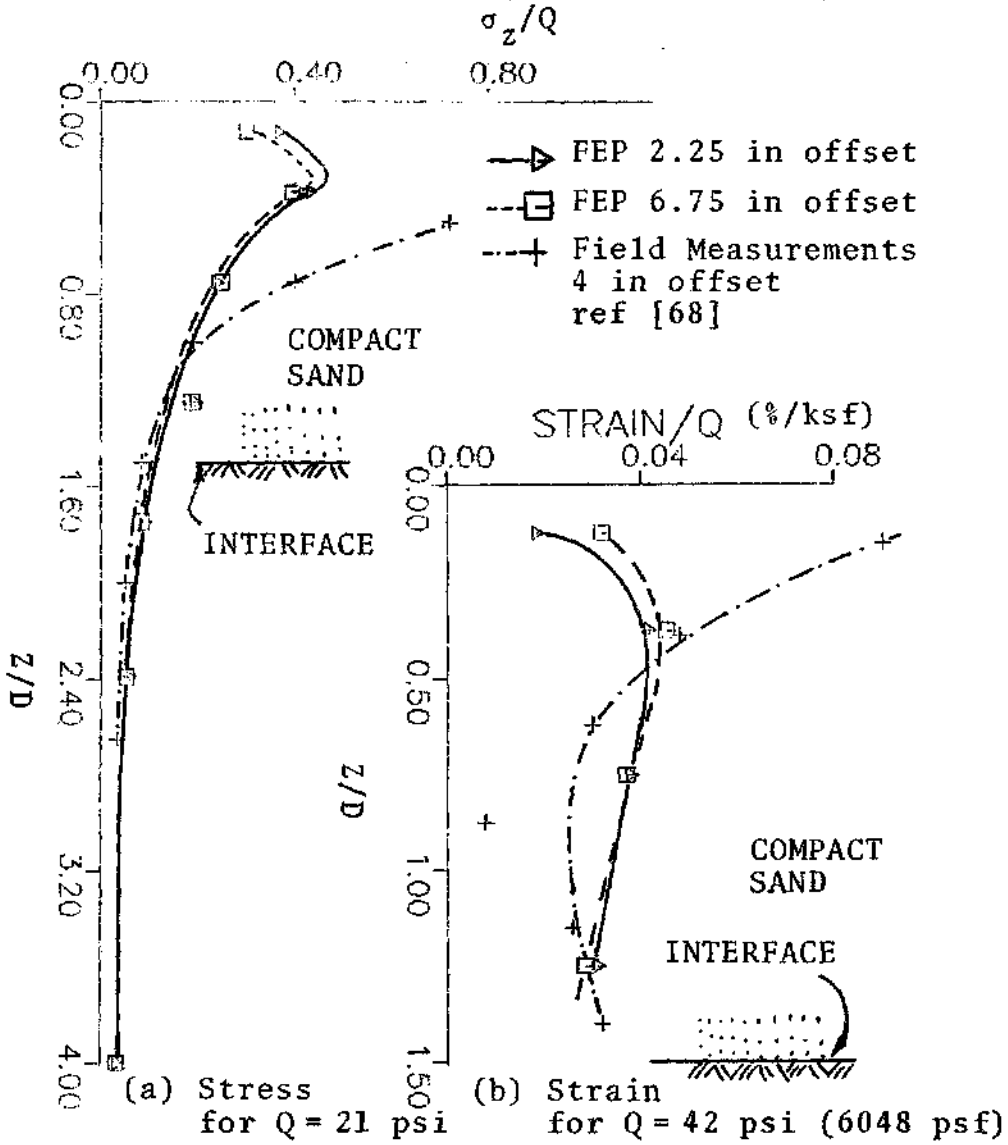

Figure 10-17. Vertical Stress and Strain Distributions. Example No. 6

of the compacted sand in the laboratory model.

Also the sand had a water content of 8-11% which could have induced large surface tension stresses in the sand which could have increased the modulus of elasticity due to the apparent confining effect.

Example No. 7: Analysis of a Soil-Fabric System Laboratory Test

Using the finite element formulation the analysis is presented of a soil-fabric system model. The laboratory tests of the system consisted of the application of a dynamic repeated load over a two layer fabric reinforced model and the measurement of corresponding displacements and stresses for a certain number of load applications. The geometry of the laboratory model is shown in Figure 10-18. Triaxial repeated load tests were performed on the soil and crushed stone. Tests of the fabric slip against clay and gravel provided the friction parameters of the interface. The laboratory results for the soft clay and fabric are shown in Figure 10-18. For the clay and gravel the parameters were obtained from dynamic repeated triaxial tests; average values of the test results were used. Parameters for the clay are shown in Figure 10-19a. The fabric tension-strain response and the interface friction parameters are given in Figure 10-19b. The gravel tests indicate a strong linear behavior with a plasticity parameter $H' = 14490$ constant obtained from the laboratory tests. A

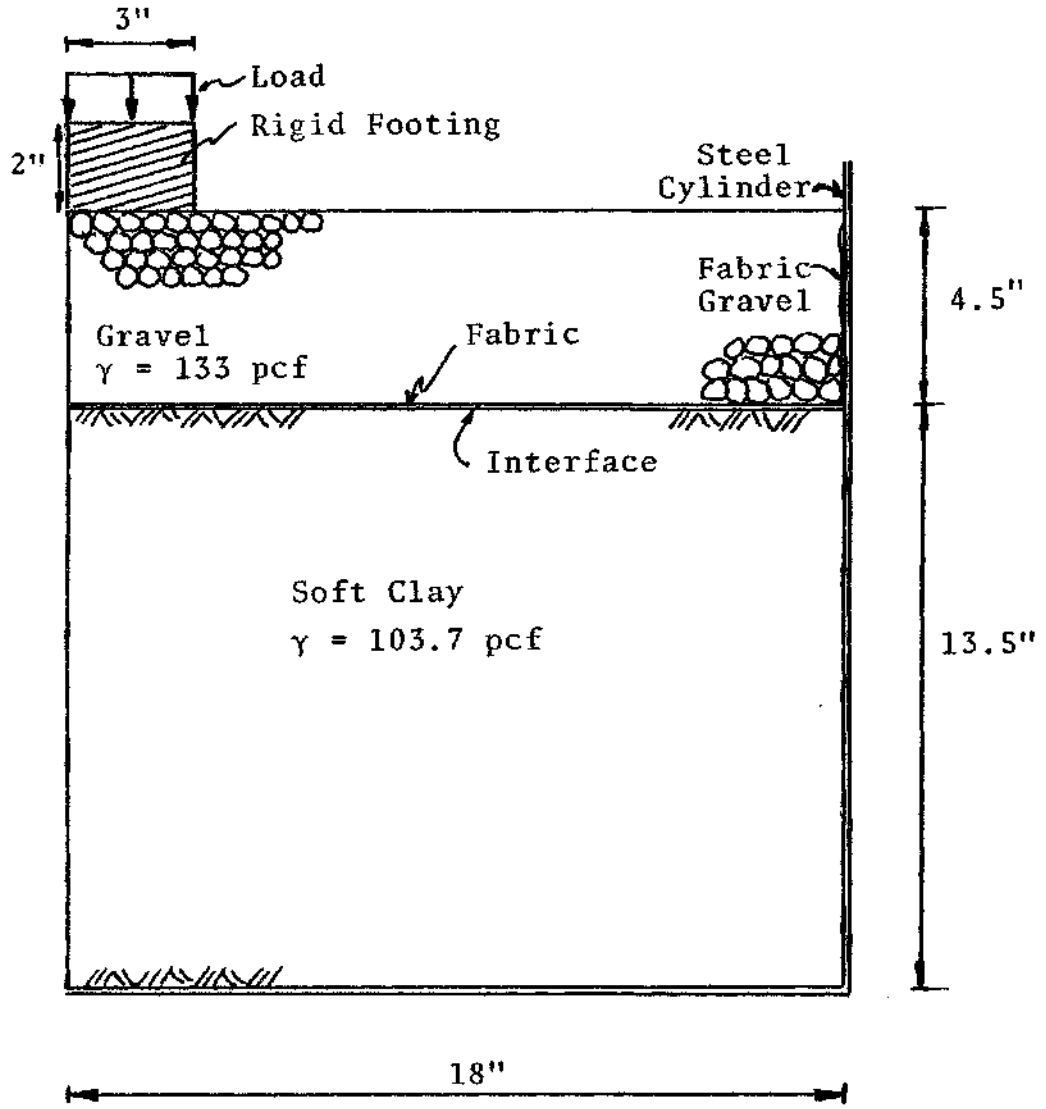

	E psi	ν	k_1	n	φ	c psi	$\bar{\sigma}_o$ psi
Gravel	2000	0.3	1242	0.762	48	0	1.0
Soft Clay	765	0.4	--	--	0	5.0	1.0
Footing	$2x10^6$	0.4					

Gravel: H' = 14490

Figure 10-18. Soil-Fabric Laboratory Model. Example No. 7

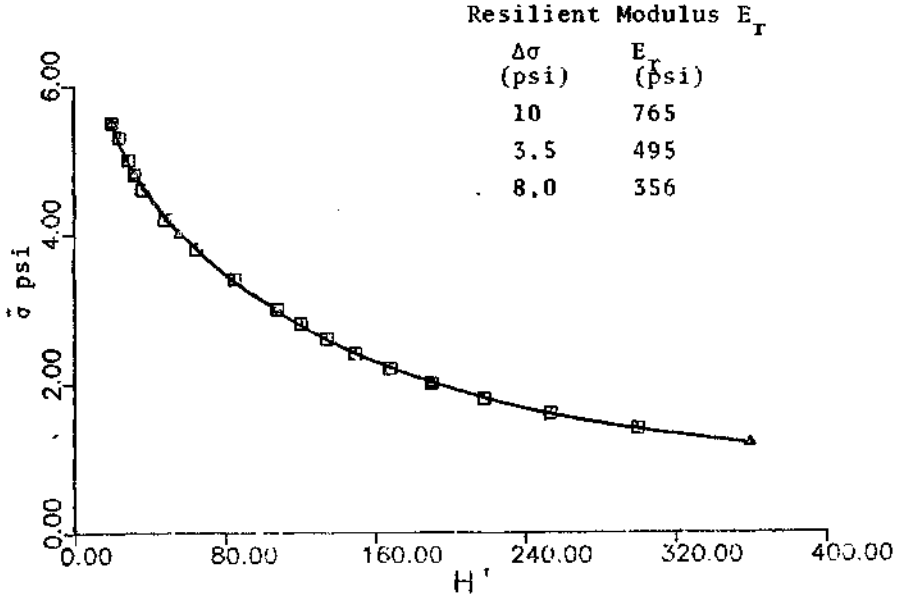

(a) Soft Clay Plasticity Parameters

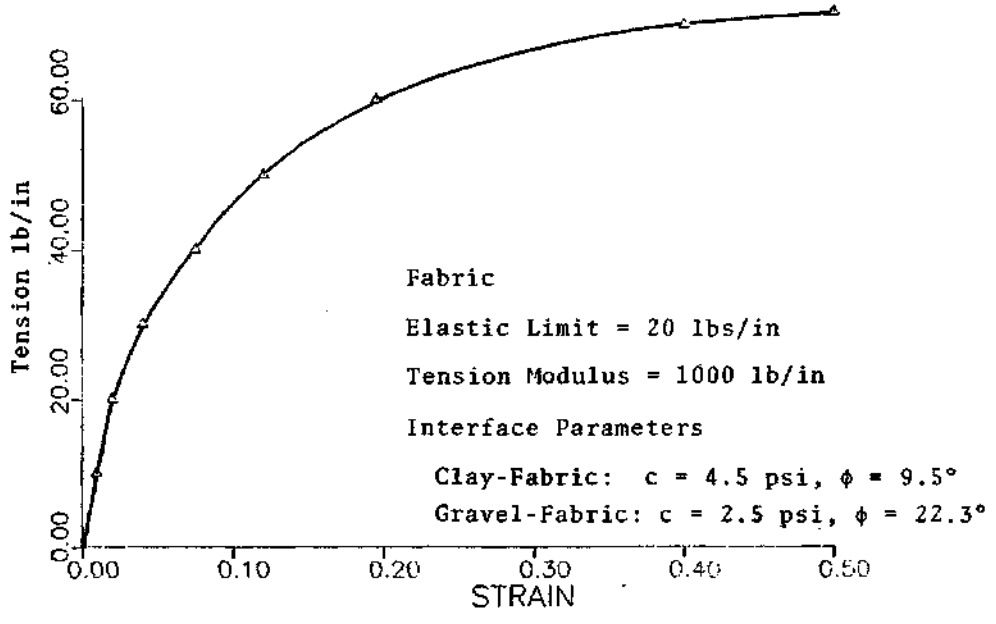

(b) Fabric Tension-Strain Behavior

Figure 10-19. Laboratory Material Parameters. Example No. 7

finite element model with fabric and one without fabric was prepared to determine the effect of the fabric. The finite element meshes used are shown in Figure 10-20. The circular surface loading was applied by a rigid plate. The complete state of stresses and deformation of the system was calculated for 7 psi load increments to 70 psi. The small strain and large strain options were used. Comparisons of a linear elastic two layer finite element analysis with the no tension procedure presented in Chapter VIII are given.

The vertical stress distributions for a vertical axis offset 2.25 in are shown in Figure 10-21a,b for applied loadings of 7 psi and 49 psi. The no tension analysis results give larger vertical stresses than the elastic analysis for 7 psi. For higher loads, most of the gravel elements are at failure and the computed vertical stresses in the gravel are smaller than the no tension analysis for the case of loading with a rigid plate. The results of a uniform loading are also shown; this condition gives larger stresses than the elastic analysis. For an applied pressure of 56 psi, the "reinforcing" action of the fabric is quite noticeable. Figure 10-21c shows the vertical stress distribution for an applied pressure of 56 psi on a horizontal plane at a depth of 5.25 inch, which is 0.75 inch below the interface. The vertical stress below the loaded area is 14% smaller with the fabric than without. The vertical stresses from the fabric model are higher outside the loaded area with a maximum

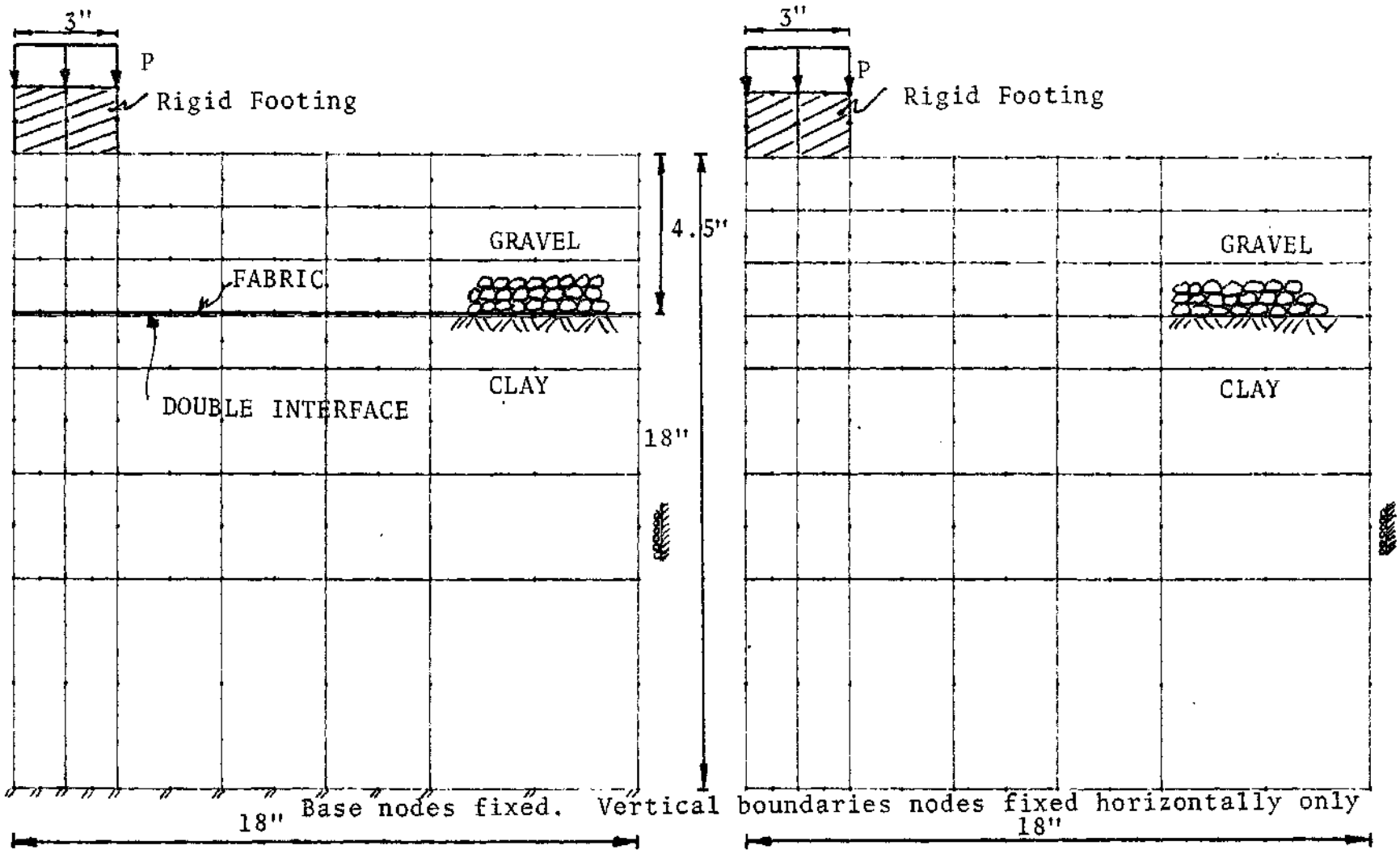

(a) With Fabric

(b) Without Fabric

Figure 10-20. Finite Element Models With and Without Fabric. Example No. 7

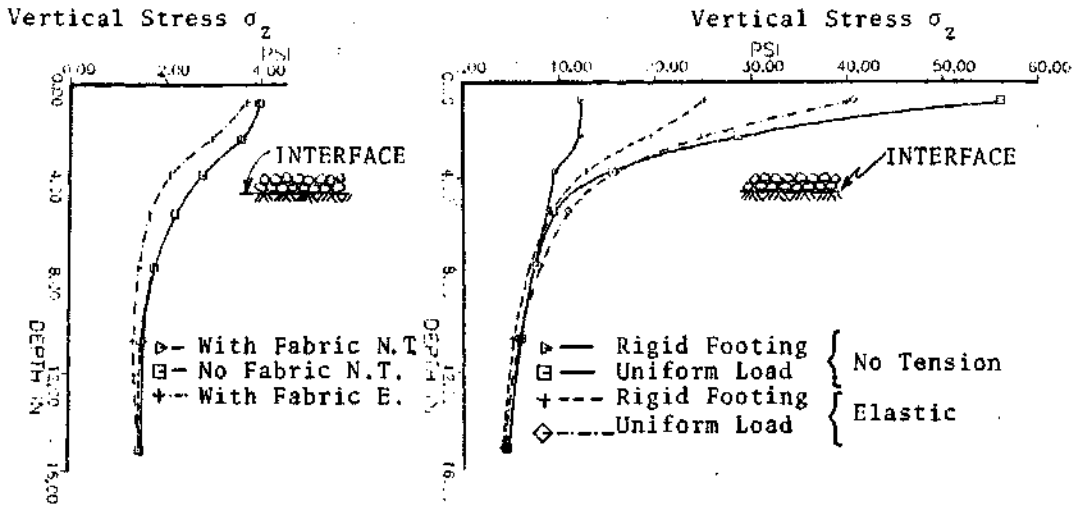

(a) Applied Pressure 7 psi Vertical stresses for a vertical axis 2.25 inch offset from centerline

(b) Applied Pressure 49 psi Vertical stresses for a vertical axis 2.25 inch offset from centerline with fabric

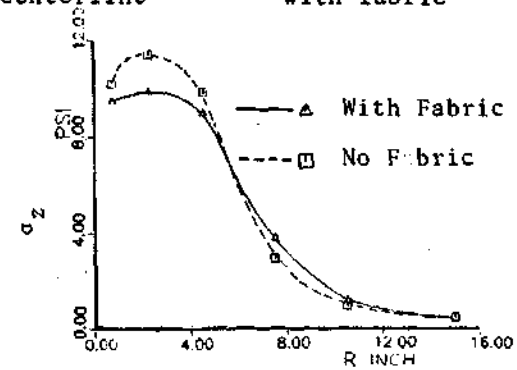

(c) Applied Pressure 56 psi. Vertical stresses for a horizontal plane 0.75 inch below the fabric.

Figure 10-21. Finite Element Program Computed Stress Distributions. Example No. 7.

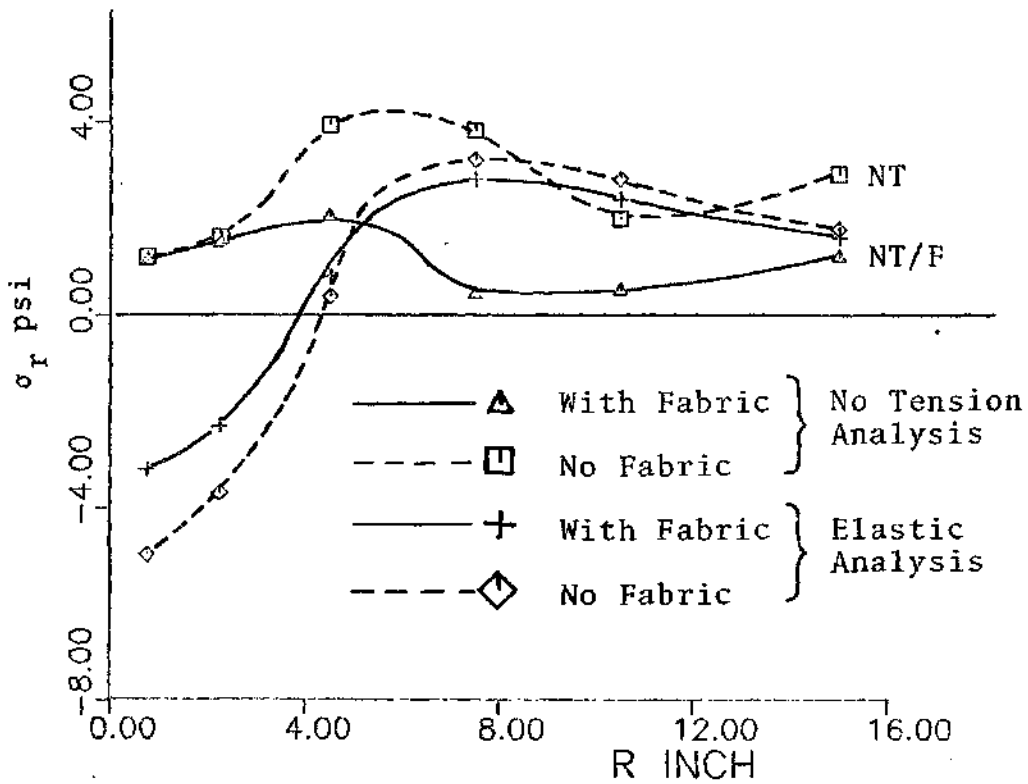

Figure 10-22. Radial Stresses at 0.75 inch Above the Interface. Example No. 7.

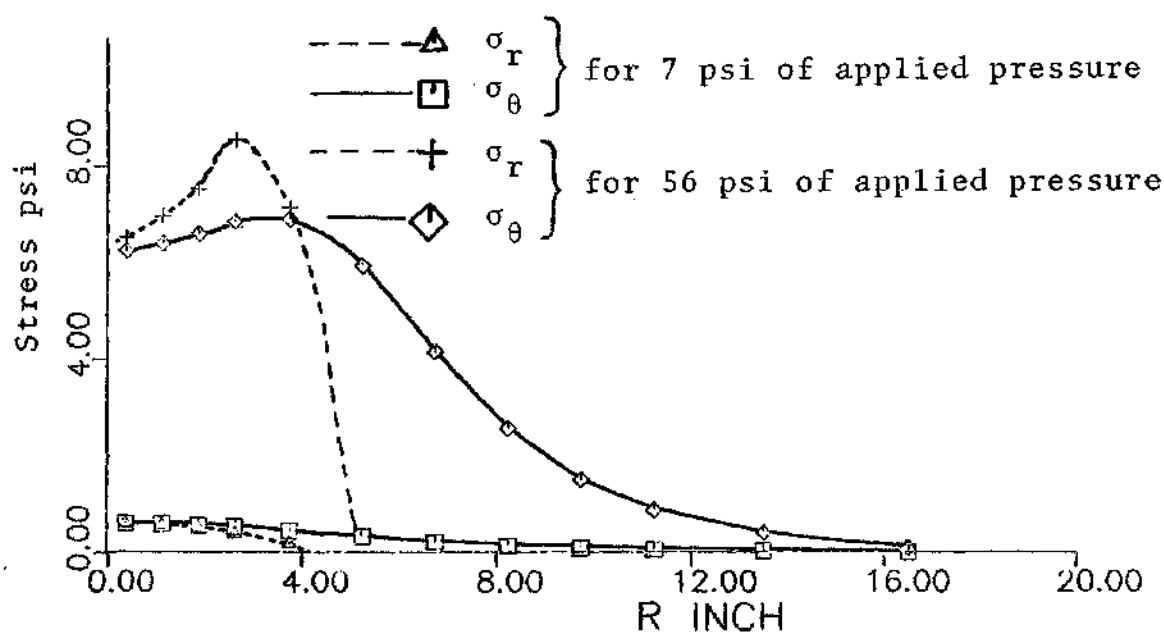

Figure 10-23. Fabric Stresses. Example No. 7.

difference of 25%.

The fabric action improves the confining condition of the model. The radial stresses at a depth of 3.75 inch (0.75 inch above the interface) are given in Figure 10-22. The no tension and elastic analysis results are shown for models with and without fabric. The tensile stresses in the cohesionless materials given by the elastic analysis are modified to compressive stresses as described in Chapter VIII. The model with fabric results in a large reduction in the radial stresses developed in the bottom part of the gravel layer. The computed tensions in the fabric are shown in Figure 10-23 for the low load level of 7 psi and for the 56 psi loading. A large increase in the tensile stress in the fabric with load increase is obtained mainly due to the increase vertical deformation and the more effective geometry condition of the fabric to take the tensions developed by the external load. Slip started to occur at 63 psi between the fabric and the gravel at the element shown in Figure 10-24b, for a computed shear higher than the maximum shear stress at the interface. The elements in failure for 7 psi and 56 psi load levels are shown in Figure 10-24 for both models. At 7 psi only the gravel elements in the tension zones are at failure. By a load of 56 psi almost all gravel elements are in failure, with the exception of the sampling points located under the rigid footing. Without fabric at the same loading all sampling points under the load except one are at failure.

For 10 load increments of 7 psi of applied pressure the total load displacement history of the footing is shown in Figure 10-25 considering elastic-plastic material response. The total deformation at the surface and at the interface is compared in Figure 10-26 showing that under the rigid footing the gravel deformed uniformly. The models with and without fabric were analyzed for elastic effects with no tension analysis. The difference of the elastic-plastic and the elastic displacements provides an estimate of the plastic, nonrecoverable displacements of the system for the corresponding load application for the number of cycles for which the initial parameters were given.

With the results obtained and given in Table 10-1 using a weighted value for the permanent deformations for each of the average conditions from the laboratory tests, an estimate of the total permanent deformation for 100 cycles was computed and compared with the measured values. The results are shown in Table 10-2. They show a maximum difference of 25%, an acceptable difference for a 100 times repeated load test. The deformed mesh is shown in Figure 10-27 for a single load application.

Finally, a finite element model with an initially deformed bowl shape fabric with a maximum centerline vertical displacement of 1.5 inch was analyzed to establish the reduction in vertical displacements with a more efficient position of the fabric. The total elastic-plastic settlement was

Table 10-1. Computed Response of the Soil-Fabric Model. Vertical Deformations for the Center of the Loaded Area. Example No. 7

Total Applied Pressure 70 psi. in 10 Load Increments.

Model	Gravel Thickness inch	δ_{ep} inch	δ_e inch	δ_p inch	Execution Time sec
No Fabric	4.5	0.364	0.198	0.166	790
With Fabric	4.5	0.289	0.194	0.095	750
No Fabric	7.0	0.226	0.175	0.051	571
With Fabric	7.0	0.207	0.175	0.032	620

where

δ_{ep} = Elastic-Plastic Deformation
δ_e = Elastic Deformation
δ_p = Plastic Deformation

Table 10-2. Permanent Deformation for 100 Cycles of Load Applications. Example No. 7

Model	Gravel Thickness Inch	Computed Value Inch	Measured Value Inch	Ratio Computed Measured
With Fabric	4.5	2.7	2.4	1.13
No Fabric	4.5	4.72	4.6	1.03
With Fabric	7.0	0.90	1.2	0.75
No Fabric	7.0	1.44	1.8	0.80

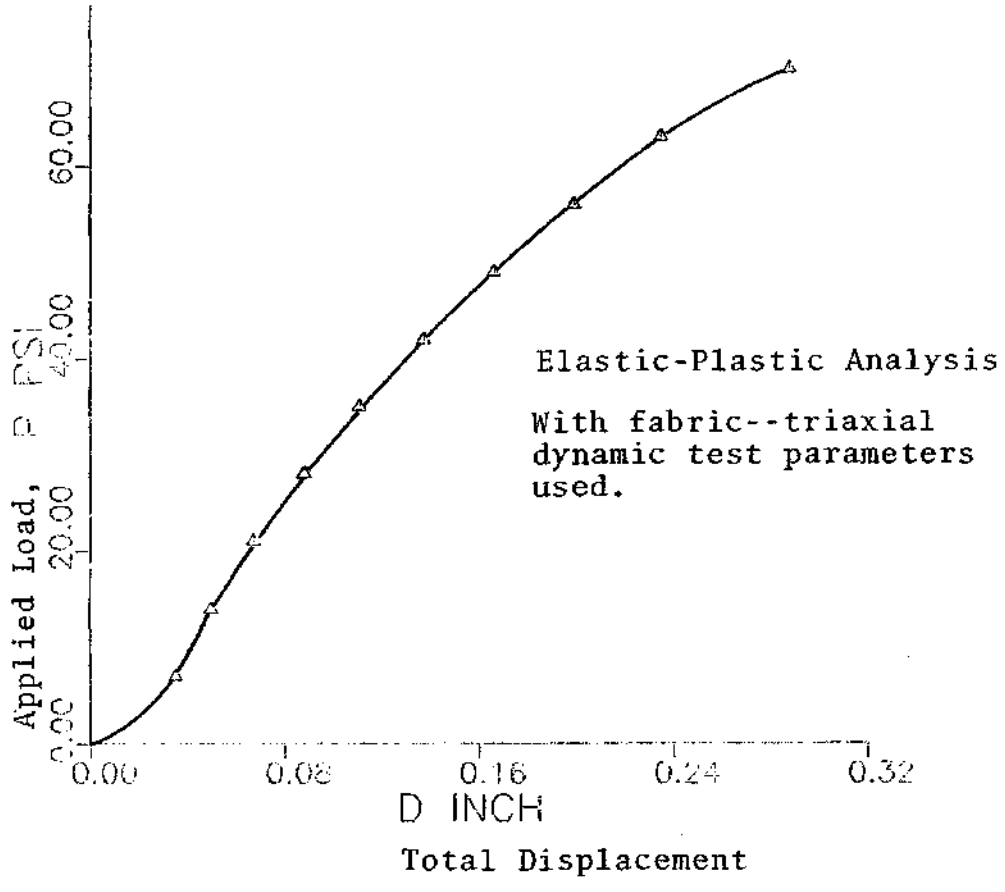

Figure 10-25. Total Load Displacement at the Surface. Example No. 7

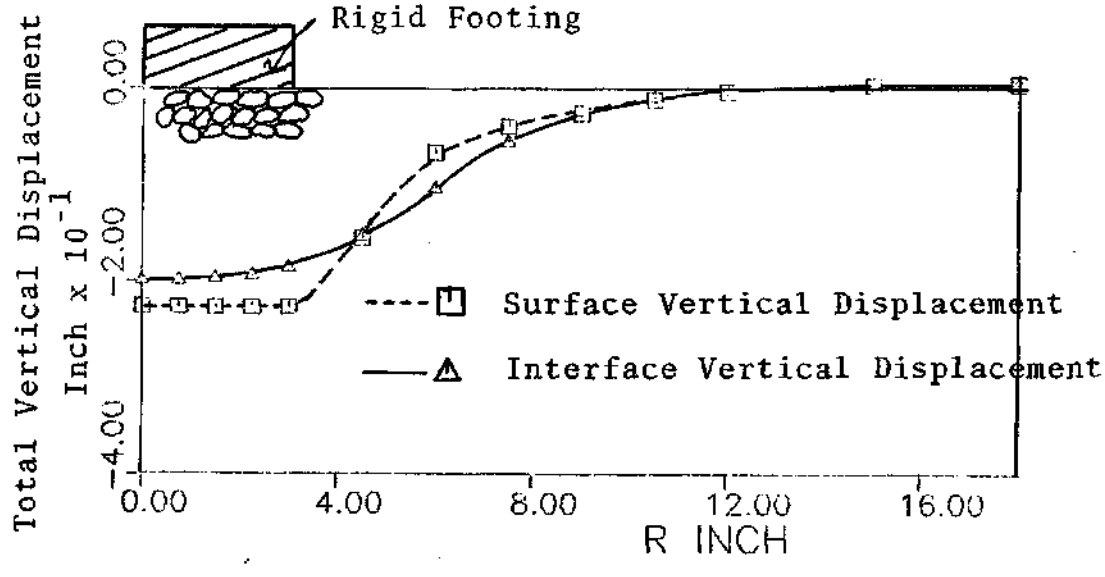

Figure 10-26. Surface versus Interface Vertical Displacement. Example No. 7

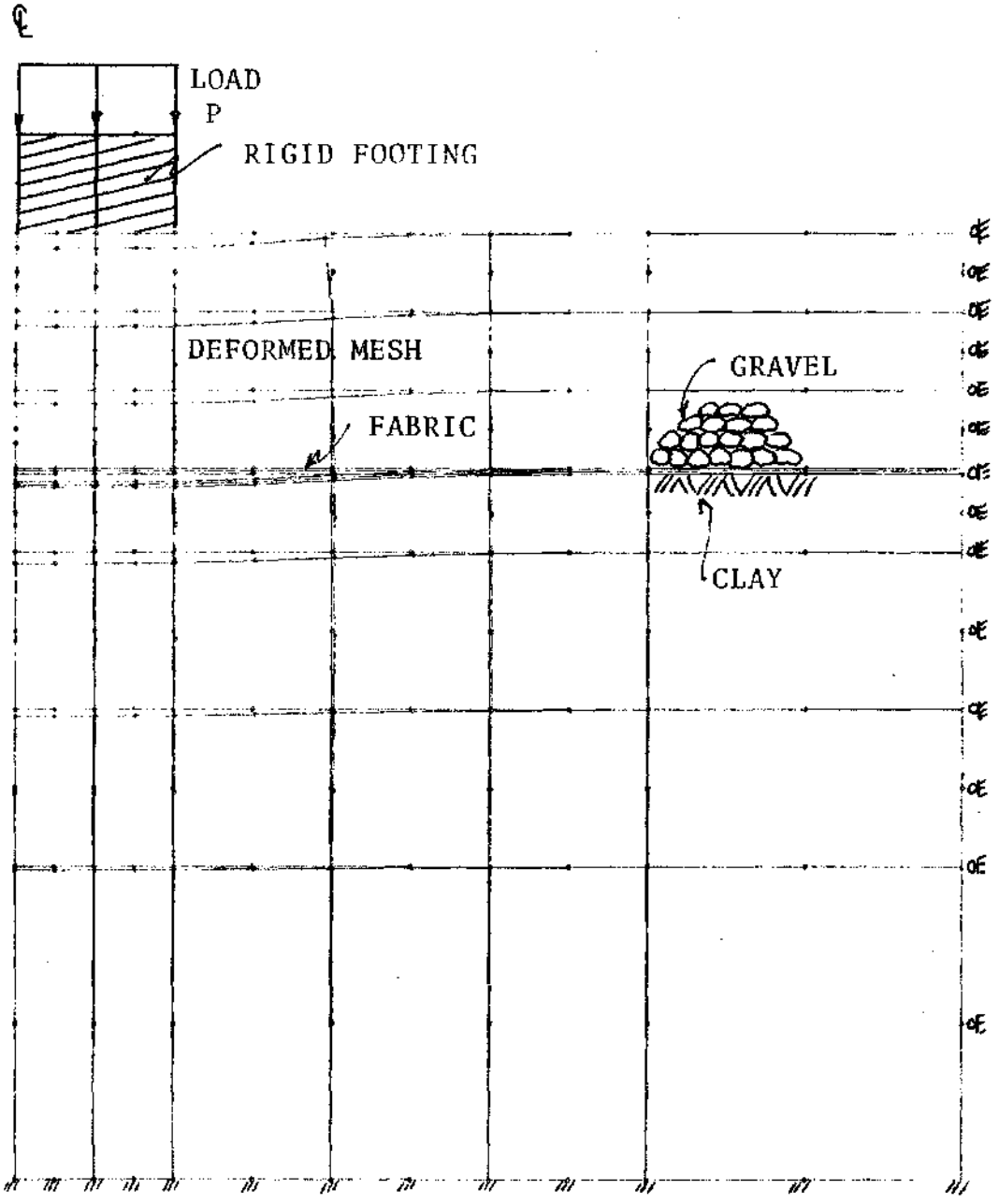

Figure 10-27. Deformed Mesh for the Soil-Fabric System. Example No. 7

reduced by 33% at 60 psi of applied pressure, compared with 20% reduction with an initial horizontal fabric, with respect to the no fabric model. The finite element models used in Example No. 7 were also analyzed with the large displacement option of the program. Results for the model with 7 inches of gravel are very close to the results obtained using the small displacement option. The total elastic-plastic displacements were 0.22 inch and 0.24 inch with and without fabric, respectively. Small displacement theory resulted in displacements of 0.21 and 0.22 inch which is a 10% difference.

For the model having a 4.5 inch layer of gravel the results of the large displacement option show a large increase in deformations compared with the small displacement option. For the thinner gravel layer the elements began failing earlier during the application of the loads. The large displacement option for the model without fabric resulted in a total displacement of 0.52 inch compared with 0.36 inch for the small displacement option. For the model with fabric, slip also occurred at a load of 63 psi. Slip first occurred at 63 psi with the small displacement option. For the large displacement option at 70 psi the elements below the rigid plate are all in failure and the applied loads can not be equilibrated. Therefore, the program stopped at this point.

The attempt to use the experimental results to validate the finite element program is limited since important

parameters that define the soil behavior are not included in the formulation. In general the computations of the settlement with the program give an acceptable approximation for the complex soil-fabric multiple load application problem.

CHAPTER XI

CONCLUSIONS

A mathematical finite element formulation was presented to analyze the soil fabric problem. The program was verified with theoretical and laboratory measurements. The theoretical verification consisted in separate analysis of various components of the system. The result of the computations show that the program provided very good answers for this type of verification. Measured response during laboratory tests provided a second verification of the program. The plasticity solution was compared with laboratory measurements and resulted in good approximations for small displacements. For the two layer soil fabric problem the program provides reasonably good answers accounting for the complexity of a multi load application problem. The general limitations of the finite element formulation presented include no provision to consider viscosity and consolidation effects, although laboratory tests can be performed to at least indirectly consider these effects. Inertia forces, rotation of local axis in the individual elements, strain softening and pore pressure effects are also not included. Laboratory measurements are needed for the verification of the plastic behavior of the elements with large displacements and the no tension conditions developed in cohesionless materials. The present

formulation is a definite improvement over current analysis of multilayer interface reinforced systems. The following specific conclusions can be made:

1. An axisymmetric finite element formulation for the computation of multilayer soil-fabric systems with interfaces, plasticity, nonlinear response, large displacements and no tension analysis was presented. The formulation can be successfully used to approximate the complex soil-fabric behavior under repeated load application.

2. The eight node isoparametric element is useful to reduce the total number of elements and corresponding number of equations of the system. This is a very important advantage when the system is solved a number of times for incremental analysis.

3. A soil-fabric model can be represented by approximately 50 element mesh formed by isoparametric and interface elements.

4. The load increments should be kept small to about 1/10 of the total applied load to compute the fabric response accurately and not to be too far out off bounds of the failure criteria for the individual elements.

5. Repeated load tests for soil and gravel used in the soil mechanics practice can be used to obtain representative elastic and plastic parameters of the materials and interfaces of the problem.

6. The present model can be applied to study the

relative behavior of different types of fabrics and geometry of the models to compare their behavior.

7. The present formulation does not include the consideration of local punching of individual particles of aggregate into the fabric or the soil if a fabric is not present.

8. For the examples presented the soil-fabric system had a better response to the applied loads, and the computed elastic-plastic and plastic deformations were smaller than the system without fabric. The behavior of the fabric with only 4.5 inch of gravel was more effective than with 7 inches.

9. The soil-fabric computations and parameters with respect to repeated load tests needs further comparisons with experimental models.

10. With the use of the soil plasticity theory failure zones can be determined along with the distribution of stresses for the elastic-plastic condition.

11. The no tension analysis resulted in general in increased vertical stresses in comparison with an elastic analysis. Under a rigid loaded plate the elements near the centerline give a lower stress with respect to the elastic analysis and elements or sampling points very near the edge of the plate increase their vertical stresses as their confining stress increases.

12. The initial no tension analysis resulted in increased vertical stresses in the gravel and clay layers.

13. The strain distribution in the gravel loaded with a rigid plate results in low strains near the rigid plate with maximum strains at a depth of z/D = 0.5

14. The failure zones in a two layer model increase very rapidly in the gravel layer due to the initial horizontal tensile stresses. In the soil-fabric model the failure conditions develop slower than in the no fabric model.

15. The interface model presented provides a simple way to compute shear stresses at both sides of a reinforcing element.

16. For the examples presented the large displacement option resulted in larger deformations than the small displacements option. However, in the literature large displacement computations show larger or smaller computed values of deformations than the small strain computation, depending on the problem type [22,137]. New research on large displacement computation for soils, including plastic effects should incorporate the corotational stress rate in the development of the constitutive relationship. For certain problems the effect of the rotation of the elements might not be significant, due to small total displacements. Updating the geometry of the soil-fabric problem will take care of geometry and stiffness changes and could improve the results.

17. The equilibrium condition of the system has to be maintained so that meaningful results of a nonlinear problem

are obtained. The number of load increments used might change the number of iterations per load increment needed to satisfy the equilibrium conditions of the system.

18. Viscosity, consolidation or time effects are not included in the present formulation. Instantaneous deformations which include the plasticity effect are computed. This plasticity effect depending on the laboratory test used to evaluate the properties might already include viscosity, consolidation or time effects in a general way. The need of defining appropriate parameters and laboratory verification is needed.

19. The relative dimensions of the laboratory model and the computer model shows that the effects of the rigid lateral boundary of the model are important for the behavior of the fabric in the system, these effects affect the performance of the fabric.

20. The computer hardware used can affect the solution of equations involving large stiffness of interface elements. A CDC-CYBER 74 computer was used which provides 16 decimal points in single precision and 32 in double precision. Single precision was used in the solution of the soil-fabric model.

CHAPTER XII

RECOMMENDATIONS FOR FURTHER STUDY

The computer formulation presented can be applied to other geotechnical problems directly. Piles and anchors are easily analyzed with the program. Elastic-plastic, no tension materials, and nonlinear fabric elements can be included in the formulation. Additional work is needed in the following important areas:

1. Full measurements of the response in a granular material under the application of rigid and semirigid footings. The results need to be compared with the analytical no tension solution presented. The conditions of the initial state of the granular material and the mechanical properties including the fictitious tension capability, due to grain interlocking needs to be measured.

2. The repeated load application analysis can be included in the formulation with the appropriate parameters. Analysis of the resulting stresses and deformations after each load application are needed for subsequent analysis.

3. The implementation and testing of the plane strain solution of the finite element model can give additional information and provide solutions to other geotechnical problems.

4. The formulation of the fabric finite element model

to incorporate different tension modulus in orthogonal directions is needed, also laboratory tests to define the fabric material properties and their influence in the actual response of the fabric in the soil-fabric system.

5. The finite element model should be extended to include incremental construction.

6. For soil plasticity applied to large displacements, an appropriate rate of stress should be incorporated in the development of the elasto-plastic constitutive relationship. The corotational rate also called the Jaumann rate of stress should be implemented in the formulation to improve the large displacement plastic predictability.

7. The appropriate laboratory parameters and the computer solution compared to the laboratory measurements can provide more confidence in the use of the program.

8. The laboratory parameters input to the program need to comply with the derivations developed for the finite element model. Complete sets of laboratory parameters should be determined to correctly model the problem.

9. The mesh size of example No. 7 with 56 elements provided with good approximation. Improvement can be achieved by using smaller elements with the corresponding increase in computer time. Here the total storage required for the largest example, 56 elements and 187 nodes, was 165000 bits and 1840 sec. of running time.

10. The soil-fabric system for the resilient modulus computations performed can give acceptable answers. If a static analysis is performed with the mathematical formulation presented, viscosity and consolidation effects need to be included and a new formulation has to be developed. The material laboratory testing techniques need to be developed and carefully programmed to provide the parameters needed in the computation.

APPENDIX A

DEFINITIONS

The definitions given here follow reference [85].

True Cauchy Stress Tensor--τ_{ij}

The true Cauchy Stress Tensor also called true stress tensor or Euler stress tensor is the stress that results from the application of the force acting on an oriented surface in the deformed configuration of the body (Figure A1-a). The stress vector $\underset{\sim}{T}$ per unit area in the deformed configuration is given by: $\underset{\sim}{T} = \frac{dF}{ds}$ and the Cartesian components of the Cauchy stress τ_{ij} are defined by:

$$\nu_i \, \tau_{ij} = T_j = \frac{dF_j}{ds}$$

or

$$\underset{\sim}{dF} = (\nu_i \tau_{ij} ds)\underset{\sim}{e}_j$$

where

$\underset{\sim}{e}_j$ = unit base vectors

$\underset{\sim}{dF}$ = force acting on the deformed surface

ds = differential area in the deformed surface

ν_i = components of the unit normal to the deformed surface

First Piola-Kirchhoff Stress Tensor--t_{ij}

The first Piola-Kirchhoff stress tensor, also called Piola-Lagrange stress tensor or nominal stress tensor, is the stress per unit area in the undeformed configuration of the body. First we translate the force vector $d\underset{\sim}{F}$ acting on the deformed area ds to the undeformed area ds_o (Figure A1-b). The stress vector per unit undeformed area is $\underset{\sim}{t} = \frac{dF_i}{ds_o} \underset{\sim}{e}_i$ and the Cartesian components of the Piola-Kirchhoff stress t_{ij} are defined by:

$$n_i t_{ij} = \frac{dF_j}{ds_o}$$

or

$$d\underset{\sim}{F} = (n_i \; t_{ij} \; ds_o)\underset{\sim}{e}_j$$

where

n_i = components of the unit normal

dF_j = component of the force acting on the undeformed surface

ds_o = undeformed surface

$\underset{\sim}{e}_j$ = base vectors in the undeformed surface

Second Piola-Kirchhoff Stress Tensor--S_{ij}

The second Piola-Kirchhoff stress tensor also called second Piola stress tensor or Kirchhoff-Trefftz stress is a

stress per unit area in the undeformed configuration of the body and is a purely mathematical quantity. The force vector is decomposed with respect to the convected base vectors $\underset{\sim}{g}_i$ defining an alternative force vector $d\hat{\underset{\sim}{F}}$, with: $d\underset{\sim}{F} = d\hat{F}\ \underset{\sim}{g}_i$ and the respective Cartesian components: $d\hat{\underset{\sim}{F}} = d\hat{F}\ \underset{\sim}{e}_i$. This vector is translated to the undeformed area ds_o (Figure A1-c). The stress vector $\hat{\underset{\sim}{t}}$ per unit area in the undeformed configuration is: $\hat{\underset{\sim}{t}} = \dfrac{d\hat{F}_i}{ds_o}\ \underset{\sim}{e}_i$ and the Cartesian components of the second Piola-Kirchhoff stress, S_{ij}, are defined by:

$$n_i\ S_{ij} = \hat{t}_j = \frac{d\hat{F}_j}{ds_o}$$

or

$$d\underset{\sim}{F} = d\hat{F}_j\ \underset{\sim}{g}_j = (n_i\ S_{ij}\ dS_o)\underset{\sim}{g}_j$$

where

n_i = components of the unit normal

ds_o = undeformed surface

$\underset{\sim}{g}_i = \dfrac{\partial y_j}{\partial x_i}\ \underset{\sim}{e}_j$

y_j = coordinate system for the deformed configuration

x_i = Cartesian coordinate system in the undeformed configuration

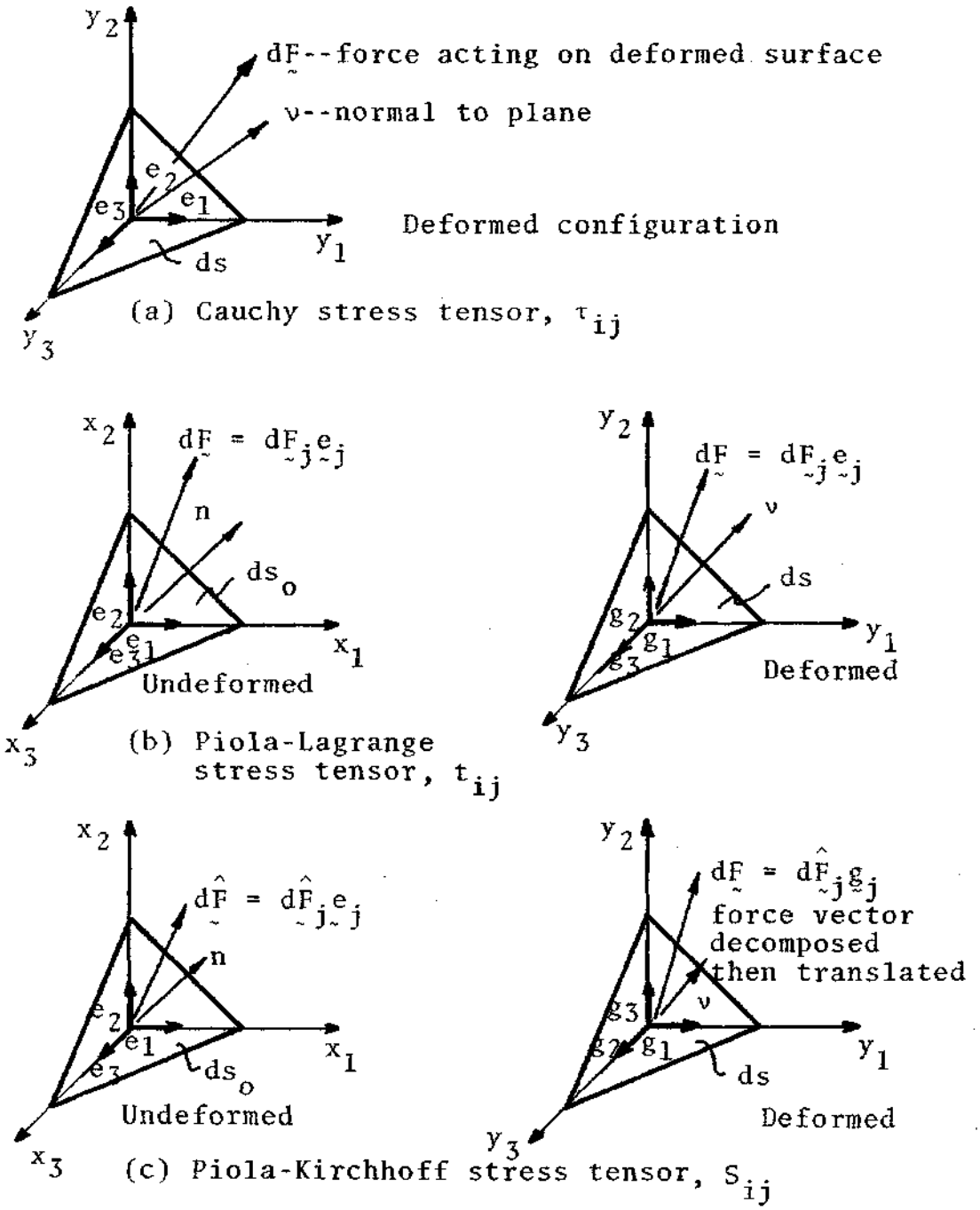

Figure A1. Stress Tensor Definitions

Now the force vector $d\underset{\sim}{F}$ can be related to the three stress measures given:

$$d\underset{\sim}{F} = (\nu_i \tau_{ij} ds)\underset{\sim}{e}_j \quad \text{(Cauchy)}$$

$$d\underset{\sim}{F} = (n_i t_i ds_o)\underset{\sim}{e}_j \quad \text{(Piola-Lagrange)}$$

$$d\underset{\sim}{F} = (n_i S_{ij} ds_o)\underset{\sim}{g}_j \quad \text{(Piola-Kirchhoff)}$$

The change in volume of an infinitesimal element can be related by J where $Jdv_o = dv$ and $J = \det \left|\frac{\partial y_i}{\partial x_j}\right|$.

For the axisymmetric axes the following transformation formulas apply:

1. Transformation of coordinates

   $x = r \cos\theta$

   $y = r \sin\theta$

   $z = z$

   θ = angle (Figure A-2)

where

(x,y,z) Cartesian coordinates

(r,z,θ) Cylindrical coordinates

2. Base vectors

   $e_r = \cos\theta\, e_1 + \sin\theta\, e_2$

   $e_\theta = -r \sin\theta\, e_1 + r \cos\theta\, e_2$

   $e_z = e_3$

3. Metric tensor

   $e_{ij} = e_i e_j$ the covariant components

   $e_{rr} = 1 \qquad e_{r\theta} = 0 \qquad e_{rz} = 0$

   $e_{\theta r} = 0 \qquad e_{\theta\theta} = r^2 \qquad e_{\theta z} = 0$

   $e_{zr} = 0 \qquad e_{z\theta} = 0 \qquad e_{zz} = 1$

and using also the contravariant components:

$$e_r = e_r \qquad e_z = e^z \qquad e_z \cdot e_z = 1$$
$$e_r \cdot e_r = 1 \qquad e_r \cdot e_z = 0 \qquad e_\theta \cdot e_\theta = r^2$$
$$e_\theta \cdot e^\theta = 1 \qquad e^\theta \cdot e^\theta = \frac{1}{r^2}$$

4. Deformed state

$$\delta = z + w$$

where δ = position vector in the deformed state

$\underset{\sim}{w}$ = displacement

$$w = ue_r + ve_z$$

Note $\theta = 0$ and $\frac{\partial u}{\partial \theta} = \frac{\partial v}{\partial \theta} = 0$

5. Deformation gradient, F, the transpose is given by:

$$F^T = \begin{bmatrix} 1 + \frac{\partial u}{\partial r} & \frac{\partial v}{\partial r} & 0 \\ \frac{\partial u}{\partial z} & 1 + \frac{\partial v}{\partial z} & 0 \\ 0 & 0 & 1 + \frac{u}{r} \end{bmatrix}$$

from [4A] and [85] additional notes.

6. Green Lagrange strain, e.

$$e = \frac{1}{2}(G - I) = e_{ij}\, e^i\, e^j$$

G = deformation tensor, I = Identity Matrix

and $$e_{rr} = \frac{\partial u}{\partial r} + \frac{1}{2}\left[\left(\frac{\partial u}{\partial r}\right)^2 + \left(\frac{\partial v}{\partial r}\right)^2\right]$$

$$e_{rz} = e_{zr} = \frac{1}{2}\left[\frac{\partial u}{\partial z} + \frac{\partial v}{\partial r} + \frac{\partial u}{\partial r}\frac{\partial u}{\partial z} + \frac{\partial v}{\partial r}\frac{\partial v}{\partial z}\right]$$

$$e_{zz} = \frac{\partial v}{\partial z} + \frac{1}{2}\left[\left(\frac{\partial u}{\partial z}\right)^2 + \left(\frac{\partial v}{\partial z}\right)^2\right]$$

$$e_{\theta\theta} = ru + \frac{1}{2}(u)^2$$

7. Physical components of the Green-Lagrange strain, e^*_{ii}

$$e^{\theta} = \frac{1}{r}\left[2ru + (u)^2\right]e^{\theta}e^{\theta} = \left[2\frac{u}{r} + \left(\frac{u}{r}\right)^2\right](re^{\theta})(re^{\theta})$$

where re^{θ} = unit vector

Then the other components are,

$$e^*_{rr} = e_{rr}$$

$$e^*_{rz} = e_{rz} = e^*_{zr} = e_{zr}$$

$$e^*_{zz} = e_{zz}$$

and $$e^*_{\theta\theta} = \frac{u}{r} + \frac{1}{2}\left(\frac{u}{r}\right)^2$$

8. The strain expressions for the axisymmetric case are then:

$$\varepsilon_r = \frac{\partial u}{\partial r} + \frac{1}{2}\left[\left(\frac{\partial u}{\partial r}\right)^2 + \left(\frac{\partial v}{\partial r}\right)^2\right]$$

the engineering definition of $\gamma_{rz} = e^*_{rz} + e^*_{zr}$, then

$$\gamma_{rz} = [\frac{\partial u}{\partial z} + \frac{\partial v}{\partial r} + \frac{\partial u}{\partial r}\ \frac{\partial u}{\partial z} + \frac{\partial v}{\partial r}\ \frac{\partial v}{\partial z}]$$

$$\varepsilon_z = \frac{\partial v}{\partial z} + \frac{1}{2}\ [(\frac{\partial u}{\partial z})^2 + (\frac{\partial v}{\partial z})^2]$$

$$\varepsilon_\theta = \frac{u}{r} + \frac{1}{2}\ (\frac{u}{r})^2$$

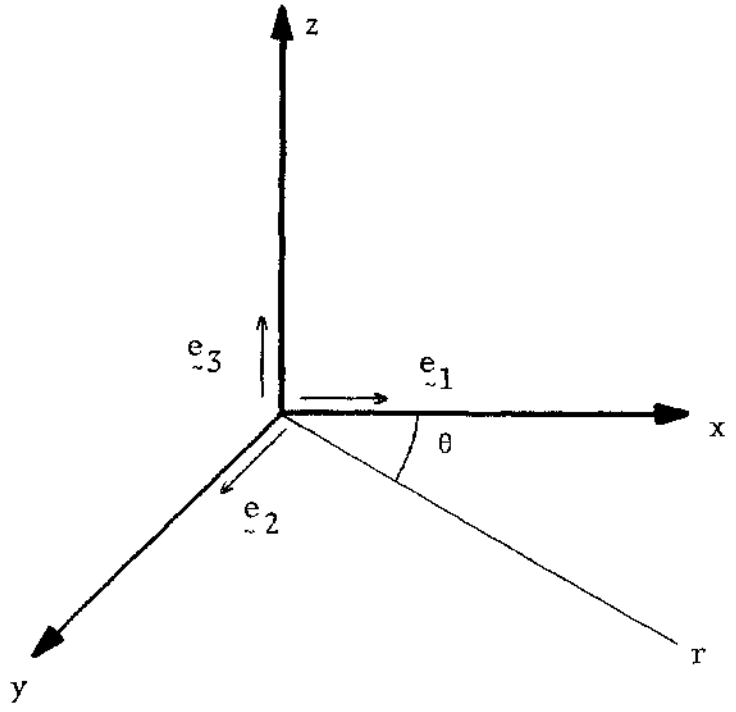

Figure A2. Axisymmetric Axes r,z,θ and Cartesian Axes x,y,z

BIBLIOGRAPHY

1. Argyris, J. H. (1965), "Matrix Analysis of Three-Dimensional Elastic Media. Small and Large Displacements," AIAA J., Vol. 3, No. 1, Jan., pp. 45-51.

2. Atluri, S. N. (1973), "On the Hybrid Stress Finite Element Model for Incremental Analysis of Large Deformation Problems," Int. J. Solids Struct., Vol. 9, No. 10, pp. 1177-1191.

3. Atluri, S. N. and Murakawa, H. (1977), "On Hybrid Finite Element Models in Nonlinear Solid Mechanics," International Conference on Finite Elements in Nonlinear Mechanics, Vol. 1, Tapir, Norway, August.

4. Atluri, S. N. (1980), "On Some New General Complementary Energy Theorems for the Rate Problems in Finite Strain. Classical Elasto-Plasticity," Georgia Institute of Technology, also in Journal of Structural Mechanics, March.

4A. Atluri, S. N. (1979), Class Notes, Georgia Institute of Technology Course on Finite Elements.

5. Baligh, M. M. and Scott, R. F. (1976), "Analysis of Wedge Penetration in Clay," Geotechnique, No. 1, pp. 165-208.

6. Barksdale, R. D. (1969), "Analysis of Layered Systems," Georgia Institute of Technology, Project B-607, July.

7. Barksdale, R. D. and Hicks, R. G. (1973), "Material Characterization and Layered Theory for Use in Fatigue Analysis," HRB-14-Special Report, pp. 20-48.

8. Barksdale, R. D. (1972), "Laboratory Evaluation of Rutting in Base Course Materials," Proceedings International Conference on the Structural Design of Asphalt Pavements, London.

9. Bathe, K. J., Wilson, E. L. and Iding, R. (1974), "NONSAP--A Structural Analysis Program for Static and Dynamic Response of Nonlinear Systems," Report UCSESM 74-3, University of California, Berkeley, February.

10. Bathe, K. J., Ramm, E. and Wilson, E. L. (1975), "Finite Element Formulations for Large Deformation Dynamic Analysis," Int. J. Num. Meth. Engng., Vol. 9, pp. 353-386.

11. Bathe, K. J., Wilson, E. L. (1976), Numerical Methods in Finite Element Analysis, Prentice Hall.

12. Bathe, K. J., Oden, J. T., Wunderlich, W., Ed. (1976), "Formulations and Computational Algorithms in Finite Element Analysis," U.S.-Germany Symposium, MIT, August.

13. Bell, J. R., Greenway, D. R. and Vischer, W. (1977), "Construction and Analysis of a Fabric Reinforced Low Embankment," Cr. Coll. Int. Sols., Textiles, Paris.

14. Busnell. D. (1977), "A Strategy for the Solution of Problems Involving Large Deflections, Plasticity and Creep," Int. J. Num. Meth. Engng., Vol. 11, pp. 683-708.

15. Carter, J. P., Booker, J. R. and Davis, E. H. (1977), "Finite Deformation of an Elasto-Plastic Soil," Int. J. Num. Ana. Meth. Geomechanics, Vol. 1, pp. 25-43.

16. Carter, J. P., Booker, J. R. and Small, J. C. (1979), "The Analysis of Finite Elasto-Plastic Consolidation," Int. J. Num. Ana. Meth. Geomechanics, Vol. 3, pp. 107-129.

17. Chang, J. C., Forsyth, R. A. and Beaton, J. L. (1974), "Performance of a Reinforced Earth Fill," California Department of Transportation, Division of Highways, Highway Research Report, Transportation Laboratory, presented at the 53rd Annual Meeting of the HRB, January.

18. Chang, C. Y., Nair, K., and Singh, R. D. (1974), "Finite Element Methods for the Nonlinear and Time Dependent Analysis of Geotechnical Problems," Analysis and Design in Geotechnical Engineering, Vol. 1, ASCE, Austin, Texas, June, pp. 269-302.

19. Chang, J. C., Hannon, J. B. and Forsyth, R. A. (1976), "Pull Resistance and Interaction of Earthwork Reinforcement and Soil," TRR 640, December, pp. 1-7.

20. Chang, J. C., Forsyth, R. A. (1977), "Finite Element Analysis of Reinforced Earth Wall," J. Geotech. Engng. Div., ASCE, GT 7, July, pp. 711-724.

21. Chen, W. F. (1975), Limit Analysis and Soil Plasticity, Elsvier Scientific.

22. Chen, W. F. and Davidson, H. L. (1977), "Large Deformation Response of Clay to Loads," Finite Elements in Nonlinear Mechanics, Vol. 2, Tapir, Norway, pp. 478-511.

23. Chen, W. F. (1980), "Plasticity in Soil Mechanics and Landslides," J. Engng. Mech. Div., EM3, June, pp. 443-463.

24. Committee on Computer Applications of the Geotechnical Engineering Division (1976), "A Standard for Computer Program Distribution," J. Geotech. Engng. Div., ASCE, GT 10, October, pp. 1049-1057.

25. Cook, R. D. (1974), Concepts and Applications of Finite Element Analysis. John Wiley.

26. Cormeau, I. (1975), "Numerical Stability in Quasi-Static Elasto/Visco-Plasticity," Int. J. Num. Meth. Engng., Vol. 9, pp. 109-127.

27. Corotis, R. B., Farzin, M. H., and Krizek, R. T. (1974), "Nonlinear Stress-Strain Formulation for Soils," J. Geotech. Engng. Div., ASCE, GT 9, September, pp. 993-1008.

28. Dario, N. P. and Bradley, W. A. (1973), "A Comparison of First and Second Order Axially Symmetric Finite Elements," Int. J. Num. Meth. Engng., Vol. 5, pp. 573-583.

29. Desai, C. S. and Reese, L. C. (1970), "Analysis of Circular Footings on Layered Soils," J. Soil Mech. and Found. Div., ASCE, SM4, July, pp. 1289-1310.

30. Desai, C. S. (1971), "Nonlinear Analyses Using Spline Functions," J. Soil Mech. and Found. Div., ASCE, SM 10, pp. 1461-1480.

31. Desai, C. S. and Wu, T. H. (1976), "A General Function for Stress-Strain Curves," Numerical Methods in Geomechanics, Ed. C. S. Desai, ASCE, Vol. 1, Virginia, pp. 306-317.

32. Desai, C. S. and Saxena, S. K. (1977), "Consolidation Analysis of Layered Anisotropic Foundations," Int. J. Num. Ana. Meth. Geomechanics, Vol. 1, pp. 5-23.

33. Desai, C. S. and Christian, J. T. Ed. (1977), Numerical Methods in Geotechnical Engineering, McGraw-Hill.

34. Desai, C. S. (1979), "Some Aspects of Constitutive Models for Geologic Media," Proceedings 3rd International Conference in Numerical Methods in Geomechanics, Aachen, April.

35. DiMaggio, F. L. and Sandler, I. S. (1971), "Material Model for Granular Soils," J. Eng. Mech. Div., ASCE, EM3, June, pp. 935-950.

36. Doherty, W. P., Wilson, E. L. and Taylor, R. L. (1969), "Stress Analysis of Axisymmetric Solids Utilizing Higher Order Quadrilateral Finite Elements," Report No. 69-3, Structural Engineering Laboratory, University of California, Berkeley, January.

37. Domaschuk, L. and Valliappan, P. (1975), "Nonlinear Settlement Analysis by Finite Elements," J. Geotech. Engng. Div., ASCE, GT7, July, pp. 601-614.

38. Drucker, D. C. and Prager, W. (1952), "Soil Mechanics and Plastic Analysis or Limit Design," Q. J. Applied Math., 10 pp. 157-165.

39. Duncan, J. M., Monismith, C. L. and Wilson, E. L. (1968), "Finite Element Analyses of Pavements," Highway Research Board, No. 228, pp. 18-33.

40. Duncan, J. M. and Chang, C. Y. (1970), "Nonlinear Analysis of Stress and Strain in Soils," J. Soil Mech. and Found. Div., ASCE, SM3, September, pp. 1629-1653.

41. Durocher, L. L., Gasper, A. and Roades, G. (1978), "A Numerical Comparison of Axisymmetric Finite Elements," Int. J. Num. Meth. Engng., Vol. 12, pp. 1415-1427.

42. Evans, R. J. and Pister K. S. (1966), "Constitutive Equations for a Class of Nonlinear Elastic Solids," Int. J. Solids Struct., Vol. 2, pp. 427-445.

43. Fardis, M. N. and Buyokozturk, O. (1979), "Shear Transfer Model for Reinforced Concrete," J. Engng. Mech. Div., ASCE, EM2, April, pp. 255-275.

44. Fenves, S. J., Perrone, N., Robinson, A. and Schnobrich, W. C., Ed. (1973), Numerical and Computer Methods in Structural Mechanics, Academic Press, Inc.

45. Fenves, S. J. (1967), Computer Methods in Civil Engineering, Prentice Hall.

46. Fung, Y. C. (1965), Foundations of Solid Mechanics, Prentice Hall.

47. Gallager, R. H. (1975), Finite Element Analysis Fundamentals, Prentice Hall.

48. Gerrard, C. M. (1969), "Tables of Stresses, Strains and Displacements in Two-Layer Elastic Systems," Australian Road Research Board, Special Report No. 3.

49. Ghaboussi, J., Wilson, E. L. and Isenberg, J. (1973), "Finite Element for Rock Joints and Interfaces," J. Soil Mech. and Found. Div., ASCE, SM10, October, pp. 833-848.

50. Goodman, R. E., Taylor, R. L. and Brekke, T. L., (1968), "A Model for the Mechanics of Jointed Rock," J. Soil Mech. and Found. Div., ASCE, SM3, May, pp. 637-659.

51. Goodman, R. E. (1976), Methods of Geological Engineering in Discontinuous Rocks, West Publishing Co.

52. Gudehus, G., Ed. (1977), Finite Elements in Geomechanics, John Wiley.

53. Haisler, W. E., Stricklin, J. A., and Stebbins, F. T., (1972), "Development and Evaluation Solution Procedures for Geometrically Nonlinear Structural Analysis," AIAA Journal, Vol. 10, No. 3, March, pp. 264-272.

54. Harr, M. E. (1977), Mechanics of Particulate Media, McGraw Hill.

55. Herrmann, L. R. (1972), "Interpretation of the Finite Element Procedure as Stress Error Minimization Procedure," J. Engng. Mech. Div., ASCE, EM5, October, pp. 1330-1335.

56. Herrmann, L. R. (1973), "Efficiency Evaluation of a Two Dimensional Incompatible Finite Element," Computers and Structures, Vol. 3, pp. 1377-1395.

57. Herrmann, L. R. (1977), "Nonlinear Finite Element Analysis of Frictional Systems," Finite Elements in Nonlinear Mechanics, Vol. 2, Tapir, Norway, pp. 825-844. International Conference on Finite Elements in Nonlinear Mechanics.

58. Herrmann, L. R. (1976), "General Two Dimensional Soils and Reinforced Earth Analysis Program, REA, University of California, Davis, January.

59. Herrmann, L. R. and Al Yassin, Z. (1978a), "Numerical Analysis of Reinforced Soil Systems," ASCE, Spring Convention, Preprint 3125, Pittsburg, April.

60. Herrmann, L. R. (1978b), "Finite Analysis of Contact Problems," J. Engng. Mech. Div., ASCE, EM5, October, pp. 1043-1057.

61. Herrmann, L. R. (1978c), "Additional Work on the Mechanics and Analysis of Reinforced Earth," University of California, Davis, September.

62. Heuze, F. E., Goodman, R. E. and Bornstein, A., (1971), "Numerical Analysis of Deformability Tests in Jointed Rock-Joint Perturbation and No Tension," Finite Element Solutions, Rock Mechanics, 3, pp. 13-24.

63. Hibbit, H. D., Marcal, P. V. and Rice, J. R. (1970), "A Finite Element Formulation for Problems of Large Strain and Large Displacement," Int. J. Solids Struct., Vol. 6, pp. 1069-1086.

64. Hill, R. (1950), The Mathematical Theory of Plasticity, Oxford University Press, London.

65. Hinton, E. and Campbell, J. S. (1974), "Local and Global Smoothing of Discontinuous Finite Element Functions Using a Least Squares Method," Int. J. Num. Meth. Engng., Vol. 8, pp. 461-480.

66. Hinton, E., Scott, F. C. and Ricketts, R. E. (1975), "Local Least Squares Smoothing for Parabolic Isoparametric Elements," Int. J. Num. Meth. Engng., Vol. 9, pp. 235-239.

67. Hofmeister, L. D., Greenbaum, G. A., and Evensen, D. A. (1971), "Large Strain, Elasto-Plastic Finite Element Analysis," AIAA Journal, Vol. 9, No. 7, pp. 1248-1255.

68. Intraprasart, S. (1979), "Experimental Studies and Analysis of Compacted Fills Over Soft Subsoils," Ph.D. Thesis, Georgia Institute of Technology.

69. Irons, B. M. (1970), "A Frontal Solution Program for Finite Element Analysis," Int. J. Num. Meth. Engng., Vol. 2, pp. 5-32.

70. Isenberg, J. (1973), Analytic Modeling of Rock Structure Interaction, Vol. 1, Advanced Research Projects Agency of the Department of Defense, Agbabian Associates, April.

71. Jaeger, J. C. (1962), Elasticity, Fracture and Flow, 2nd Edition, Methuen and Co., London.

72. Jaeger, J. C. and Cook, N. G. W. (1976), Fundamentals of Rock Mechanics, 2nd Ed., Chapman and Hall, London, John Wiley, New York.

73. Jessberger, H. L. (1977), "Load-Bearing Behavior of Gravel Subbase Non Woven Fabric-Soft Subgrade System," Cr. Coll. Int. Sols. Textiles, Paris.

74. Kaare Hoeg (1972), "Finite Element Analysis of Strain-Softening Clay," J. of the Soil Mech. and Found. Div., ASCE, SM1, Jan., pp. 43-57.

75. Katona, M. G., Smith, J. M., Odello, R. S. and Allgood, J. R., (1976), "CANDE, A Modern Approach for the Structural Design and Analysis of Buried Culverts," FHWA, Rd. 77-5, October.

76. Kinney, T. C. (1979), "Fabric Induced Changes in High Deformation Soil-Fabric-Aggregate Systems," Ph.D. Thesis, University of Illinois, Urbana.

77. Kost, E. G. (1972), Nonlinear Dynamic Analysis of Frames with Filler Panels, John Blume & Associates, U. S. Atomic Energy Commission, November.

78. Lade, P. V. and Duncan, J. M. (1975), "Elastoplastic Stress-Strain Theory for Cohesionless Soil," J. of the Geotech. Engng. Div., ASCE, GT10, October, pp. 1037-1053.

79. McMeeking, R. M. and Rice, J. R. (1975), "Finite-Element Formulations for Problems of Large Elastic-Plastic Deformation," Int. J. Solids Struct., Vol. 11, pp. 601-616.

80. Mitchell, J. K. and Gardner, W. S. (1971), "Analysis of Load Bearing Fills Over Soft Subsoils," J. Soil Mech. and Found. Div., ASCE, Vol. 97, SM11, pp. 1549-1571.

81. Mondkar, D. P. and Powell, G. H. (1974a), "Towards Optimal In-Core Equation Solving," Computers and Structures, Vol. 4, pp. 531-548.

82. Mondkar, O. P. and Powell, G. H. (1974b), "Large Capacity Equation Solver for Structural Analysis," Computers and Structures, Vol. 4, pp. 699-728.

83. Murakawa, H. and Atluri, S. N. (1978), "Finite Elasticity Solutions Using Hybrid Finite Elements Based on a Complementary Energy Principle," ASME Journal of Applied Mechanics, Vol. 45, No. 3, September, pp. 539-547.

84. Murakawa, H. and Atluri, S. N. (1979), "Finite Elasticity Solutions Using Hybrid Finite Elements Based on a Complementary Energy Principle," Part 2: Incompressible Materials, Journal of Applied Mechanics, Paper No. 79-APM-6, ASME. Joint ASME-CSME Applied Mechanics Fluids Engineering and Bioengineering, June.

85. Murakawa, H. (1978), "Incremental Hybrid Finite Element Methods for Finite Deformation Problems," Report GIT-ESM-SA-78-7, Georgia Institute of Technology, August.

86. Murray, D. W. and Wilson, E. L. (1969), "Finite-Element Large Deflection Analysis of Plates," J. Engng. Mech. Div., ASCE, EM1, Vol. 95, February, pp. 143-165.

87. Nadai, A. (1931), Plasticity, McGraw-Hill.

88. Nagtegaal, J. C., Parks, D. M. and Rice, J. R. (1974), "On Numerically Accurate Finite Element Solutions in the Fully Plastic Range," Computer Methods in Applied Mech. and Eng., 4, pp. 153-177.

89. Nath, P., (1977), "The Analysis of Composite Structures with Prescribed Frictional Conditions at the Interfaces," Int. J. Num. Ana. Meth. Geomechanics, Vol. 1, pp. 387-396.

90. Nayak, G. C. and Zienkiewicz, O. C. (1972a), "Elasto-Plastic Stress Analysis, A Generalization for Various Constitutive Relations Including Strain Softening," Int. J. Num. Meth. Engng., Vol. 5, pp. 113-135.

91. Nayak, G. C. and Zienkiewicz, O. C. (1972b), "Note on the Alpha Constant Stiffness Method for the Analysis of Non-Linear Problems," Int. J. Num. Meth. Engng., Vol. 4, pp. 579-582.

92. Nayak, G. C. and Zienkiewicz, O. C. (1972c), "Convenient Form of Stress Invariants for Plasticity," J. Structural Div., ASCE, ST4, pp. 949-954.

93. Needelman, A. (1972), "A Numerical Study of Necking in Circular Cylindrical Bars," Journal Mechanics Physics of Solids," Vol. 20, pp. 111-127.

94. Nemat-Nasser, S. and Taya, M. (1976), "Model Studies of Ductil Fracture I. Formulation," Journal of the Franklin Institute, 302, pp. 463-472.

95. Ngo, D. and Scordelis, A. C. (1967), "Finite Element Analysis of Reinforced Concrete Beams," ACI Proceedings, Title 64-14, March, pp. 152-163.

96. Oden, J. T. and Sato, T. (1967), "Finite Strains and Displacements of Elastic Membranes by the Finite Element Method," Int. J. Solids Struct., Vol. 3, pp. 471-488.

97. Oden, J. T. and Key, J. E. (1970), "Numerical Analysis of Finite Axisymmetric Deformations of Incompressible Elastic Solids of Revolution," Int. J. Solids Struct., Vol. 6, pp. 497-518.

98. Oden, J. T. (1972), Finite Elements of Nonlinear Continua, McGraw-Hill.

99. Okamoto, N. and Nakazawa, M. (1979), "Finite Element Incremental Contact Analysis with Various Frictional Conditions," Int J. Num. Meth. Engng., Vol. 14, pp. 337-357.

100. Osias, J. R. and Swedlow, J. L. (1974), "Finite Elasto-Plastic Deformation I. Theory and Numerical Examples," Int. J. Solids Struct., Vol. 10, pp. 321-339.

101. Pande, G. N., Owen, D. R. J. and Zienkiewicz, O. C. (1977), "Overlay Models in Time-Dependent Non-Linear Material Analysis " Computer and Structures, Vol. 7, pp. 435-443.

102. Pande, G. N. and Sharma, K. G. (1979), "On Joint/ Interface Elements and Associated Problems of Numerical III-Conditioning," Int.J. Num. Ana. Meth. Geomechanics, Vol. 3, pp. 293-300.

103. Pappin, J. W. and Brown, S. F. (1980), "Resilient Stress-Strain Behavior of a Crushed Rock," Int. Symposium of Soils Under Cyclic and Transient Loading, Swansea, Jan., pp. 169-177.

104. Peterson, H. (1977), "Application of the Finite Element Method in the Analysis of Contact Problems," Finite Elements in Nonlinear Mechanics, Vol. 2, Tapir, Norway, pp. 845-862, International Conference on Finite Elements in Nonlinear Mechanics.

105. Pian, T. H. H. (1976), "Variational Principles for Incremental Finite Element Methods," Journal of the Franklin Institute, 302, pp. 474-488.

106. Potyondy, J. C. (1961), "Skin Friction Between Various Soils and Construction Materials," Geotechnique, Vol. XI, December, pp. 339-353.

107. Poulos, H. G. and Davis, E. H. (1974), Elastic Solutions for Soil and Rock Mechanics, John Wiley.

107A. Prager, W. (1961), "An Elementary Discussion of Definitions of Stress Rate," Quart. Appl. Math, 18, pp. 403-407.

108. Raad, L. and Figueroa, J. L. (1980), "Load Response of Transportation Support Systems," Transportation Engineering Journal, ASCE, TE1, January, pp. 111-128.

109. Rice, J. R., McMeeking, R. M., Parks, D. M. and Sorensen, E. P. (1979), "Recent Finite Element Studies in Plasticity and Fracture Mechanics," Computer Methods in Applied Mechanics and Engineering, 17/18, pp. 411-442.

110. Rich, T. P. (1978), "Closed Form Elasto-Plastic Stiffness Matrix for Axisymmetric Finite Elements," Int. J. Num. Meth. Engng., Vol. 12, pp. 59-65.

111. Romstad, K. M., Herrmann, L. R. and Shen, C. K. (1976), "Integrated Study of Reinforced Earth-I," J. Geotech. Engng. Div., ASCE, GT5, May, pp. 457-471.

112. Rowe, R. K., Booker, J. R. and Balaam, N. P. (1978), "Application of the Initial Stress Method to Soil Structure Interaction," Int. J. Num. Meth. Engng., Vol. 12, pp. 873-880.

113. Runesson, K., Tagnfors, H. and Wiberg, N. E. (1977), "Computer Implementation of Non-Linear Finite Element Analysis Applied to Some Geotechnical Problems," Finite Elements in Nonlinear Mechanics, Vol. 2, Tapir, Norway, pp. 561-584, International Conference on Finite Elements in Nonlinear Mechanics.

114. Schmertmann, J. H., Hartman, J. P. and Brown, P. R. (1978), "Improved Strain Influence Factor Diagrams," J. Geotech. Engng. Div., GT8, August, pp. 1131-1135.

115. Seed, H. B., Mirty, F. G., Monismith, C. L. and Chan, C. K. (1967), "Factors Influencing the Resilient Deformation of Untreated Aggregate Base in Two-Layer Pavements Subjected to Repeated Loading, Highway Research Record, 190, pp. 19-57.

116. Seed, H. B., Mirty, F. G., Monismith, C. L. and Chan, C. K. (1965), "Prediction of Pavement Deflections from Laboratory Repeated Load Tests," Report No. TE 65-6, Department of Civil Engineering, University of California at Berkeley.

117. Segerlind, L. J. (1976), Applied Finite Element Analysis, John Wiley.

118. Sharma, H. D., Nayak, G. C., and Maheshwari (1976), "Generalization of Sequential Non-Linear Analysis," A Study of a Rookfill Dam with Joint Elements, Numerical Methods in Geotechnical Engineering, Ed. Desai, C. S., Vol. II, ASCE, Virginia, June, pp. 662-685.

119. Shen, C. K., Romstad, K. M. and Herrmann, L. R. (1976), "Integrated Study of Reinforced Earth II," J. Geotech. Engng. Div., GT6, June, pp. 577-591.

120. Sowers, G. F. (1979), Fourth Edition, Introductory Soil Mechanics and Foundations: Geotechnical Engineering, MacMillan.

121. Stricklin, J. A., Haisler, W. E. and von Riesemann, W. A. (1971), "Geometrically Nonlinear Structural Analysis by Direct Stiffness Method," J. Structural Div., ASCE, ST9, pp. 2299-2314.

122. Stricklin, J. A., Haisler, W. E. and von Riesemann, W. A. (1973), "Evaluation of Solution Procedures for Material and/or Geometrically Nonlinear Structural Analysis," AIAA Journal, Vol. 11, No. 3, March, pp. 292-299.

123. Terzaghi, Karl (1943), Theoretical Soil Mechanics, John Wiley.

124. Terzaghi, Karl and Peck, R. B. (1968), Soil Mechanics in Engineering Practice, 2nd Ed., John Wiley.

125. Timoshenko, S. P. and Goodier, J. N. (1970), Theory of Elasticity, McGraw Hill, 3rd Ed.

126. Venkateswara Rao, G. and Krishna Murty, A. V. (1971), "An Alternate Form of the Ramberg-Osgood Formula for Matrix Displacement Analysis," Nuclear Engineering and Design, 17, pp. 297-308.

127. Westergaard, H. M. (1952), Theory of Elasticity and Plasticity, Harvard University Press, John Wiley.

128. Wood, R. D. and Schrefler, R. (1978), "Geometrically Non-Linear Analysis, a Correlation of Finite Element Notations," Int. J. Num. Meth. Engng., Vol. 12, pp. 635-642.

129. Wifi, A. S. (1976), "An Incremental Complete Solution of the Stretch-Forming and Deep-Drawing of a Circular Blank Using a Hemispherical Punch," International Journal Mech. Sci., 18, No. 1, pp. 23-31.

130. Wilhite, T. (1979), "Computer Modeling of Aggregate Fabric-Soil Systems," Special Problem, Georgia Institute of Technology.

131. Wilson, E. L. (1965), "Structural Analysis of Axisymmetric Solids," AIAA Journal, Vol. 3, No. 12, December, pp. 2269-2274.

132. Wilson, E. L. (1969), "Elastic Dynamic Response of Axisymmetric Structures," Report No. 69-2, Structural Engineering Laboratory, University of California, Berkeley, January.

133. Wilson, E. L., Taylor, R. L., Doherty, W. P. and Ghaboussi, J. (1973), "Incompatible Displacement Models," Numerical and Computer Methods in Structural Mechanics, Ed., Fenves, S. J., et al., pp. 43-57.

134. Yaghmai, S. and Popov, E. P. (1971), "Incremental Analysis of Large Deflections of Shells of Revolution," Int. J. Solids Structures, Vol. 7, pp. 1375-1393.

135. Yamada, Y., Yoshimura, N. and Sakurai, T. (1968), "Plastic Stress-Strain Matrix and Its Application for the Solution of Elastic-Plastic Problems by the Finite Element Method," Int. J. Mech. Sci., Vol. 10, pp. 343-354.

136. Yamada, Y. (1976), "Formulation of a Solution Procedure for Non-Linear Material and Structural Behaviors--Theoretical Bases for Program Composite III," Proceedings Conference on Computer Simulation for Material Applications, National Bureau of Standards, Gaithersburg, pp. 826-837.

137. Yamada, Y. and Wifi, A. S. (1977), "Large Strain Analysis of Some Geomechanics Problems by the Finite Element Method," Int. J. Num. Ana. Meth. Geomechanics, Vol. 1, pp. 299-318.

138. Zeevaert, L., (1972), Foundation Engineering for Difficult Subsoil Conditions, Van Nostrand.

139. Zienkiewicz, O. C., Cheung, Y. K. and Stagg, K. G. (1966), "Particular Reference to Problems of Rock Mechanics," Journal of Strain Analysis, Vol. 1, No. 2, pp. 172-182.

140. Zienkiewicz, O. C., Valliappan, S. and King, I. P. (1968), "Stress Analysis of Rock as a 'No Tension' Material," Geotechnique, 18, pp. 56-66.

141. Zienkiewicz, O. C., Valliappan, S. and King, I. P. (1969), "Elastic-Plastic Solutions of Engineering Problems 'Initial Stress' Finite Element Approach," Int. J. Num. Meth. Engng., Vol. 1, pp. 75-100.

142. Zienkiewicz, O. C., Best, B., Dullage, C., and Stagg, K. G. (1970), "Analysis of Nonlinear Problems in Rock Mechanics with Particular Reference to Jointed Rock Systems," Proceedings Second International Conference in Rock Mechanics, pp. 8-14, Yugoslavia.

143. Zienkiewicz, O. C. and Cormeau, I. (1974), "Visco-Plasticity and Creep in Elastic Solids--A Unified Numerical Solution Approach," Int. J. Num. Meth. Engng., Vol. 8, pp. 821-845.

144. Zienkiewicz, O. C. and Lewis, R. W. and Humperson, C. (1975), "Associated and Non-Associated Visco-Plasticity and Plasticity in Soil Mechanics," Geotechnique, 25, No. 4, pp. 671-689.

145. Zienkiewicz, O. C., Norris, V. and Naylor, D. J. (1977), "Plasticity and Viscoplasticity in Soil Mechanics with Special Reference to Cyclic Loading Problems," Finite Elements in Nonlinear Mechanics, Vol. 2, Tapir, Norway, International Conference on Finite Elements in Nonlinear Mechanics.

146. Zienkiewicz, O. C. and Pande, G. N. (1977), "Time Dependent Multilaminate Model of Rocks--A Numerical Study of Deformation and Failure of Rock Masses," Int. J. Num. Ana. Meth. Geomechanics, Vol. 1, pp. 219-247.

147. Zienkiewicz, O. C. (1977), The Finite Element Method, 3rd Edition, McGraw-Hill.

148. Zienkiewicz, O. C., Lewis, R. W., Stagg, K. G., Ed. (1978), Numerical Methods in Offshore Engineering, John Wiley.

149. Zienkiewicz, O. C., Rodin, E. Y. and Glowinski, R. (1979), Energy Methods in Finite Element Analysis, John Wiley.

VITA

Adolfo Enrique Zeevaert was born on September 6, 1944 in Mexico City, México. He attended 14 years in the German School "Alexander von Humboldt" and graduated in 1962 from the Preparatory. In 1963 he enrolled in the Universidad Nacional Autónoma de México where in 1967 he graduated third among 500 students and received diplomas for 2nd highest grades in his junior and senior years. On April 3, 1968 he presented his Professional Examination for his Civil Engineering title with the thesis: "Comportamento de Muros de Mampostería Reforzada ante Carga Lateral" (Behavior of Reinforced Hollow Masonry Walls Subjected to Lateral Loads) obtaining Mención Honorífica (Highest Honors). In September 1968 he came to the United States to study with a half-time research assistantship at the University of Illinois where he got his Master of Science in Structural Engineering in February 1970. He then returned to Mexico City and worked for Dr. Leonardo Zeevaert as a design engineer and teaching assistant where he got interested in soil mechanics. From 1973 to 1976 he worked at SICARTSA, a Mexican government owned steel plant, on the geotechnical and structural design of a complete steel plant. Starting as a design engineer, in 1975 he was named chief of the department of special studies for the civil engineering department of the company.

He became involved in several geotechnical and soil-structure interaction problems and decided to obtain a degree in the geotechnical area. He returned in September 1977 to the United States with teaching and research assistantships in the School of Civil Engineering, Georgia Institute of Technology, where he began to work toward a Ph.D. in geotechnical engineering.

His professional activities include memberships in the American Society of Civil Engineers, American Concrete Institute, Sociedad Mexicana de Mécanica de Suelos, International Society of Soil Mechanics, Sociedad Mexicana de Ingeniería Sísmica and Colegio de Ingenieros Civiles de México. He is a registered professional engineer in Mexico City and registered supervisor for the public works department of Mexico City.